U.S.NRC
United States Nuclear Regulatory Commission
Protecting People and the Environment

NUREG/CR-7238

Guidance Document: Conducting Paleoliquefaction Studies for Earthquake Source Characterization

Office of Nuclear Regulatory Research

AVAILABILITY OF REFERENCE MATERIALS IN NRC PUBLICATIONS

NRC Reference Material

As of November 1999, you may electronically access NUREG-series publications and other NRC records at the NRC's Public Electronic Reading Room at http://www.nrc.gov/reading-rm.html. Publicly released records include, to name a few, NUREG-series publications; *Federal Register* notices; applicant, licensee, and vendor documents and correspondence; NRC correspondence and internal memoranda; bulletins and information notices; inspection and investigative reports; licensee event reports; and Commission papers and their attachments.

NRC publications in the NUREG series, NRC regulations, and Title 10, "Energy," in the *Code of Federal Regulations* may also be purchased from one of these two sources.

1. **The Superintendent of Documents**
   U.S. Government Publishing Office
   Washington, DC 20402-0001
   Internet: http://bookstore.gpo.gov Telephone:
   1-866-512-1800
   Fax: (202) 512-2104

2. **The National Technical Information Service**
   5301 Shawnee Road
   Alexandria, VA 22161-0002
   http://www.ntis.gov
   1-800-553-6847 or, locally, (703) 605-6000

A single copy of each NRC draft report for comment is available free, to the extent of supply, upon written request as follows:

U.S. Nuclear Regulatory Commission
Office of Administration
Publications Branch
Washington, DC 20555-0001
E-mail: distribution.resource@nrc.gov
Facsimile: (301) 415-2289

Some publications in the NUREG series that are posted at the NRC's Web site address http://www.nrc.gov/reading-rm/doc-collections/nuregs are updated periodically and may differ from the last printed version. Although references to material found on a Web site bear the date the material was accessed, the material available on the date cited may subsequently be removed from the site.

Non-NRC Reference Material

Documents available from public and special technical libraries include all open literature items, such as books, journal articles, transactions, *Federal Register* notices, Federal and State legislation, and congressional reports. Such documents as theses, dissertations, foreign reports and translations, and non-NRC conference proceedings may be purchased from their sponsoring organization.

Copies of industry codes and standards used in a substantive manner in the NRC regulatory process are maintained at—

The NRC Technical Library
Two White Flint North
11545 Rockville Pike
Rockville, MD 20852-2738

These standards are available in the library for reference use by the public. Codes and standards are usually copyrighted and may be purchased from the originating organization or, if they are American National Standards, from—

American National Standards Institute
11 West 42nd Street
New York, NY 10036-8002
http://www.ansi.org
(212) 642-4900

Legally binding regulatory requirements are stated only in laws; NRC regulations; licenses, including technical specifications; or orders, not in NUREG-series publications. The views expressed in contractor-prepared publications in this series are not necessarily those of the NRC.

The NUREG series comprises (1) technical and administrative reports and books prepared by the staff (NUREG-XXXX) or agency contractors (NUREG/CR-XXXX), (2) proceedings of conferences (NUREG/CP-XXXX), (3) reports resulting from international agreements (NUREG/IA-XXXX), (4) brochures (NUREG/BR-XXXX), and (5) compilations of legal decisions and orders of the Commission and Atomic and Safety Licensing Boards and of Directors' decisions under Section 2.206 of NRC's regulations (NUREG-0750).

DISCLAIMER: This report was prepared as an account of work sponsored by an agency of the U.S. Government. Neither the U.S. Government nor any agency thereof, nor any employee, makes any warranty, expressed or implied, or assumes any legal liability or responsibility for any third party's use, or the results of such use, of any information, apparatus, product, or process disclosed in this publication, or represents that its use by such third party would not infringe privately owned rights.

U.S.NRC
United States Nuclear Regulatory Commission
Protecting People and the Environment

NUREG/CR-7238

Guidance Document: Conducting Paleoliquefaction Studies for Earthquake Source Characterization

Manuscript Completed: January 2017
Date Published: January 2018

Prepared by:

M. Tuttle[1]
L. Wolf[2]
P. Mayne[3]
K. Dyer-Williams[4]
R. Lafferty[5]

[1]M. Tuttle & Associates, P.O. Box 345, Georgetown, ME 04548

[2]Auburn University, Geosciences, Auburn, AL 36849

[3]Georgia Institute of Technology, Civil and Environmental Engineering, Atlanta, GA 30332-0355

[4]VanLeen Associates, P.O. Box 156, Columbia, MD 21045

[5]Lafferty-Hess Consultants, 16400 Sigmond Lane, Lowell, AR 72745

Sarah Tabatabai, NRC Project Manager

Office of Nuclear Regulatory Research

ABSTRACT

Destructive earthquakes, both recent and historical, demonstrate the critical need for paleoliquefaction data to assist with the assessment of the potential for damaging earthquakes around the world. Paleoliquefaction studies, along with other paleoseismic studies such as fault studies, supplement seismicity studies and provide information about the long-term behavior of earthquake sources. Paleoliquefaction studies focus on soft-sediment deformation features, including sand blows and sand dikes, and related ground failures that result from large earthquakes. Most paleoliquefaction studies have been conducted in intraplate geologic settings, but a few such studies have been carried out in interplate settings as well. Paleoliquefaction studies have provided valuable information about timing, location, and magnitude of large paleoearthquakes, particularly those with moment magnitude, **M**, greater than 6, during the past 50,000 years. Although the results of paleoliquefaction studies have greatly increased the understanding of seismic hazards in a few regions where Holocene (0.01 million years ago, or Ma, to present) and Late Pleistocene (0.126 to 0.01 Ma) age deposits occur, the specific type, level of detail, and quality of paleoliquefaction data vary from one study area to another. This variation is due in part to the lack of standardized procedures for paleoliquefaction studies. There is also a shortage of qualified and experienced paleoliquefaction experts and few comprehensive resources for new investigators or regulators interested in obtaining results from paleoliquefaction studies for characterization of earthquake sources. In order to overcome some of the current deficiencies and advance the field of paleoliquefaction, this document provides detailed guidance for conducting paleoliquefaction studies that will generate high-quality paleoliquefaction data for use in seismic source characterization and seismic hazard assessment. Intended as a comprehensive resource for investigators and regulators interested in the field of paleoliquefaction, this report includes background information on earthquake-induced liquefaction and related ground failures and the resulting soft-sediment deformation features that may be preserved in the geologic record, relevant information derived from the disciplines of geology, geophysics, and geotechnical engineering, an extensive bibliography, and recommendations for future research.

FOREWORD

The U.S. Nuclear Regulatory Commission (NRC) requires an evaluation to determine the Safe Shutdown Earthquake Ground Motion (SSE) for a nuclear power plant site as specified in 10 CFR Part 100. A performance based approach to define site-specific earthquake ground motion is one component in the development and evaluation of the SSE. Regulatory Guide 1.208 provides guidance on this performance based approach which implements a probabilistic seismic hazard analysis. The probabilistic seismic hazard analysis is dependent on the characterization of seismic (earthquake) sources, with the key parameters in characterizing seismic sources being their location, timing, and size. The historical record of measured earthquakes is limited; therefore, the study of prehistoric earthquakes is extremely valuable in characterizing seismic sources. The study of prehistoric liquefaction features, paleoliquefaction, is one method used to characterize seismic sources.

Regulatory Guide 1.208, A Performance-Based Approach to Define the Site-Specific Earthquake Ground Motion, and the Standard Review Plan for the Review of Safety Analysis Reports for Nuclear Power Plants: LWR Edition (NUREG-0800), Section 2.5.1, provides guidance to license applicants and NRC staff, respectively, on the review of seismic sources. This document provides valuable guidance on how to conduct a paleoliquefaction study and evaluate data with consideration of uncertainties encountered in the various phases of the study for seismic source characterization. This guidance document will be a resource for staff as updates to regulatory and staff guidance are developed on characterizing seismic sources.

TABLE OF CONTENTS

LIST OF FIGURES

LIST OF TABLES

EXECUTIVE SUMMARY

The primary goal of this document is to provide detailed guidance for conducting paleoliquefaction studies in order to generate high-quality data for use in seismic source characterization and seismic hazard assessment. Towards this end, the document includes a review of many of the geological, geophysical, and geotechnical techniques applied in paleoliquefaction studies and of approaches used to incorporate paleoliquefaction data in seismic hazard assessment. Furthermore, this document advances procedures for quantification of uncertainties of paleoliquefaction results. The intended audience includes scientists new to the field who may be interested in pursuing paleoliquefaction studies, government and consulting personnel interested in using paleoliquefaction data in seismic hazard assessments, regulators seeking a better understanding of paleoliquefaction in order to evaluate the results of specific studies, and experienced paleoliquefaction experts planning future research. This document was written by an interdisciplinary team with more than ninety years of combined experience in paleoliquefaction and the related fields of paleoseismology, Quaternary geology, structural geology, neotectonics, seismology, geophysics, geotechnical engineering, soil science, and archeology.

Originally developed in California as a subdiscipline of paleoseismology, the study of paleoliquefaction is a type of empirical science that documents, dates, and analyzes soft-sediment deformation structures and related ground failures that resulted from large earthquakes, particularly those of moment magnitude, **M,** greater than 6, that occurred during the past 50,000 years, and possibly earlier. Evidence of these events may be preserved in the geologic record for thousands to tens of thousands of years in the form of soft-sediment deformation structures such as sand blows, dikes, sills, diapirs, foundered clasts, convolute bedding, pseudonodules, and load casts, as well as fissured, subsided, and tilted ground. Paleoliquefaction has emerged as a significant contributor to the understanding of the earthquake hazard in intraplate geologic settings of the Central and Eastern United States (CEUS) and southeastern Canada. In these regions, paleoliquefaction data supplement historical seismicity data and extend knowledge of the behavior of earthquake sources back in time. Paleoliquefaction studies have been conducted primarily in intraplate regions because active faults, the preferred target of most paleoseismic studies, are rarely expressed on the surface or are otherwise difficult to identify in these intraplate seismotectonic regions. However, recent earthquakes in interplate settings, such as the 2010 **M** 7.0 event in southern Haiti and the 2011 **M** 6.2-6.3 earthquake in Christchurch, New Zealand, induced severe liquefaction over large areas but were not associated with surface ruptures. Therefore, paleoliquefaction studies are likely to be more broadly applied in both interplate and intraplate settings in the future than they have been in the past.

In 2012, the CEUS seismic source characterization (SSC) project was completed. It was a multi-year project funded by the Electric Power Research Institute, the U.S. Department of Energy, and the U.S. Nuclear Regulatory Commission to develop a new generation of regional seismic source models for the CEUS. Recognizing their significance to seismic hazard assessment, paleoliquefaction data were used in the development of the new seismic source models. As part of the SSC project, a paleoliquefaction database was developed that included all major regional datasets. In addition, a technical report was written summarizing the current state of knowledge for each region and reviewing uncertainties related to the identification and interpretation of earthquake-induced liquefaction features. During the course of that effort, it became evident that the type, level of detail, and quality of paleoliquefaction data vary from one region to another. It was found that, even in regions where large paleoearthquakes have been recognized, significant uncertainties remain regarding their sources, magnitudes, and recurrence times, largely due to insufficient data. One of the recommendations of the report was the development of a manual of

best practices to provide guidance in conducting paleoliquefaction studies and to promote the collection of accurate and complete paleoliquefaction data. Following up on that recommendation, this document provides a comprehensive overview of paleoliquefaction studies. The intent of the document is to help standardize methodologies, to promote paleoliquefaction studies in areas where new or additional data are needed to better characterize seismic sources, and to encourage further development of the field through multidisciplinary research.

Similar to the paleoseismology field in general, paleoliquefaction studies provide information about the timing, location, magnitude, and recurrence times of large paleoearthquakes and are especially useful in regions where recurrence times of large earthquakes are longer than the historical record of earthquakes. Unlike fault studies, paleoliquefaction studies focus on soft-sediment deformation structures and related ground failures resulting from earthquake-induced liquefaction. Paleoliquefaction studies are inherently regional in scope and require observations and interpretations of liquefaction features at many sites over a large area. The field of study is interdisciplinary and requires expertise in paleoseismology, Quaternary geology, and the affiliated fields of sedimentology, geomorphology, soil science, geochronology, and sometimes archeology. A background in structural geology, neotectonics, seismology, geophysics, and geotechnical engineering is also desirable. Knowledge of ground motion is also relevant, as this is key to linking observed liquefaction features to potential sources. Qualified and experienced investigators should be involved in planning and execution of paleoliquefaction studies in order to avoid misidentification of soft-sediment deformation features and misinterpretation of the presence or absence of earthquake-induced liquefaction features. It is beneficial for more than one experienced investigator to be involved in the observation and interpretation of liquefaction features. If possible, site reviews should be conducted by paleoliquefaction experts during or soon after field investigations in order to discuss uncertainties and to avoid erroneous interpretation and results.

Characteristics of earthquake-induced liquefaction features and criteria for identifying them are well established, but the pool of experienced paleoliquefaction experts is small. Although there are numerous scientific articles and reports on various topics related to liquefaction studies, there are few resources that summarize all the relevant information. Therefore, this document was designed as a comprehensive resource for investigators and regulators to help remedy the shortage of practitioners in the field of paleoliquefaction for characterization of earthquake sources. It draws upon case studies of modern earthquakes that induced liquefaction, well-documented paleoliquefaction studies, and efforts to incorporate paleoliquefaction results into the seismic source models used in the national probabilistic seismic hazard maps and in probabilistic seismic hazard analyses for nuclear facilities.

This document presents background information on paleoseismology, earthquake-induced liquefaction and related ground failures, and soft-sediment deformation structures that form as a result of liquefaction. It also provides guidance on all aspects of paleoliquefaction studies, including selection of study areas and the various types of information that should be consulted, performance of site investigations and surveys of river cutbanks and other exposures, relative and absolute dating techniques used to constrain ages of liquefaction features and thus important for estimating the timing and recurrence of paleoearthquakes, and geological and geotechnical approaches to estimating source areas and magnitudes of paleoearthquakes. The report identifies factors that contribute to uncertainty in paleoliquefaction data and observations and analyses that can help to reduce those uncertainties. In addition, procedures are offered for the quantification and expression of uncertainty in estimates of timing, location, magnitude, and recurrence of paleoearthquakes. The report also includes a discussion of the use of paleoliquefaction data in seismic hazard assessment through the development of regional seismic

source models and presents recent examples of the use of paleoliquefaction data in seismic source models of the New Madrid seismic zone in the central U.S. The document concludes with recommendations for future research, ranging from liquefaction induced by recent earthquakes, to geophysical methods for mapping buried sand blows and sand dikes, and to geotechnical *in situ* testing devices and procedures, as well as improved methodologies, for assessing liquefaction.

ACKNOWLEDGMENTS

The development of this guidance document is sponsored by the U.S. Nuclear Regulatory Commission (NRC) under contract NRC-HQ-11-C-04-0041. The views and conclusions contained in the document are those of the authors and should not be interpreted as necessarily representing the official policies of the U.S. Government. Many thanks to Thomas Weaver who provided valuable guidance and support during the first year of the contract. Others who encouraged the development of this document include Annie Kammerer, Jon Ake, and Russ Wheeler. Gail Atkinson reviewed the entire document, and Russell Green, Shannon Mahan, and Julie Morrow reviewed sections of the report on the geotechnical approach to estimating magnitudes, optically-stimulated luminescence dating of sand blows, and archeological excavation protocols, respectively. Thomas Holzer contributed to the section on the liquefaction potential index. Taylor Busch, Caroline Moseley, and Cameron Schroeder assisted with editing portions of the manuscript and Kathleen Tucker modified several figures. Many thanks to reviewers Gail Atkinson, Russell Green, Thomas Holzer, Shannon Mahan, and Julie Morrow as well as NRC staff members Alice Stieve, Gerry L. Stirewalt, Thomas J. Weaver, and Sarah Tabatabai whose comments and suggestions contributed to and improved this document. We are very grateful to Rasool Anooshehpoor who helped to complete the editing process for this document.

ABBREVIATIONS AND ACRONYMS

3-D	Three-dimensional
ADAMS	Agencywide Documents Access and Management System
AMS	Accelerator mass-spectrometry
CEUS	Central and Eastern United States
CFR	Code of Federal Regulations
CHT	Crosshole test
CPT	Cone penetration test
CSR	Cyclic stress ratio
CRR	Cyclic resistance ratio
DHT	Downhole test
DMT	Flat dilatometer test
EM	Electromagnetic
ER	Electrical Resistivity
ETM+	Enhanced Thematic Mapper Plus
FC	Fines content
FS	Factor of safety
GPR	Ground-penetrating radar
IBC	International Building Code
LDI	Lateral displacement index
LiDAR	Light Detection and Ranging
LPI	Liquefaction potential index
LSI	Liquefaction severity index
M	Moment magnitude
MSF	Magnitude Scaling Factor
N	Blow count
NCEER	National Center for Earthquake Engineering and Research
NEHRP	National Earthquake Hazards Reduction Program
NMSZ	New Madrid seismic zone
NRC	Nuclear Regulatory Commission
OSL	Optically-stimulated luminescence
PGA	Peak ground acceleration
RLME	Repeated large-magnitude earthquake

SBT	Soil behavioral type
SCPTu	Seismic piezocone test
SPT	Standard penetration test
SSC	Seismic source characterization
SDMT	Seismic flat dilatometer test
TM	Thematic Mapper
UCD	University of California-Davis
USGS	U.S. Geological Survey

1 INTRODUCTION

The field of paleoliquefaction has developed over the past forty years and is now providing important information on source areas, magnitudes, and recurrence times of large paleoearthquakes. Recently, paleoliquefaction data have been used in the development of the national seismic hazard maps and in the central and eastern U.S. (CEUS) seismic source characterization for nuclear facilities. Paleoliquefaction studies, along with other paleoseismic studies such as fault studies, supplement seismicity studies and provide information on earthquake potential that will be necessary for seismic hazard assessments of nuclear facilities. This document provides an overview of paleoliquefaction, including recent advances, to facilitate the broader application of this relatively new field of inquiry for such assessments.

1.1 Paleoseismology and the Paleoliquefaction Approach

Paleoseismology is the study of fault ruptures and the effects of strong earthquakes as preserved in the geologic record. This scientific discipline extends our knowledge of seismic activity into the prehistoric period, thereby improving our understanding of the long-term behavior of fault zones and seismic sources (e.g., McCalpin, 1996 and 2009). Paleoliquefaction studies, which focus on the effects of strong shaking preserved in the geologic record, are especially valuable in regions where seismogenic faults may not rupture the surface or are otherwise difficult to identify (Tuttle, 2001; Tuttle et al., 2003). Paleoseismology, including paleoliquefaction studies, is especially useful in regions like central and eastern North America where strain rates are relatively low and recurrence times of large earthquakes are longer than the historical record. In such regions, the seismicity catalog is insufficient to characterize the expected rates of large events, a critical issue for uncertainty in seismic hazard estimation.

The paleoliquefaction approach is based on field observations of surface effects and soft-sediment deformation structures resulting from soil liquefaction induced by historical and modern earthquakes. The 1819 Cutch (Kachchh) earthquake in India is an example of a large historical earthquake that induced liquefaction and ground failure. Accounts of the earthquake reported by Captain J. MacMurdo (1822) and later discussed by Oldham (1926) describe “the occurrence of sand vents” “frequent and widespread throughout Cutch,” “spots of ground in circles” that “threw out water to a considerable height, and subsided into a slough,” and rivers, generally dry except during the monsoon, “filled to their banks for a period of a few minutes…to half an hour." The 2001 moment magnitude, **M**, 7.7 Bhuj earthquake also in the Kachchh region of India is a modern example of earthquake-induced liquefaction and ground failure. Accounts of this event describe fountains of water 1 to 2 m high during and immediately following the earthquake, formation of sand blows and ground fissures, and water flowing temporarily in previously dry channels (Tuttle et al., 2002a). Fuller (1912), who studied the 1811-1812 New Madrid earthquakes in the central U.S. almost a century after the event, describes the appearance of sand blows, sand sloughs, sand scatters, sand dikes, and simple and compound fissures (Figure 1-1).

Figure 1-1 Photograph of large sand blow with central crater that formed during 1811-1812 New Madrid earthquakes (from Fuller, 1912).

Fuller (1912) also recognized “geologic evidence of shocks long antedating that of 1811.” The evidence included “certain sand sloughs, …cracks as large as any of those of the last great disturbance…with trees fully 200 years old grown on their bottoms and slopes” and sloughs with “all the characteristics of sunk lands except the dead timber”…pointing “to a considerably earlier origin.” Fuller was an early paleoseismologist. Applying the principle of uniformitarianism, that suggests: "the present is the key to the past," he recognized paleoliquefaction features (or prehistoric liquefaction features) and related ground failures and used them to interpret the occurrence of paleoearthquakes similar to those in 1811-1812. Following the 1971 San Fernando, California earthquake, Sims (1973) described three zones of soft-sediment deformation structures in lacustrine deposits that had accumulated in the Van Norman reservoir. The three zones of deformation structures were attributed to liquefaction induced by three separate seismic events: the 1971 earthquake, and two prior earthquakes in 1952 and 1930. Recognizing the potential usefulness of soft-sediment deformation structures in developing long-term earthquake histories, Sims (1975) suggested criteria for distinguishing seismically from non-seismically induced structures. These and many other post-earthquake studies, including geological and geotechnical investigations, have provided valuable information used to identify earthquake-induced liquefaction features in the geologic record, to develop empirical relations, and to make interpretations about paleoearthquakes from paleoliquefaction features.

The paleoliquefaction approach has been most broadly applied in central and eastern North America. Paleoliquefaction studies have been conducted in the New Madrid (e.g., Saucier, 1991; Tuttle, 1999; Tuttle et al., 2002b and 2005), the Charleston (e.g., Talwani and Cox, 1985; Obermeier et al., 1989; Amick et al., 1990; Talwani and Schaeffer, 2001), and the Charlevoix (Tuttle and Atkinson, 2010) seismic zones, where large historical earthquakes are known to have occurred. In addition, paleoliquefaction studies have been conducted in the Wabash Valley (e.g., Munson et al., 1997; Obermeier, 1998) and the Eastern Tennessee (Hatcher et al., 2012) seismic zones, where only small to moderate earthquakes have occurred during the historical period. Other studies have been conducted outside recognized seismic zones, including those in the

meizoseismal areas of the 1727 Newburyport, Massachusetts, earthquake (Tuttle and Seeber, 1991), along the mid-Atlantic Seaboard (Amick and Gelinas, 1991), in southwestern Illinois (McNulty and Obermeier, 1999; NUREG/CR-5730), along the Clarendon-Linden fault zone in western New York State (Tuttle et al., 2002c), and near the southwestern terminus of the Reelfoot Rift fault system in east-central Arkansas (Tuttle et al., 2006; Al-Shukri et al., 2009). In the northeastern Caribbean, paleoliquefaction studies have been carried out in the Dominican Republic (Tuttle et al., 2003) and in Puerto Rico (Tuttle et al., 2005a; Tuttle, 2011) to help assess the earthquake potential of onshore and offshore faults. A paleoliquefaction study is currently underway in the Central Virginia seismic zone, the source of the 2011, **M** 5.8, Mineral earthquake that led to the temporary shutdown of the North Anna nuclear power plant located 18 km from the epicenter (Tuttle, pers. comm., 2015). The study will compare liquefaction features that formed during the 2011 **M** 5.8 earthquake (Green et al., 2015) with several weathered sand dikes found during a paleoliquefaction study in the mid-1990s, (Obermeier and McNulty, 1998; Agencywide Documents Access and Management System [ADAMS] Accession No. ML042800292).

The goals of paleoliquefaction studies are to estimate the timing, source areas, magnitudes, and recurrence times of strong earthquakes during the past 50,000 years, and possibly earlier. Results of paleoliquefaction studies increasingly are being used as input parameters for seismic hazard analyses and probabilistic risk assessments. In developing the U.S. national seismic hazard maps, the results of several paleoliquefaction studies were incorporated into the source model for the New Madrid seismic zone (Petersen et al., 2008). The CEUS Seismic Source Characterization Project developed a paleoliquefaction database that included all major datasets and used the paleoliquefaction data to identify earthquake source areas, to estimate recurrence times, and to weight maximum magnitudes in the new regional seismic source model (NUREG-2115).

1.2 Earthquake-Induced Liquefaction

Since the 1960s, when the 1964 Alaska, U.S., 1964 Niigata, Japan, and 1967 Caracas, Venezuela, earthquakes, caused catastrophic liquefaction-related failures, earthquake soil dynamics has been a major research focus of the geotechnical engineering community (Seed and Idriss, 1982). Due to this concerted research effort, the process of liquefaction, the conditions contributing to liquefaction and the mechanisms of ground failure are much better understood than before.

1.2.1 Process of Liquefaction

Liquefaction is the phenomenon that occurs when saturated sands exhibit reduced strength and stiffness due to increased pore water pressure, most often associated with cyclic loading imposed during earthquakes (Youd, 1973; Seed and Idriss, 1982; Boulanger and Idriss, 2014). There are two primary types of liquefaction: (a) flow liquefaction; associated with static monotonic loading; and (b) cyclic liquefaction, caused by repeated (earthquake) loading (Robertson and Wride, 1998). The term "liquefaction" is reserved for sands and granular deposits, while similar but rarer "cyclic softening" can occur in soft fine-grained clays and silts (Idriss and Boulanger, 2008). Sediment must be water-saturated in order for pore water pressures to develop during ground shaking. High pore water pressure can lead to a buoyancy effect on sediment grains causing a significant drop in the shear strength of the sediment (Kramer et al., 2011). During earthquakes, seismic waves propagate towards the ground surface and cyclic shear waves distort the structure of near-surface sediment through which they pass. Loose sands and gravels will tend to compact and reduce in volume (termed *contractive* behavior), leading to a reduction in strength and stiffness, i.e. "liquefaction". In contrast, dense sands and gravels will exhibit *dilative* behavior (i.e.,

increase in volume) and are less likely to liquefy, however, they may accumulate deformations of limited magnitude in a phenomenon termed "cyclic mobility".

At the micromechanics level, sediment is composed of individual grains or particles (e.g., sand) and each particle is in contact with a number of neighboring particles (Figure 1.2). The weight of the overlying particles produce contact forces between the particles by gravity (termed *overburden stresses*) and these forces hold individual particles in place and give the sediment its strength and structure. For saturated sediment below the water table, some of the weight of the overlying particles is carried by the pore water creating a buoyancy effect. Under level ground conditions and where no shear stresses are applied from foundations or other structures, a stable matrix of granular particles exists as long as the overburden stress (gravity) exceeds the pore water pressure (buoyancy). In contrast, liquefaction occurs when the structure of water-saturated, loose, granular sediment breaks down due to rapidly applied and repetitive loading caused by earthquakes. As the sediment structure breaks down, the loosely packed particles attempt to move into a denser configuration (termed *contraction*). During an earthquake, however, there is not enough time for the water in the pores of the sediment to be squeezed out. Instead, the water is trapped and prevents the particles from moving closer together. This is accompanied by an increase in pore water pressure that reduces the contact forces between the individual particles, thereby softening and weakening the sediment.

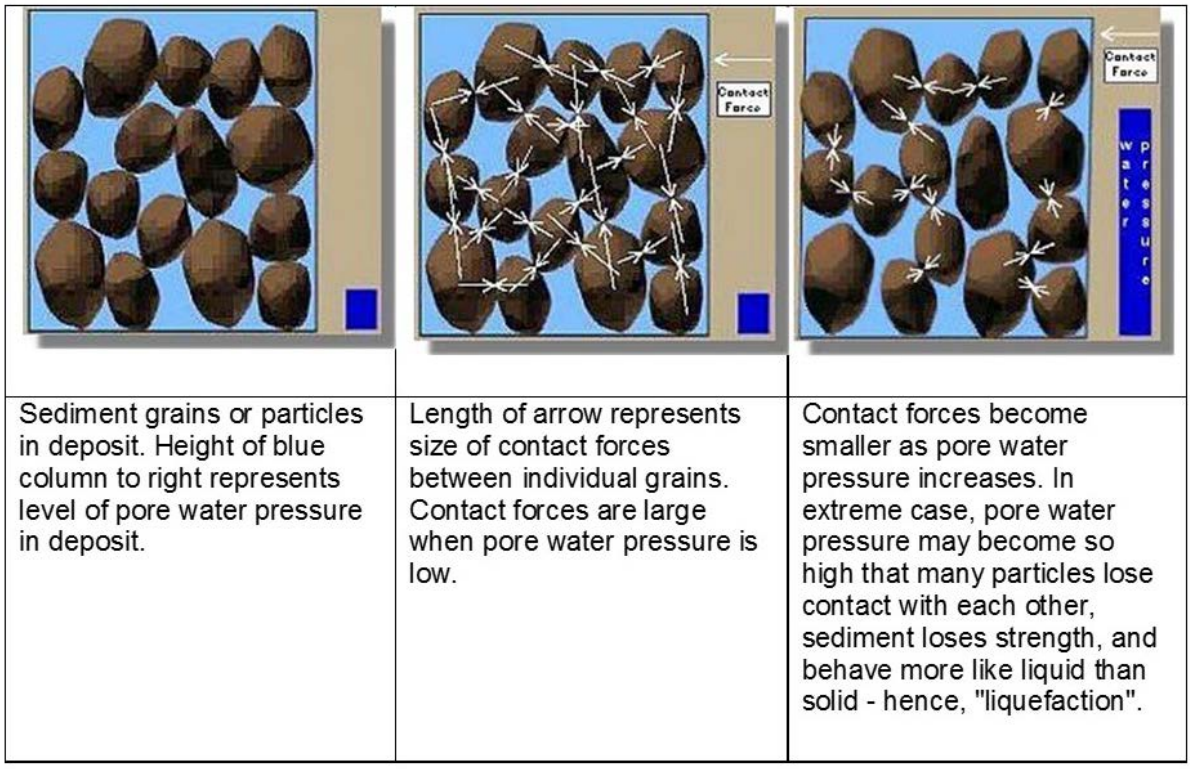

Sediment grains or particles in deposit. Height of blue column to right represents level of pore water pressure in deposit.	Length of arrow represents size of contact forces between individual grains. Contact forces are large when pore water pressure is low.	Contact forces become smaller as pore water pressure increases. In extreme case, pore water pressure may become so high that many particles lose contact with each other, sediment loses strength, and behave more like liquid than solid - hence, "liquefaction".

Figure 1-2 Schematic representation of changes in grain-to-grain contacts and pore water pressure as a volume of water-saturated granular sediment experiences ground shaking. The blue column represents the pore water pressure (from Johansson, 2000).

The state of stress in a soil or sediment is best represented by the effective stress condition:

$$\sigma' = \sigma - u$$

where σ is the total (vertical) overburden stress, u = pore water pressure, and σ' is the effective (vertical) stress. This is classically referred to as the principle of effective stress (Terzaghi 1943). See Appendix A for an explanation of the evaluation of overburden stress.

Soil behavior is complex during soil liquefaction, as illustrated in Figure 1.3. *Cyclic liquefaction* results from the accumulation of excess pore water pressure as repeated load cycles are applied by earthquake ground motions. Cyclic liquefaction of sands is the most common type of behavior. In the phenomenon of *cyclic mobility*, deformations accumulate in sands under the repeated cycles of earthquake loading, however the soil strength is not significantly reduced. *Cyclic softening* can occur in soft sensitive clays and silts. *Flow liquefaction* occurs during first-time (monotonic static) loading of unstable soils, including sands, silts, and clays. In cases of both cyclic and flow liquefaction, a significant loss of soil strength occurs.

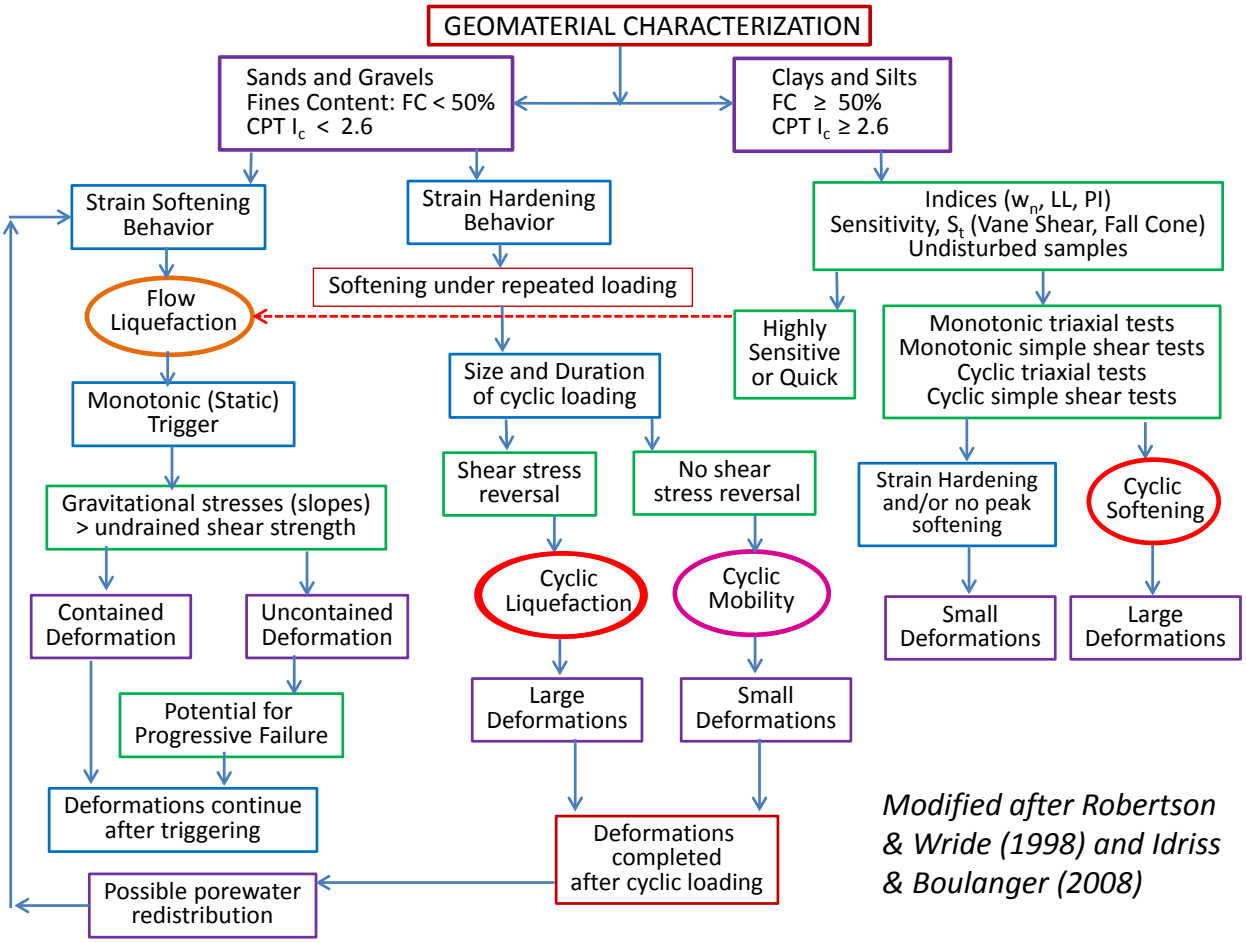

Figure 1-3 Flow chart showing the different types of soil liquefaction: flow liquefaction, cyclic liquefaction, cyclic mobility, and cyclic softening.

In the well known concept of "quicksand", a *flow liquefaction* condition can occur where the total vertical overburden stress equals the ambient hydrostatic pore water pressure (probably high due to artesian conditions), such that the effective stress equals zero:

$$\sigma = u \quad and \quad \sigma' = 0$$

Contractive soils undergo flow liquefaction when gravitational shear stresses (loads on the soil) are greater than the residual undrained shear strength (strength of liquefied soil). Flow liquefaction results in large deformations. Examples of flow liquefaction failures include the Fort Peck Dam (Casagrande, 1965) and Aberfan flowslide (Bishop, 1973) among others.

At most documented liquefaction sites, the more common mechanism is cyclic liquefaction where earthquakes cause the generation of pore water pressures that accumulate during repeated cycles of back-and-forth shearing. In loose contractive sand, the development of positive pore water pressure reduces the effective stress state and when the effective strength envelope is reached, the onset of *cyclic liquefaction* occurs (Figure 1.4; Robertson and Wride 1998; Robertson 2010).

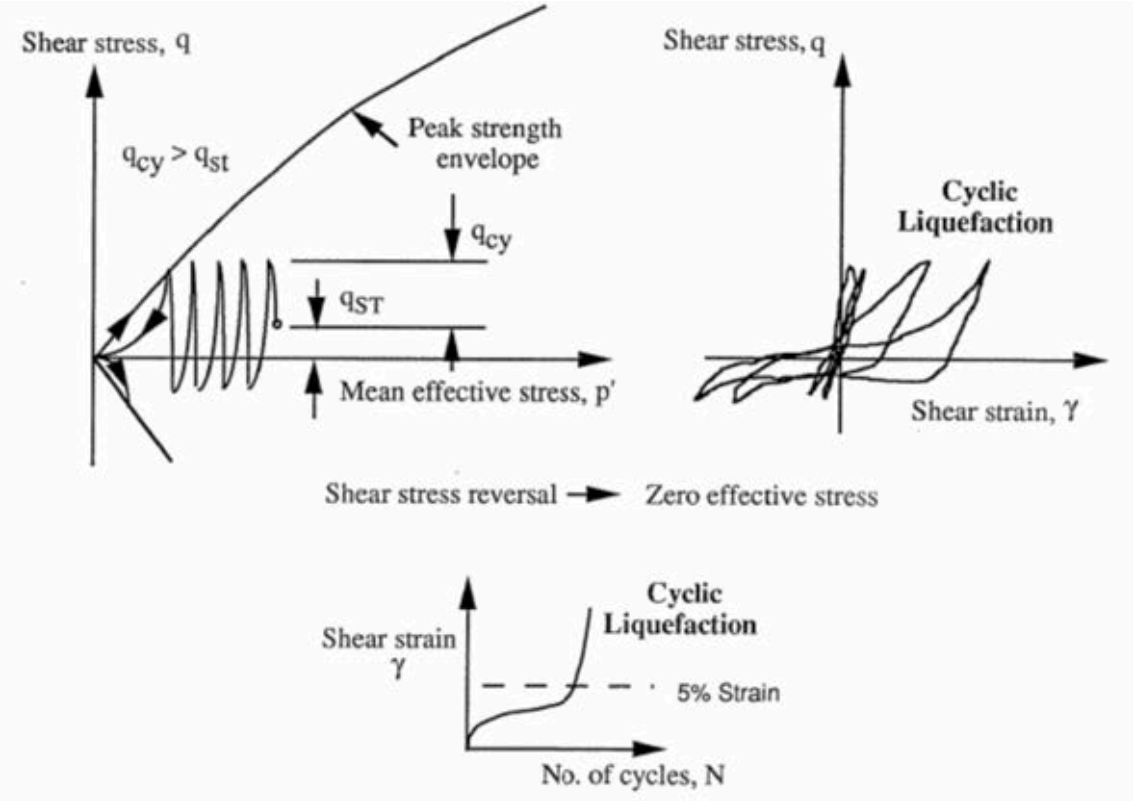

Figure 1-4 Schematic of undrained cyclic behavior of sand illustrating cyclic liquefaction, where q_{cy} represents the cyclic shear stress and q_{st} is the initial geostatic static shear stress (from Robertson and Wride 1998).

During large earthquakes, the excess pore water pressures can force the liquefied sand upward towards the ground surface from several meters below the ground. During this process, an upward flow of water is initiated in the layer that liquefied, which can further cause liquefaction in overlying non-liquefied sandy deposits, producing a quicksand effect (Kramer et al., 2011). If the slurry of water and sediment intrudes the overlying layers, it will form sand dikes and (Figure 1.5) small sand diapirs. Sand dikes are tabular in morphology and have some lateral continuity; whereas, sand diapirs are intrusive structures with little lateral continuity. Sometimes the upward flowing slurry of water and sediment intrudes laterally below the basal contact of a relatively

impermeable layer, forming sills (Tuttle, 2001). If the slurry of water and sediment erupts on the ground surface, sand blows or sand boils will form. These features are also described as sand volcanoes because they resemble small volcanic cones, some with small craters at the surface, aligned along ground fissures (Figure 1.5).

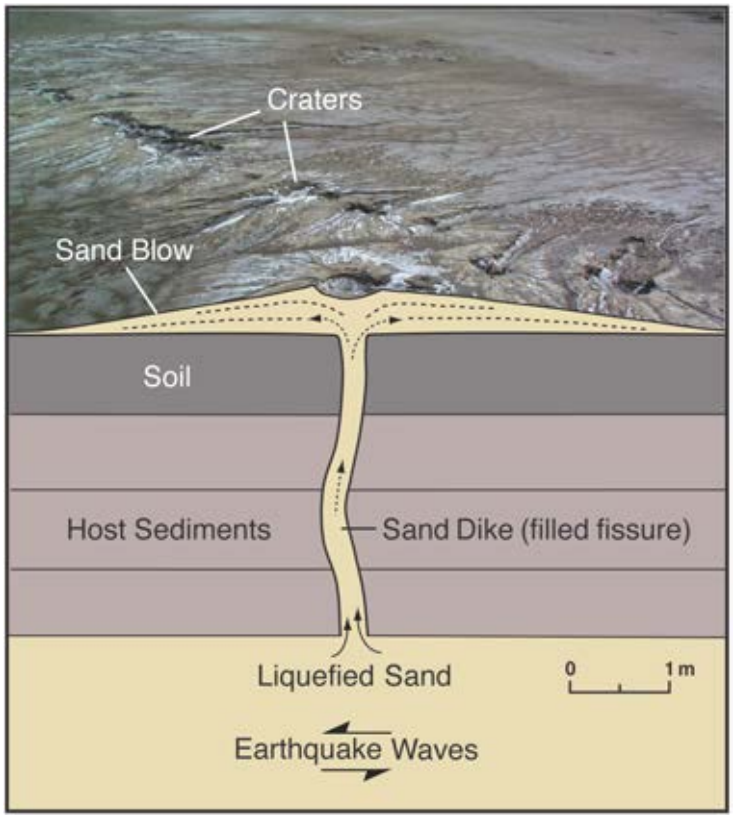

Figure 1-5 Sand blows or sand volcanoes resulting from liquefaction of water-saturated loose, granular sediment and subsequent venting of water and entrained sediment onto the ground surface (from NUREG-2115). Upper: photograph of moderate-sized sand blow (12 m long, 7 m wide, and 14 cm thick) that formed above ground fissure about 40 km from epicenter of 2002 M 7.7 Bhuj, India, earthquake (Tuttle et al., 2002a). Lower: schematic diagram illustrating structural and stratigraphic relations of sand blow, sand dike, and liquefied sediment at depth (after Sims and Garvin, 1995).

For additional discussion of the process of liquefaction, see Seed (1979), Seed and Idriss (1981), Ishihara (1985), Castro (1987 and 1995), Dobry (1989), Robertson and Wride (1998), Youd et al. (2001), and Robertson (2010).

1.2.2 Conditions that Influence Liquefaction and the Formation of Liquefaction Features

Liquefaction features commonly form in fluvial, lacustrine, beach, and estuarine deposits of Holocene age (0.01 Ma to present) where sand is interbedded with silt and clay and shallow groundwater conditions prevail (e.g., Sims, 1973; Youd, 1984; Tuttle et al., 1990, 2002; Obermeier, 1996; Reid et al., 2012). Sedimentological and hydrological conditions in these environments favor liquefaction during earthquakes and result in deformational structures that can be recognized by the trained professional. Liquefaction features also have formed in similar

deposits of Late Pleistocene age (0.126 to 0.01 Ma) that are characterized by loose to moderate soil density and have not been cemented (e.g., Tuttle et al., 2006; Tuttle and Atkinson, 2010; Tuttle and Dyer-Williams, 2010). Although much less common, liquefaction features have been reported in sediment as old as 200,000-240,000 yr B.P. (Obermeier et al., 1990).

The physical properties of sediment that influence liquefaction susceptibility, or their tendency to liquefy during earthquakes, include the size, shape, and packing arrangement of the sediment grains. Well-rounded, well-sorted, loose to moderately loose, fine sand with a high void ratio would be especially susceptibility to liquefaction, so long as it is saturated. Generally, coarser grained sediment, such as coarse sand or pebbles, would be less susceptible to liquefaction than fine sand due to its greater permeability, making the buildup of pore water pressure during ground shaking more difficult. Poorly sorted sand, with lower void ratio as well as lower permeability, also would be less susceptible to liquefaction. Liquefaction susceptibility decreases with increasing fines content, especially if the fines include clay (Seed et al., 1983). For fine-grained soils (clays and silts), shaking ground can possibly result in significant deformations, particularly with soft or sensitive soils, and this is now termed cyclic softening (Idriss & Boulanger, 2008).

Aging can have a significant effect on the strength of soil, and thus may influence the liquefaction susceptibility of sediment (e.g., Leon et al., 2006; Andrus et al., 2007). Over time, sediment consolidates, especially if buried by subsequent deposits, becoming more densely packed and less susceptible to liquefaction. In addition, cementation of sand grains by clay, calcium carbonate, and iron and manganese oxides will strengthen the sediment and reduce its liquefaction susceptibility (Sowers, 1979). Cementation can increase the soil liquefaction resistance particularly where the water table fluctuates. Wetting and drying cycles in the depth range of a fluctuating water table can promote the precipitation and concentration of clays, carbonates, and oxides. In situations with considerable groundwater flow, however, carbonates and other potential cementing agents may be flushed out of the sandy deposits (Green et al., 2005). Due largely to aging effects, Pleistocene (2.58 to 0.01 Ma; Gibbard et al., 2010) deposits tend to be less susceptible to liquefaction than Holocene (0.01 Ma to present) deposits, and pre-Pleistocene (before 2.58 Ma) deposits tend to have a very low likelihood of being susceptible to liquefaction (Youd and Hoose, 1977; Youd and Perkins, 1978).

Layering in sediment plays an important role in liquefaction and the formation of liquefaction features. Upper capping layers of clay or silt form impermeable barriers that prevent or retard the flow of water upward through the sediment from underlying sandy layers (e.g., Friedman and Sanders, 1978). By preventing or retarding the flow of water, layers of clay or silt promote the buildup of pore water pressure in sandy layers during ground shaking that can lead to liquefaction (Idriss & Boulanger, 2008). In addition, distinctive types of liquefaction features form in interbedded coarse-grained and fine-grained sediment that can be fairly easily recognized. These features include foundered clasts, load casts, convolute laminations, ball and pillow structures, and pseudonodules that formed in the layer that liquefied as well as sand diapirs, dikes, and sills that intruded overlying layers, and sand blows or sand volcanoes that resulted from venting of liquefied sediment onto the ground surface. A more detailed discussion of these earthquake-induced liquefaction features is provided in Section 1.4.

As mentioned above, sediment must be saturated in order to liquefy. Therefore, the elevation of the water table relative to the sediment that is susceptible to liquefaction is an important factor. The water table is often high in fluvial, lacustrine, and estuarine environments contributing to the liquefaction susceptibility of sediment in these settings. The water table fluctuates in response to precipitation and therefore varies from season to season and from year to year. In coastal settings, the water table fluctuates in response to ocean tides as well as to precipitation. Long-term changes in relative sea-level cause large fluctuations in the water table in coastal and nearby inland areas and can have significant impact on liquefaction potential of sediment.

1.2.3 Ground Motions that Cause Liquefaction

The key index parameters of ground motion include ground acceleration, ground velocity, ground displacement, and duration of ground shaking (Seed and Idriss, 1982). These combined with the frequency characteristics of ground motion account for the intensity of ground shaking. Characteristics of earthquake ground motions at a particular site, that may or may not suffer liquefaction, will depend on several seismological and geological factors. These factors include magnitude of the earthquake, the source mechanism of the earthquake, distance from the site to the earthquake source, directivity of seismic energy related to the direction and speed of fault rupture, characteristics of the rocks along the wave path from source to site, and local soil conditions at the site.

Earthquake-induced liquefaction is caused by the buildup of excess pore water pressure due to cyclic shear stresses imparted by ground motions. In particular, the amplitude of the cyclic shear stresses and the number of cycles of shearing contribute to liquefaction (Seed and Idriss, 1982). Maximum shear stress is related to maximum ground acceleration and the number of cycles depends on the duration of the earthquake and also implicitly its frequency content. Earthquakes in the eastern US with higher frequency content cause higher peak ground accelerations (PGAs) than western earthquakes at the same magnitudes and distances (Atkinson and Boore, 2000). Both maximum ground acceleration and duration of ground shaking generally increase with earthquake magnitude and may also increase as a result of seismotectonic setting, site conditions, and bedrock topography (i.e., basin effects). The default or reference magnitude value for liquefaction analyses in the U.S. is **M** 7.5, which is considered to impart 15 cycles of uniform stress (Youd et al., 2001; Idriss and Boulanger 2004; Boulanger and Idriss, 2014).

In liquefaction analyses, the level of ground shaking from seismic loading is expressed in terms of the cyclic stress ratio (CSR), which is the ratio of the cyclic shear stress (τ) to the effective overburden stress (σ'_{vo}) at any given elevation, or CSR= τ/σ'_{vo}. Using the conventional simplified procedures, the cyclic stress ratio (CSR) is expressed as (Seed and Idriss, 1971):

$$CSR = \frac{\tau_{ave}}{\sigma'_{vo}} = 0.65 \cdot \left(\frac{a_{max}}{g}\right) \cdot \left(\frac{\sigma_{vo}}{\sigma'_{vo}}\right) \cdot r_d$$

where τ_{ave} is the average equivalent uniform shear stress generated by the earthquake (assumed to be 65 percent of the maximum induced stress), a_{max} is the peak (horizontal) ground acceleration (or PGA), g = the gravitational acceleration constant (g = 9.8 m/s^2 = 32 ft/s^2), σ_{vo} and σ'_{vo} are the total and effective vertical stresses, respectively, and r_d is a stress reduction coefficient that accounts for the flexibility of the model soil column ($r_d \leq 1.0$). See Appendix A for additional details concerning the calculations of σ_{vo} and σ'_{vo}.

The PGA is taken as the maximum of either horizontal component, or alternately as the geometric mean of both peak horizontal components, however, is not calculated as the resultant value from the two measured axes from accelerogram records (Youd and Idriss, 1997).

The magnitude of PGA = a_{max}/g can be estimated using three basic approaches: (a) empirical PGA distance plots, (b) seismic hazard maps, and/or (c) site-specific amplification analyses and acceleration records. Point source methods have been used to develop PGA distance relations (e.g., Boore 1983, 2005). Seismic hazard maps showing the expected PGAs are published by the U.S. Geological Survey (USGS) and various state geological agencies, the Federal Emergency Management Agency, the International Building Code (IBC), and by international sources for regions outside of the United States. Figure 1.6 is an example of a USGS seismic hazard map showing estimated PGA across the US.

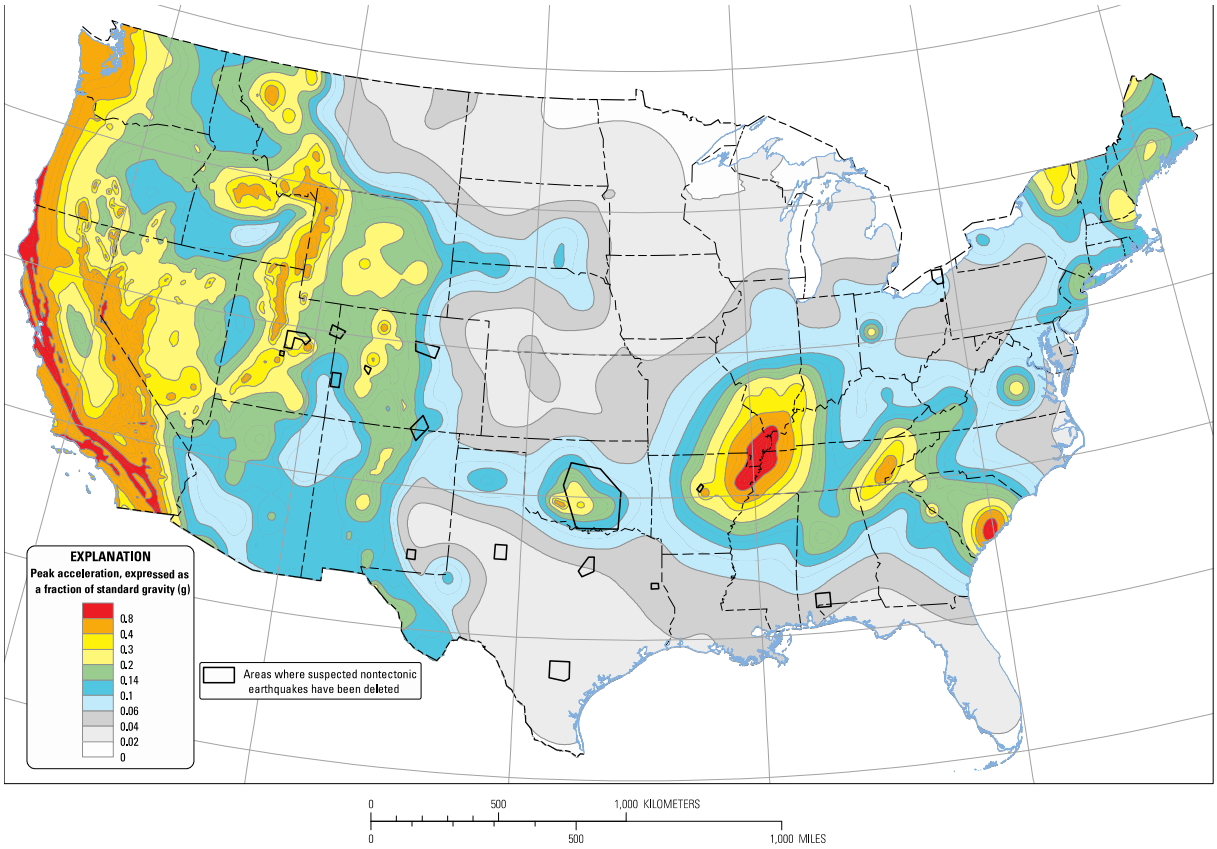

Figure 1-6 Peak ground acceleration (PGA) for 2% probability of exceedance in 50 years on a uniform firm-rock site condition with a shear wave velocity in upper 30 m of 760 m/s (from Petersen et al., 2012).

The value of CSR can be more properly evaluated using site-specific values of soil stiffness, in particular, the small-strain shear modulus: $G_{max} = \rho_t \cdot V_s^2$, where ρ_t = total soil mass density and V_s = shear wave velocity. Thus, measured V_s for each of the various soil layers at depth provide the corresponding G_{max} stiffness values that are input directly into computer codes such as SHAKE (Schnabel et al., 1972), EduSHAKE (www.proshake.com), ProSHAKE (www.proshake.com), SHAKE2000 (www.geomotions.com), and DEEPSOIL (Hashash and Park, 2001; Hashash et al., 2010: http://deepsoil.cee.illinois.edu). A full acceleration-time record from a reference earthquake event can be used as input in the generation of the expected dynamic stress levels. Alternatively, the value a_{max} is taken from the appropriate design events for a given project (i.e., the 2%, 5%, or 10% probability earthquake for a certain return period; the maximum credible event for a known fault located a certain distance from the site; or a code-based response spectrum).

The stress reduction factor (r_d) can be obtained via alternate approaches, including: (a) simplified approach that uses a mean value from probabilistic studies; or (b) a site-specific analyses for the particular location and soil shear wave velocity profile (e.g., SHAKE, DEEPSOIL). The magnitude of the factor r_d decreases with depth ($r_d \leq 1$) with the mean relation shown in Figure 1.7 plus upper and lower bounds following the original study by Seed and Idriss (1971).

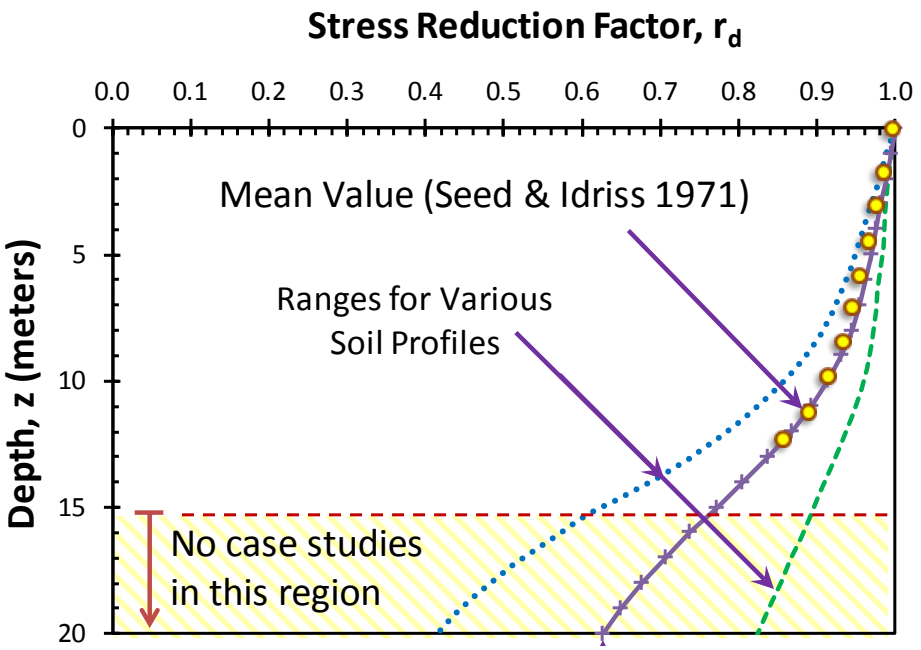

Figure 1-7 Simplified relation for stress reduction factor (rd) as a function of depth (from Youd et al., 2001).

Per the recommendations of the National Center for Earthquake Engineering and Research (NCEER) Workshop on soil liquefaction, a continuous function for r_d can be expressed in terms of depth z (in meters) for the simplified procedure (Youd et al., 2001) which is given by:

$$r_d = \frac{1 - 0.411z^{0.5} + 0.0405z + 0.00175z^{1.5}}{1 - 0.418z^{0.5} + 0.0573z - 0.00621 + 0.00121z^2}$$

While the above expression provides a quick deterministic value for r_d in the CSR evaluation, in truth, site-specific values show considerable variance and wide possible ranges, thereby adding significant uncertainty in the outcome. Studies by Idriss and Boulanger (2010) showed that r_d depends not only on depth (z) but also on earthquake magnitude (M), as described in Appendix B. Moreover, extensive analyses conducted by Cetin et al. (2004) offer a more detailed look at the r_d parameter that provides more complex expressions which depends upon depth (z), moment magnitude (M), PGA, and shear wave velocity (V_s), as summarized in Appendix B.

Much of the research and documentation on earthquakes have focuses on a reference earthquake of magnitude M_w = 7.5 lasting approximately 15 seconds duration with level ground conditions. Thus, a more generalized cyclic stress ratio can be detailed as:

$$CSR_{7.5} = \frac{\tau_{ave}}{\sigma'_{vo}} = 0.65 \cdot \left(\frac{a_{max}}{g}\right) \cdot \left(\frac{\sigma_{vo}}{\sigma'_{vo}}\right) \cdot r_{d} \cdot \frac{1}{MSF \cdot K_\sigma \cdot K_\alpha}$$

where MSF = magnitude scaling factor, K_σ = overburden factor, and K_α= ground slope factor (Idriss and Boulanger 2004; Robertson 2009). In reality, a range of earthquake magnitudes may occur in nature and thus the MSF allows for a direct adjustment of the methodology to a common event (Boulanger and Idriss 2012). The K_σ and K_α factors are applicable for more specialized cases, such as large earthen dams and reservoirs, where loose natural sands might lie beneath slopes and may be situated under several hundred meters of overburden. For the simplified

procedures of the NCEER approach where case histories are restricted to depths of z < 15 m and effective overburden stresses are generally σ'_{vo} < 2 atm, the value of K_σ ≈ 1 and for flat horizontal ground conditions, K_α ≈ 1.

The recommended magnitude scaling factor (MSF) to adjust the CSR for the NCEER approach is given by Youd et al. (2003):

$$MSF = (7.5/M_w)^{-3.3}$$

1.3 Ground Failure Resulting from Liquefaction

The understanding of ground failure comes largely from case studies following modern earthquakes (e.g., Bray et al., 2010; Cetin et al., 2011; Cubrinovski et al., 2011; Tuttle et al., 2002a). Earthquake-induced liquefaction can cause several types of ground failure, including loss of bearing strength, ground settlement, ground oscillation, lateral spreads, and flow failures (National Research Council, 1985; Robertson et al., 1992). Soil or sediment properties that influence the location and type of ground failure include permeability, thickness, strength, and spatial relations (Tuttle and Barstow, 1996). Nature and severity of ground failure is related to the reduction in shear strength and the magnitude of the static shear loads supported by the layer that liquefies (Ishihara and Yoshimine, 1992). See Appendix C for additional information on the evaluation of ground deformation, including settlements and lateral spreads.

Loss of Bearing Strength: This type of failure, also referred to as bearing capacity failure, usually results in settling or tipping of a building or some other engineered structure into a near surface layer that has liquefied (Figure 1.8). Bearing strength failures also can affect soils or sediment overlying the layer that liquefied. Loss of strength of the liquefied layer or formation of a water-interlayer below a relatively impermeable surface layer, such as a weathered clay or silt, can lead to sinking of pieces of the overlying layer into the weak layer below.

Ground settlement: Settlements due to liquefaction can occur as the layer that liquefies compacts and excess pore water pressures dissipate. This type of failure can result in drowning of low-lying areas, including forests, and shifting of drainage patterns.

Ground oscillation: This type of ground failure occurs on flat ground. It is thought that the layer that liquefies sloshes back and forth as shaking continues. The overlying soil is jostled and broken, ground cracks open and close, and water or mud may erupt or vent through them. A recent example of this phenomenon was videotaped in Tokyo's Central Park during the 2011 Tohoku earthquake (http://www.youtube.com/watch?v=I3hJK1BoRak).

Figure 1-8 Bearing strength failure during 2010 M 7.0 earthquake in Haiti (from Kattenhorn, 2011).

Lateral spreads: Lateral spreads occur on gently sloping ground (0.3-3°) and involves lateral movement of large blocks of soil as a consequence of liquefaction in a subsurface layer (e.g., Youd et al., 2002). Figure 1.9 illustrates a lateral spread during the Bhuj earthquake in India (Tuttle et al., 2002a). Horizontal movements of 3-5 m are common, but may be as great as 30-50 m, if slopes are unfavorable and ground shaking lasts for a long time. Lateral spreads often break up internally, forming numerous fissures, scarps, and hummocky ground. Lateral spreads typically occur along riverbanks with fissures forming perpendicular to the direction of movement.

Flow Failures: This type of failure occurs on slopes greater than 3° and involves lateral movement of a layer of sediment or blocks of sediment riding on the liquefied sediment or water interlayer (Robertson, 2010). Figure 1-10 shows a flow failure induced by the Saguenay earthquake in Canada 180 km from the epicenter (Tuttle et al., 1989 and 1990). Flow failures are the most catastrophic type of ground failure caused by liquefaction. Horizontal movements can range from several meters to several tens of kilometers. Although they can occur on land or underwater, the largest flow failures have occurred underwater in coastal areas.

Figure 1-9 Lateral spread adjacent to river during 2001 M 7.7 Bhuj earthquake in India. Sand blows also formed on surface of block that moved towards river (from Tuttle et al., 2002a).

Familiarity with the various types of ground failure resulting from liquefaction is helpful in interpreting the geologic record of past liquefaction events. Certain liquefaction features, described in Section 1.4 below, are likely to form during different types of ground failure. Sand diapirs and foundered clasts are likely to be associated with bearing strength failures. Sand blows and sand dikes are likely to form during ground oscillations and lateral spreads (Figure 1-11). Chaotic deposits with destroyed bedding and large soil clasts may result from flow failures, and drowned forests may be indicative of ground settlement. Earthquake-triggered landslides on slopes greater than 3° can exhibit many of the same characteristics as landslides triggered by non-seismic causes such as saturated soil conditions resulting from intense rainfall or rapid snowmelt and erosion of the slope toe by fluvial or wave action. In order to attribute mass movements to a paleoearthquake, it is usually required to find many landslides that formed at the same time over a large area (e.g., Adams, 1982; Goldfinger, 2011; Aylesworth and Lawrence, 2003; Brooks, 2013).

Figure 1-10 **Flow failure, about 88 m wide and extending 150 m across the valley below, triggered by M 5.9 Saguenay earthquake in Canada (from Tuttle et al., 1989 and 1990). Photograph taken looking down slope. Note blocks of soil and debris pile at toe of slide.**

Figure 1-11 Small sand blow noted following 2011 M 7.2 van Tabanli earthquake in Turkey (from Cetin et al., 2011). For scale, pencil adjacent to vent.

1.4 Earthquake-Induced Liquefaction Features

The types of sedimentary features that result from earthquake-induced liquefaction can be divided into two categories: those related to deformation extending beyond the layer that liquefies and those related to deformation within the sedimentary layer that liquefies (Figures 1.12-1.18 and 1.20). Features that extend beyond the liquefied layer, such as intrusive dikes, sills, and diapirs and extrusive sand volcanoes or blows, are most commonly used in paleoliquefaction studies. Features that form within the liquefied layer include foundered clasts, load casts, convolute lamination, ball-and-pillow structures, and pseudonodules. Because these in-layer features can form as the result of other sedimentary processes, they are rarely used alone in paleoliquefaction studies. In the best of circumstances, both types of features and their interrelationships can be observed in a single exposure.

1.4.1 Dikes, Sills, Diapirs, and Blows

As described above, strong ground shaking can induce liquefaction and fluidization of water-saturated, loose, sandy sediment and lead to various types of ground failure. This can result in intrusion of pressurized water and entrained sediment into adjacent and overlying deposits, and extrusion of water and sediment onto the ground surface (Figure 1.12). Because sandy sediment is more easily liquefied and fluidized than finer-grained sediment, the intrusive and extrusive features resulting from liquefaction are most often sandy in nature. However, silt also is known to liquefy and form intrusive and extrusive features. For example, liquefaction was observed in silty soils in Adapazari during the 1999 Kocaeli, Turkey, earthquake (Bray and Sancio, 2006).

Dikes are sheet-like or tabular-shaped intrusive bodies that crosscut bedding in the host deposits. Dikes usually have well-defined margins and can be differentiated from the host deposit by

differences in grain size and weathering characteristics (Figure 1.13). Dikes typically originate in a layer of sandy sediment (i.e., the source layer) and are composed of sediment derived from the source layer (Figure 1.14). The dikes may contain clasts of the intruded host deposits and exhibit flow structure or lineations. They often become narrower and finer-grained, and sometimes branch, up section. Dikes may pinch out or terminate within the stratigraphic section or extend through the entire section to the ground surface. Tree root casts, animal burrows, dessication cracks, and other voids or weak spots near the ground surface can be utilized as pathways to the surface (e.g., Audemard and de Santis, 1991; Tuttle, 1999; Martin, 2011). Diapirs are similar to dikes but are relatively small intrusions of sediment extending from the layer that liquefied into the base of the overlying layer (Figures 1.12 and 1.15). In contrast to dikes and diapirs, sills are intruded parallel to bedding of host deposits and usually take the form of lenses intruded below low-permeability layers. The source layer of dikes, diapirs, and sills may contain foundered clasts of the overlying layer and exhibit deformation structures, such as dish structures, ball-and-pillow structures, and convolute bedding, as well as flow structure or lineations (Figure 1.14). Alternatively, the source layer may be massive if bedding has been completely destroyed.

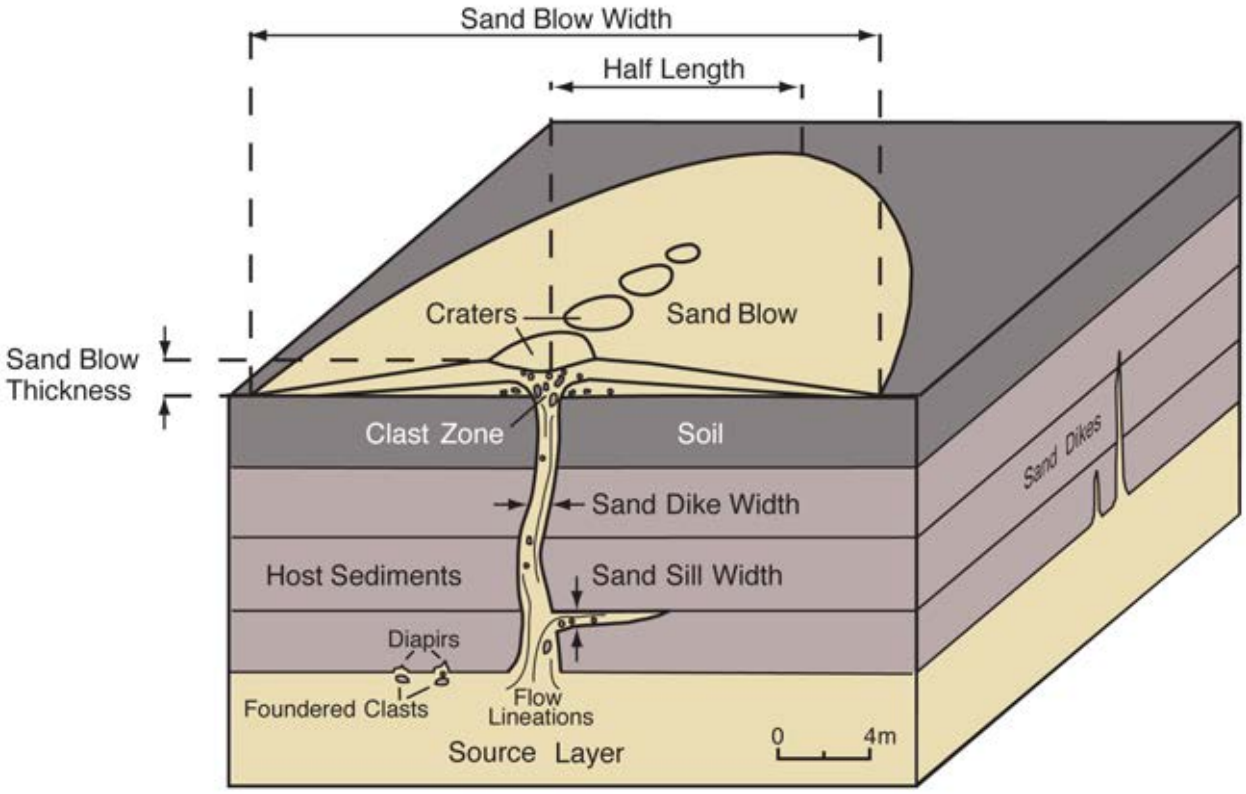

Figure 1-12 Block diagram showing relationship between the liquefied layer and overlying liquefaction features including intrusive sand dikes and sills and an extrusive sand blow (from NUREG-2115).

Blows are extrusive deposits resulting from venting of water and entrained sediment onto the ground surface (Figures 1.5, 1.12, and 1.16). The opening at the ground surface through which the slurry of water and sediment flows is referred to as the vent. As vented water flows across the ground surface, the entrained sediment is deposited to form constructional cones or to fill subsided areas. In plan view, the shape of a blow is related to the shape of the void through which the slurry of water and sand vented. Linear to elliptical blows result from venting through

fissures (Tuttle and Barstow, 1996). Circular blows result from venting through tubular-shaped conduits such as root casts. In cross section, blows overlie soil horizons and other depositional units and are connected to dikes or other sediment-filled conduits below the vent.

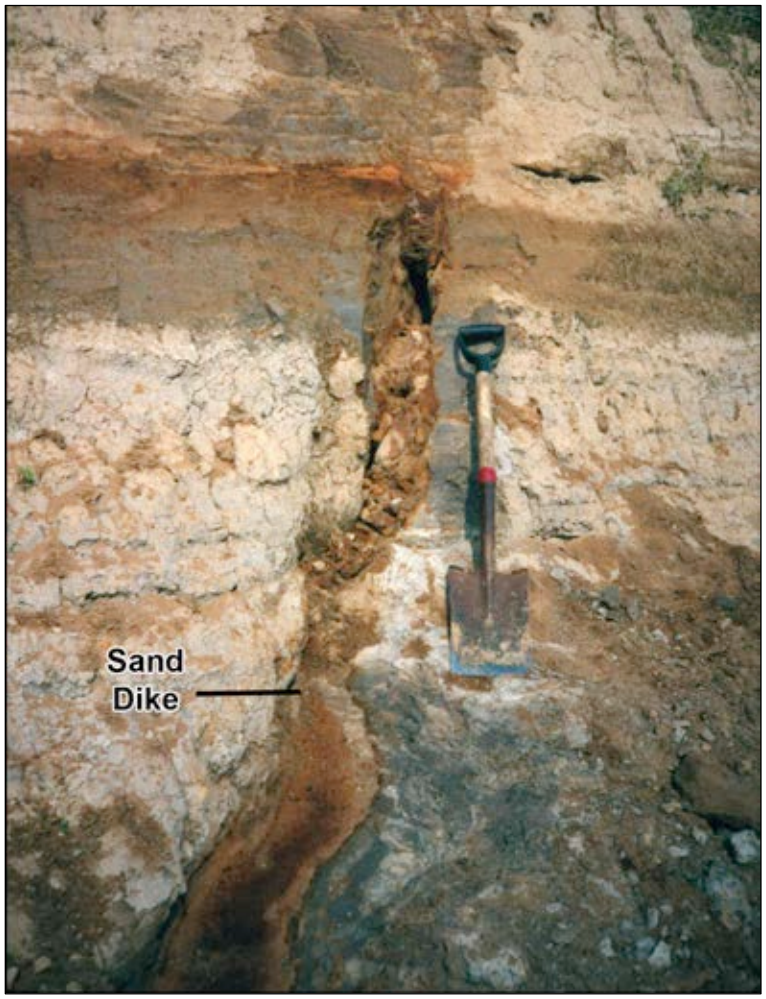

Figure 1-13 Photograph of sand dike exposed in a cutbank of the Meramec River near St. Louis, Missouri (NUREG/CR-5730). The dike crosscuts and is coarser grained than the silty deposit it intrudes. For scale, shovel is 1 m long. Photograph by M. Tuttle.

Typically, sediment composing the blows is thickest and coarsest-grained immediately above the vent and, generally, thins and fines away from the vent. The sand blows often contain clasts of the underlying deposits through which the slurry of water and sand flowed. Clasts within the blows tend to be larger and more abundant in close proximity to the vent. In cases where a large volume of subsurface sediment has vented to the surface or where there has been lateral spreading, the soil horizon buried beneath the blow may dip toward the vent or be displaced downward across the vent due to ground subsidence (Figure 1.16; Tuttle and Barstow, 1996). In cases, where craters form at the ground surface, vented sediment is deposited within the craters and around the crater rims. Over time, the craters are filled with reworked sand blow deposits, slack-water deposits, and organic material.

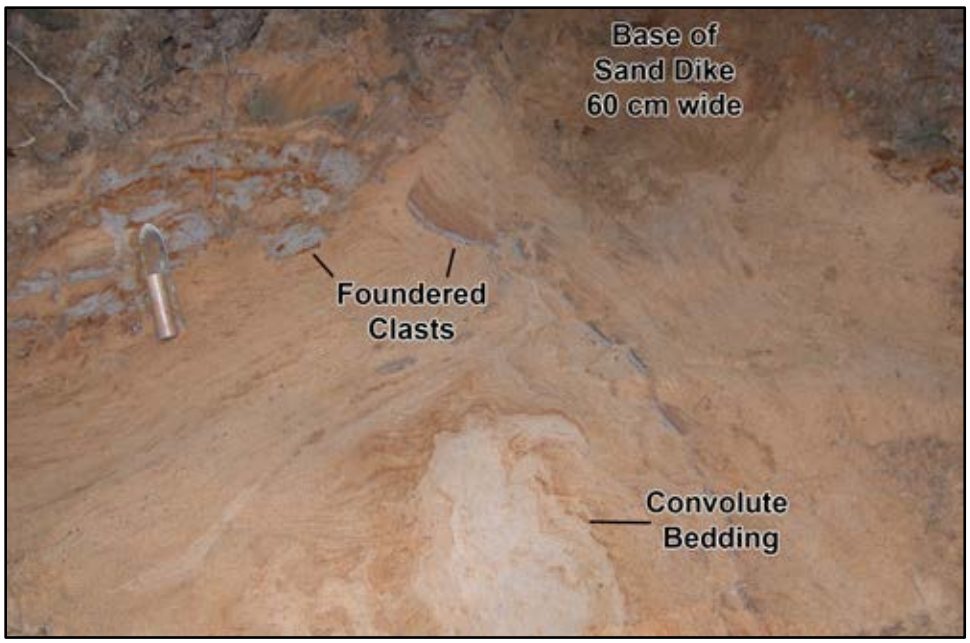

Figure 1-14 **Photograph of convolute bedding, foundered clasts in liquefied layer and base of related sand dike intruding overlying mottled silt. Photograph by M. Tuttle.**

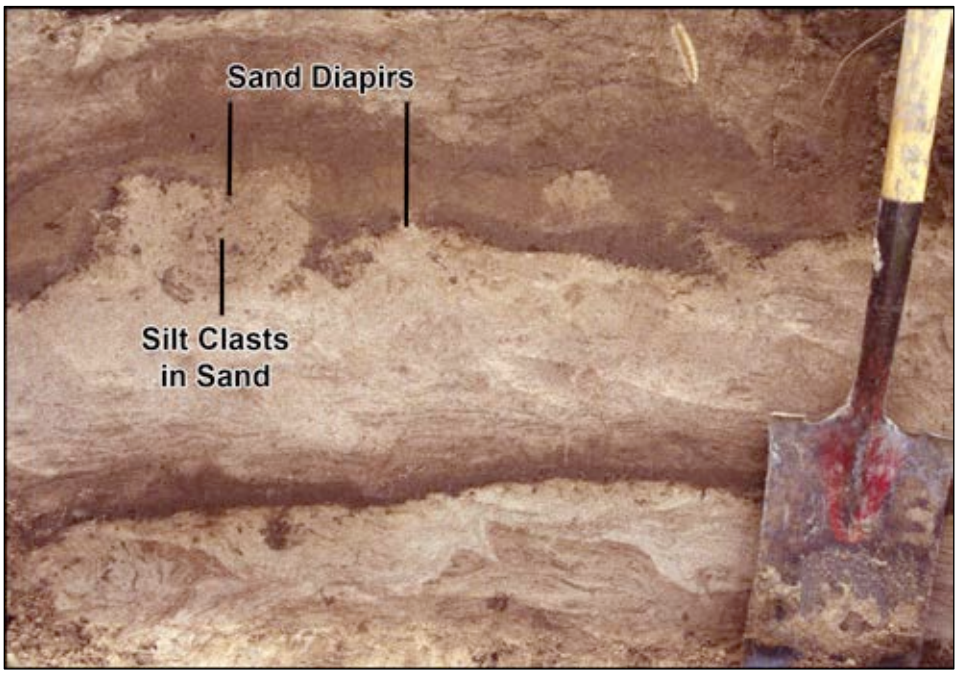

Figure 1-15 **Photograph of sand diapirs intruding base of overlying silt layer exposed in a cutbank of Big River southwest of St. Louis, Missouri (NUREG/CR-5730). Notice foundered clasts of silt in the sand layer that liquefied. Photograph by M. Tuttle.**

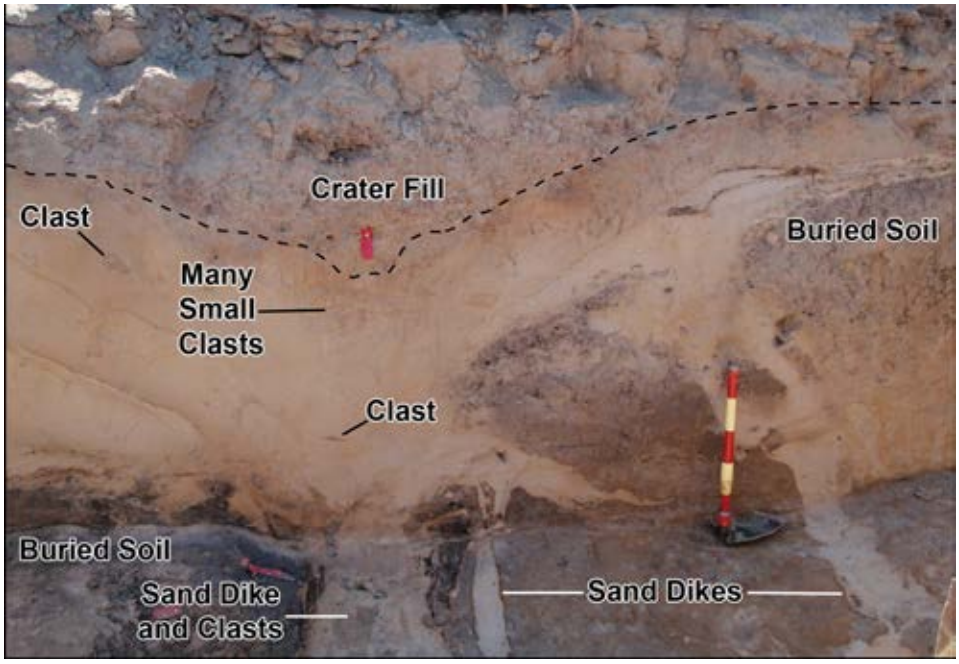

Figure 1-16 **Photograph of sand blow and related sand dikes exposed in a trench in the New Madrid seismic zone. Brown soil horizon is crosscut by two sand dikes, displaced downward ~1 m, and buried by the sand blow. Clasts of the soil horizon occur within dikes and overlying sand blow. Each colored intervals on shovel handle represents 10 cm. Photograph by M. Tuttle.**

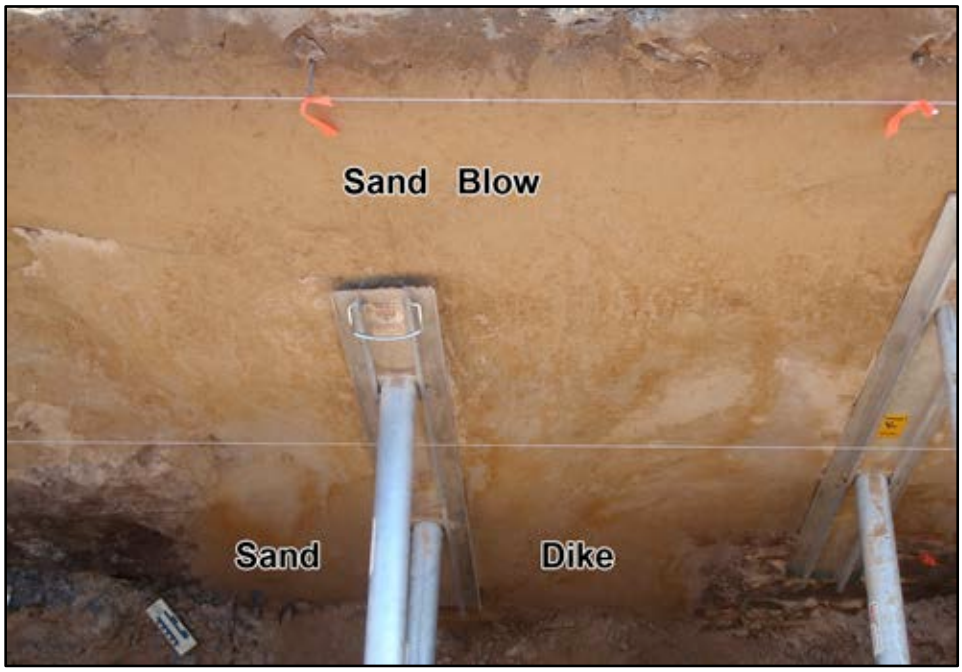

Figure 1-17 **Very weathered sand blow and related feeder dike (1.3 m wide) exposed in trench near Marianna, Arkansas, 80 km south of the New Madrid seismic zone (Tuttle et al., 2010a). Dating indicates that the liquefaction features formed about 9,900 yr B.P. Distance between level lines is 1 m. Photograph by M. Tuttle.**

Subsequent to their formation, blows and blow craters may or may not be buried by other deposits, such as overbank deposits in fluvial systems or lagoonal deposits in estuarine systems. Burial of blows and blow craters helps to preserve them in the geologic record. Those features that form on higher or relatively stable positions of the landscape will be subjected to soil-forming processes. If the features are small, they are likely to be destroyed within decades or centuries, leaving truncated and weathered sand dikes below. If the blows and blow craters are large, they can persist for thousands of years and develop soil characteristics indicative of their age (Figure 1.17; NUREG/GR-0018 and Tuttle et al., 2006). Other blows subjected to reworking or erosion may be partially or wholly destroyed, leaving only vent structures and related dikes as evidence of earthquake-induced liquefaction (Reid et al., 2012; Tuttle et al., 2012).

1.4.2 Soft Sediment Deformation Features within the Liquefied Layer

Features that form within sediment layers that liquefy include load casts, convolute bedding and laminations, ball-and-pillow structures, and pseudonodules. These deformation structures have been attributed to earthquake-induced liquefaction on the basis of laboratory experiments (Kuenen, 1958) and field studies (e.g., Sims, 1973 and 1975; Obermeier, 1996; Tuttle, 1999). A large body of sedimentological literature also discusses non-seismic mechanisms of formation of these deformation structures (e.g., Lowe and LoPicollo, 1974; Lowe, 1975; Allen, 1982; and Owen, 1987). Chief among the mechanisms is a gravitational unstable density gradient often due to high rates of sedimentation.

Sims (1975), who pioneered the use of these types of features in paleoliquefaction studies, developed recognition criteria by studying earthquake-induced structures that formed in different environments during modern and historic earthquakes. He noted that these liquefaction features typically form in interbedded fine- and coarse-grained deposits close to the sediment-water interface as a result of bearing strength failure due to liquefaction of the coarse-grained layers. In a recent overview paper, Sims (2012) provides a detailed discussion of the characteristics of liquefaction features and the conditions under which these liquefaction features form. In the case of load casts, fine-grained layers sag into the liquefied coarse-grained layer but without completely detaching (Figure 1.18). If the sagging layers detach, convolute laminations and ball-and-pillow structures form as they sink into the liquefied coarse-grained layer.

Pseudonodules form when the coarse-grained layer separates into domains or irregular masses. See Sims (2012) for additional photographs of soft-sediment deformation structures. In his early research, Sims (1973) found that load casts form at lower intensities of about VI, whereas convolute laminations and pseudonodules form at higher intensities of VIII-IX. Therefore, the occurrence of the different types of strata-bound liquefaction features may help to constrain the locations and magnitudes of paleoearthquakes. However, further research is needed to determine whether these features can provide reliable magnitude estimates.

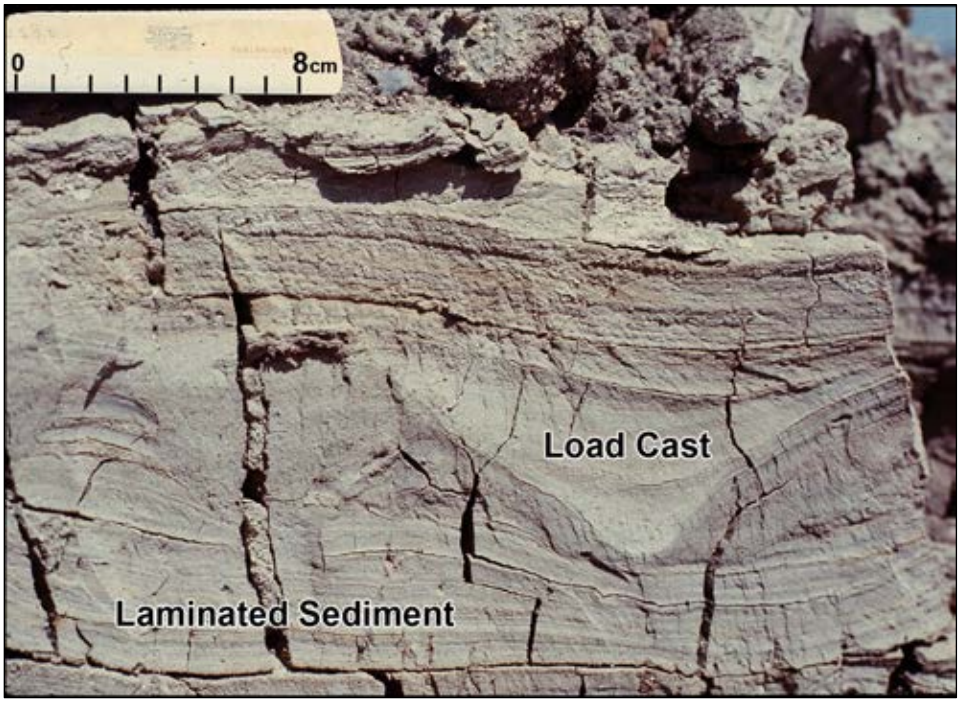

Figure 1-18 Load cast that formed in laminated sediment of Van Norman Lake during the 1952 Kern County, California, earthquake (from Sims, 1975).

1.4.3 Diagnostic Criteria and Characteristics of Liquefaction Features

Criteria used to identify and utilize paleoliquefaction features in paleoseismology studies have been developed over the past forty years. Focusing primarily on intrusive and extrusive features extending beyond the layer that liquefies, the following general criteria are recommended for identifying earthquake-induced liquefaction features: (1) sedimentary characteristics consistent with case histories of earthquake-induced liquefaction; (2) sedimentary characteristics indicative of a sudden, strong, upwardly directed hydraulic force of short duration; (3) occurrence of more than one type of liquefaction feature and of similar features at multiple nearby locations; (4) occurrence in geomorphic settings where hydraulic conditions described in (2) would not develop under non-seismic conditions; and (5) age data to support both contemporaneous and episodic formation of features over a large area (Obermeier, 1996; Tuttle, 2001). Criteria (1)-(3) are required and (4) and (5) preferred to attribute a sedimentary structure to earthquake-induced liquefaction. The more criteria that are satisfied, the greater the confidence is in the interpretation.

Dikes, blows, and blow craters have been documented following historical (e.g., Dutton, 1889; Fuller, 1912) and modern (e.g., Tuttle et al., 1990: Tuttle et al., 2002a; Sims and Garvin, 1995) earthquakes and are considered diagnostic of earthquake-induced liquefaction. Tuttle and Hartleb (2012) compiled the following list of structural and sedimentary characteristics of earthquake-induced liquefaction features to assist in their recognition in the geologic record:

Dikes:

- Dike sidewalls typically subparallel, usually widen downward; also may broaden upward into vent structure at the ground surface (event horizon),

- Typically a few meters to tens of meters long (in map view); therefore, often, but not always, exposed in both walls of a trench,
- Sand within dikes often fines upward,
- Often characterized by flow structure or lineations,
- Often contain clasts of host deposit(s),
- Near-vertical dikes may exhibit grading, with finer material along dike margins; inclined dikes may exhibit bedding,
- May be characterized by subsidiary dikes and/or sills,
- Source layer may lack original sedimentary structure where fluidized or may exhibit flow structure or lineations, as well as soft-sediment deformation structures such as ball-and-pillow structures and dish structures.

Blows and blow craters:

- Typically elliptical or linear, sometimes circular, in map view,
- Connected to feeder dikes below,
- Often characterized by “cut-and-fill” structure and flow structures, or flow lineations, above the feeder dike,
- Vented sediment typically fine to coarse sand and may include some silt and clay,
- Often becomes finer-grained up-section and laterally away from feeder dike/vent,
- Usually thins laterally away from feeder dike/vent,
- May comprise multiple fining-up depositional units related to a sequence of earthquakes; seismites may be separated by layers of fines, such as silty clay or clay that accumulated between earthquakes,
- May contain clasts of host deposit, especially near feeder dike; clast size generally decreases with distance from vent,
- Volume of vented deposit should be reasonable relative to size and number of sand dikes,
- Subsidence structures may be seen near vent, including localized down warping of surface soil and host strata and possible vertical displacement across feeder dikes,
- Blow craters often form in organic-rich soils or clay-rich host deposits,
- Blow craters contain vented sand deposits and clasts of host material; overlain by crater fill deposits and/or reworked material.

Sims (1975) suggested the following criteria for distinguishing seismically from non-seismically induced deformation structures:

- Liquefiable sediment is present or potentially present,
- Deformational structures observed are similar to those formed experimentally or shown to have formed during seismic events,
- Structures are restricted to or originate from a single stratigraphic interval,
- Zones of structures are correlated over large areas,
- Absence of detectable influence by slopes, slope failures, or other sedimentological, biological, or deformational processes.

Wheeler (2002) later expanded the criteria and further evaluated limitations related to determining the origin of these deformation structures. Recognizing these limitations, Tuttle and Atkinson (2010) urged that these structures be used in combination with blows and dikes in paleoliquefaction studies. Although these deformation structures can provide information about paleoearthquakes, additional research is needed to further explore the full range of expression of stratabound liquefaction features as well as the ground motions and site conditions under which they form.

Table 1-1 Summary of tests for determining seismic origin of soft-sediment structures (from Wheeler, 2002; Sims, 2012).

Test Name	Observation	Limitations
Sudden formation	Structure formed more suddenly, and perhaps more violently, than any non-seismic alternative	May be unable to rule out some nonseismic origins without additional evidence
Synchronous formation	Nearby structures of same type formed at times indistinguishable from each other	May be unable to rule out some nonseismic origins; dating and correlation lack resolution to distinguish synchronous from near-synchronous formation
Zoned distribution	Size of structure decreases away from a central area	Cannot rule out earthquake origin
Size	Structure not larger than similar structures formed by historical earthquakes	Maximum size may be unknown; cannot rule out an earthquake origin for small structures
Tectonic setting structure	Seismic shaking strong enough to form the structure occurs more frequently than nonseismic alternatives in modern analog settings	Threshold magnitudes and accelerations for formation are only generally known
Depositional setting	Seismic shaking by itself forms the structure in similar modern deposits	Difficulty in recognizing some newly formed structures in the field

1.4.4 Non-Seismic Features Not To Be Confused with Earthquake-Induced Liquefaction Features

There are many features that can be misidentified as earthquake-induced liquefaction features by an inexperienced investigator. One way to distinguish non-seismic from earthquake-induced liquefaction features is to compare the features in question with features whose origins are known (e.g., sand-blow craters that formed during modern earthquakes; craters resulting from tree throw during recent storms). A few of the most commonly misinterpreted features are briefly discussed below with respect to the depositional environments in which they occur.

All sedimentary environments: Root casts and dessication cracks occur in near-surface sediment in almost all depositional settings. Both root casts and dessication cracks pinch downward and are filled from above (Figure1.19). Root casts also branch downward. These characteristics are opposite to those of sand dikes, which branch and pinch upward and are filled from below. It should be noted that root casts, cracks, animal burrows, and other voids and weaknesses in near-surface sediment provide pathways for venting water and entrained sand resulting from earthquake-induced liquefaction. In these cases, a sand dike or other sediment-filled conduit that increases in size with depth occurs below these features.

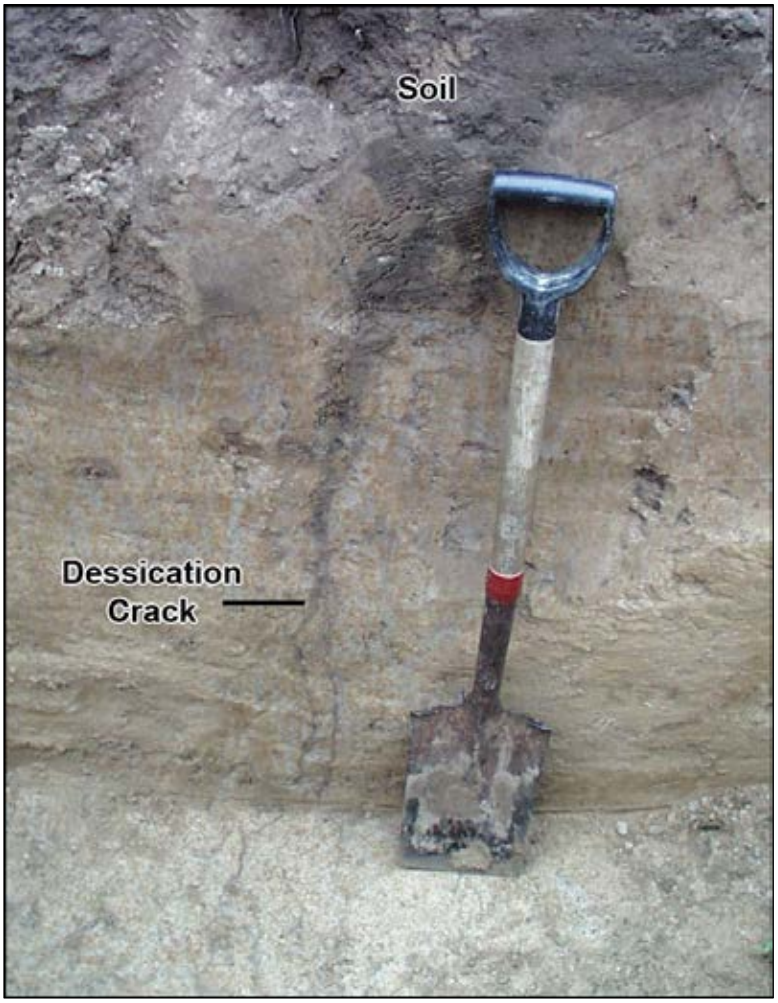

Figure 1-19 Desiccation crack filled with soil from above, exposed in wall and floor of trench. For scale, short handled shovel is 1 m in length. Photograph by M. Tuttle.

Fluvial environment: Fluvial deposits that may be sandy and limited in extent, such as point-bars or crevasse splays, should not be confused with sand blows. Blows are connected to sand dikes that crosscut soil horizons and underlying deposits, whereas fluvial deposits are not.

Lacustrine and estuarine environments: Dewatering structures, including ball-and-pillow structures, are common in deltaic deposits that experience high sedimentation rates, such as where rivers debauch into lakes or bays (Figure 1.20). Depositional context is key to recognizing these structures as non-seismic in origin.

Figure 1-20 Ball and pillow structures in glaciofluvial deposits exposed along Rouge River near Toronto, Ontario (Tuttle et al., 2010b). Photograph by M. Tuttle

Periglacial environment. Two commonly occurring deformation structures in periglacial deposits are involutions and ice-wedge casts. Involutions caused by cryoturbation (i.e., disturbance from freeze and thaw cycles) are characterized by distortion and mixing of the upper meter of sediment (Figure 1.21). Ice-wedge casts are downward-narrowing, nearly vertical, tabular features that result from thermal contraction of frozen ground. Both types of structures form over relatively long periods of time, compared to earthquake-induced liquefaction features.

Glacial environment. In glacial deposits, there is an abundance of deformation features related to ice tectonics. Deformation features that might be misinterpreted as earthquake-induced liquefaction features include stringers of sediment incorporated into diamictons and fluid-injection structures below glacial tills (Figure 1.22). However, these features often occur in association with sheared sediment, are very irregular in shape, and lack characteristics of earthquake-induced liquefaction features, such as source beds with soft-sediment deformation structures.

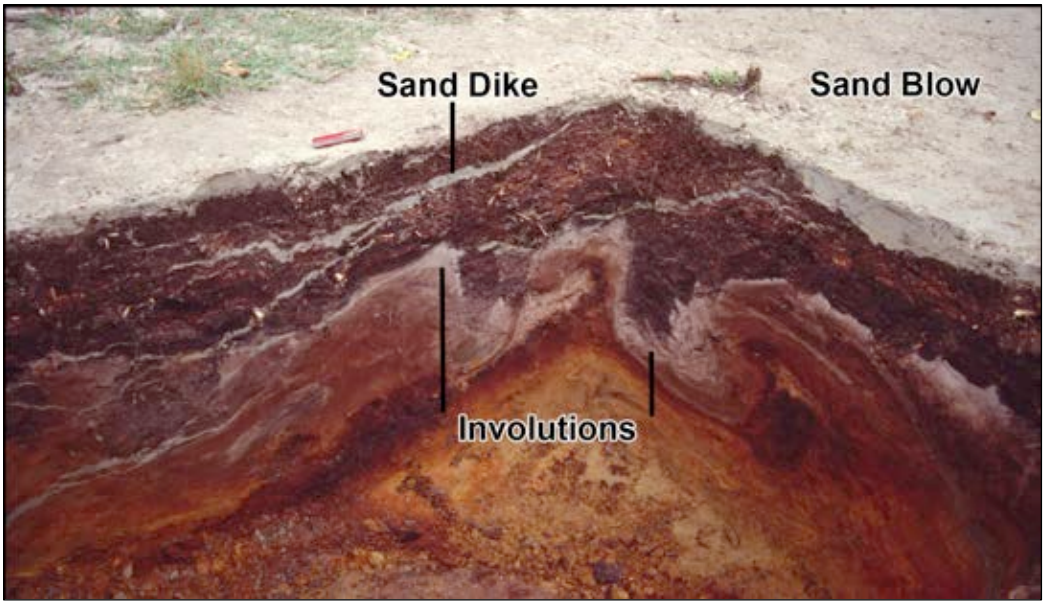

Figure 1-21 **Deformation of sediment due to cryoturbation exposed in trench excavated in sand blow that formed during 1988 M 5.9 Saguenay, Quebec, earthquake (NUREG/CP-0119). For scale, red pocketknife is 9 cm long.**

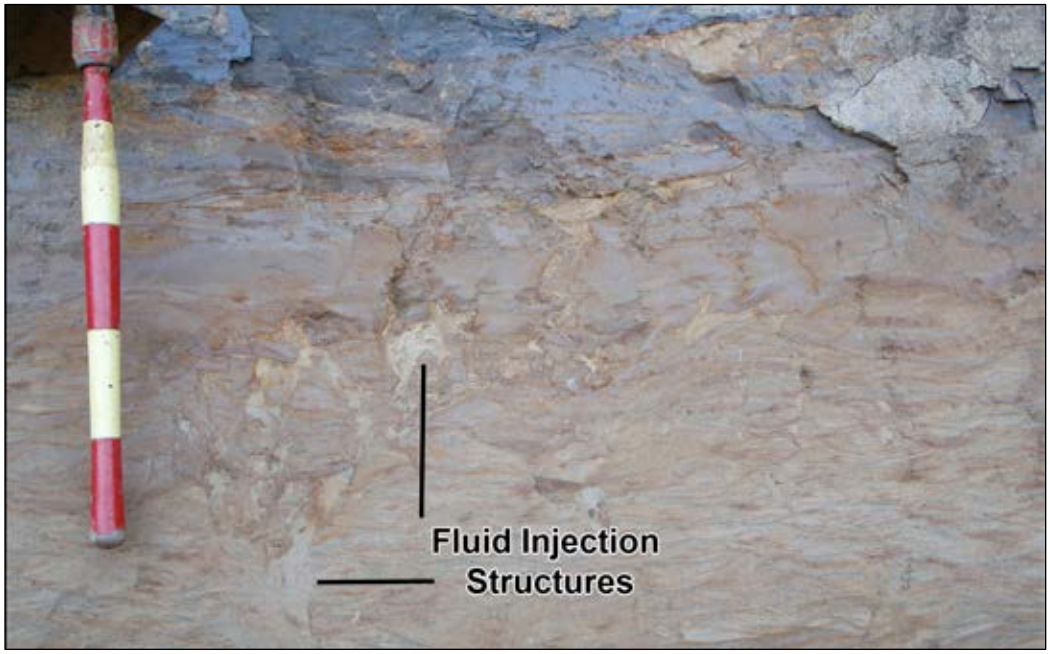

Figure 1-22 **Fluid injection structures in glaciofluvial deposit below diamicton or glacial till (dark gray) (Tuttle et al., 2010b). Each colored intervals on the shovel handle represents 10 cm. Photograph by M. Tuttle.**

2 PLANNING AND CONDUCTING PALEOLIQUEFACTION STUDIES

The components of a paleoliquefaction study include the following:

- Selection of the study area;
- Field investigations;
- Dating of liquefaction features; and
- Interpretation of liquefaction features.

Each of these components is discussed in detail in the following sections.

As previously stated, the primary goals of paleoliquefaction studies are to estimate the timing, source areas, magnitudes, and recurrence times of strong earthquakes during the Late Quaternary. The results of paleoliquefaction studies increasingly are being used as input parameters for seismic hazard assessments. Like paleoseismology in general, paleoliquefaction requires expertise in Quaternary geology, and the affiliated fields of sedimentology, geomorphology, soil science, geochronology, and sometimes archeology. Background in structural geology, neotectonics, seismology especially ground motion, geophysics, and geotechnical engineering is also desirable. It is advisable that experienced, qualified investigators be involved in planning and execution of paleoliquefaction studies in order to avoid misidentification of features in the geologic record and misinterpretation of the presence and absence of liquefaction features (NUREG-2115). Along these lines, it is advantageous to have at least two experienced investigator involved in field investigations so that they can discuss observations and interpretations of liquefaction features onsite. If possible, site reviews should conduct by paleoliquefaction experts during or soon after field investigations while features are intact and sites accessible. Some knowledge of ground motion is also relevant, as this is key to linking observed liquefaction features to potential sources. Uncertainties related to all aspects of paleoliquefaction studies - from the indentification and dating of liquefaction features to the interpretation of the timing, source area, and magnitude of paleoearthquakes - should be quantified and represented in results of the studies.

2.1 Federal Regulations

Federal agencies must comply with the National Environmental Policy Act and the National Historic Preservation Act when conducting or funding a paleoliquefaction field study. Compliance with the National Environmental Policy Act may require the federal agency to perform an environmental assessment and/or an environmental impact statement to assess the effects of field activities on the environment. Some federal agencies have categorical exclusions for geologic reconnaissance activities that preclude the need for performing these environmental studies. In addition, the National Historic Preservation Act requires the federal agency to comply with the 106 process described in the Code of Federal Regulations (36 CFR 800). This process requires coordination and communication with State Historic Preservation Officers and Native American Tribes prior to initiating ground disturbing activities.

2.2 Information Used in the Selection of the Study Area

A variety of information is helpful in selecting the best area for a paleoliquefaction study. This information includes accounts of ground failure indicative of liquefaction during modern and historical earthquakes, aerial photographs and satellite images, data on Quaternary geology and geotechnical properties of soil or sediment, and conditions in the field. For the results of a paleoliquefaction study to be useful in assessing seismic hazards, the study area must possess sedimentological and hydrological conditions that are conducive to the formation and preservation of liquefaction features (Sims, 1975; Obermeier, 1996; Tuttle, 2001). In addition, there must be an adequate exposure of sediment to be able to identify and study liquefaction features.

Conditions necessary for the formation of liquefaction features include (1) the presence of loose to moderately dense sandy sediment usually within 15 m of the ground surface, and (2) a water table or perched water table above the liquefiable sediment so that it is saturated at the time of the earthquake. In addition, a relatively impermeable capping layer promotes the increase in pore water pressure in and liquefaction of saturated sandy sediment during ground shaking. Liquefaction features are most likely to be preserved in geologic settings that are relatively stable or are experiencing sediment accumulation. For example, sand blows may endure for millennia on surfaces of abandoned plains or high terraces or they may be buried and preserved by subsequent deposits in coastal, fluvial, and lacustrine environments. Even in these settings, however, liquefaction features can be destroyed by natural processes such as river channel migration and mass movements. In addition, human modification of the landscape can destroy liquefaction features. For example, the agricultural practice of plowing commonly disturbs the upper 10-25 cm (4-10 inches) of the topsoil. Land leveling removes variations in topography by cutting and filling and can disturb up to several meters of the land surface. Therefore, plowing can destroy relatively small (<10 cm thick) sand blows and land leveling can destroy even large (1-2 m thick) sand blows. Finding and interpreting paleoliquefaction features is very difficult in areas that have been severely altered by human activity.

2.2.1 Accounts of Ground Failure Indicative of Liquefaction

For many large modern and historical earthquakes, there are eyewitness accounts of water and sand venting from the ground often through cracks or fissures. This type of ground failure is almost always due to earthquake-induced liquefaction of subsurface sediment. Often there are reports of springs forming or shutting down and riverbanks collapsing in the same area.

Modern and historical accounts of ground failure indicative of liquefaction can provide helpful information. For example, the accounts likely (1) indicate that sedimentological and hydrological conditions exist for the formation of liquefaction features, (2) point to possible study sites where paleoliquefaction features may be found in addition to modern or historical features, and (3) can be used along with information about the location and magnitude of the modern or historical earthquakes to interpret paleoliquefaction features in the study area. Accounts of liquefaction were used in these ways in the meizoseismal areas of the 1727 felt-area magnitude (**M**fa) 5.5 Newburyport, Massachusetts earthquake (Tuttle and Seeber, 1991; Tuttle, 2007 and 2009); the 1811-1812 moment magnitudes, **M** 7 to 8, New Madrid earthquakes in the central U.S. (Tuttle, 1999; Tuttle et al., 2002b); the 1925 **M** 6.2 Charlevoix, Quebec, earthquake (Tuttle and Atkinson, 2010); the 1944 **M** 5.8 Cornwall, Ontario-Massena, New York, earthquake (NUREG/CR-6495); and the 1988 **M** 5.8 Saguenay, Quebec, earthquake (Tuttle et al., 1990 and 1992).

2.2.2 Aerial Photography and Satellite Imagery

Aerial photography and satellite imagery can provide a bird's eye view of surficial sand blow deposits. As long as the deposits are not obscured by forest canopy and other vegetation or destroyed by development and agricultural practices, sand blows appear as circular, elliptical, and linear, light-colored patches on the ground surface (Figures 2.1 and 2.2). Historical aerial photographs that predate modern development can be especially useful in identifying and mapping sand blows, which are especially apparent if the surrounding soils are fine grained and therefore have a greater moisture-holding capacity. Sand blows are obvious on river floodplains characterized by silty and clayey soils developed in overbank deposits. The lower moisture-holding capacity of sand blows also may be reflected in vegetation type and in crop growth. For example, crops growing on large sand blows in the New Madrid seismic zone in the central U.S. often wilt and die during the course of the growing season (Tuttle et al., 2011). In agricultural settings, relatively small (< 0.25-0.5 m thick) sand blows may be destroyed over time by plowing. However, large sand blows, like those in the New Madrid seismic zone (up to 2 m), will be recognizable on aerial photographs and satellite imagery despite plowing of the upper decimeter or more.

Figure 2-1 **Aerial photograph showing light-colored sand blow deposits near the Pemiscot Bayou east of Lepanto, Arkansas (Tuttle, 1999). Sand blows are aligned above point bar deposits within the meander scroll bars. Photograph taken on January 26, 1964 by U.S. Department of Agriculture.**

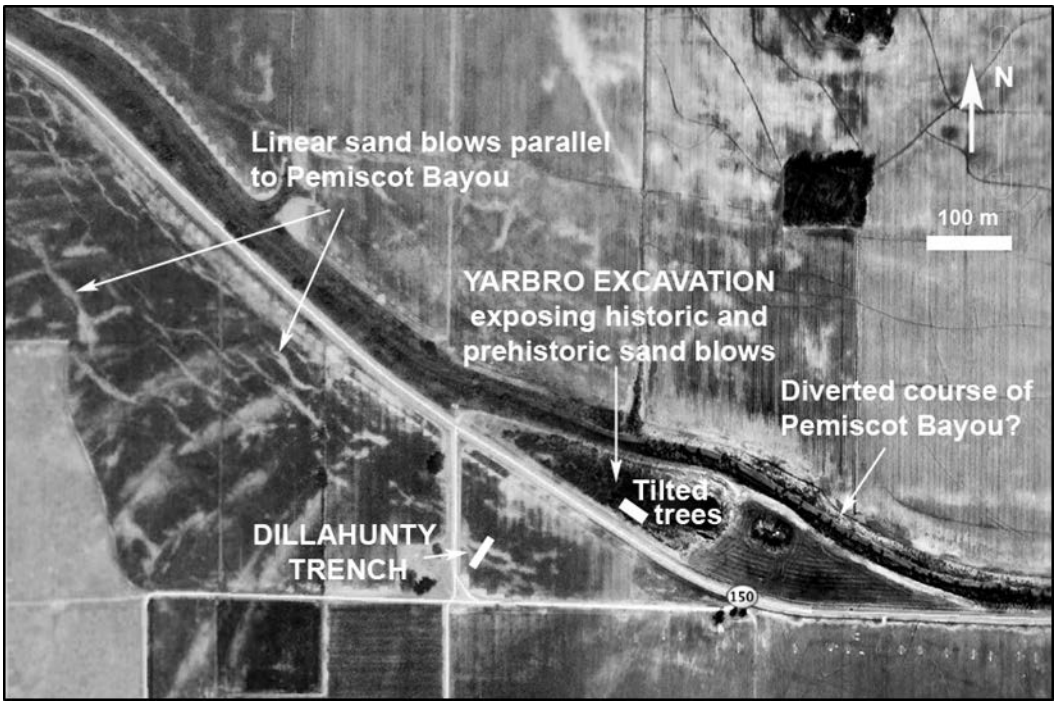

Figure 2-2 Google Earth satellite image showing linear sand blows parallel to and within 300 m of Pemiscot Bayou north of Blytheville, Arkansas. These features probably formed during lateral spreading towards the bayou. Historic and prehistoric sand blows and related sand dikes have been documented and dated in nearby excavations (Tuttle, 1999).

Satellite imagery has been acquired relatively recently, and therefore, reflects ground conditions as they exist today. Therefore, sand blows that have been disturbed by farming may appear less distinct on satellite images than on historical aerial photographs. However, satellite imagery, image processing software, and geographical information systems now provide the opportunity to combine data sets within a geographical framework and to classify and map sand blows over large areas based on their spectral characteristics. LANDSAT-7 Enhanced Thematic Mapper Plus (ETM+) imagery may be especially useful in this regard.

ETM+ imagery can provide information on reflected or emitted radiation from the Earth's surface in the blue-green (band 1), green (band 2), red (band 3), near-infrared (band 4), mid-infrared (bands 5 and 7), and the far-infrared (band 6) portions of the electromagnetic spectrum. In addition, ETM+ imagery includes a panchromatic band 8 with a high resolution of 15 m. For mapping sand blows less than 15 m in diameter, higher resolution panchromatic imagery is also available. The TM infrared bands reflect the character of the soil and rock materials. Band 4 is ideal for near-infrared reflectance peaks in healthy green vegetation and for detecting water-land interfaces. The two mid-infrared bands are useful for vegetation and soil moisture studies and discriminating between rock and mineral types. The far-infrared band is designed to assist in thermal mapping and for soil moisture and vegetation studies. Band ratio images are often created to remove effects of illumination differences and to accentuate the spectral differences between materials (e.g., Rencz, 1999; Rattan, 2006). This involves dividing the values of pixels in one band by the values of pixels in a second band. By computing ratio images using TM infrared bands, it may be possible to map sand blows of different ages based on soil characteristics that develop over time. Resulting liquefaction maps, like all maps based on remotely sensed data,

must be calibrated with field data or otherwise verified in the field. Although satellite imagery has been used extensively to map soils, only pilot studies have been conducted to date for mapping sand blows. This is an area of research that appears to hold much promise.

Light Detection and Ranging (LiDAR) is an optical remote sensing technology that can provide high-resolution elevation data. The data are processed to produce detailed bare earth models and therefore are particularly useful for mapping faults in densely vegetated regions. Typical accuracies range between 20-100 cm horizontally and between 9-18 cm vertically but can be further improved with closer pulse spacing (> 4 pulses/sq m) during data acquisition. LiDAR data are being used in paleoseismology to map fault ruptures that offset topography. Their application in paleoliquefaction studies has been very limited so far. In the greater Christchurch region of New Zealand, LiDAR data are being used to study the environments in which liquefaction features formed during the 2010-2011 Canterbury earthquake sequence (Villamore et al., 2014). With additional research, LiDAR may be found to be useful in mapping medium to large sand blows, especially when combined with other remotely-sensed data that can reflect sediment and soil types. Currently, high-resolution LiDAR data are not readily available and are expensive to acquire.

Aerial photography and satellite imagery have been used successfully to identify sand blows on the ground (e.g., Tuttle et al., 1999 and 2006). In addition, they are readily available and relatively inexpensive. With soil characteristics and seasonal growth patterns in mind, it is advantageous to select aerial photographs and satellite imagery that was acquired when sand blows would be more apparent. In northern forested areas, the best acquisition time is probably late fall following leaf off and prior to the wet or snowy season. In agricultural areas where floodplains are under cultivation, these times include late winter or early spring following plowing and prior to crop growth, late summer or early fall when soils have dried out and crops have been adversely affected by droughty soil conditions, and late fall following harvest and prior to the beginning of the wet or snowy season. Times to avoid image acquisition include the rainy season when all soils would tend to be wet and when floodplains may be flooded, as well as spring and summer before crops have been adversely affected by droughty soil conditions.

2.2.3 Quaternary Geology

As discussed above, liquefaction features tend to form in response to strong ground shaking where saturated, loose to moderately loose sandy deposits are overlain by less permeable sediment that may include silt and clay. These sedimentological and hydrological conditions often exist in Holocene fluvial, lacustrine, esturine, deltaic, and lagoonal deposits and sometimes in similar deposits of Late Pleistocene age. Therefore, surficial geology maps, as well as articles and reports about the Quaternary geology of a region, provide essential information about the presence and distribution of conditions where liquefaction features are most likely to occur, if they have formed in a region. Therefore, it is important to consult relevant geologic resources before undertaking, or during the early stages of, a paleoliquefaction study.

A systematic review of surficial geology maps, in combination with aerial photographs and/or satellite images, can help to identify areas where suitable conditions are likely to exist and where exposure of sediment may be available for examination in plowed fields, sand and gravel pits, and river cutbanks. Based on such a review, a reconnaissance plan can be developed to verify conditions and exposure prior to conducting systematic searches along rivers or subsurface investigations at selected sites. Many geologic maps are now available in digital and georeferenced formats and can be downloaded over the internet. These georeferenced maps can be imported into a Geographical Information System to be displayed and analyzed in combination with other datasets such as satellite imagery, soils maps, and topography.

2.2.4 Geotechnical Data

Geotechnical data that characterize the material properties of subsurface soil, or sediment, at a site also can be used to assess whether or not suitable conditions are present for the formation of liquefaction features. Properties of sediment measured today are likely to differ from what they were in the past. Therefore, age effects and stress history of the sediment should be considered when assessing past conditions. Geotechnical data are often used to identify the layer that liquefied. The liquefied layer can only be known with certainty, however, if liquefaction features are observed originating in this layer. Once areas of interest are identified based on characteristics related to Quaternary geology, site-specific geotechnical data can be sought for these areas.

Geotechnical data used in the design of bridge foundations are often collected prior to their construction at crossings of rivers, lakes, estuaries, and lagoons, environments where conditions tend to be suitable for the formation of earthquake-induced liquefaction features. These data include borehole logs, geophysical logs, results of laboratory tests, and engineering reports. The borehole logs typically show the type and depth of soil, or sediment, (e.g., clay, silt, sand, gravel, organics), blow counts (N), and the depth to the water table. Laboratory analyses may include information on specific gravity, void ratio, grain size, liquid and plastic limits, water content, and unconfined compressional strength.

Blow counts are the number of hammer blows, with a 140-lb hammer dropped a distance of 30 inches that are required to advance a 2-inch (outside diameter) split-barrel sampler one foot (ASTM D1586). Non-standard hammers, samplers, and distances of drop have been used, in which case, correction factors generally have been applied to the blow counts. However, any geotechnical study carried out with the intent of using the data for liquefaction analyses should be performed with standard equipment. The blow count (N) is correlated to soil density and has been empirically related to liquefaction of soil or sediment during actual earthquakes. In recent years, the electronic cone penetrometer and seismic piezocone have been employed more frequently in site characterization because of the continuous readings, direct logging of measured data to the computer, and repeatability and reliability of the cone penetration test (ASTM D5778). If needed, relations have been developed between tip resistance (qt) and blow counts (N) (Kulhawy and Mayne, 1990; Idriss and Boulanger, 2004). Liquefaction susceptibility in sandy soils generally increases with decreasing blow counts and cone tip resistance. Of particular interest for paleoliquefaction studies are saturated, sandy soils, with blow count values in the 0-30 range and tip resistance in the 0-18 MPa (megapascal; measurement unit of pressure; 1 MPa = 10 bars) range, that occur below a fine-grained confining layer and usually less than 15 m or 49.2 ft below the surface (Obermeier et al., 2001; Tuttle, 2001).

Geotechnical data generated for bridge projects are often available at local, state, or federal transportation agencies. Some data have been digitized and entered into databases making the information more accessible. Even so, it can be labor intensive to identify bridge projects, download or copy geotechnical data, review the data, and extract information useful for paleoliquefaction studies. However, it is well worth the effort since this information related to material properties helps in the selection of suitable areas for reconnaissance. Furthermore, if they are collected at paleoliquefaction study sites, geotechnical data can be used in liquefaction analysis of scenario earthquakes (see Section 2.5.4.3).

2.3 Field Studies

Paleoliquefaction field studies should be designed to fully characterize the ages, sizes, and spatial distribution of paleoliquefaction features in a region. These studies often include initial reconnaissance, site investigations, and river surveys, in order to achieve well-constrained age

estimates of paleoliquefaction features, as well as to gather information about the size and spatial distribution of paleoliquefaction features over a large area. During every phase of a field program, it is recommended that a paper or electronic site description form be used to record information about liquefaction sites, liquefaction features, and samples collected. The use of a form ensures that relevant information is consistently collected at all liquefaction sites (see Appendix D for an example of such a form). To fully characterize the ages of liquefaction features, suitable sediment of Holocene to Late Pleistocene age should be included in the studies. In areas where liquefaction features are small and sparse, including areas far from the epicenters of causative earthquakes, more exposures will need to be examined to find and characterize liquefaction features. Fieldwork should be conducted at times of the year, and even at times of the day in coastal areas, when exposure is optimal in order to minimize chances that liquefaction features are missed due to high water, heavy vegetation, or snow cover. It is important to conduct investigations in areas of suitable conditions and exposure and to determine where liquefaction features have and have not formed.

Utmost care must be taken to correctly identify earthquake-induced liquefaction features and not to confuse them with features that formed as the result of other processes. In plan view, sand blows have circular, elliptical, and linear shapes and can range up to tens of meters in width and hundreds of meters in length. In cross-section, sand blows commonly take the form of constructional cones that can range up to 1 to 2 m in thickness. Deposits and features that have been misidentified as earthquake-induced liquefaction feature include fluvial deposits, sediment-filled dessication cracks, chemical weathering, tree-throw, and cultural features. Liquefaction features have certain characteristics, described in Sections 1.4.1-3, that help to distinguish them from other deposits and features (Figure 1.12). For example, the presence of feeder dikes helps to distinguish earthquake-related sand blows from fluvial deposits and deformation related to tree throw. With close examination of deposits and features by an experienced eye, earthquake-induced liquefaction features can be identified and analyzed with confidence.

2.3.1 Initial Reconnaissance

A reconnaissance plan must be developed and may be based on a variety of information including eyewitness accounts of liquefaction effects during modern or historical earthquakes, interpretation of aerial photographs and satellite imagery, and information about geological, geotechnical, and ground water conditions. The plan identifies locations to visit in order to assess whether or not sand blows occur at the ground surface, exposure is adequate to warrant searches for liquefaction features along rivers and ditches and in borrow pits, and conditions appear favorable for formation and preservation of liquefaction features. The results of reconnaissance are used to refine plans for field studies, including searches for and site-specific investigations of paleoliquefaction features.

Reconnaissance involves inspection of sites for which possible sand blows were identified on aerial photographs and/or satellite imagery. Once permissions are arranged with property owners and farmers, the site is walked and the possible sand blow identified on the ground. State Archeological Surveys, State Historic Preservation Offices, and Tribal Historic Preservation Offices should be contacted prior to excavation. If the possible sand blow appears sandier on the surface than the surrounding soils, several test pits about 1-1.5 m deep are dug by hand to observe the sedimentary characteristics of the deposit. Color, grain size, sedimentary structures, and thickness of the soil horizons and sediment layers are documented. If the deposit is found to be sandier than surrounding soils, to be deposited on top of the surrounding soil, to contain clasts of the underlying soil, and to be characterized by irregular bedding or flow structures, it is likely to be a sand blow and may warrant further study.

Likely sand blows found in this manner are evaluated, and those deemed the most likely to provide crucial information about paleoearthquakes are selected for further investigation (see Section 2.3.2 below).

Reconnaissance also includes inspection of rivers and borrow pits, where suitable conditions for the formation of liquefaction features may occur. For rivers, conditions and exposures are inspected at bridge crossings, boat ramps, parks, and other public access points. For each location, photographs are taken and information is recorded about access, cutbank exposure, type of sediment, and river level. For borrow pits, permission and access must first be arranged with sand and gravel companies. Inspections of borrow pits include taking photographs and describing exposure, type of sediment, and deformation structures, including liquefaction features. Those portions of rivers and borrow pits with the most suitable conditions and best exposure are selected for systematic searches for liquefaction features (see Section 2.3.3 below).

2.3.2 Site Investigations

Detailed investigations are conducted at sites where sand blows have been identified and that hold promise for providing information about the timing, locations, and magnitudes of paleoearthquakes. Sand blows that occur in association with cultural horizons and features (e.g., pits, post molds, wall trenches) are often selected for site investigations because cultural artifacts and abundant organic material found in these horizons and features can be used to estimate the ages of the liquefaction features. For example, many of the better-constrained age estimates of sand blows in the New Madrid seismic zone in the central U.S. have come from investigations at archeological sites (e.g., Bauer, 2006; Tuttle, 1999; Tuttle et al., 2005b). If investigations are to be conducted at archeological sites, it is imperative to involve professional archeologists in the endeavor, to take steps to minimize impacts to the site, and to comply with the National Historic Preservation Act.

Site investigations often include geophysical surveys followed by trenching. As explained below in more detail, geophysical techniques are used to map the extent of the sand blow, to locate the main feeder dikes of the sand blow, and to identify cultural features that may be associated with the sand blow. The results of geophysical surveys help to position trenches to reveal critical relationships between the liquefaction features and cultural horizons and features, while minimizing the impact to the archeological site. Excavation of trenches is necessary to study and document characteristics of the liquefaction features and their relationships with host sediment, soil horizons, and cultural horizons and features, as well as to collect carefully controlled samples for dating the time of formation of the liquefaction features. In addition, archeologists document and sample cultural horizons and features found to be associated with the liquefaction features.

2.3.2.1 Geophysical Techniques

Geophysical techniques offer a non-invasive tool for mapping the three-dimensional (3-D) morphology of sand blows and locating sand dikes and sand blows in the subsurface. Although sand blow deposits are often identified by careful examination of surface deposits and natural understanding of subsurface relationships and can help guide trench excavations necessary to collect samples for dating sand blows and their causative earthquakes. The physical properties of surficial deposits and their three-dimensional morphology strongly influence the distribution of sand blows and other liquefaction features. The ability of geophysical techniques to detect vertical and lateral changes in sedimentary properties makes them an effective mapping tool in paleoliquefaction studies. This section discusses the types of geophysical methods that can be used in paleoliquefaction studies and the factors important for planning geophysical surveys to optimize their effectiveness and utility.

Electrical resistivity, ground penetrating radar, seismic methods, magnetic methods and ground conductivity surveys have all been used in paleoliquefaction investigations. All methods are useful for locating subsurface features, although each has its advantages and its limitations. These relative assets and disadvantages should be carefully considered when choosing the technique or combination of techniques to be employed at a given site. All methods derive their success from their sensitivity to variations in the physical properties of the sediment, and all are best used following surface reconnaissance to determine and narrow the general survey area. The geophysical methods discussed here are not ideal for large-scale, regional reconnaissance, but rather, are best employed once a liquefaction site has been identified using the geological techniques described above in Section 2.3.1.

Electrical Resistivity (ER): ER methods use a low-frequency alternating current that is introduced through an electrode pair, while a potential difference is measured by another electrode pair. The ratio of the voltage at the receiver electrodes to the current input by the transmitting pair is the impedance. The ability for current to travel through the subsurface is a function of the physical properties of the medium. Resistivity, the inverse of conductivity, is a measure of the resistance of a volume to the applied electric current. In general, rocks are associated with high resistivity, whereas sediment, due to its higher porosity, can be associated with either high or low resistivity depending upon the degree of saturation or clay content. Saturated sediment or those containing salt or clay, because of their ionic content, increase the ability for current to flow and thus decrease the resistivity of the material.

Although electrical methods have been in use for resource exploration since Schlumberger's early work in the last century (Oristaglio and Dorozynski, 2009), the method was first applied to studies of earthquake-induced liquefaction in the mid-1990's (Wolf et al., 1998; Tuttle et al., 1999). The time required to perform surveys and their imaging capability have since improved with the use of equipment offering multichannel, automated switching capability and 3-D inversion algorithms for estimating the true subsurface distribution of resistivities (Wolf et al., 2006).

The calculation of apparent resistivity is based on the style of array, or electrode configuration, selected. The factors affecting the measured values are the input current, the spacing between electrodes, and the physical properties of the material. If 3-D data acquisition is not employed, profile lines should be oriented perpendicular to the strike of elongated sand blows, if observed at the surface. In map view, sand dikes and related sand blows often form *en echelon* patterns and parallel profile lines help to determine their orientation (Figure 2.3).

Important to all geophysical surveys are the depth and scale of the imaging desired. For ER surveys, the depth of imaging is greatly affected by the conductive properties of the near-surface layers and the spacing of the electrodes. Early geophysical studies of paleoliquefaction features used a basic four-electrode layout, usually in a Wenner constant-spread array (Wolf et al., 1998). For a Wenner style or mixed Dipole-Dipole array, the spacing between electrodes or dipoles should be no more than twice the size of the features to be imaged, and approximately equal to the desired imaging depth (Wolf et al., 2006). Tighter spacing will resolve smaller features, but there will be a trade-off in the maximum depth imaged. For example, with an electrode spacing of 3 m, sand dikes as small as 18 cm in width that crosscut silty deposits at a depth of less than 1 m have been imaged (Figure 2.3; Wolf et al., 1998).

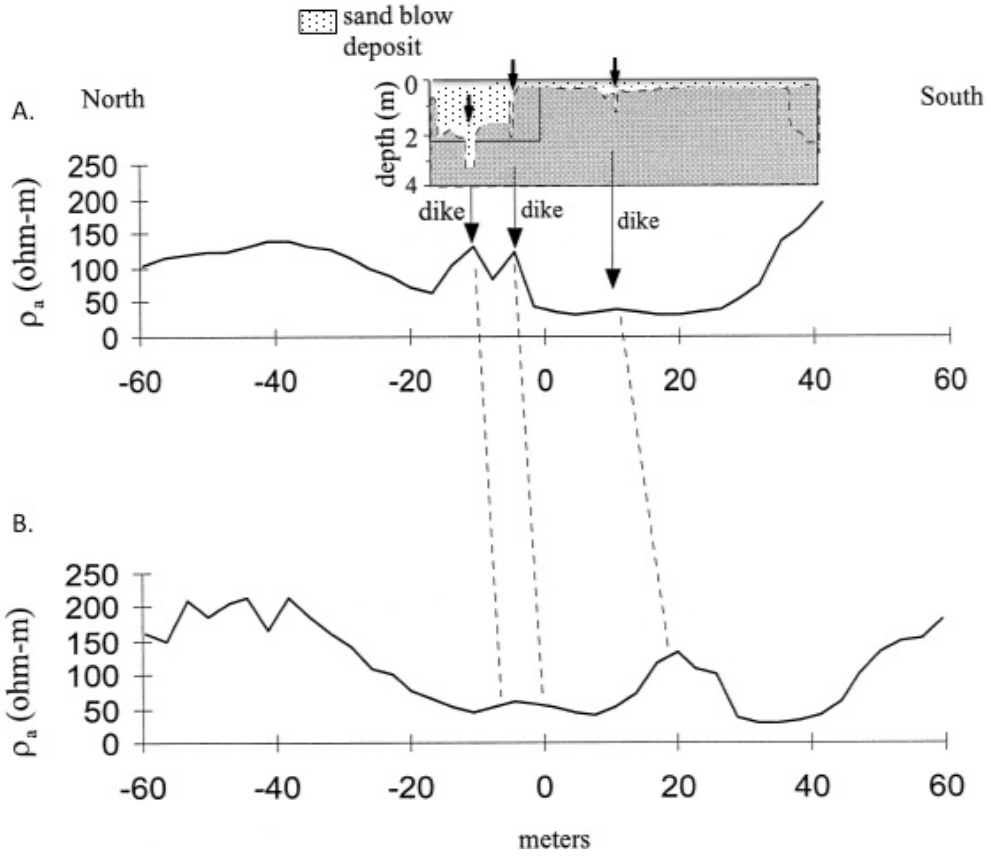

Figure 2-3 Example of correlation between two parallel apparent resistivity profiles offset by ~ 16.5 m showing en echelon expression of sand dikes (indicated by arrows). (A) Apparent resistivity highs show position of sand dikes later exposed in trench excavation. Dike at -5 meters is 18 cm wide. (B) Apparent resistivity along parallel profile to south of (A) shows dike at -15 meters getting smaller and dike at +12 meters getting larger (after Wolf et al., 1998).

When done correctly in suitable environs, the imaging capability and resolution of the ER method is excellent. Figure 2.4 contains an example of an electrical resistivity profile that has been correlated with a log of a wall of an excavated trench. The location for the excavation was chosen based on the results of the site reconnaissance (e.g., archeological surveys, soil test pits, etc.) and geophysical survey. Warm colors in the geophysical cross-sections denote more resistive material (e.g., fine to coarse sand associated with sand blow deposits and dikes).

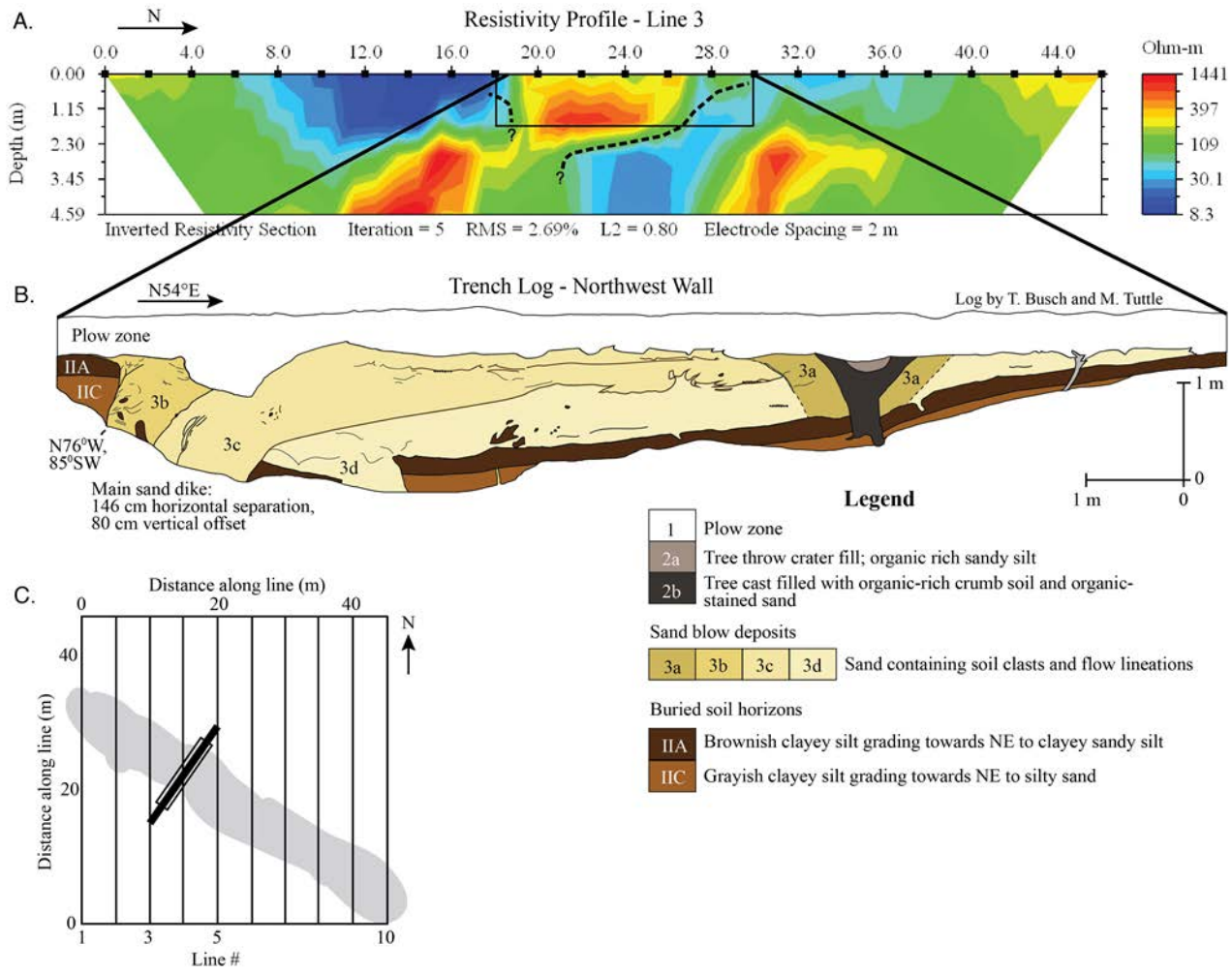

Figure 2-4 **(A) Example of a resistivity profile at a liquefaction site in the New Madrid seismic zone in northeastern Arkansas. Dotted line outlines approximate contact between sand blow deposit and host sediments. Warm colors reflect sediment associated with sand blow deposits and sand-filled dikes, which typically have higher resistivities than surrounding fine-grained sediment. Blue colors reflect material with higher percentages of clay and moisture, which are more conductive. The resistivity profile is correlated with a trench log (B) that runs at an angle to the resistivity profile. The trench log reveals only the portion of the resistivity section outlined by the black rectangle in (A). Dark brown colors correlate with green to blue colors in the resistivity profile, while yellow to red colors correlate to sand blow deposits and the top of the feeder dike. Note cross-cutting relationship of sand-filled dike with finer-grained sediment of buried soil horizons. (C) Inset map shows location of the trench (heavy black line) and trench log (open rectangle) in relation to the N-S oriented geophysical profiles and northwest oriented sand blow (shaded gray) as seen on satellite imagery and in the field.**

Blue colors reflect sediments with higher percentages of fines, such as silts and clays. Important in the interpretation of the geophysical data is the recognition of patterns and geometries

commonly associated with liquefaction deposits, as discussed in Sections 2.2.2, 2.3, and 2.3.1, because interbedded fine- and coarser-grained sediment is common in fluvial environments.

In addition to the electrode spacing, success in imaging is determined by the contrast in physical properties between the liquefaction deposit or feature, and the surrounding host material. The contrast in grain sizes between the coarser grained, sandy liquefaction features and the finer grained host deposits provides a good indication of the potential success of the survey. Wolf et al. (2006) compared the grain-size distribution of sediment sampled from liquefaction deposits with that of the surrounding host sediment at seven sites in the New Madrid seismic zone in the central U.S. (Figure 2.5). Results showed that, when the contrast in grain-size is large, imaging by resistivity surveys is excellent. However, at sites where the contrast is low, results are relatively poor and success is only achieved through decreasing the electrode spacing, which can greatly increase the time needed to perform the survey. For a more detailed discussion of ER arrays and their utility, the reader is referred to standard texts, such as Burger et al. (2006) or Parasnis (1997). For representative ranges of resistivity values for different sediment and rock types, the reader is referred to Telford et al. (1990).

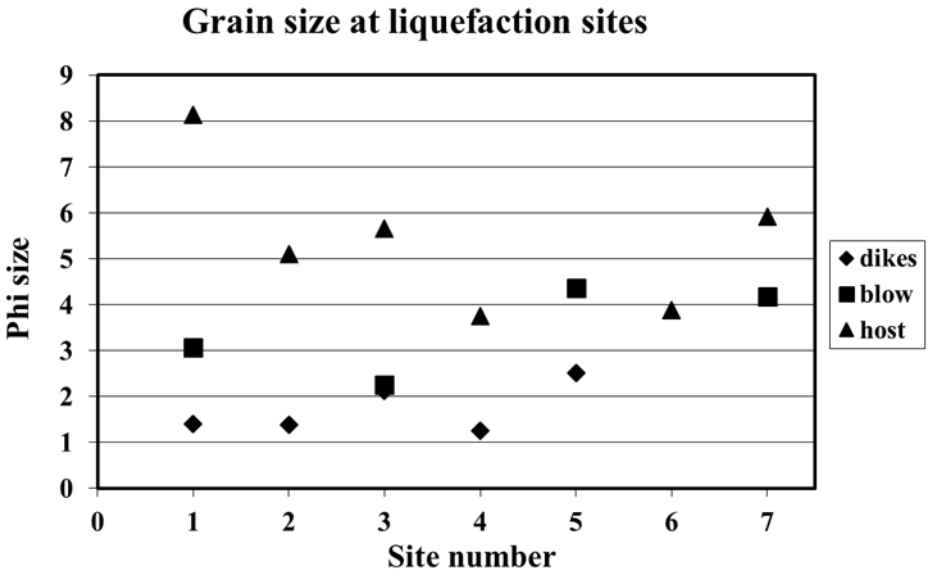

Figure 2-5 Measured grain sizes at seven sites in the New Madrid seismic zone in phi size, ϕ, where particle diameter =1 mm · 2-ϕ. Host sediment (triangles) corresponds to sediment sizes of silts and clays; sand blows correspond to fine to very fine sand; sand dikes correspond to mostly medium sand. Where difference in grain sizes between liquefaction features and host sediment is small, resolution is poor (e.g., sites 5 and 7). Where contrast is greater (e.g., sites 1 and 2), resolution is good. Site numbers 5 and 6 represent two trenches at the same site.

Ground-Penetrating Radar (GPR): GPR methods involve the transmission and reflection of electromagnetic energy. Like seismic methods, transmitted waves (in this case electromagnetic fields) are scattered, reflected and partitioned at interfaces in the subsurface due to contrasts in impedance such that some energy is returned to the surface. This partitioning is determined by the contrast in physical properties at stratigraphic and structural boundaries. GPR systems operate over a range of frequencies, and the ability for waves to propagate is a function of the dielectric permittivity of the medium, the operating frequency of the system (antenna choice) and

the propagation dispersion (radar response to small-scale heterogeneities in the subsurface). GPR is best used in areas of dry, sandy soils, as the signal penetration through clayey soils and saturated soils can be poor. An important decision to be made before beginning GPR surveys is the target depth and size of the features being imaged and the appropriate antenna to achieve this depth and resolution. An excellent source for a thorough discussion of the relations affecting GPR theory and practice can be found in Annan (2005). With the proper choice of antenna frequency and suitable soils, GPR methods offer a fast, efficient tool for locating subsurface sand dikes, feeder dikes and deformation structures at depths less than 5 m.

The use of GPR methods for earthquake-related liquefaction studies was pioneered by Liu and Li (2001) and later further developed by Al-Shukri et al. (2006). Liu and Li (2001) used both a 400 and 100 MHz antenna to study three sites in the New Madrid seismic zone. As with ER methods, there is a trade-off between depth of signal penetration and feature resolution; lower frequencies penetrate deeper, but lose their resolving capability. Similarly, the success of the method is dependent on the physical properties of the near-surface sediment. Like electrical methods, GPR works best when there is a contrast in grain size between the sandy liquefaction features and the surrounding host sediment. However, a key limitation of GPR surveys is the loss of signal penetration associated with conductive overburden. Clays and clayey soils are very good conductors and effectively prevent electromagnetic energy from penetrating to strata below. Penetration depths in such conditions can be less than one meter. Because true 3-D data acquisition is not common in most GPR surveys, parallel profile lines are oriented perpendicular to elongated sand blows. The profiles can later be combined to form a pseudo-3-D data set.

Al-Shukri et al. (2006) had good success using a 400-MHz antenna in their work on paleoliquefaction deposits in east central Arkansas south of the New Madrid seismic zone. They noted that, because the sand blow thickness was less than 4 m, this antenna frequency provided the necessary penetration depth as well as the spatial resolution needed to image sand dikes crosscutting silty host deposits, contacts between buried soils and overlying sand blows, and displacements of those contacts due to liquefaction-related ground failure (Al-Shukri et al., 2006; Tuttle et al., 2006). Resolution was also improved by post-processing the data (e.g., filtering for noise reduction, removal of direct wave arrival) following acquisition. Results of Al-Shukri et al. (2006) show clear reflectors similar to what one might achieve with seismic reflection surveys (Figure 2.6). A key advantage to GPR surveys is the speed with which surveys can be accomplished relative to seismic surveys. In addition, GPR surveys require only minimal personnel (e.g., Liu and Li, 2001; Salvi et al., 2003) and preliminary data processing can be accomplished in the field.

Seismic Methods: Seismic refraction and reflection have been used in paleoliquefaction studies, but have not had the success of other methods. Generally, the resolution of the surveys are influenced by sediment properties, such as layer impedance (velocity x density), layer thickness relative to geophone spacing, type of energy source, and the dynamic range of recording system. Although refraction methods are good for determining velocities and depth to stratigraphic interfaces, they work best in relatively flat-lying layers. They can be used to determine the thickness of overburden, depth to the water table, and potentially depth to underlying buried sand blows or source sands. However, refraction methods are limited in their ability to image vertical boundaries, such as crosscutting sand dikes, and require long profile lengths for reliable determination of crossover distances, which are needed to determine layer thickness. In contrast, seismic reflection methods are more useful for imaging offset host horizons, displaced reflectors, and sand conduits or vents.

Several sources (e.g., the mini-Sosie, explosives, Betsy gun and hammer) have been used in earthquake hazard studies and shallow investigations. However, most of these do not resolve features at less than several meters depth (e.g., Sexton and Jones, 1988; Bray and Frost, 2010). Hammer sources achieve the best resolution at shallow depths, but are labor-intensive for long profiles.

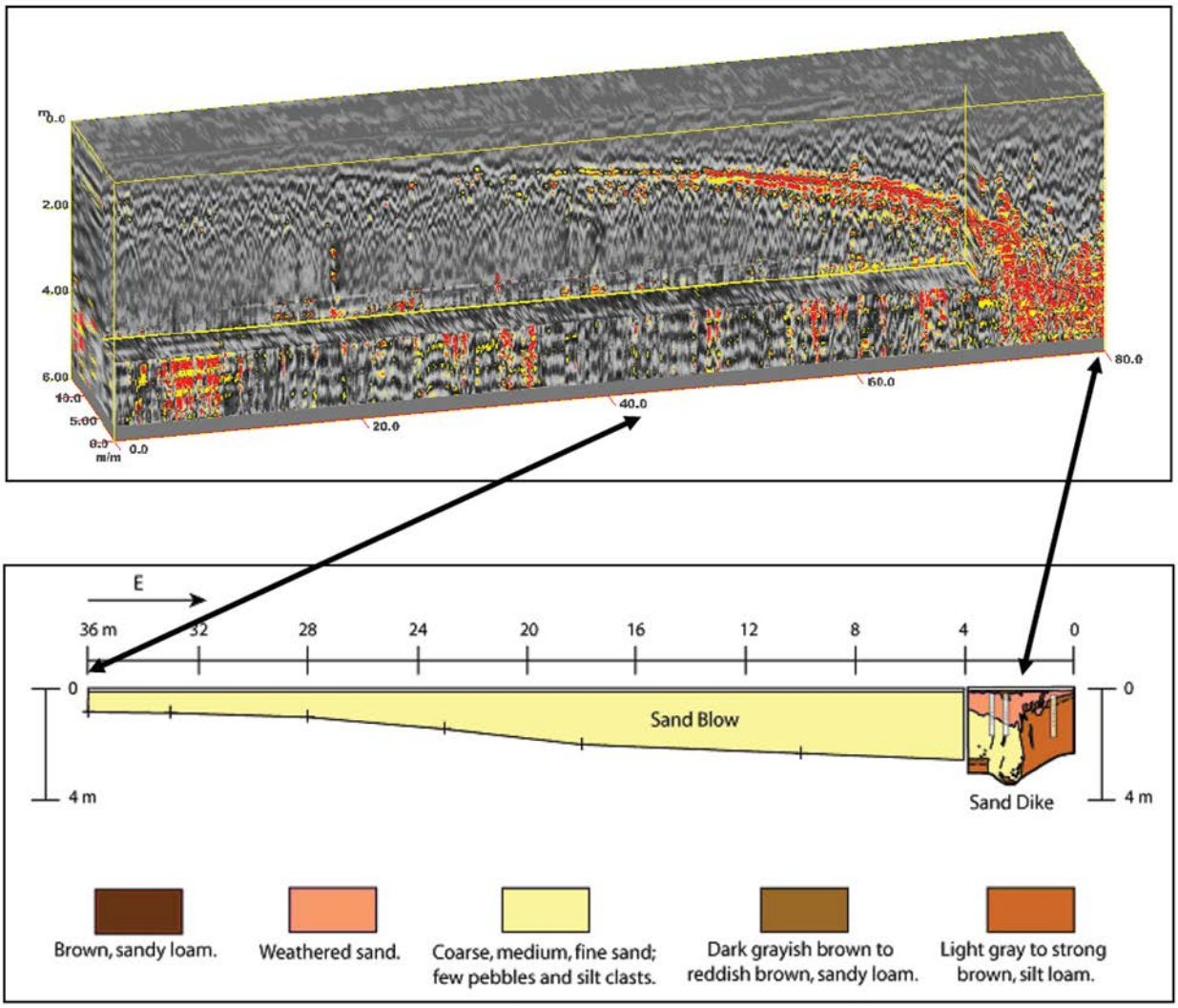

Figure 2-6 (Above) Pseudo-three dimensional GPR image correlated with (Below) log of trench excavation showing large sand blow and related sand dike near Marianna, Arkansas (from Al-Shukri et al., 2006).

Seismic reflection surveys, although useful for locating faults and structural deformation, have limited utility for paleoliquefaction studies because they do not lend themselves to mapping sand blows and sand dikes at depths that can be trenched for the study of liquefaction features and collection of samples for dating. They can be used in combination with electromagnetic (EM) and GPR to study the relationship of liquefaction features, shallow subsidence, and offset strata with possible faulting of deeper horizons. In addition to their limitations in imaging shallow layers, the data acquisition time in seismic surveys, compared to GPR and ER, is significantly longer and data processing is much more involved.

Magnetic Surveys: Magnetic gradiometric surveys have been used in archeological studies for some time. However, their use in paleoliquefaction studies to locate cultural features and horizons in close association with sand blows is more recent (e.g., Wolf et al., 1998; Tuttle et al., 1999). As discussed in Section 2.4.3 below, these cultural horizons and features contain organic materials and artifacts that can be used to constrain the ages of associated sand blows and sand dikes.

Magnetic anomalies are frequently observed at archeological sites due to the contrast in magnetic properties of cultural objects, such as pottery and daub relative to the surrounding host sediment (Figure 2.7). The artifacts possess a remanent magnetism acquired from magnetite or other similar minerals as they are heated and then cooled causing the magnetic domains within the minerals to realign with the applied field. Thus, objects made from baked clay, such as bricks, pottery, hearths, and cooking pits, or points containing magnetite can often be located by magnetic surveys. Also, buried features or objects that are not in themselves magnetic sometimes can be located as a result of soil disturbance at the site (e.g., shallow graves). A characteristic of anomalies associated with cultural features is their morphology, as they are often quasi-circular (in the case of pits, post holes, etc.) or elongate (walls) in map view (Figure 2.7).

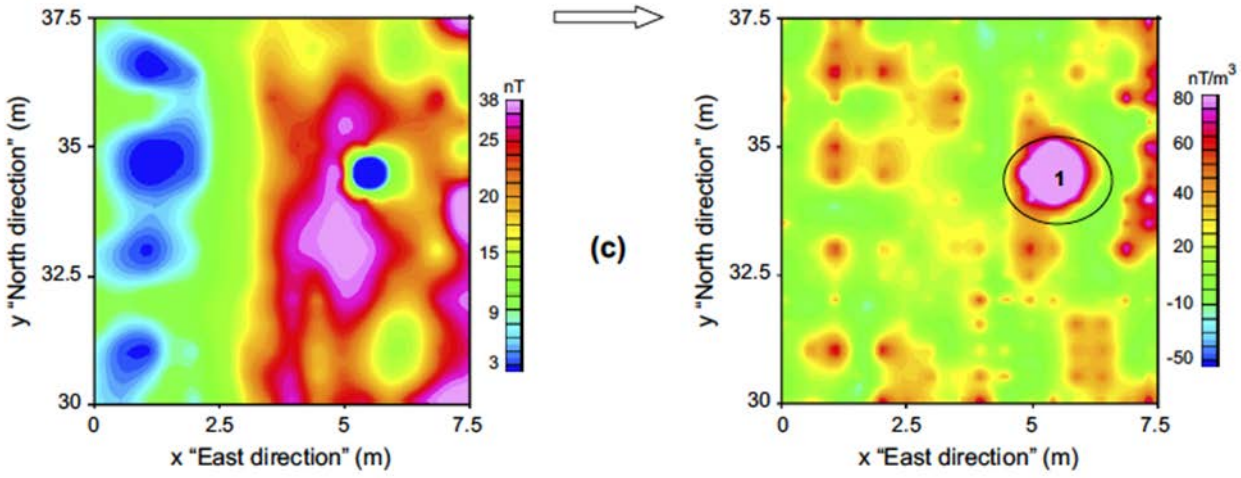

Figure 2-7 Magnetic anomaly maps from an archeological site in Turkey showing location of buried graves. Left panel shows observed magnetic anomalies. Right panel shows anomalies after data processing (from Arlsoy et al., 2007).

Although some success has been achieved by total magnetic field surveys made with portable magnetometers, gradiometer surveys are known to be most successful for finding artifacts and cultural features. Portable magnetometers can be modified to operate as a gradiometer. In gradiometer surveys, the gradient, or change in intensity with distance, is measured. To be useful, the measurement spacing must be small relative to the distance to the sources of the anomalies. Results of gradiometer surveys can be difficult to interpret, often because of noise sources in the near surface. For instance, the presence of daub or baked soil, commonly found at archeological sites such as those studied in the New Madrid seismic zone, can be hard to distinguish from clay-rich deposits or lenses. A preliminary investigation to determine the contrast in magnetic properties of the host sediment relative to a known cultural feature at the site is one approach for overcoming this problem. This approach can guide the choice of measurement spacing and subsequent interpretation of the data.

Electromagnetic Surveys: Electromagnetic surveys using ground conductivity meters have been used for paleoliquefaction studies and provide a rapid, easily used reconnaissance tool. Wolf (2004) used a Geonics EM31 at several sites in the New Madrid seismic zone. The EM31 generates a primary magnetic field via a transmitter coil, which in turn, produces eddy currents in the ground. These currents generate a secondary magnetic field that is measured by the receiver coil. The difference between the primary and secondary fields is a complex quantity reflecting the physical properties of the earth materials. The EM31 is limited by a fixed transmitter frequency and coil separation, resulting in little control over the imaging depth of the instrument. The measured value is a function of the material properties within about five meters of the surface. If the liquefaction features are large (e.g., sand dikes > 1 m wide) and the contrast between liquefaction deposits and host sediment is notable (see Figure 2.5), the instrument can provide useful information. For smaller features, the instrument does not provide adequate resolution, and it is best utilized for broad reconnaissance. Other EM instruments allow a range of transmitting frequencies or coil separations, which control the depth of imaging and might, consequently, yield better success with smaller features.

In summary, although there is a range of geophysical methods that can be used for site investigations, the choice of technique depends strongly on (1) the site geology, (2) the scale of the survey, (3) the resolution required (i.e., the estimated size and depth of liquefaction features), and (4) the presence of cultural features. To date, the most reliable techniques for imaging subsurface sand blows and sand dikes are ER and GPR; however, the limitations of each method should be considered in the context of the site characteristics. In general, the highest resolution is achieved with ER methods, whereas GPR affords faster data acquisition. At sites where clays are prevalent in the near-surface sediment, the penetration depth and resolving capability of GPR is very limited (possibly < 1 m) due to strong signal attenuation. Although ER also will suffer signal attenuation in the presence of near-surface clays (which can channel energy), the investigator can adjust the electrode configuration for improved imaging. At sites in which there is little contrast between the host sediment and that of the liquefaction features, the resolving ability of ER will be limited. In these cases, GPR may be superior for locating features such as sand dikes and vents, where the sedimentary layering has been disturbed by ground failure and dike intrusion, which cause scattering and diffraction of the transmitted energy. The optimal methodology for sites is a combination of the two techniques - GPR for initial reconnaissance and ER for detailed imaging. Magnetic methods (particularly gradiometry) are useful at sites that contain cultural features because pottery and other clay-rich artifacts have remanent magnetism. Geophysical imaging of liquefaction sites prior to trenching can help the investigator to identify relationships critical for interpreting liquefaction features, locate material for estimating the timing of the liquefaction-inducing earthquake, and minimize disruption of sensitive cultural deposits.

2.3.2.2 Paleoseismic Trenches

As mentioned above in Section 2.3.1, trenches are excavated in surface sand blows that are thought to hold the most promise for providing information about past earthquakes. Trenches are typically 1.5 to 2 m deep, depending on the thickness of the sand blow. To ensure safe working conditions, it is recommended that trenches in sandy soils have sloped walls at a horizontal to vertical ratio of 1.5:1, or be shored if walls are vertical. Stable trenches deeper than 2 m are not feasible in environments where the water table is fairly close to the ground surface. Trenches are usually excavated roughly perpendicular to the strike of the liquefaction feature, which is determined from aerial photography and/or satellite imagery, geophysical surveys, and field observations. It is recommended that the trenches be dug with a backhoe or excavator with a smooth-blade bucket, sometimes referred to as a sand bucket or mop-out bucket. A smooth-

blade bucket makes a clean cut in the bottom of the trench, making it easier to recognize features of interest and to clean the surface for further examination.

If there is a plow zone at the site, it is removed with the backhoe in thin, 2-5 cm thick, cuts until the base of the plow zone is reached. The contact with the underlying sand blow is carefully cleaned and examined for intruding root casts or cultural features such as post molds, pits, and wall trenches (Figure 2.8). Any intruding features are documented, photographed, and sampled. The excavation continues through the sand blow, with frequent cleaning and examination of the walls and floor and documentation of biological, cultural, and geological features encountered. This procedure is followed until the soil or sediment layer buried beneath the sand blow is reached. The contact of the buried soil or sediment layer is carefully examined for and samples collected of buried leaves, tree debris, tree trunks, and other organic materials. If cultural artifacts are found in the buried soil, backhoe excavation ceases and an archeological excavation, referred to as a test unit by archeologists, is planned and excavated by an archeologist. If no cultural artifacts are found in the buried soil, backhoe excavation continues as needed to reveal the feeder dikes of the sand blow.

Figure 2-8 Paleoseismic investigation at archeological site 3MS306 in the New Madrid seismic zone (NUREG/GR-0017). Contact between the plow zone and the underlying sand blow is carefully examined for features, such as cultural pits and tree-root casts, that may help to constrain the minimum age of the sand blow. Photograph by M. Tuttle.

After trench excavation is completed, trench walls are cleaned with shovels and trowels and logged at an appropriate scale (1" = 25 cm or 50 cm) depending on the complexity of the features (Figure 2.9). Logging, a fundamental technique employed in paleoseismic studies, requires careful observations and recording of crucial relationships. Logs are created of the trench walls, and sometimes the trench floor, by gridding the surfaces and measuring points of interest relative to the grid or by surveying points of interest using a total station. During logging, liquefaction features and their sedimentological, stratigraphical, and structural relations are studied. Liquefaction features are described in terms of size (i.e., width of dikes, and lateral extent and

thickness of sand blows and sills), orientation, vertical and horizontal displacements, sedimentary structures, cross-cutting relations, soil development, and stratigraphic context. Liquefaction-related ground failure and the amount of vertical and horizontal displacements are measured and described. The characteristics of the host sediment also are documented, including sediment type, bedding, thickness, lateral continuity, and soil development. Organic samples are collected for radiocarbon dating and sediment samples are collected for optically-stimulated luminescence (OSL) dating. The locations of the samples are carefully noted on the trench log.

During the excavations, artifacts collected by an archeologist are bagged and tagged according to provenance. Cultural features that intrude or are intruded by liquefaction features also are excavated. Later in the archeological laboratory, feature fill is processed by flotation to recover small artifacts and organic materials for radiocarbon dating. In addition, artifacts are described in terms of sherd sizes and types, lithic types and sources, and tool types. Information about the artifact assemblage of a site and results of radiocarbon and OSL dating are used to estimate the ages of liquefaction features. See Appendix E for archeological excavation protocol developed for paleoseismic investigations at archeological sites in Arkansas.

It is critical that the ages of the liquefaction features be well constrained if they are to be correlated across the region and used to estimate the source areas and magnitudes of the prehistoric events. Samples collected during site investigations, and during surveys of river cutbanks and other exposures as described below in Section 2.3.3, are later reviewed and the best samples selected for dating of the sand blows and sand dikes. To reduce uncertainties in radiocarbon ages, the accelerator mass-spectrometry (AMS) technique is recommended. Although more expensive than radiometric dating, AMS yields errors of only +/- 40 years. Various methods can be used to calibrate radiocarbon ages (e.g., Vogel et al., 1993; Stuiver et al., 1998). As described in Section 2.4.5, uncertainties in OSL dates can be quite large due to a variety of factors (LDRL, 2010). However, OSL dating can provide age control at liquefaction sites where organic samples needed for radiocarbon dating are not available. To narrowly constrain age estimates of individual liquefaction features, it is advisable to date multiple samples at each site. Furthermore, since paleoliquefaction studies are regional in scope, it is often necessary to date liquefaction features at many sites across the study area.

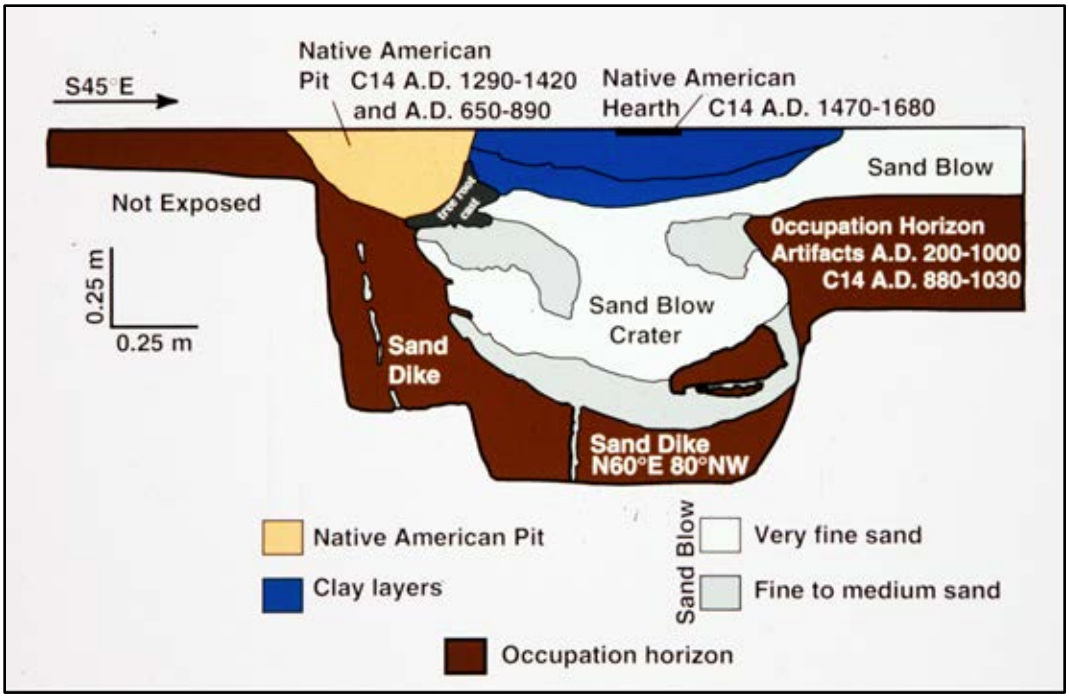

Figure 2-9 **(Above) Photograph of excavations and (Below) log of trench wall at archeological site 3MS306 in northeastern Arkansas, showing relationships between the sand-blow crater, sand blow, sand dikes, and Native American hearth, pit, and occupation horizon (from NUREG/GR-0017). Also shown are 2-sigma calibrated radiocarbon dates of organic samples collected from cultural features and horizon. On the basis of the artifact assemblage and radiocarbon dates, the earthquake-induced liquefaction features are estimated to have formed in A.D. 900 ± 100 yr.**

2.3.3 Surveys of River Cutbanks and other Exposures

Eroding river cutbanks, recently excavated drainage ditches, and active borrow pits provide exposures of Holocene and Late Pleistocene deposits in which liquefaction features may occur. Surveys of selected rivers, ditches, and borrow pits should be conducted when water levels are low and exposure is at an optimum. Where possible, it is recommended that surveys be conducted by motorboat or canoe so that a larger area can be surveyed in the time available.

During the river surveys, all exposures are carefully examined for the presence of liquefaction features and other deformation related to earthquakes. This often involves checking subvertical features, such as cracks and soil discontinuities, to determine if they are sand dikes. If the features appear to be sand dikes, they are tracked up section to determine if they terminate within the host deposit or if they are connected to sand blows (Figure 2.10).

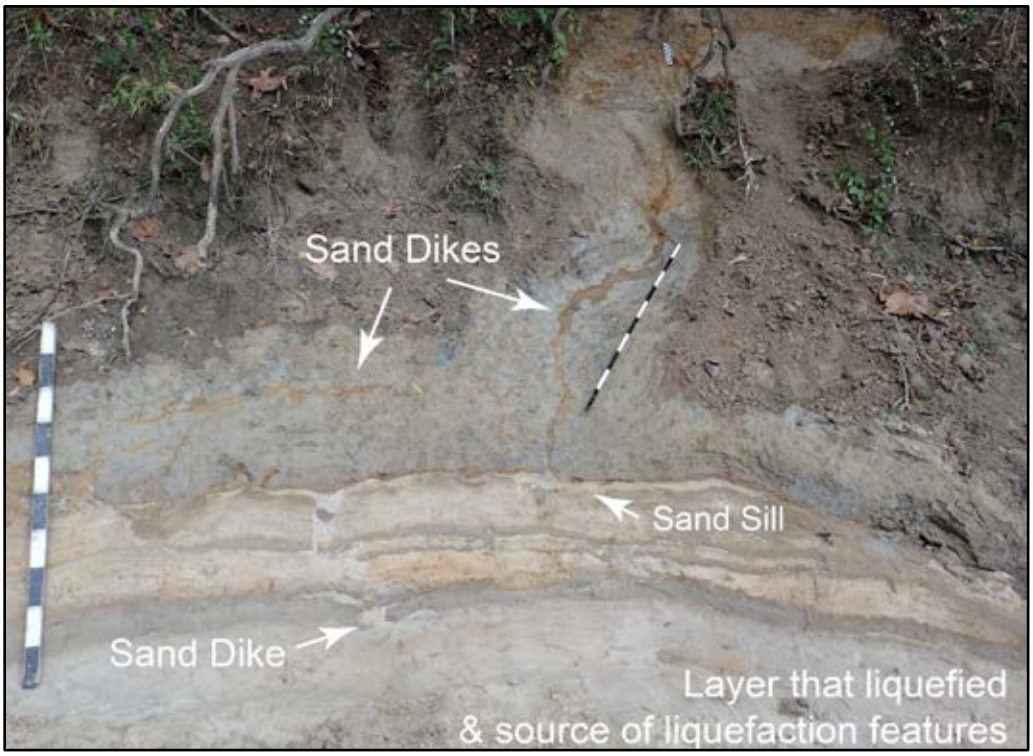

Figure 2-10 Earthquake-induced liquefaction features found along a river cutbank during reconnaissance in the region surrounding the New Madrid seismic zone. Note that the layer that liquefied is visible as well as the sand dikes and sill that intrudes the overlying deposits. One dike extends about 2 m up section and terminates near the top of the photograph. On the two larger scales, black and white intervals represents 10 cm; on smaller scale near dike tip, intervals represents 1 cm. Photograph by M. Tuttle.

As during trench investigations, liquefaction features are described in terms of their size (width of dikes, thickness and lateral extent of sand blows and sills), orientation, vertical and horizontal displacements, sedimentary structures, crosscutting relations, soil development, and stratigraphic context. The main liquefaction features, and their context and relationships, are photographed. Wood, charcoal, and other organic samples are collected for radiocarbon dating, and sediment samples are collected for OSL dating. It is often necessary to scrape the exposure with a trowel

or shovel to find organic samples in close association with liquefaction features, such as in soils buried by or developed in sand blows or near dike terminations. OSL samples are often collected at the contacts between the sand blows and the underlying soils or sediment in order to date the time of burial. The locations of liquefaction sites are measured with a global positioning system and marked on topographic maps. In addition, it is important to document the sedimentary conditions and amount of exposure where liquefaction features are not found.

2.4 Dating of Liquefaction Features

Liquefaction features are dated to estimate the ages of the paleoearthquakes that were responsible for their formation. It is important to constrain the ages of liquefaction features as narrowly as possible to differentiate closely timed events and to correlate similar-age features across a region. Sand blows usually provide the best opportunity for estimating the ages of paleoearthquakes with relatively small uncertainties, because it is often possible to determine both maximum and minimum age constraints for sand blows and thus bracket their age of formation (Figure 2.11; Tuttle, 2001). Close maximum age constraints can be determined by dating plant material, such as twigs and leaves, and sediment that was at or near the ground surface and buried by the sand blows at the time of the event.

Similarly, plant material derived from surface soils and incorporated in the vented deposits of sand blows and sand-blow craters also provides close maximum age constraints. In addition, minimum age constraints, and sometimes, close minimum age constraints, can be determined for sand blows and sand-blow craters. For example, a close minimum age constraint can be achieved by dating plant material and sediment that accumulated in craterlets in the upper surface of sand blows soon after they formed. More commonly, minimum age constraints come from dating plant material in soils that developed in the sand blows over time and from tree roots and cultural pits that extend down into sand blows from above (Figure 2.11).

Estimating the ages of sand dikes and sand sills usually involves greater uncertainty than for sand blows and sand-blow craters, because dikes and sills may terminate several meters below the ground surface at the time of the paleoearthquake (Figures 1.12 and 2.10; Tuttle, 2001). Maximum age constraints can be determined by dating the uppermost stratigraphic units that the dikes crosscut or the sills overlie, but these ages may be hundreds to thousands of years older than the liquefaction feature (Tuttle et al., 1999). Minimum age constraints of dikes and sills can be determined by dating roots, animal burrows, and cultural pits that clearly intrude and postdate the liquefaction features or by dating deposits that overlie unconformities truncating the liquefaction features. However, it is fairly uncommon to find circumstances such as these that help to constrain the minimum age of dikes and sills (Tuttle, 2001). Therefore, age estimates of sand dikes and sills often have large uncertainties. Some investigators will make educated guesses as to the ages of these types of liquefaction features based on weathering characteristics of the features themselves or the approximate age of the deposits in which they occur. There can be large uncertainties on the order of thousands of years in these estimates.

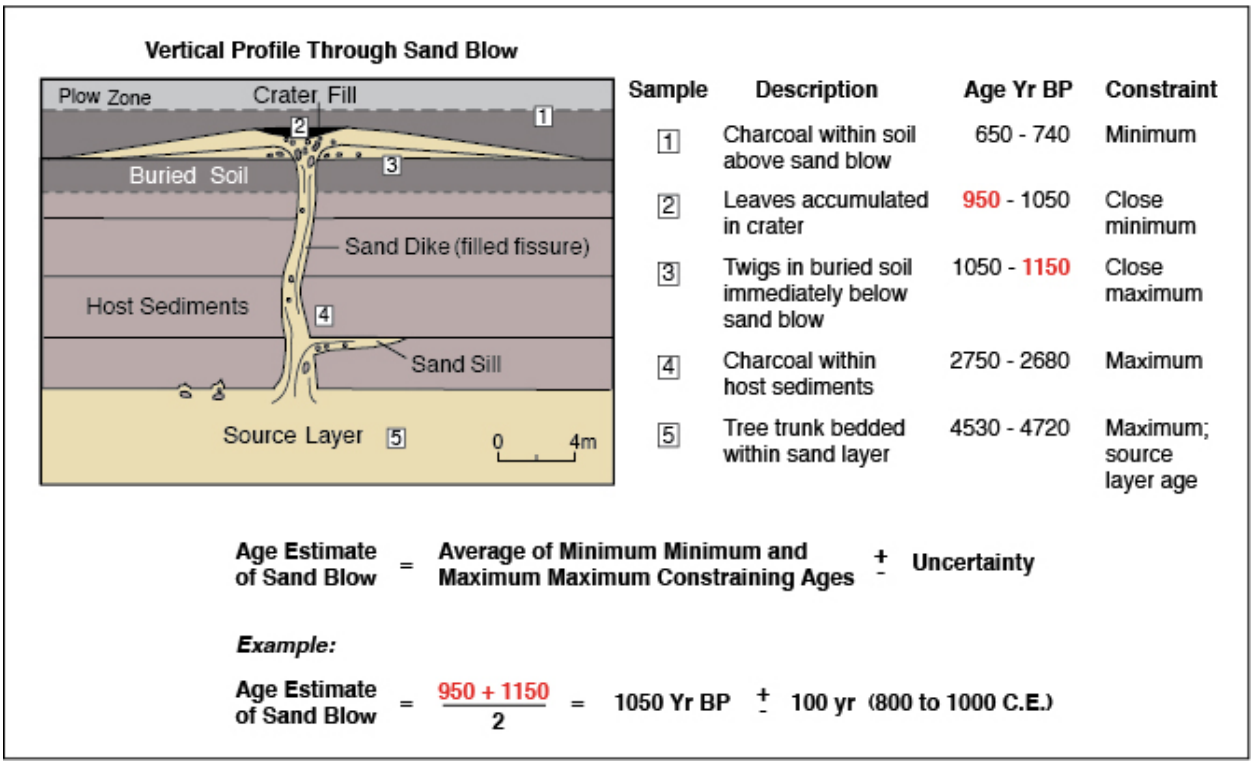

Figure 2-11 Diagram illustrating sampling strategies and age estimation of liquefaction features (after NUREG-2115).

Pseudonodules, load casts, and related folds typically form close to the sediment-water interface at the time of sediment deposition (Sims, 1975). Age estimates and related uncertainties for causative earthquakes can be derived by dating the deformed sediment itself or by dating plant material above and below the deformed sediment. There often are much larger uncertainties in estimating the ages of sand diapirs and foundered clasts because these soft-sediment deformation structures may have formed anytime following deposition of the stratigraphic units involved. Maximum age constraints can be established by dating the deformed deposits, but the deformation may be hundreds or thousands of years younger than the deposits.

A variety of dating techniques are used in paleoliquefaction studies (Table 2.1). A brief summary of the most commonly used dating techniques is provided below.

2.4.1 Soil Development and Weathering Characteristics

The state of a soil system is defined as a function of five soil-forming factors: climate, biological activity, topography, parent material, and time (Jenny, 1941, 1961; Birkeland, 1999). In genetically related suites of soils in which all soil-forming factors except for time are about equal, soil profiles, as well as certain soil properties, develop systematically with age (Harden, 1982; Harden and Taylor, 1983). These soil properties include rubification (i.e., reddening and brightening of soil colors), clay and organic accumulation, soil structure, consistence, and pH. Therefore, soil profiles and properties can be used to estimate the age of a soil if they are calibrated with numerical techniques, such as radiocarbon dating and OSL dating as described below in Sections 2.3.4 and 2.3.5 (Table 2.1).

Table 2-1 Summary of dating techniques used in paleoliquefaction studies (after NUREG-2115).

Dating Technique	Applicable Time Period (Years BP)	Dating Precision (Years)	Applied in CEUS Regions[1]	Selected References[2]
Soil development	1–100,000+	Varies with soil property	(1) NMSZ	(1) NUREG/GR-0018
Stratigraphic context	1–100,000+	100's–1,000's	(1) NMSZ (2) WVSZ	(1) Tuttle, 1999 (2) Hajic et al., 1995; Munson and Munson, 1996
Archeological context	1–12,000	10's–1,000's	(1) NMSZ (2) STL (3) WVSZ	(1) NUREG/GR-0018; Tuttle et al., 2005, 2011 (2) Tuttle, Chester, et al., 1999 (3) Munson and Munson, 1996
Radiocarbon	1–50,000	10's–100's	(1) NMSZ (2) MAR (3) STL (4) WVSZ (5) ALM (6) CSZ (7) AC-CVA (8) NEWBURY (9) CxSZ	(1) Tuttle et al., 2005b (2) Tuttle et al., 2006 (3) Tuttle, Chester, et al., 1999 (4) Munson and Munson, 1996 (5) Cox, Larsen, et al., 2004 (6) Talwani and Schaeffer, 2001 (7) Obermeier and McNulty, 1998 (8) Tuttle and Seeber, 1991 (9) Tuttle and Atkinson, 2010
Optically stimulated luminescence	100–700,000	10's–1,000's	(1) NMSZ (2) MAR (3) WVSZ (4) ALM	(1) Mahan et al., 2009 (2) Tuttle et al., 2006 (3) Mahan and Crone, 2006 (4) Cox, Larsen, et al., 2004
Dendro-chronology	1–1,000s	Annual, possibly seasonal	(1) NMSZ	(1) Van Arsdale et al., 1998; Tuttle, 1999

1. NMSZ = New Madrid seismic zone and surrounding region; MAR = Marianna Area; STL = St. Louis and surrounding region; WVSZ = Wabash Valley seismic zone and surrounding region; ALM = Arkansas-Louisiana-Mississippi region; CSZ = Charleston seismic zone; AC-CVA = Atlantic Coast and Central Virginia reconnaissance; NEWBURY = Newburyport, Massachusetts, and surrounding region; CxSZ = Charlevoix seismic zone and surrounding region.
2. Selected references shown here. See references at end of report.

In most paleoliquefaction studies, soil development is used as a relative dating technique to distinguish young, unweathered features from significantly older, weathered features. In the New Madrid seismic zone, for example, the thickness of A soil horizons developed in sand blows has been used to distinguish paleoliquefaction features from those that formed during the 1811-1812 earthquake sequence and to estimate the age of prehistoric sand blows (NUREG/GR-0018). The age estimates are based on a rate of A horizon development derived from measurements of A horizon thickness of sand blows whose ages were determined by radiocarbon dating. Age estimates derived in this manner typically have uncertainties on the order of 100-200 years, similar to the uncertainties of radiocarbon dating on which the rate of A horizon development is based.

In a few regions where sand dikes have terminated within the stratigraphic section and organic material and cultural artifacts have not been available for constraining the ages of the features, soil characteristics such as iron staining and accumulation of fine-grained sediment have been

used to correlate features over large distances. This practice is not recommended unless the soil characteristics have been calibrated and the uncertainties associated with their rates of development quantified. Otherwise, the spatial correlation of features and the interpretations related to the spatial distribution of those features may be erroneous (Tuttle, 2001).

2.4.2 Stratigraphic Context

Stratigraphic context and relationships can be used as a means to estimate the relative ages of buried sand blows and sand dikes, and to correlate paleoliquefaction features between exposures. The law of superposition, crosscutting relationships, and identification of paleosurface indicators preserved in the stratigraphic record can be used to help determine the relative ages of paleoliquefaction features. Moreover, in an area with laterally continuous stratigraphy or prominent marker beds, age equivalence can be established between different exposures or sites. If the ages of some or all of these continuous strata are determined by numerical or other means at one site, these ages can be extrapolated to other nearby sites. However, correlation of paleoliquefaction features identified in similar-age deposits is potentially problematic. For example, most of the mid- to late-Holocene sand-blow craters identified in the Charleston, South Carolina, region are found in beach ridge deposits that are 100 ka and older (McCartan et al., 1984). If only the host deposits had been used to correlate and date paleoliquefaction features, the timing of the events may have been overestimated and the number of paleoearthquakes underestimated. Ages derived through other methods reveal that earthquakes separated by a significant time period have produced paleoliquefaction features within correlative stratigraphic units.

In addition, stratigraphic context and relationships can be used to place maximum ages on, for example, sand dikes that terminate upward at a stratigraphic level that may be lower than the paleo-ground surface at the time of the causative earthquake (Figures 1.12 and 2.11). Sand dikes that terminate below the event horizon, or a horizon that represents the ground surface at the time of the earthquake, commonly are encountered outside of active seismic zones and at greater distances from the seismic source than sand blows. By numerical or relative dating of the host deposits, it is possible to place at least a maximum age constraint on the timing of dike formation (Figure 2.11).

Although stratigraphic context can be used to estimate the relative ages of paleoliquefacion features, this approach is typically less precise and less accurate than numerical dating techniques. Therefore, it should be calibrated using radiocarbon or OSL numerical dating methods where possible. Even so, uncertainties in age estimates of paleoliquefaction features based on their stratigraphic context are likely to be on the order of several hundreds to several thousands of years at best (Table 2.1).

2.4.3 Archeological Context

Regional archeological chronologies are developed primarily on the basis of two methodologies: (1) seriation, or the sequence of artifact and ceramic types particularly within cultural horizons and (2) radiocarbon dating of organic material associated with artifacts and cultural horizons (Aiken, 1990; Morse and Morse, 1983; O'Brien and Lyman, 1999). Artifacts found at liquefaction sites can help to estimate the ages of the liquefaction features (Saucier, 1991; Tuttle and Schweig, 1995; Lafferty, 1996; Munson et al., 1997). Some artifact types are narrowly tied to specific cultural periods while others are not. Age estimates of liquefaction features based on their archeological context will have uncertainties at least as great as those based on radiocarbon dating (Tuttle, 2001; Table 2.1).

Cultural artifacts found in, or associated with, liquefaction features during reconnaissance can provide a preliminary estimate of the ages of the features. The stratigraphic relationships between liquefaction features and cultural features and horizons, as well as the assemblage of artifacts (especially if diagnostic artifact types are present) can help to further constrain the ages of the liquefaction features (e.g., Tuttle et al., 1996, 2005, and 2011). For example, the assemblage of artifacts within an A soil horizon buried by a sand blow can provide an estimate of the maximum age of the liquefaction feature (Figures 2.9 and 2.12; Tuttle et al., 1999). The assemblage of artifacts within an occupation horizon developed in a sand blow or cultural features, such as a storage pit or wall trench dug into a sand blow, can provide an estimate of the minimum age of the sand blow (Table 2.2). It is important to study assemblages of artifacts at a site since there are still many uncertainties regarding the temporal and geographical ranges of artifact types.

Due to the common abundance of organic-rich material, archeological sites often provide good opportunities for finding samples suitable for radiocarbon dating and constraining the age(s) of any liquefaction feature that is present. In these cases, it is desirable to conduct both archeological analyses and radiocarbon dating of organic samples to provide a means of independently verifying results and add confidence to the age estimates of liquefaction features.

The archaeological context of a sand blow or sand dike is defined by the presence of artifacts and/or cultural features that may occur stratigraphically above, below, or within the geologic feature. In the broadest sense, an artifact is an object that has been modified by human beings. This can range from bringing an object, such as a cobble from a river, onto a site, to building large structures such as long houses and bridges. Portable artifacts are divided conceptually by some theoreticians (i.e., Taylor, 1948) into two categories: (1) intentionally produced artifacts, such as knives, projectile points, pottery, and (2) cultural debris, such as the flakes produced when making a projectile point, bones from a meal, or seeds that were charred by cooking. All of these artifacts incorporated into the soil matrix make up the archaeological site or a stratum at the site. On intensively occupied sites, there will often be 100s or even 1,000s of square meters of continuous matrix of archaeological deposits, which are called sheet middens.

Cultural features are constructed (e.g., mounds, burials, hearths, house walls, trash pits, and pottery kilns) or are large accumulations of artifacts (e.g., a midden, stone tool quarry, pottery waste piles). Unlike artifacts, cultural features cannot be removed from the field as a single entity. Instead, they must be carefully documented before and as they are recovered via excavation. Features are time capsules that often contain deposits from a short duration of time, usually on the order of decades. Pits and postholes are generally the most common feature types encountered on prehistoric archaeological sites. Most pits manifest as dark stains in the host deposits. These deposits often have an abundance of small charred seeds, as well as wood and nut fragments ranging in density up to hundreds or even thousands per liter. These remains are dateable and many are identifiable to a species. Moreover, the seeds and nut fragments are annuals and provide radiocarbon dates with small standard deviations.

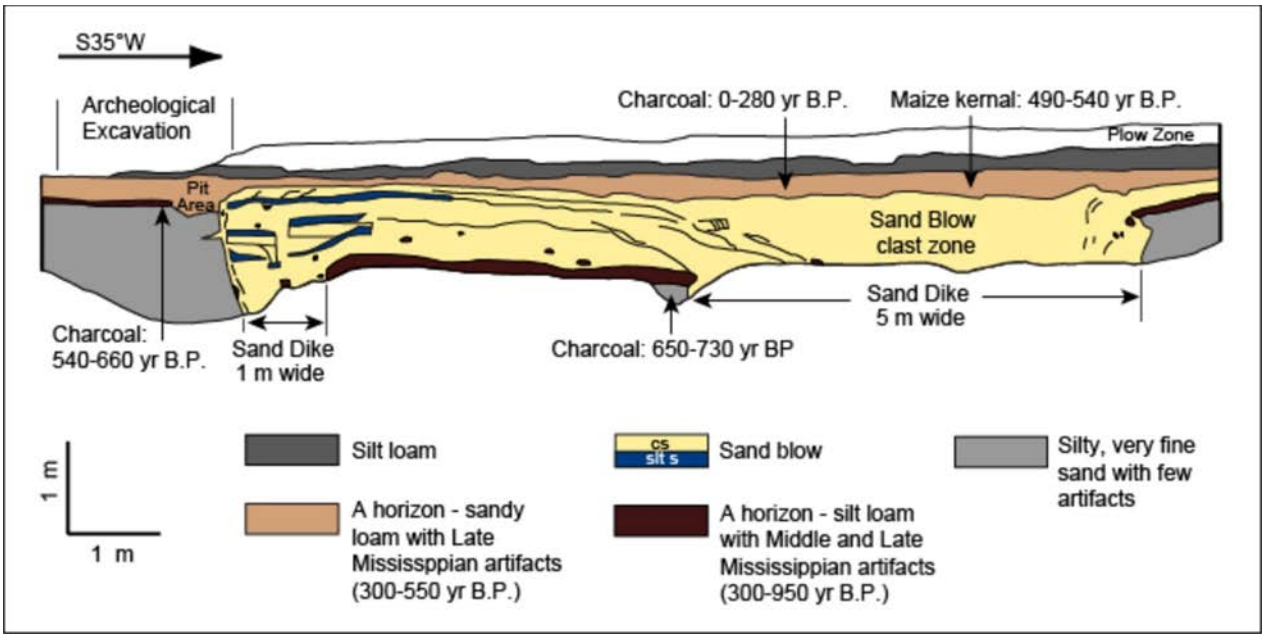

Figure 2-12 Log of sand blow and uppermost portions of related sand dikes exposed in a trench wall at the Dodd site in the New Madrid seismic zone (after NUREG-2115). Sand dikes were also observed in trench floor and opposite wall. Radiocarbon dating of charcoal from a pit in soil below the sand blow and a maize kernel from a cultural feature excavated in the top of the sand blow bracket the age of formation of the sand blow between 490 and 660 yr B.P. Artifacts in the A horizon buried by the sand blow and in the A horizon developed in the top of the sand blow indicate that the sand blow formed during the late Mississippian cultural period (300-550 yr B.P. or A.D. 1400-1670).

Diagnostic artifacts, such as pottery, projectile points, and axes, change through time. For example, from about 200 B.C to A.D. 400, Native Americans in the Lower Mississippi Valley begin producing fabric-decorated, grog-tempered ceramic wares (Table 2.2; Morse and Morse 1983 and 1996). From about A.D. 400 to 1000, cord marked and plain pottery predominate. After about A.D. 1000, potters consistently added shell as a tempering agent to their ceramic paste. During the succeeding 600 years, scores of decorative techniques were used. Many of these ceramic types have been dated in their archaeological context and the occurrences and relative frequencies of ceramic types can be used for establishing the general age of a site.

Plant remains that commonly occur at cultural sites also can help to constrain the age of liquefaction features, and thus paleoearthquakes. From about 1000 B.C. until historic time, the eastern North American Indians cultivated a variety of plants. During the early part of this development, Native North American seed plants, including goosefoot/lambs quarter (*Chenopodium berlandiera*), sunflower may grass (*Phalaris carolina*), little barley (*Hordeum pusillum*), knot weed (*Polygonum erectum*), sunflower (*Helianthus annuus*), and sumpweed (*Iva annua*), dominated. Later, tropical cultivars from Mesoamerica (i.e., southern Mexico and Guatemala) were added and proliferated. Remains of tropical plants, most notably maize (*Zea mays*), beans (*Phaseolus vulgarius*), and squash (*Cucurbita spp*.), occur only in trace amounts in cultural assemblages dating to about 1000 B. C. After about 400 B.C., however, the quantity of tropical cultivars increased, and by A. D. 1100, they dominated the botanical assemblages.

Changes in botanical assemblages such as these allow for fairly accurate (+/- 200 years) age estimates of the feature or horizon from which plant remains are collected.

Table 2-2 Cultural periods, time spans, and associated diagnostic artifacts (from Tuttle et al., 2005b).

Cultural Periods	Years (A.D./ B.C.)	Diagnostic Artifacts
Historic	A.D. 1673[1]- present	Iron, glass, glazed pottery, plastic
Late Mississippian	A.D. 1400-1673	Shell-tempered pottery - Parkin Punctate, Campbell Applique, Matthews Incised, Bell Plain, and Memphis rim mode; Nodena points
Middle Mississippian	A.D. 1000-1400	Shell-tempered pottery - Parkin Punctate and Old Town Red (exterior slipped); Madison points
Early Mississippian	A.D. 800-1000	Pottery transition - shell-tempered pottery, Varney Red Filmed pottery (interior slipped) and mixed temper wares; Madison points
Late Woodland	A.D. 400-1000[2]	Cordmarked and plain, sand- (Barnes) and grog- (Baytown, Mulberry Creek) tempered pottery; Madison points and Table Rock Stemmed points
Middle Woodland	200 B.C.-A.D. 400	Sand- and grog-tempered pottery; dentate, stamped, and fabric-marked pottery;
Early Woodland	500-200 B.C.	Punctated pottery; baked clay objects
Late Archaic	3000-500 B.C.	Stemmed projectile points; baked clay objects

1. Dougan, 1995.
2. Morse and Morse (1983 and 1996) use A.D. 400-700. Radiocarbon dating performed for paleoliquefaction sites indicates Late Woodland period extends to A.D. 1000.

2.4.4 Radiocarbon Dating

Radiocarbon dating, or 14C dating, is the most common dating technique used in paleoliquefaction studies (Table 2.1). Although reliable for only the past 50,000 years, radiocarbon dating is useful for the time period of interest for most paleoseismic studies. Uncertainties in the results are related to the dating techniques, to conversion of radiocarbon ages to calibrated ages, and to sampling of materials that are used in dating liquefaction features.

Two different radiocarbon dating techniques are used, depending on the size of the sample (Aiken, 1990). The radiometric technique is used for larger samples (e.g., charcoal ≥ 15 grams, wood ≥ 25 grams, and soil ≥ 200 grams) and the accelerator mass spectrometry (AMS) technique is used for smaller samples (charcoal ≥ 20 milligrams, wood ≥ 20 milligrams, and soil ≥ 2 grams). Using the radiometric technique, a precision of better than ± 1%, corresponding to ± 80 radiocarbon years, can usually be achieved for samples that are less than 10,000 years in age. High-precision measurements can be made on wood samples of ≥ 1 kilogram by measuring the beta activity of the sample in a proportional gas counter (Stuiver et al., 1998). For these very large samples, a precision ± 0.25%, corresponding to ± 20 radiocarbon years, can be obtained. With the AMS technique, precision of about ± 0.5%, corresponding to ± 40 radiocarbon years, can be achieved. Although more expensive, the AMS technique is more often used in paleoliquefaction studies because of its higher precision.

Radiocarbon dating results are reported as both measured and conventional 14C ages. Conventional ages are derived from measured ages by normalizing them to the modern standard through the use of 13C/12C ratios. 14C in the atmosphere has fluctuated over time due to variations in cosmic radiation and, recently, to burning of fossil fuels and testing of nuclear devices (Stuiver et al., 1993). Therefore, it is desirable to convert conventional ages to actual or calendar years by using the radiocarbon calibration curve (Figure 2.13; Tuttle, 1999). Although the recent part of the curve (12 k.y. or thousand years) based on tree-ring records is the most reliable, the calibration curve now extends to 50 k.y. B.P. (Walker, 2005; Reimer et al., 2009). Calibration procedures that are commonly used in paleoliquefaction studies and that yield similar results include CALIB, OxCal, and Pretoria (Stuiver and Reimer, 1993; Talma and Vogel, 1993; Vogel et al., 1993; Bronk Ramsey, 1995 and 2001; and Stuiver et al., 2005). It is preferable to use 2-sigma calibrated dates to either bracket or approximate the ages of the liquefaction features. This assures with a high probability that the actual ages of the liquefaction features fall within the estimated age range. Calibrated ages rarely have 2-sigma ranges of less than 100 years, more often have 2-sigma ranges of about 200–300 years, and sometimes have two or three ranges depending on the number of intercepts of the conventional radiocarbon age with the calibration curve.

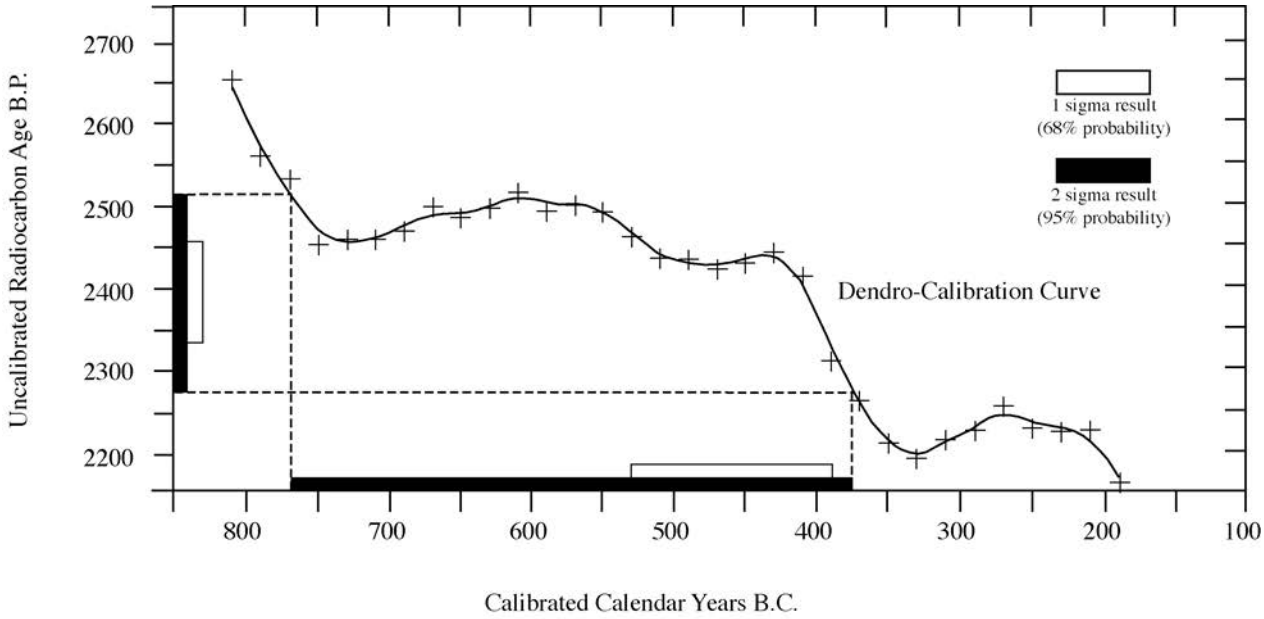

Figure 2-13 Portion of dendrocalibration curve illustrating conversion of radiocarbon age to calibrated date in calendar years. For example, 2-sigma radiocarbon age of 2,280-2,520 BP is converted to calibrated date of 770-380 BC (from Tuttle, 1999).

The type and location of samples collected for radiocarbon dating affect the uncertainty of the age estimate of the liquefaction features. Plant remains that occur in close stratigraphic position to a sand blow will fairly closely reflect its age. For example, leaves or burned wood that occur at the contact of a buried soil horizon and an overlying sand blow would provide a close maximum age constraint for the sand blow. Similarly, maize kernels, leaves, or burned wood incorporated into the top of a sand blow would provide a close minimum age constraint (Figures 2.9 and 2.12). In contrast, a piece of charcoal within the buried soil or underlying sediment would provide a maximum age constraint, but could be hundreds or even thousands of years older than the sand blow. Unless associated with in situ cultural or biological features such as fire pits and tree trunks,

a charcoal sample could be reworked, in which case its age relationship to the sand blow would be even more uncertain.

Bulk samples of soils buried by or developed in sand blows can also be dated. However, radiocarbon dates of soils reflect the mean residence time of carbon in those samples (Trumbore, 1989; Walker, 2005). Also, contamination by young (e.g., modern humic acids) and old (e.g., lignite and calcium carbonate) carbon can be a significant problem in soils. Therefore, dating soils is usually a last resort and requires a sampling strategy to help minimize the uncertainties (Tuttle, 1999).

2.4.5 Optically-Stimulated Luminescence

Luminescence techniques, including OSL dating, provide an estimate of the time since quartz and feldspar grains were last exposed to light, which sets the luminescence signal to zero. OSL dating is a type of radiation exposure dating that determines the age of a deposit based on its last exposure to light or intense heat (>150 °C). When a mineral is exposed to naturally occurring radiation, electrons accumulate at defects within the crystal lattice, or "electron traps". Exposure to light will free electrons from light-sensitive traps, a process referred to as bleaching. Bleaching serves to reset the clock, and the mineral will not begin to accumulate trapped electrons until deposition and burial. Ideally, all sediment grains will be reset at the time of deposition (Duller, 2008; Rhodes, 2011). In other words, OSL is a numerical method used to determine the amount of time that has passed since sediment was last exposed to light. OSL can be used to estimate the ages of sand blows, and thus their causative earthquakes, by dating sediment that pre- and post-dates sand blows (Mahan and Crone, 2006; Tuttle et al., 2006; Mahan et al., 2009).

OSL dating can be employed in a variety of terrestrial stratigraphic settings, can date sediment 100 years to <700,000 years old, and is particularly useful for dating sediment that receive brief exposure to sunlight prior to deposition (Table 2.1; Lian and Roberts, 2006; Duller, 2008; Rhodes, 2011; LDRL, 2010). Uncertainties in OSL dates are increased according to the variations in the population of equivalent doses that are measured from the grains of the deposit. The preferred grain size of sediment for OSL dating is coarse silt to medium sand (quartz or feldspar) that has had at least one to two minutes of sunlight exposure. Quartz is preferred to feldspar if the deposit has had limited exposure to sunlight and is not older than 150,000 years.

There are multiple sources of uncertainty that can limit the accuracy of OSL dating. The most common problem is that the sediment has not received enough sunlight exposure prior to burial in order to rid the sample of previously acquired luminescence (Lian, 2007). In addition, silt and sand grains that are coated with clay during their erosional travel path may be shielded from the bleaching effects of sunlight. Because cosmic radiation often fluctuates and attenuates quickly with depth, uncertainties in the depositional elevation of the sediment sample also may contribute to the uncertainty in the resulting OSL age estimates. In addition, the accuracy of OSL dating may be limited by estimates of past water content in the deposit (e.g.. water table fluctuations and disequilibrium in the U series, etc.) because of the radiation-absorbing characteristic of water.

To minimize the impact of the sources of uncertainties described above, it is preferable that OSL samples come from a relatively homogeneous stratigraphic unit that is at least 30 cm thick, and has not undergone significant bioturbation, water-content variations, or diagenetic changes following burial (LDRL, 2010). Therefore, careful selection and sampling of sediment are crucial as well as early guidance on sampling techniques and sample handling from the luminescence dating facility.

2.4.6 Dendrochronology

Dendrochronology is the dating of past events through the study of the tree ring records. This technique was first developed to date prehistoric timbers of pueblos in the southwestern U.S. and later used to date historic log cabins and prehistoric waterlogged wood in the east (Douglass, 1936). As trees grow, they add annual growth bands, or rings, to their circumference. Tree ring width varies from species to species and from year to year depending on the amount of annual rainfall and other environmental factors. Therefore, tree-ring chronologies are both species and region specific. Master chronologies are constructed by starting with tree-ring sequences for modern trees and adding antecedent and overlapping sequences back through time (Douglass, 1941; Pierce, 1986; Stahle et al., 1985). Dating a sample of an ancient tree is accomplished by matching the sequence of rings with the master chronology. It is desirable to have a sequence of one hundred rings for dating purposes. Accurate dating of the death of a tree requires having the exterior ring of the specimen.

Dendrochronology has the potential to date paleoearthquakes to the year and even the season (Table 2.1; Pierce, 1986; Stahle et al., 2004). For example, trees killed by coseismic subsidence along the coast of Washington State helped to provide exact dates of megathrust earthquakes along the Cascadia subduction zone (Atwater et al., 2004). In the New Madrid seismic zone, bald cypress in Reelfoot Lake in westernmost Tennessee showed a dramatic increase in ring width following the 1811-1812 earthquakes; whereas bald cypress in the St. Francis sunkland in northeastern Arkansas showed decreased ring widths for about 45 years following the earthquakes (Figure 2.14; Van Arsdale et al., 1998). Enhanced growth of bald cypress in Reelfoot Lake is attributed to increased water depth resulting from subsidence. Suppressed growth of bald cypress in the St. Francis sunkland is thought to be due to tissue damage inflicted by earthquake shaking.

So far, dendrochronology has been used very little in paleoliquefaction studies but it has the potential to better constrain age estimates of paleoearthquakes, especially in regions where liquefaction-related ground failures were severe (Table 2.1). Abrupt changes in soil-moisture conditions due to liquefaction-related subsidence of the ground surface and/or burial by thick sand blows, as well as disruption of tree root systems by lateral spreading, may affect tree ring growth and even lead to tree death (Figure 2.15; Tuttle, 1999). Therefore, trees buried and preserved below sand blows may provide accurate dates of paleoearthquakes. Before dendrochronology can be used to date paleoliquefaction features, however, regional chronologies that extend beyond the historic period must be developed for long-lived tree species.

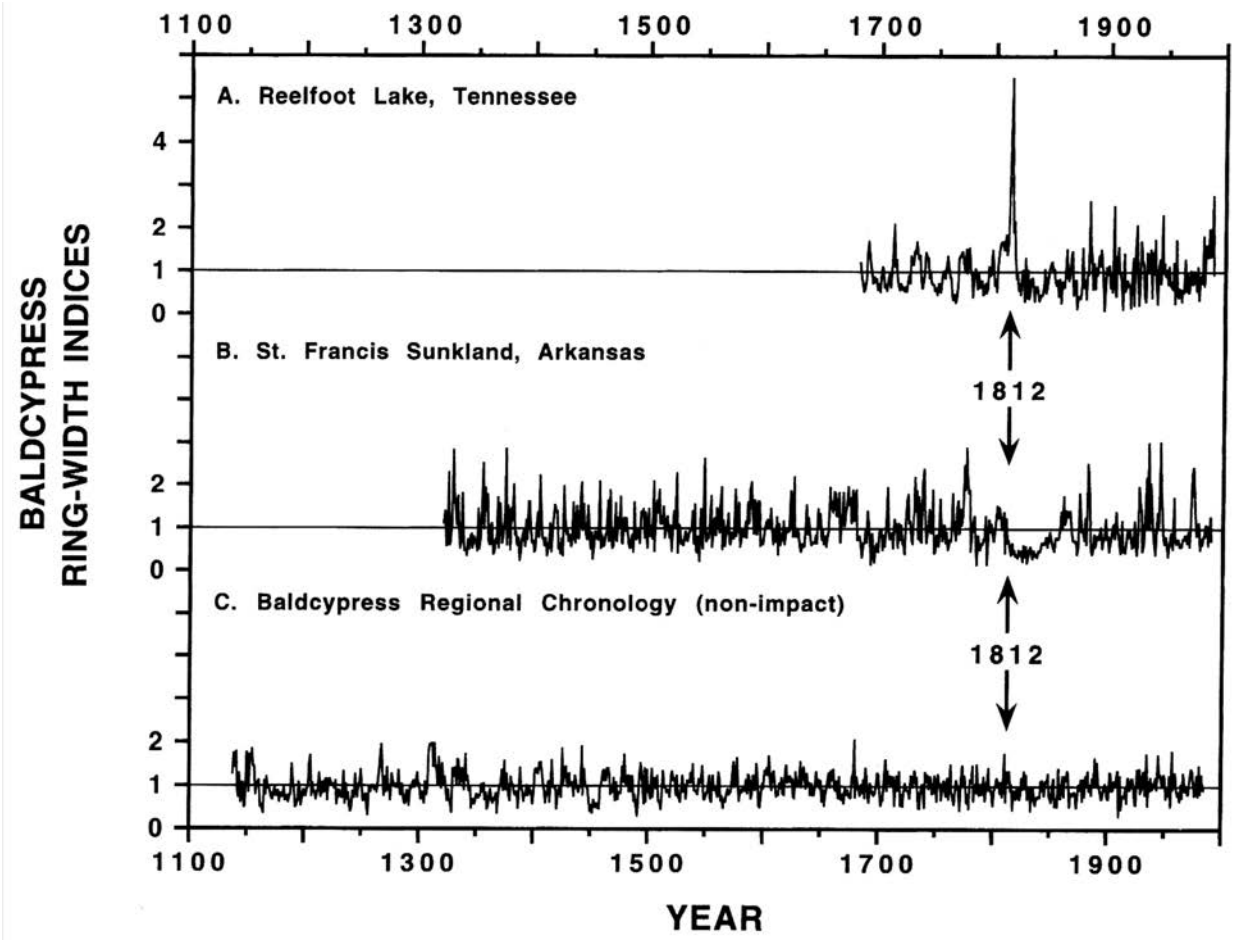

Figure 2-14 **Bald cypress tree-ring chronologies from Reelfoot Lake, Tennessee (A), St. Francis sunkland, Arkansas (B), and regional chronology based on four bald cypress chronologies in central Arkansas (C). Note growth surge at Reelfoot Lake that peaked in 1814 and prolonged growth suppression at St. Francis sunkland following New Madrid earthquakes of 1811-1812 (from Van Arsdale et al., 1998).**

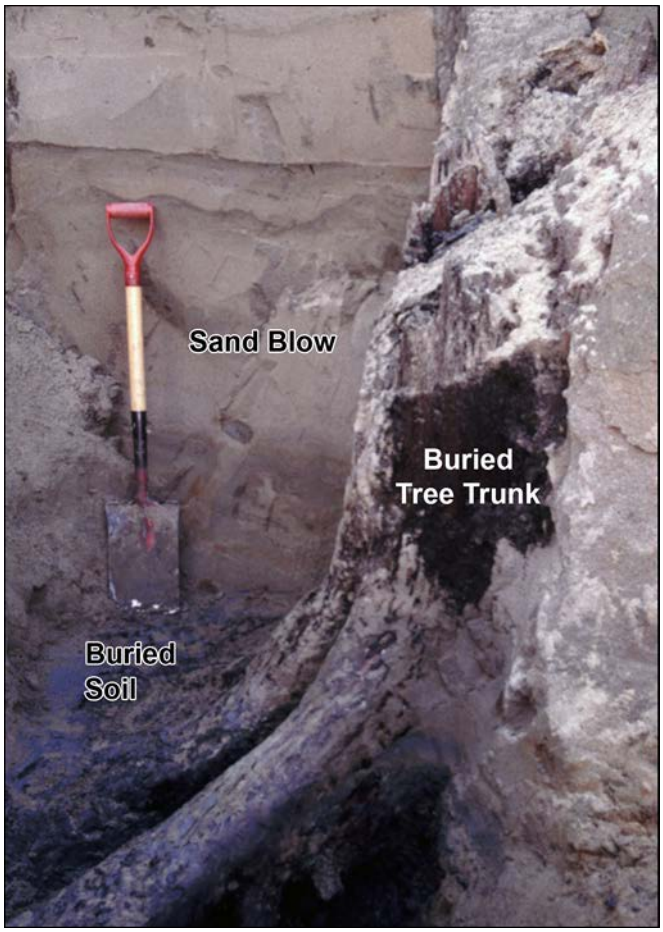

Figure 2-15 ***In situ*** **tree trunk buried, and likely killed, by sand blow deposit in the New Madrid seismic zone presents opportunity to date paleoearthquakes to the year and even season of occurrence. For scale, shovel is 1 m long. Photograph by M. Tuttle.**

2.5 Interpretation of Liquefaction Features

Following field studies and dating of samples found in association with liquefaction features, interpretations are made regarding the ages of the features and the timing of causative earthquakes, the source areas and magnitudes of paleoearthquakes, and the recurrence times of large earthquakes and long-term behavior of earthquake sources. These interpretations are based on information about the locations, sedimentary and structural characteristics, and sizes of liquefaction features, as well as their archeological and stratigraphic context, and results of radiocarbon and OSL dating of liquefaction features. There are numerous factors that contribute to uncertainties in earthquake parameters (timing, location, magnitude, and recurrence time) interpreted from liquefaction features. However, these uncertainties can be reduced by conducting a broad and balanced field program, by making careful and thorough field observations, by collecting samples to constrain the ages estimates of liquefaction features, and by wisely employing analysis tools in the interpretation of liquefaction data (Table 2.3).

Table 2-3 Uncertainties related to interpretation of paleoearthquake parameters (from NUREG-2115).

Earthquake Parameter	Range in Uncertainty	Factors that Contribute to Uncertainty	Observations and Analyses that Reduce Uncertainty
Timing	10's–1,000's of years	(1) Dating of liquefaction features (2) Use of sand dikes in absence of sand blows	(1) Well-constrained age estimates of liquefaction features (2) Space-time diagrams (3) Statistical analysis of uncertainty range of age estimates of multiple liquefaction features
Location	Few–100's of km	(1) above (2) Correlation of features across region (3) Size and spatial distribution of contemporaneous features a. Style of faulting b. Earthquake source characteristics c. Directivity of seismic energy d. Attenuation and amplification of ground motion e. Relative density of sediment f. Distribution of liquefiable sediment g. Water table depth (4) Field sampling and exposure	(1) through (3) above (4) Size distribution of features (5) Information regarding uncertainty factors (3a) through (3g). (6) Field studies conducted where sedimentary and hydrologic conditions suitable for formation and preservation of liquefaction features, and when adequate exposure available to find features, if present (7) Comparative study with calibration event in same region (8) Relationship to active fault
Magnitude	0.25–1+ unit	(1) through (4) above (5) Epicentral distance to farthest sand blow unlikely to be known (6) Changes in source sediment due to liquefaction or to postliquefaction effects such as cementation and compaction	(1) through (8) above (9) Empirical relations based on global database of earthquakes that induced liquefaction (10) Evaluation of scenario earthquakes using liquefaction potential analysis
Recurrence time	10's–1,000's of years	(1) Uncertainty in timing of paleoearthquakes (2) Completeness of paleoearthquake record in space and time	(1) Well-constrained age estimates of paleoearthquakes (2) Space-time diagrams (3) Consideration of history of sedimentation and erosion as well as of changes in water table

2.5.1 Correlation of Liquefaction Features

Correlation of liquefaction features is an important and necessary step in the interpretation of the timing, location, and magnitude of paleoearthquakes. Correlation of liquefaction features is based on available information, including one or more of the following (from NUREG-2115):

- Chronological control: Paleoearthquakes are distinguished based on grouping paleoliquefaction features that have overlapping age estimates. As described above in

Section 2.4, sand blows are best to use because the event horizons are more easily identified and their age estimates are usually better constrained, whereas the event horizon and age estimates associated with sand dikes are often poorly constrained.

- Size distribution: In general, feature size diminishes as ground shaking decreases. Therefore, the size distribution of liquefaction features relates to magnitude and distance from the causative earthquake. The size distribution of features is also important for interpreting whether similar-age features formed during a single large earthquake or multiple smaller earthquakes.
- Stratigraphic control: Paleoearthquakes are distinguished based on grouping paleoliquefaction features found in deposits of similar age (see caveats described in Section 2.4.2).
- Pedologic or weathering characteristics: Paleoearthquakes are distinguished based on grouping paleoliquefaction features with similar soil or weathering characteristics (see caveats described in Section 2.4.1).

If the different types of information described above provide conflicting correlations for a specific field study, the investigator must assess the relative quality of the information and provide a preferred interpretation. Additional field reconnaissance may be necessary to identify areas for targeted studies that might be necessary to resolve these conflicts.

2.5.2 Timing of Paleoearthquakes

Estimates of the timing of paleoearthquakes are based on dating of many individual liquefaction features, and possibly other paleoseismic deformation structures, across a region. If ages of liquefaction features cannot be constrained within a few hundred years, it may not be possible to correlate features chronologically or to resolve the timing of paleoearthquakes with confidence. Therefore, it is paramount to date many liquefaction features across a region and to constrain the age estimates of those features as narrowly as possible. Uncertainty in the estimates of the timing of events decreases as the number and spatial distribution of well-constrained age estimates increases for a region (Table 2.3).

It is more difficult to recognize older liquefaction features, due to effects of soil development, weathering, and bioturbation, and to narrowly constrain their ages. Liquefaction features that are more than 50,000 years old are beyond the reach of radiocarbon dating, the most precise dating technique. For these ancient liquefaction features, age estimates may be provided by stratigraphic context and OSL dating of the host deposit but the uncertainties may be on the order of 1000s of years.

Clustering of age estimates of liquefaction features that can be reasonably correlated across a region is thought to reflect the timing of paleoearthquakes (Figures 2.16 and 2.17). For a particular cluster, the union of well-constrained age estimates of liquefaction features represents the time period during which the paleoearthquake is likely to have occurred. It is not uncommon for this time period to have a range of 100 to 1,000 years. Using the intersection of overlapping age estimates of sand blows may provide an event time with a range of tens to hundreds of years, as long as there is a high degree of confidence in the accuracy of the age estimates. Statistical analysis data clusters that include several well-constrained age estimates can lead to a more narrowly defined range of several to tens of years and thus smaller uncertainties in the estimated timing of the paleoearthquakes (Figure 2.16).

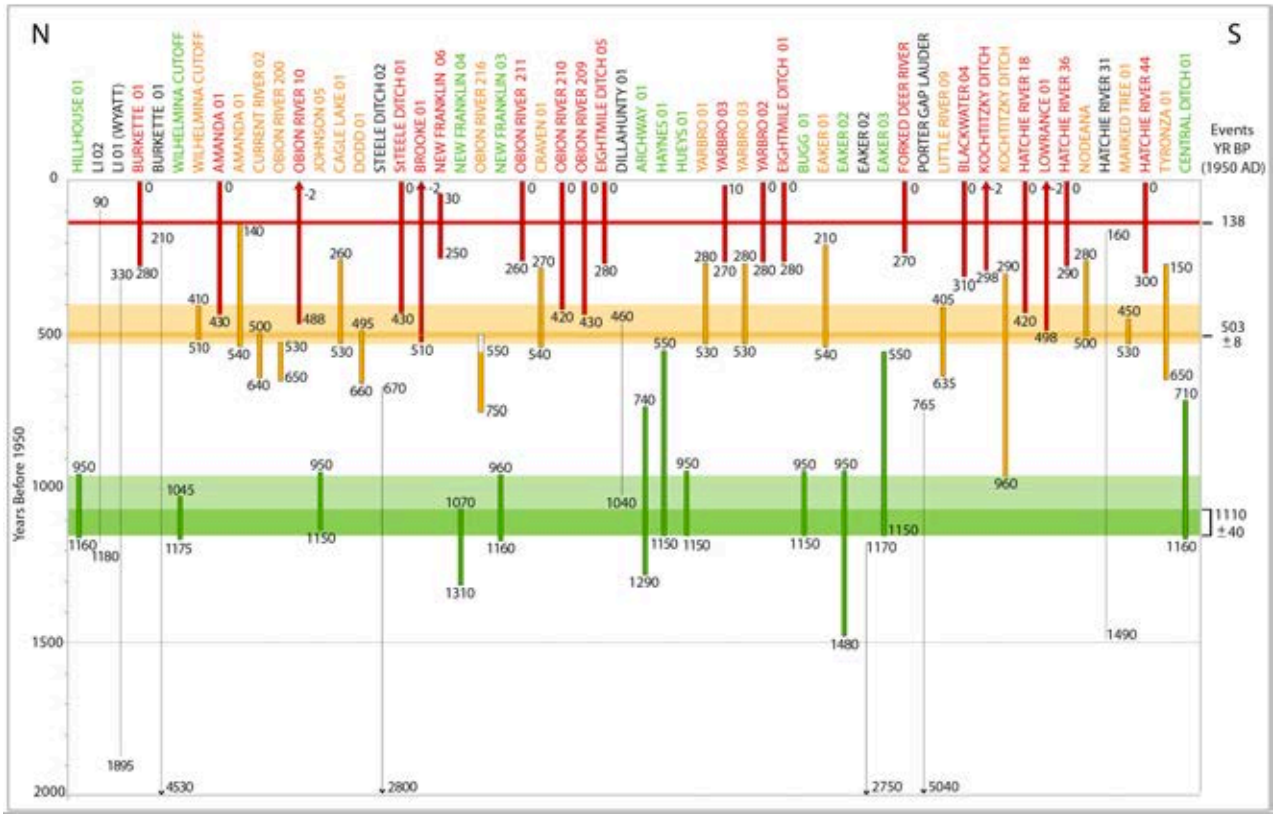

Figure 2-16 Earthquake chronology of the New Madrid seismic zone for the past 2,000 years based on paleoliquefaction studies (e.g., Tuttle et al., 2002b and 2005; NUREG-2115). Vertical bars represent age estimates of individual sand blows, and horizontal bars represent inferred event times based on intersection of overlapping age estimates: 138 yr BP (AD 1811-1812); 500 yr BP ± 150 yr; 1,050 yr BP ± 100 yr. Statistical analysis resolved event times with narrower uncertainty ranges of 503 yr BP ± 8 yr and 1,110 yr BP ± 40 yr as indicated by darker portions of the horizontal bars.

2.5.3 Locations of Paleoearthquakes

Once liquefaction features have been correlated across a region on the basis of one or more of the criteria described above in Section 2.4 (e.g., chronological or stratigraphic control), these features, specifically sand blows and sand dikes, can be used to infer the approximate locations of paleoearthquakes. The regional distribution of contemporaneous liquefaction features, sometimes referred to as the liquefaction field, is thought to reflect the meizoseismal (i.e., strongest shaking) area or source area of a particular paleoearthquake, and the area in which the largest liquefaction features are concentrated is interpreted as the epicentral area or energy center (Obermeier et al., 2001; Tuttle, 2001; Castilla and Audemard, 2007). As mentioned in Section 1.4.2, soft-sediment deformation structures such as convolute bedding, pseudonodules, and load casts may be useful in defining minimum levels of ground shaking. If present, therefore, these types of structures may help to delineate the outer limits of liquefaction fields and to

constrain the locations and magnitudes of paleoearthquakes, as long as they meet certain criteria and are used in combination with sand blows and sand dikes. Lone occurrences of earthquake-induced liquefaction features may be indicators of unique site conditions and should be interpreted with care.

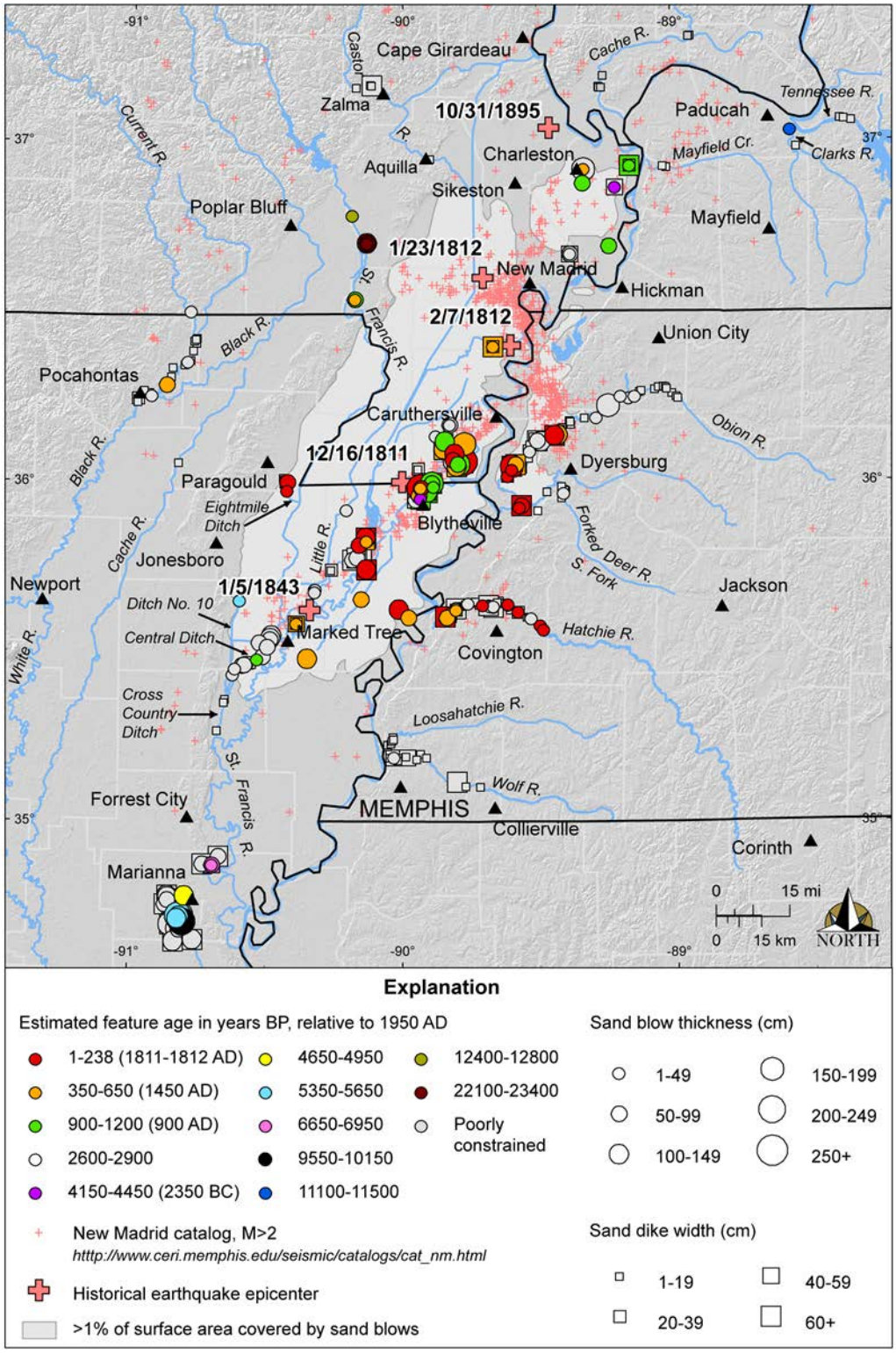

Figure 2-17 Shaded relief map of NMSZ and surrounding region showing instrumentally recorded earthquakes, inferred locations of historical earthquakes, large liquefaction field produced by large earthquakes, estimated ages and measured sizes of earthquake-induce d liquefaction features including sand blows and sand dikes (from Tuttle, 2010).

As demonstrated by modern earthquakes, sand blows generally decrease in size and frequency with increasing distance from the epicenter (e.g., Ambraseys, 1988; Castilla and Audemard, 2007). Nevertheless, the size and spatial distribution of sand blows can be influenced by a variety of factors including style of faulting, earthquake characteristics, directivity of seismic energy, attenuation and amplification of ground motion, relative density of sediment, distribution of liquefiable sediment, and water table depth. The complexity of processes and conditions influencing sand-blow formation contribute to difficulties in interpreting paleoliquefaction data. Accounting for various seismological, geological, and hydrological factors may help to reduce uncertainties to some degree. In addition, the sampling strategy and sediment exposure will affect uncertainties related to the spatial distribution of paleoliquefaction features. If searching for liquefaction features is not performed where conditions are suitable for the formation and preservation of liquefaction features, and at times when exposure is adequate to find features, information gained during paleoliquefaction studies may be incomplete and skewed spatially and/or temporally, which can lead to erroneous interpretations. Taking together the possible factors affecting the occurrence and observation of paleoliquefaction features, uncertainty in interpreting the locations of paleoearthquakes is probably on the order of tens to hundreds of kilometers (Table 2.3; NUREG-2115).

Modern and historical earthquakes that induced liquefaction can serve as calibration events for interpreting paleoliquefaction features. If the size and spatial distribution of liquefaction features generated by a paleoearthquake are similar to those for a modern or historical earthquake in the same region, the paleoearthquake can be inferred to have a similar source area to that of the modern or historical earthquake. For example, the source area of the 1886 Charleston, South Carolina, earthquake is thought to have produced several large paleoearthquakes in the past 5,500 years judging from similar spatial distributions of historical and prehistoric sand-blow craters (Talwani and Schaeffer, 2001). Similarly, the New Madrid seismic zone is thought to be the source of several sequences of large paleoearthquakes judging from the size, internal stratigraphy, and spatial distributions of historical and prehistoric sand blows (Figure 2.17; Tuttle et al., 2002b and 2005).

In comparative studies, the accuracy of the inferred locations of the paleoearthquakes is less than that for the modern or historical earthquakes, usually a few kilometers to a few tens of kilometers, respectively. If paleoliquefaction features can be directly related to a fault, such as has been done with the Reelfoot fault in the New Madrid seismic zone, uncertainty in the location of the paleoearthquake may be reduced to just a few kilometers (e.g., Kelson et al., 1996; Tuttle et al., 2002b; Table 2.3).

2.5.4 Magnitudes of Paleoearthquakes

As demonstrated by case studies of instrumentally recorded earthquakes that induced liquefaction, the size of sand blows, as well as the spatial extent of sand blows, increases with earthquake magnitude (e.g., Ambraseys, 1988; Castilla and Audemard, 2007). Therefore, the size and spatial distribution of paleoliquefaction features can help to estimate the magnitudes of paleoearthquakes (e.g., Obermeier, 1996; Tuttle, 2001). However, due to the many factors affecting the occurrence, distribution, and observation of liquefaction features, uncertainty in magnitudes of paleoearthquakes estimated from paleoliquefaction data can be fairly large, perhaps ranging up to 1 magnitude unit and above. It may be possible to reduce the uncertainty if

the size distribution of similar-age features is well constrained and by conducting comparative studies, using empirical relations, and performing geotechnical analysis (Table 2.3; Tuttle, 2001).

2.5.4.1 Comparison with Modern or Historical Analogues

In comparative studies, the size and spatial distribution of sand blows generated by a paleoearthquake are compared to those induced by a local modern or historical earthquake whose magnitude is fairly well known. For example, paleoearthquakes centered in the New Madrid seismic zone about AD 1450 (500 yr BP) and AD 900 (1,050 yr BP) are thought to be on the order of **M** 7 to 8 based on the similarity in the size and spatial distribution of sand blows with those that formed during the 1811-1812 New Madrid earthquakes (Figures 2.16 and 2.17; e.g., Tuttle et al., 2002b; NUREG-2115). A similar approach was used in the southeastern U.S. to compare the spatial distribution of paleoliquefaction features with those that formed during the 1886 **M** ~7 Charleston, South Carolina, earthquake (Talwani and Schaeffer, 2001). In studies such as these, the uncertainty related to the inferred magnitudes of the paleoearthquakes is greater than that for the modern and historical earthquakes, which usually range from 0.25 to 0.75 of a magnitude unit, respectively.

2.5.4.2 Empirical Relations

Empirical relations used in paleoliquefaction studies to estimate magnitudes of paleoearthquakes include (1) the relations between earthquake magnitude and maximum distance of surface manifestations of liquefaction, or sand blows, and (2) the relation between the liquefaction severity index and distance of liquefaction from the seismic energy source. In order to use the empirical relations to estimate magnitudes of paleoearthquakes, their source areas must first be interpreted. As described above in Section 2.5.3, the size and spatial distribution of liquefaction features are used to interpret the source areas of paleoearthquakes.

Both empirical relations are based on modern and historical cases of earthquake-induced liquefaction for which the locations and magnitudes of the earthquakes are fairly well known (Figure 2.18; e.g., Ambraseys, 1988; Papadopoulos and Lefkopoulos, 1993). Recent studies have found that style of faulting and directivity of seismic energy appears to influence the size and distance of liquefaction features, but that the greatest distance of surface manifestations of liquefaction is still a useful indicator of the magnitude of the causative earthquake (Figure 2.19; Obermeier, 1996; Tuttle et al., 2002a; Castilla and Audemard, 2007).

Paleoearthquake magnitude estimated from earthquake magnitude-liquefaction distance relations are considered minimum values since the actual epicentral distance to the farthest sand blow is unlikely to be known (Tuttle, 2001; Castilla and Audemard, 2007). A great deal of reconnaissance by an experienced investigator is often required to find and recognize distal sand blows since they become smaller and less frequent, and may occur mainly in areas characterized by sediment that is highly susceptible to liquefaction. The distance to the farthest sand dikes observed in river cutbanks should not be used to estimate magnitudes of paleoearthquakes. To do so could lead to overestimation of paleoearthquake magnitudes since sand dikes can form at greater distances than sand blows, and the magnitude-distance relations were based on “surface manifestations” of liquefaction not subsurface sand dikes.

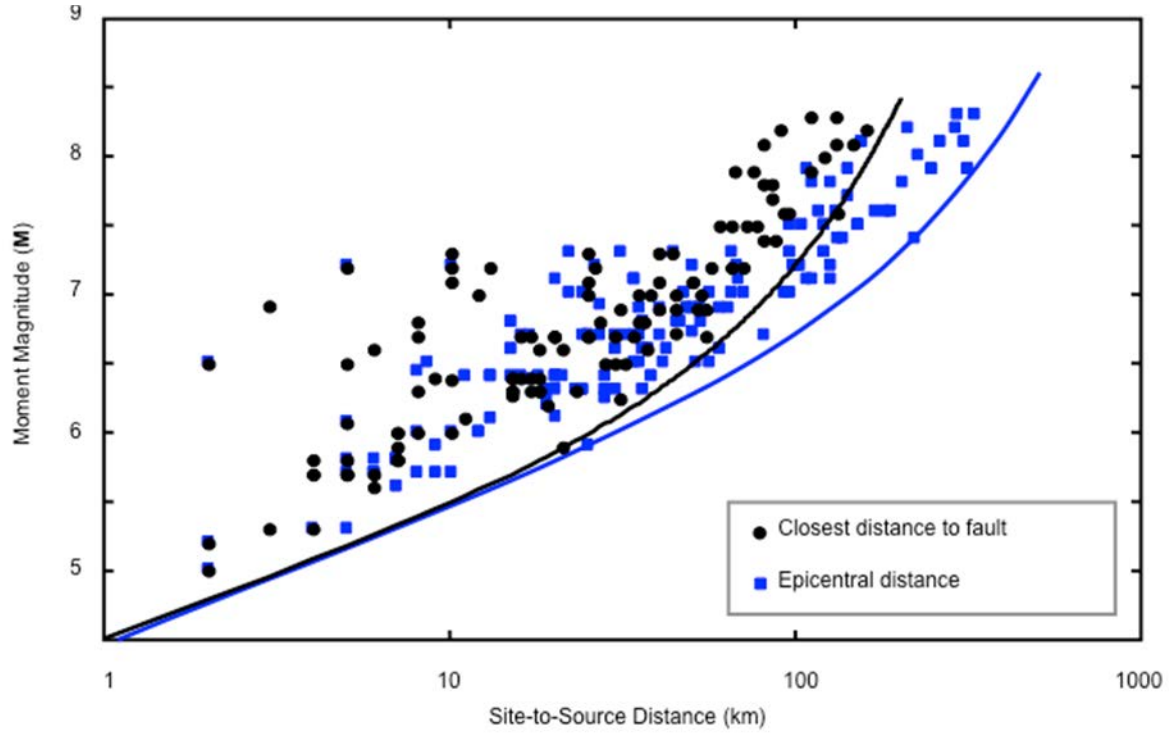

Figure 2-18 Relation between moment magnitude, M, and distance from earthquake to farthest surface expression of liquefaction (after Papadopoulos and Lefkopoulos, 1993).

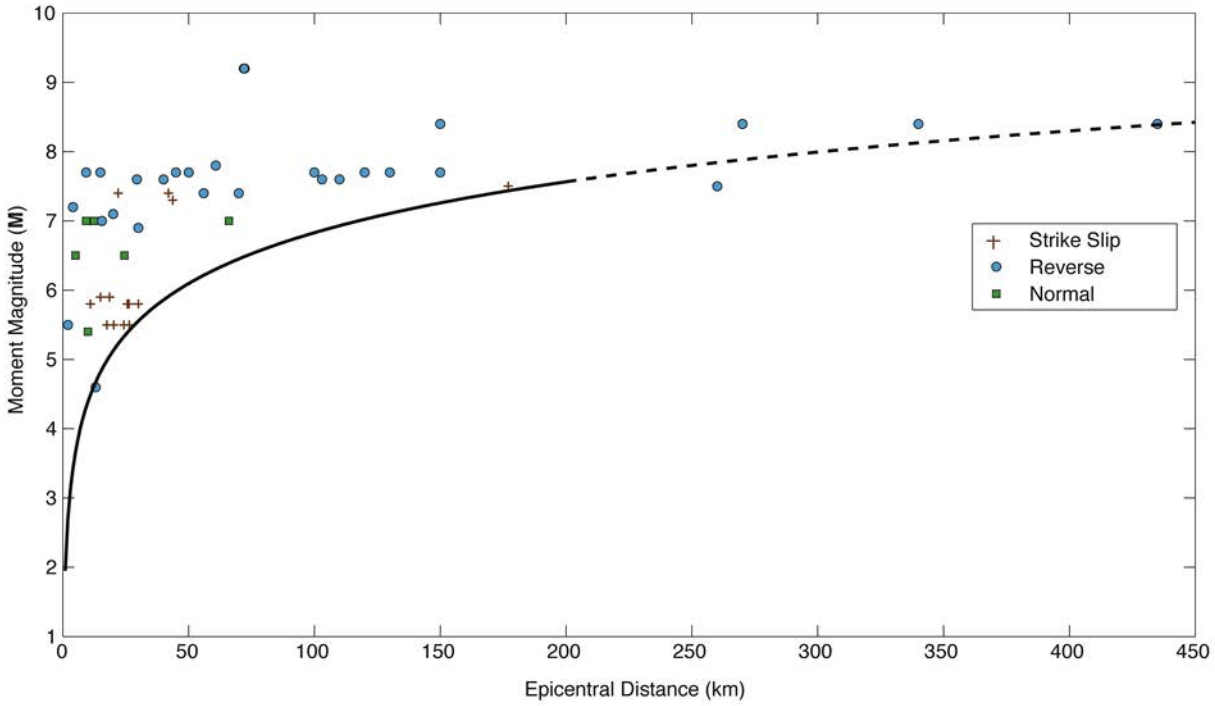

Figure 2-19 Relation between M and epicentral distance to farthest known sand blows induced by instrumentally recorded earthquakes (after Castilla and Audemard, 2007).

There are several obvious factors that contribute to uncertainties in magnitude estimates for paleoearthquakes based on the magnitude-bound method, which an empirical method based on the surface expression of liquefaction. The epicentral location may be poorly defined and the farthest sand blow is unlikely to be known. In addition, the magnitude-distance relation itself has some inherent uncertainties since the epicentral distance to the farthest sand blow may not be known even for instrumental earthquakes. Due to the sparse data for infrequent very large earthquakes, the relation is poorly constrained for earthquakes greater than magnitude 7.2. Given the various unknowns, uncertainties associated with magnitude estimates determined with the magnitude-bound method are likely to range from 0.25 to 0.6 of a magnitude unit (NUREG-2115).

Attempts have been made to reduce uncertainties in the magnitude estimates of paleoearthquakes by performing regional calibration of the magnitude-distance relation (Obermeier et al., 2001; Olson et al., 2005a). However, calibrations that rely heavily on historical earthquakes with poorly constrained locations and magnitudes are unlikely to significantly improve the magnitude-distance relation based on the worldwide database of instrumentally recorded earthquakes (e.g., Ambraseys, 1988; Papadopoulos and Lefkopoulos, 1993; Castilla and Audemard, 2007). Calibration of the magnitude-bound relation may be most fruitful for regions that have recently experienced instrumentally recorded earthquakes that induced liquefaction.

The liquefaction severity index (LSI) is a measure of ground failure displacement related to lateral spreading on gently sloping late Holocene fluvial deposits (Youd and Perkins, 1987). LSI represents the maximum observed severity of ground failure at a given locality, with displacements greater than 2.5 m receiving the limiting value of 100. Values of LSI have been determined for several earthquakes, ranging in magnitude from **M** 5.2 to 9.2, in the western U.S.

and plotted against horizontal distance from fault rupture (Youd and Perkins, 1987). A relation has been developed for one modern and two historic earthquakes in the eastern U.S. and Canada that shows liquefaction at greater distances in this region compared to similar-size earthquakes in the west (Youd et al., 1989). For example, the 1988 **M** 5.9 Saguenay, Quebec earthquake, induced liquefaction 25-30 km from its epicenter, a much greater distance than has been reported for liquefaction triggered by similar magnitude earthquakes in the western US (Tuttle et al., 1990; Youd and Perkins, 1987). Liquefaction at greater distances is probably due in part to lower attenuation of ground motion in the relatively old and hard crystalline rocks of eastern North America. Although they have been employed only rarely in paleoliquefaction studies, LSI-distance relations allow for the use of liquefaction features, including sand blows, in a meizoseismal area and do not rely on distal liquefaction features, often sand dikes, that may be difficult to date with tight age constraints and attribute to one particular paleoearthquake.

2.5.4.3 Geotechnical Approach

The geotechnical approach for evaluating the magnitudes of paleoearthquakes has involved site characterization of in situ soil properties, characterization of ground motion for scenario earthquakes, and liquefaction potential analysis (e.g., Obermeier et al., 2001; Olson et al., 2001, 2005b; Green et al., 2005). The evaluation is based on the identification of the soil or sediment layers that may have liquefied during the events, the measurement or estimation of geotechnical parameters (e.g., penetration resistance, soil density, effective overburden stress, and shear modulus) of the layers, and the groundwater level, which are used to estimate the seismic ground motions necessary to induce liquefaction in the layers. It is best to collect the geotechnical data used in the analysis at the sites of interest to ensure the data are representative of the site conditions.

Typically, liquefaction potential analysis is performed for sites where liquefaction features have and have not been observed in excavations or in natural exposures such as river cutbanks. Field observations of liquefaction features help to constrain the depth of the sediment that liquefied and to select the sediment layers used in the liquefaction potential analysis. During the analysis, minimum values of acceleration likely to induce liquefaction are determined for each site. For distal sites of liquefaction, the values may be close to the actual accelerations experienced by the sites. By comparing results of this analysis with field observations, scenario earthquakes are selected that may best reflect the source areas and magnitudes of paleoearthquakes. A variation of this approach involves determining combinations of peak ground surface acceleration and earthquake magnitude for sites that liquefied and did not liquefy (Figure 2.20; Green et al., 2005).

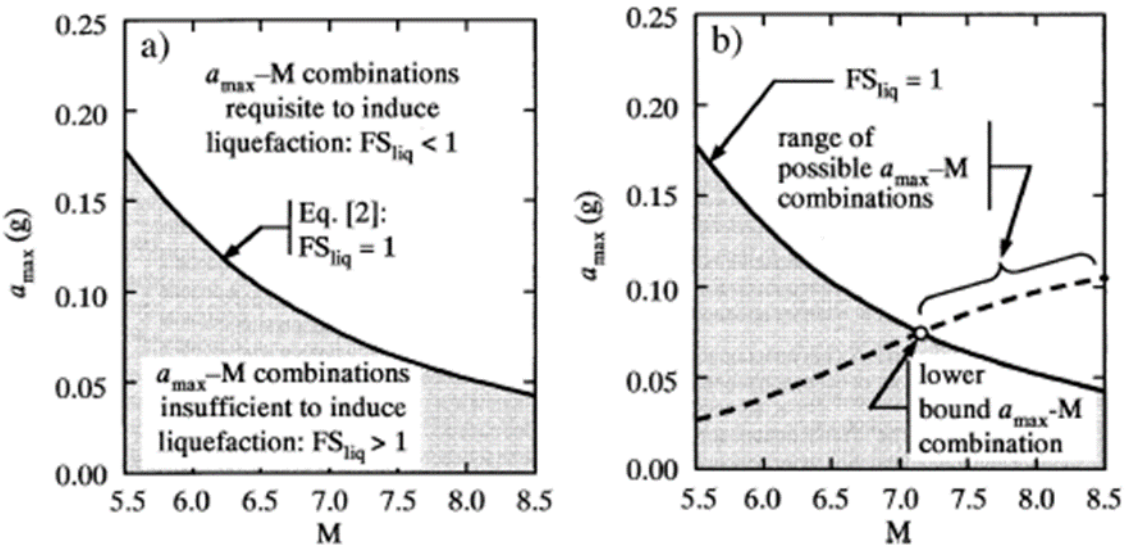

Figure 2-20 (Left) a_{max} - M combination required to induce liquefaction at an hypothetical site; (Right) lower bound a_{max} - M combination determined for the same hypothetical site (from Green et al., 2005).

The geotechnical approach has been applied in the Charleston (e.g., Hu et al., 2002a, 2002b; Leon, 2003; Leon et al., 2005; Gassman et al., 2009) and the Wabash Valley (e.g., Obermeier et al., 1993; Pond and Martin, 1997; Olson et al., 2001; Green et al., 2005; Heidari et al., 2011) seismic zones and in the St. Louis region northwest of the New Madrid seismic zone (NUREG/CR-5730). It has also been used to a more limited extent in the New Madrid (e.g., Schneider and Mayne, 2000; Schneider et al., 2001; Liao et al., 2002; Stark, 2002; Tuttle, 2004; Liao and Mayne, 2010) and the Charlevoix (e.g., Tuttle and Atkinson, 2010) seismic zones.

The geotechnical approach may suggest multiple possible source areas and a range of possible magnitudes for a given paleoearthquake. For the Wabash Valley seismic zone, the magnitude estimates range from **M** 7 to 7.8 for the Vincennes-Bridgeport paleoearthquake about 6,100 $\pm$ 200 yr B.P. and from **M** 6.3 to 7.3 for the Skelton paleoearthquake about 12,000 $\pm$ 1,000 yr BP (Pond and Martin, 1997; Green et al., 2005; Olson et al., 2005a; Castilla and Audemard, 2007). For the Charleston seismic zone, magnitude estimates for large regional paleoearthquakes range from **M** 6.8 to 7.8 (Hu et al., 2002b), **M** 5.5 to 7.2 (Leon et al., 2005), and **M** 6.7 to 7.0 (Gassman et al., 2009), depending on the study. For the region northwest of the New Madrid seismic zone in southeastern Missouri and southwestern Illinois, paleoliquefaction features that formed about 6,500 yr B.P. can be explained by one very large (M > 7) regional earthquake or two smaller earthquakes located in close proximity to the clusters of features (Figure 2.21; NUREG/CR-5730).

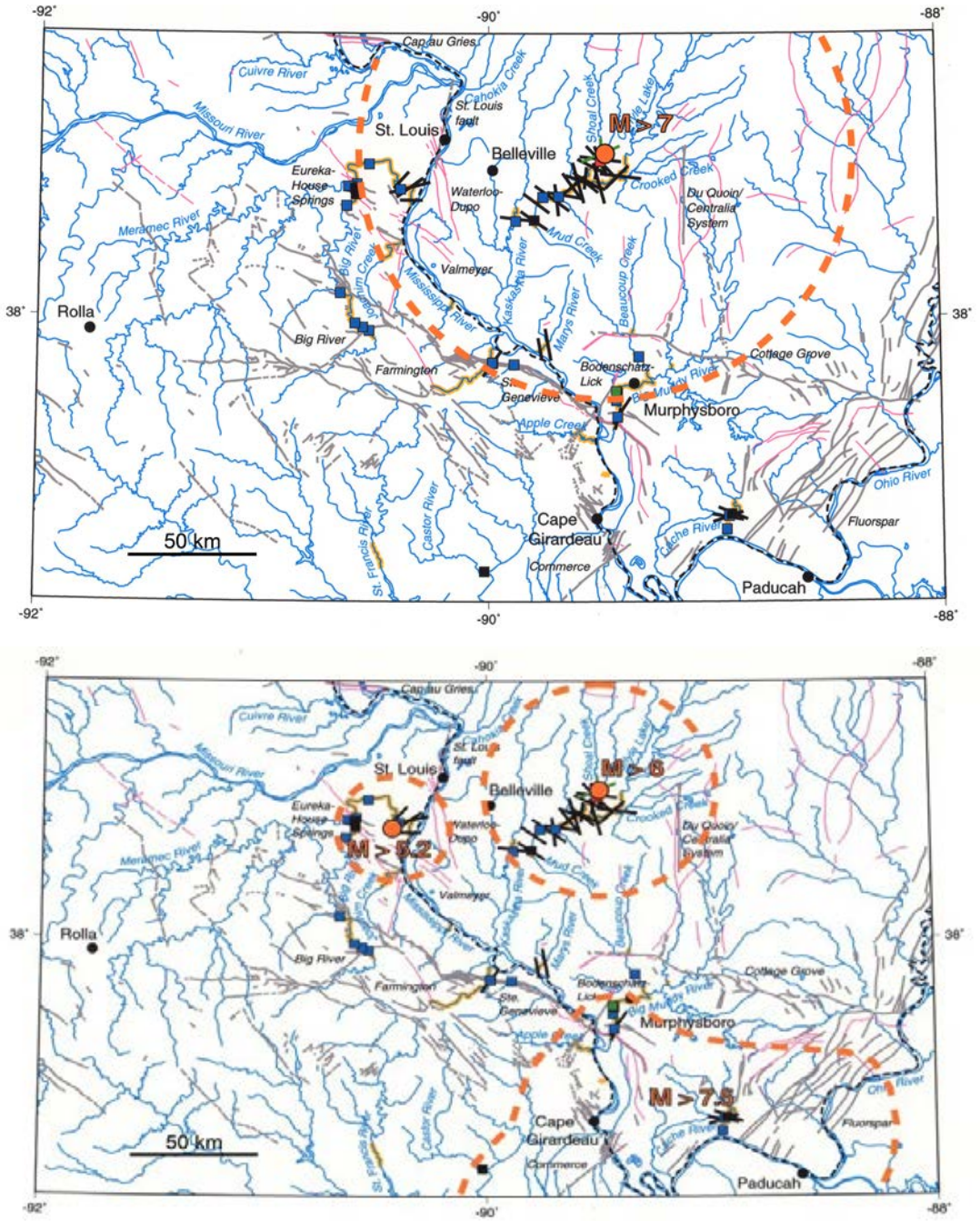

Figure 2-21 **Alternate earthquake scenarios that could explain the distribution of prehistoric liquefaction features in the greater St. Louis region (from NUREG/CR-5730): (Above) M > 7 earthquake centered near Germantown, Illinois, in vicinity of largest liquefaction features on Shoal Creek. (Below) M > 6 earthquake centered near Germantown, M > 5.2 near St. Louis, and M > 7.5 centered near New Madrid, Missouri. Solid black lines indicate location and strike of dikes, where length of lines represent dike width: 8 mm line < 1 cm width, 12 mm line = 1-10 cm width, 16 mm line > 10 cm width. Solid black squares represent dikes with unknown strike. Red and green filled squares represent sand blows and sand sills, respectively. Blue filled squares indicate soft-sediment deformation structures. Thick yellow lines identify river sections that were searched for liquefaction features. Surface traces of faults and fold axes are shown with gray lines and thin magenta lines, respectively.**

There are numerous sources of uncertainty associated with evaluating the locations and magnitudes of paleoearthquakes from geotechnical data. It is incumbent on investigators to be transparent with and describe how uncertainties are considered in their analyses. Sources of uncertainties include (1) identification of the sediment layer that liquefied during a particular event; (2) measurements of the geotechnical properties of the layer that liquefied; (3) changes in geotechnical properties of the layer due to liquefaction and to post-liquefaction effects related to aging and groundwater conditions; (4) seismic parameters (e.g., amplitude, duration, frequency, and directivity), regional ground motion attenuation, and local site effects; and (5) interpretation of site-specific results in a regional context (Tuttle, 2001; Green et al., 2005; Olson et al., 2005; NUREG-2115; Electric Power Research Institute, 2013). Improving the understanding of these sources of uncertainty and quantifying their influence on location and magnitude estimates of paleoearthquakes is an area of ongoing research

2.5.4.3.1 Liquefaction Potential Analysis

Both the cyclic-stress (e.g., Seed and Idriss, 1982; Youd et al., 2001; Cetin et al., 2004) and the seismic energy (e.g., Pond, 1996) methods of liquefaction potential analysis have been used in the evaluation of paleoearthquakes. The cyclic-stress method, also known as the simplified procedure, is the preferred method because it is well established, remains the standard in engineering practice, and is suitable for many field and tectonic settings (e.g., Seed and Idriss, 1971 and 1982; Youd et al., 2001; Robertson, 2004 and 2009; Idriss and Boulanger, 2004 and 2008; Moss et al., 2006; Cetin et al., 2004). However, progress has been made in seismic energy methods, which may be used more in the future (Green, 2001).

In the analysis, peak ground accelerations are estimated for scenario earthquakes of various moment magnitudes (e.g., **M** 5-8) at distances of interest from known or suspected earthquake sources by employing regionally appropriate ground motion prediction equations (previously known as ground motion attenuation relations) and site response analyses. Several prediction equations often are used in the calculations to capture the uncertainty inherent in the relations. Prediction equations vary significantly from one region to another, and even within regions, due to the differences in seismic source properties and geological characteristics (Heaton and Hartzell, 1988). Most prediction equations are derived from statistical modeling of recorded ground motions generated by interplate earthquakes. For intraplate tectonic settings, which are characterized by lower rates of seismicity and few recorded large magnitude earthquakes, prediction equations are based on semi-empirical seismological modeling and typically calibrated with limited data. In addition, the standard deviation of actual ground motions is about a factor of two about the median relation. It is the motions above the median that typically dominate the hazard and produce the more severe observations. Furthermore, variability in ground motions is large even over small spatial scales (e.g., a factor of two for sites within several hundred meters of each other), and liquefaction sites across a region may represent these above-median motions. Therefore, it is important to consider these two sources of variability in ground motions by including higher than median motions in the evaluation and interpretation of scenario earthquakes (Atkinson, pers. comm., 2015). As mentioned earlier, earthquakes in the eastern US with higher frequency content cause higher peak ground accelerations than western earthquakes at similar

magnitudes and distances (Atkinson and Boore, 2000). For example, the high-frequency amplitudes of the 1988 **M** 5.9 Saguenay, Quebec earthquake, which induced liquefaction farther than a similar magnitude earthquake in the western US, exceeded median predicted levels by a significant margin (Boore and Atkinson, 1992). Therefore, frequency content of eastern earthquakes may be an important factor in interpreting the distribution of liquefaction caused by paleoearthquakes. Uncertainties in prediction equations, especially for intraplate regions like the Central and Eastern United States (CEUS), as well as variability in ground motions, will have significant impacts on magnitude estimates of paleoearthquakes.

Using empirical relations between cyclic stress ratio and corrected penetration resistance, it can be determined whether or not representative layers at a site would be likely, or unlikely, to liquefy. Given the uncertainty in predicting ground motions, it is recommended that several prediction equations be used to capture the possible range of results. In addition, it is prudent to consider ground motions about a factor of two higher than the median since higher-than-average motions are likely to strongly influence the pattern of liquefaction (Atkinson, pers. comm., 2015). After computing the peak ground accelerations, cyclic stress ratios (CSR) generated by scenario earthquakes are calculated using the following expression for flat ground and depths < 15 m, as discussed earlier in Section 1.2.3:

$$CSR_{7.5} = \frac{\tau_{ave}}{\sigma'_{vo}} = 0.65 \cdot \left(\frac{a_{max}}{g}\right) \cdot \left(\frac{\sigma_{vo}}{\sigma'_{v0}}\right) \cdot r_d \cdot \frac{1}{MSF}$$

where a_{max}= PGA = peak (horizontal) ground acceleration, (a_{max}/g) is peak ground acceleration divided by gravity, σ_{vo} and σ_{vo}, are the total and effective vertical overburden stresses, respectively (see Appendix A),r_d is a stress reduction coefficient (see Appendix B), and MSF = magnitude scaling factor (see Section 1.2.3 and Appendix B). The $CSR_{7.5}$ represents the normalized shear stress (τ_{ave}/σ_v') induced in the soil by the earthquake event (i.e, the seismic demand) and commonly referenced to a benchmark case with **M** = 7.5. For ground that is sloped and for high overburden stresses (i.e., $z > 30$ m), consideration should be given towards inclusion of a slope correction factor (K_α) and/or overburden correction factor (K_σ), as discussed previously in Section 1.2.3 and Appendix B.

The ability of the soil to resist the triggering of liquefaction is quantified in terms of cyclic resistance ratio (CRR). If the CSR exceeds the CRR, liquefaction can be expected; otherwise, if CSR < CRR, liquefaction is not anticipated. The CRR has been correlated to a number of different in-situ tests including: standard penetration test (SPT), cone penetration tests (CPT), flat dilatometer test (DMT), and shear wave velocity (V_s) measurements. A summary of the standard approaches for SPT, CPT, and V_s are given in Youd et al. (2001). For illustration, selected CRR curves for **M** 7.5 earthquakes for the four test methods (SPT, V_s, CPT, and DMT) are presented in Figure 2.22. SPT and CPT are the most common test methods and additional details on the use of these methods are provided in the following sections.

2.5.4.3.2 Evaluation of Liquefaction Using the Standard Penetration Test

The procedure and tools used to perform the standard penetration test (SPT) cause variations in the measured blow count. These variations are corrected by adjusting the measured blow count (N_m) using the relation:

$$N_{1(60)} = C_N\, C_E\, C_B\, C_R\, C_S\, N_m$$

where $N_{1(60)}$ is the SPT blow count corrected for hammer energy (C_E), borehole diameter (C_B), rod length (C_R), and sampler configuration (C_S), with N_m being the measured SPT resistance or "blow count" reported in blows/foot (or blows/0.3m). Approximate values for various factors are given in Table 2.4 below. The subscript "60" refers to the average energy efficiency in the US at the time these factors were quantified (e.g., Seed et al., 1985; Skempton 1986). The magnitude of C_E is only reliably obtained by calibration measurements of dynamic force and acceleration with time per ASTM D4633.

The stress normalization of the N_{60} value is often called an "overburden correction" and provided in order to reference the data to an equivalent effective stress of one atmosphere, designated $(N_1)_{60}$ and given by:

$$(N_1)60 = C_N \, . N_{60}$$

The stress normalization factor (C_N) depends upon the specific methodology adopted, as detailed in Skempton (1986), Kulhawy and Mayne (1990), Boulanger and Idriss (2014), and ASTM D6066. A simple and commonly-adopted expression is $C_N = (\sigma_{atm}/\sigma'_{vo})^{0.5} \leq 1.7$.

Following the computations of the cyclic stress ratio and the adjusted and normalized blow count, the liquefaction potential of representative layers at borehole sites is determined by plotting computed cyclic stress ratio (CSR) versus normalized blow count [$(N_1)_{60}$] on charts such as that shown in Figure 2.22(a) for **M** 7.5 earthquakes. If the values plot above the cyclic resistance ratio (CRR) curve, then the soil is likely to liquefy. Conversely, if the values plot below the CRR, then liquefaction is considered unlikely.

The CRR curve for the corrected SPT resistance in clean quartz to silica sands is presented in Figure 2.23, following the NCEER approach. This curve was obtained from case studies at sites that experienced strong earthquakes. The CRR demarcates those seismic sites that showed clear evidence of liquefaction (i.e., bearing capacity failure, sand boils) versus seismic sites where no liquefaction was observed or evident.

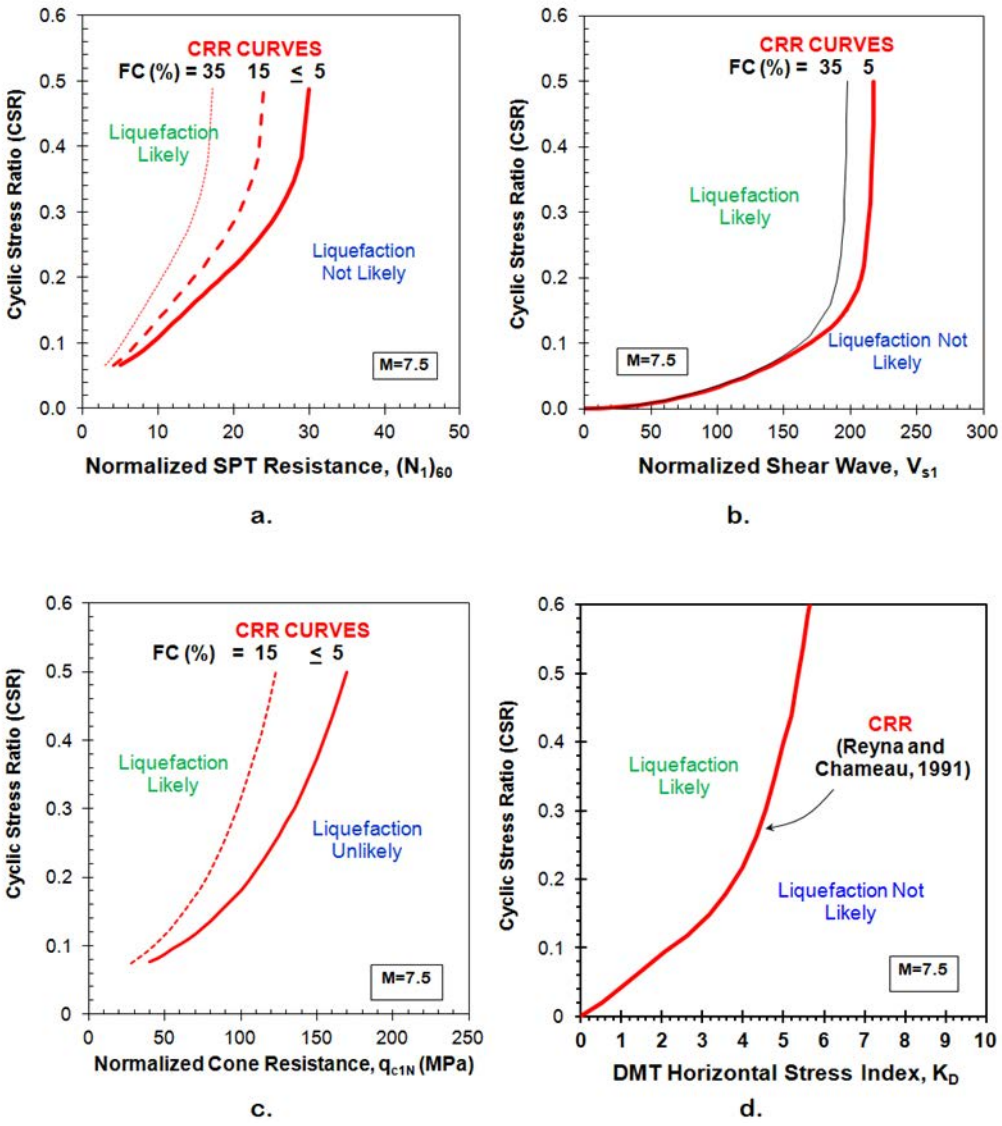

Figure 2-22 **Illustrative sets of cyclic resistance ratio (CRR) curves for M 7.5 earthquakes from in-situ tests: (a) standard penetration; (b) shear wave velocity; (c) cone penetration; and (d) flat plate dilatometer (after Schneider et al., 1999).**

Table 2-4 SPT modification factors for field procedures (modified after Skempton 1986; Kulhawy and Mayne 1990; Youd et al. 2001).

Factor	Influencing Variable	Field Case	Factor Values
C_N	Depth effect due to increasing effective overburden stress (σ_{vo}')	Note: σ_{atm}= 1 atmosphere $= 1.013$ bars $= 101.3$ kPa	$C_N = (\sigma_{atm}/\sigma_{vo}')^{0.5} \leq 1.7$
C_E	Energy ratio (ER) of drop hammer system per ASTM D4633 standards: $C_E = ER/60$	Automatic Hammer Safety Hammer Donut Hammer Pinweight Hammer	$1.0 \leq C_E \leq 1.6$ $0.8 \leq C_E \leq 1.3$ $0.6 \leq C_E \leq 0.8$ $0.5 \leq C_E \leq 0.7$
C_B	Borehole diameter, b	$65\text{mm} < b \leq 115\text{mm}$ $b = 150\text{mm}$ $b = 200\text{mm}$	$C_B = 1.00$ $C_B = 1.05$ $C_B = 1.15$
C_S	Split-barrel sampler	Sampler with liner Sampler without liner*	$CS = 1.0$ $1.1 < CS < 1.3$
C_R	Drill rod length, L	L > 10m 6m < L < 10m 4m < L < 6m 3m < L < 4m L < 3m	$CR = 1.00$ $C_R = 0.95$ $CR = 0.85$ $CR = 0.80$ $C_R = 0.75$

*Notes: normal practice in US is without a liner.

For clean sands that are tested in boreholes using the standard penetration test (SPT), the cyclic resistance ratio (CRR) for a **M** 7.5 event proposed in the NCEER approach (Youd et al., 2001) is given by the relation:

$$CRR_{7.5} = \frac{1}{34-(N_1)_{60}} + \frac{(N_1)_{60}}{135} + \frac{50}{[10\,.\,(N_1)_{60}+45]^2} - \frac{1}{200} \quad \text{for } (N_1)_{60} < 30$$

where $(N_1)_{60} = N_{60}/(\sigma_{vo}'/\sigma_{atm})^{0.5}$. The relation is presented in Figure 2.23. Note when clean sands and gravels exhibit $(N_1)_{60} \geq 30$, these granular soils are considered too dense for liquefaction and thus categorized as "nonliquefiable".

For sands that contain fines, a family of CRR curves can be developed that depends upon the fines content (FC in %), such as those presented in Figure 2.22a. Alternatively, the normalized SPT resistance $(N_1)_{60}$ can be converted to an equivalent value characteristic of clean sands, designated $(N_1)_{60\text{-cs}}$, that for the NCEER approach can be approximated by:

$$(N_1)_{60-cs} = 5\,.\,[\,1 - \frac{1}{1+(\text{FC}/15)^{3.7}}\,] + (N_1)_{60}\,.\,[\,1.2 - \frac{0.2}{1+(FC/22)^{3.3}}]$$

Then, this resistance is used in the CRR for clean sands for the specific method as shown in Figure 2.23. Thus, the aforementioned can be upgraded to:

$$CRR_{7.5} = \frac{1}{34-(N_1)_{60-cs}} + \frac{(N_1)_{60}}{135} + \frac{50}{[10\,.\,(N_1)_{60-cs}+45]^2} - \frac{1}{200}$$

for $(N_1)_{60\text{-cs}} < 30$

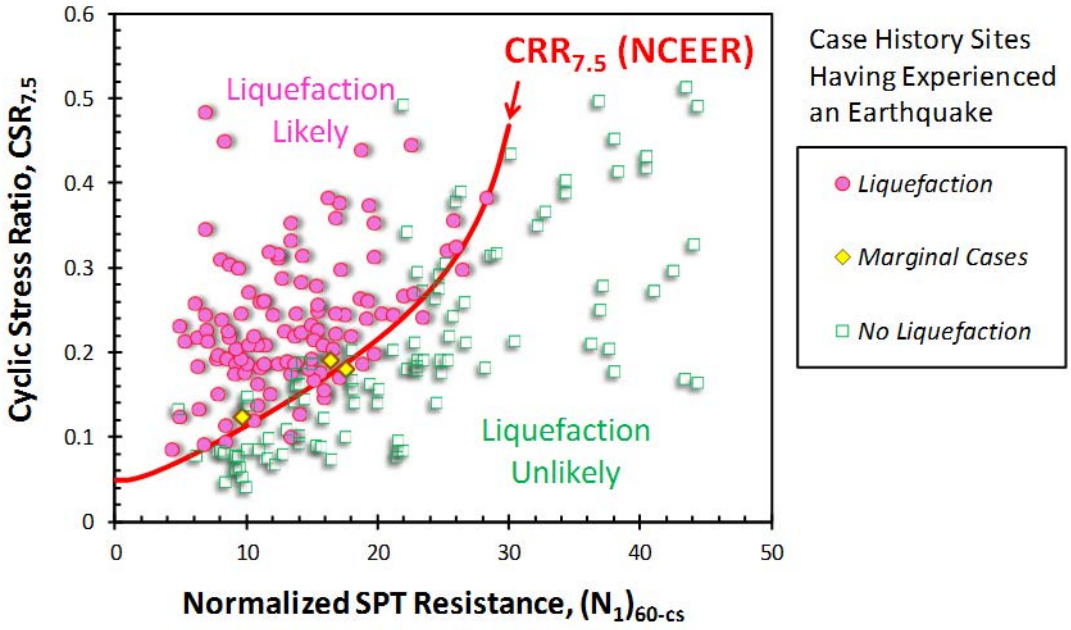

Figure 2-23 Deterministic CRR curves for adjusted SPT N-value in clean sands for NCEER method (after Youd et al., 2001).

Factor of Safety: For liquefaction analyses, a factor of safety (FS) can be calculated as:

$$FS = \frac{CRR_{7.5}}{CSR_{7.5}}$$

where $CRR_{7.5}$ = cyclic resistance ratio for a moment magnitude earthquake of **M** 7.5 and CSR is the cyclic stress ratio for **M** 7.5.

The aforementioned methods for simplified stress-based analyses of liquefaction susceptibility have been formulated in a deterministic outcome; that is, a binary decision as to "liquefaction" or "no liquefaction". As a means to better quantify the uncertainty, the stress-based methods have been re-evaluated using probabilistic analyses. In lieu of a single CRR curve, a family of CRR curves was developed to indicate the degree of probability (P_L) that liquefaction may occur. Sets of probability curves have been developed for the SPT with ranges generally given from $P_L = 5\%$ up to $P_L = 95\%$ (Liao et al., 1988; Youd and Noble 1997; Toprak et al., 1999; Juang et al., 2002; Cetin et al., 2004; Boulanger and Idriss, 2012). An example of these probabilistic CRR curves for the SPT is presented in Figure 2.24.

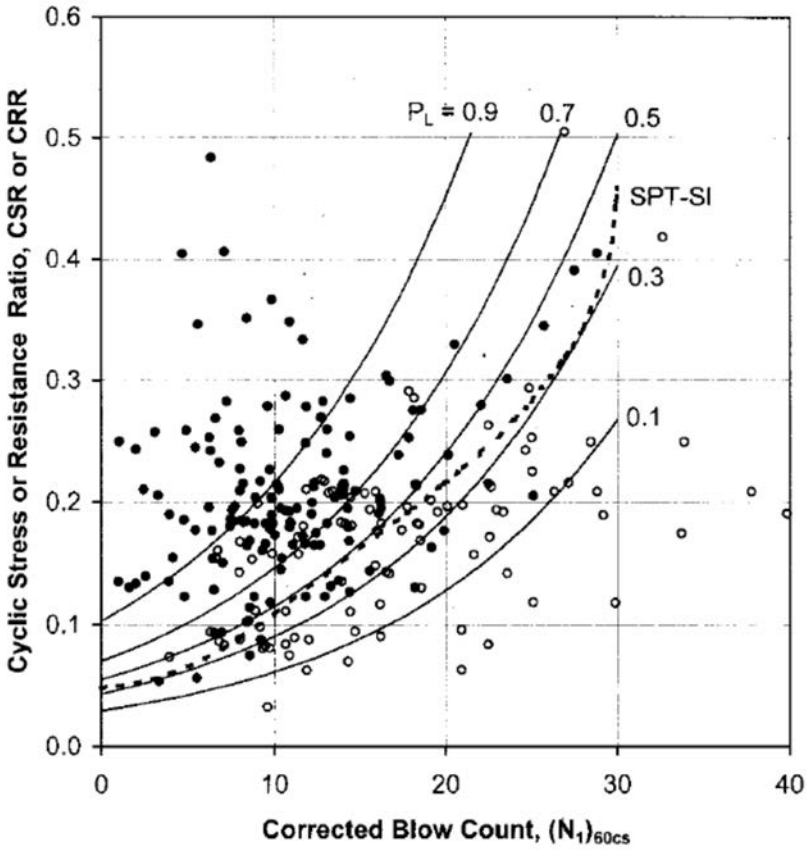

Figure 2-24 Probabilistic CRR for the SPT evaluation of liquefaction (Juang et al., 2002).

The calculated factor of safety (FS) can in fact be used to approximately assess the probability of liquefaction (P_L). For instance, for one approach detailed by Juang et al. (2002), they suggest:

$$P_L = \frac{1}{1 + (FS / 0.8)^{3.5}}$$

2.5.4.3.3 Evaluation of Liquefaction Using the Cone Penetration Test

The cone penetration test (CPT) is an excellent means for detecting the presence of loose sandy soils and evaluating their susceptibility to liquefaction because it provides continuous logging of strata and layering with at least three separate readings with depth: cone tip resistance (qt), sleeve friction (f_s), and penetration pore water pressure (u_2). The identification of loose granular soils is accomplished using a CPT material index (I_c) that determines soil behavioral type and estimates fines content. The available soil resistance (i.e., cyclic resistance ratio, CRR) in the ground is evaluated from the stress-normalized cone resistance (Q_{tn}) which is compared with the level of seismic ground motions (i.e., cyclic stress ratio, CSR) to calculate the factor of safety (FS) and/or probability of liquefaction (P_L) at the location. Furthermore, the magnitude of seismic ground deformations (i.e., settlements, subsidence) and amount of expected lateral movement also may be estimated from these results.

Of particular value, the seismic piezocone test (SCPTu) offers a hybrid technology that combines penetrometer readings with geophysical downhole testing to measure shear wave velocity (V_s) profiles, in particular the vertically-propagating and horizontally-polarized mode

(i.e., V_{sVH} waves). These shear wave measurements play a triple role in site investigations in high seismic areas and can be used for the following: (a) IBC seismic site classification; (b) site-specific amplification analyses to determine level of ground shaking; and (c) an evaluation of soil liquefaction potential (independent of the aforementioned assessment from Q_{tn}). Figure 2.25 shows a representative SCPTu from the paleoliquefaction site at Marked Tree, Arkansas that shows a predominance of sandy sediment from 3 to 28+ m depths.

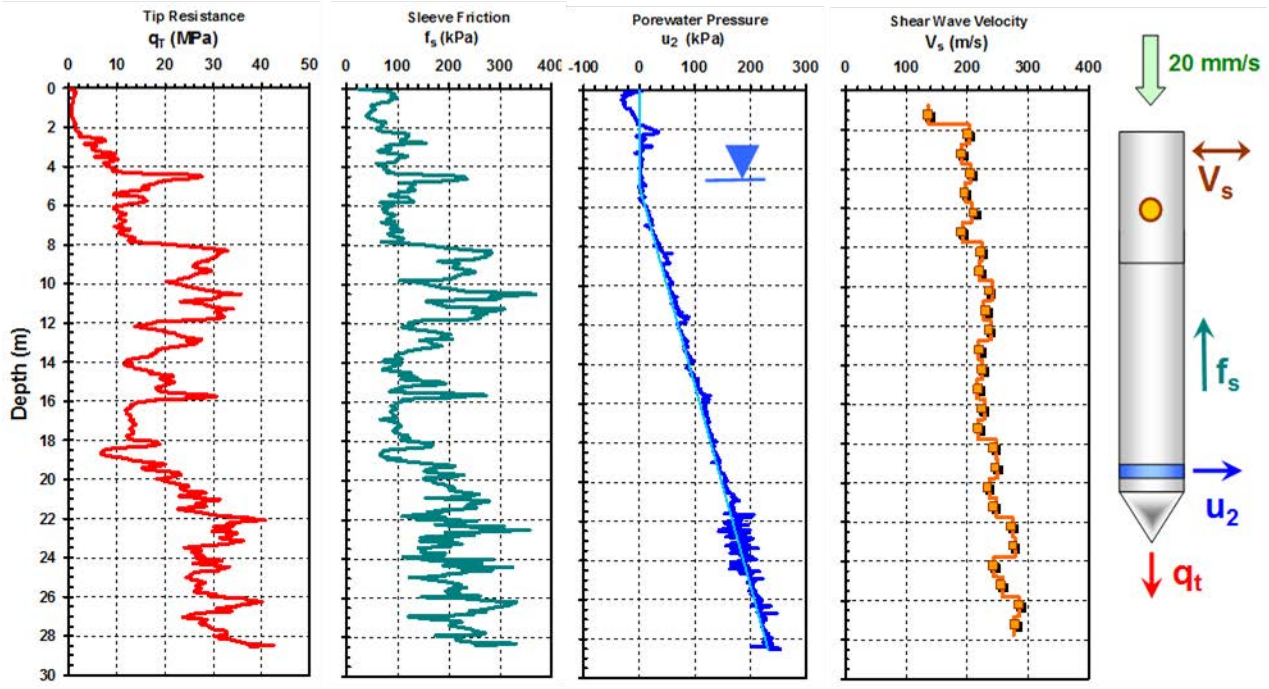

Figure 2-25 Representative seismic piezocone penetration sounding at paleoliquefaction site at a paleoliquefaction site in Marked Tree, Arkansas.

Geostratification and Soil Behavioral Type: The CPT readings are first used to delineate geostratigraphy and layering. The soil type is evaluated from the CPT material index, I_c (Robertson, 2004):

$$I_c = \sqrt{[3.47 - \log Q_{tn}]^2 + [1.22 + \log F_r]^2}$$

where Q_{tn} = stress-normalized cone resistance and F_r = normalized sleeve friction are calculated from the cone penetrometer readings:

$$Q_{tn} = \frac{(q_t - \sigma_{vo})/\sigma_{atm}}{(\sigma_{vo'}/\sigma_{atm})^n}$$

$$F_r\,(\%) = 100 \cdot \frac{f_s}{(q_t - \sigma_{vo})}$$

where σ_{vo} = total vertical overburden stress, σ_{vo}' = effective vertical stress, and σ_{atm} = a reference stress equal to atmospheric pressure ($1\ \text{atm} \approx 1\ \text{bar} \approx 100\ \text{kPa}$). In the initial evaluation, the exponent n is set to $n = 1$ to find the soil behavioral type (SBT) which is based on a 9-zonal chart developed by Robertson (1990). The SBT was modified by Robertson and Wride (1998) and Zhang et al. (2002), as shown in Figure 2.26.

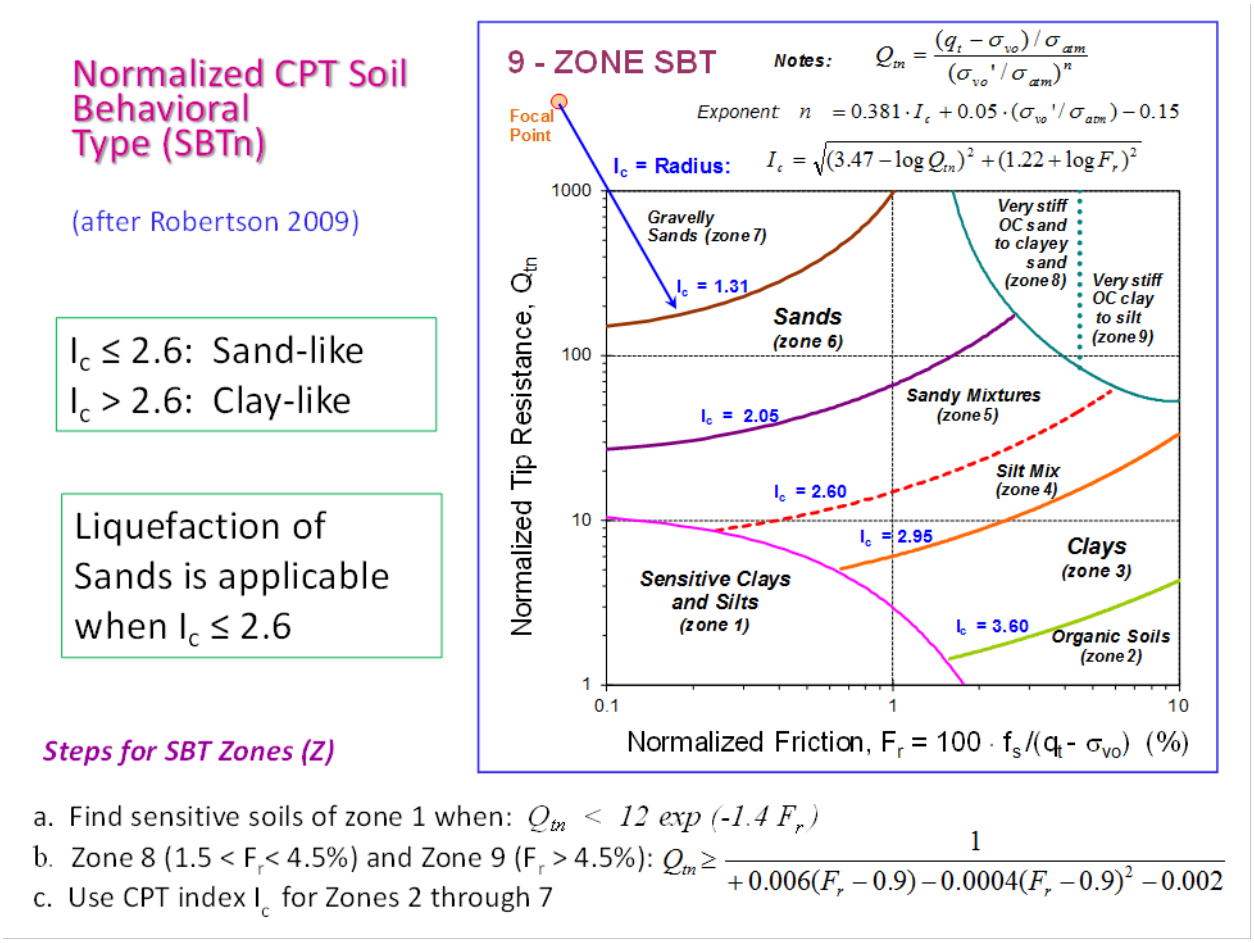

Figure 2-26 Soil behavioral type for CPT classification (after Robertson, 2004).

The exponent n is a stress-normalizing parameter that actually varies with soil type; generally taken as $n = 1$ in clays and decreasing with coarseness of geomaterials to about 0.75 in silts and around $n \approx 0.5 \pm 0.2$ in clean sands. It is found by iteration until conversion using the following expression (Robertson 2009b):

$$n = 0.381 \cdot I_c + 0.05\,(\sigma_{vo}'/\sigma_{atm}) - 0.15 \leq 1.0$$

With the center of an imaginary circle, I_c can be conceptually considered as a radius value on the Q_{tn}-F_r plot. Generally, soils that are susceptible to *cyclic liquefaction* are sandy materials identified by $I_c < 2.6$. In the more unusual case of *flow liquefaction* that may involve fine-grained materials, some additional considerations are given elsewhere (Robertson, 2010). Table 2.5 provides the ranges for I_c for each zone and additional algorithms necessary in order to identify all 9 SBT zones.

Table 2-5 Soil behavioral type and zone number as defined by CPT material index, I_c.

Soil Classification	SBT Zone Number	Range CPT Material Index I_c
Stiff clays and sands	8 and 9	(see note a)
Sands with gravels	7	$I_C < 1.31$
Sands: clean to silty	6	$1.31 < I_C < 2.05$
Sandy mixtures	5	$2.05 < I_C < 2.60$
Silty mixtures	4	$2.60 < I_C < 2.95$
Clays	3	$2.95 < I_C < 3.60$
Organic soils	2	$I_C > 3.60$
Sensitive soils	1	(see note b)

Notes:

a. Zones 8 and 9 are found when $F_r > 1.4\%$ and the following criterion is met:

$$Q_{tn} > \frac{1}{+0.006(F_r - 0.9) - 0.0004(F_r - 0.9)^2 - 0.002}$$

b. Sensitive soils of Zone 1 identified when: $Q_{tn} < 12 \exp(-1.4\, F_r)$

Fines Content: The liquefaction curves were developed initially on the basis of field performance of clean sands (identified by $I_c < 1.64$). Therefore, with the occurrence of sands with silty fines (material < 0.075 mm), the normalized cone resistance must be adjusted accordingly.

The fines content (FC in %) may be estimated from the CPT material index I_c as follows:

For $I_c < 1.64$ $\quad FC\ (\%) = 0$
For $1.64 \leq I_c \leq 3.5$: $\quad FC\ (\%) = 1.75\ (I_c)^{3.25} - 3.7$
For $I_c > 3.5$ $\quad FC\ (\%) = 100$

A correction for fines content is applied to give the equivalent value of stress-normalized cone resistance for clean sands according to (Robertson and Wride, 1998):

$$(Q_{tn})_{cs} = Kc\ .\ Q_{tn}$$

where the correction factor K_c is obtained from:

For $I_c \leq 1.64$: $\quad Kc = 1.0$
For $I_c > 1.64$: $\quad K_c = -0.403{I_c}^4 + 5.81{I_c}^3 - 21.63{I_c}^2 + 33.75I_c - 17.88$

Determination of CRR from CPT Data: At each elevation, the levels of seismic ground motion (CSR) are compared with the normalized cone tip resistances for clean sand to determine whether liquefaction will or will not occur. A critical level of loading is designated by the cyclic resistance ratio (CRR), as presented in Figure 2.27. If the CSR > CRR, then liquefaction is likely, otherwise if the CSR < CRR, liquefaction is unlikely. For clean sand, the CRR can be expressed by the following equations for an earthquake moment-magnitude of 7.5 (Youd et al., 2001; Robertson and Wride, 1998):

For $(Q_{tn})_{cs} < 50$: $\quad CRR_{7.5} = 8.33\left[\frac{(Q_{tn})_{cs}}{1000}\right] + 0.05$

For $50 \leq (Q_{tn})_{cs} < 160$: $CRR_{7.5} = 93\left[\frac{(Q_{tn})_{cs}}{1000}\right] + 0.08$

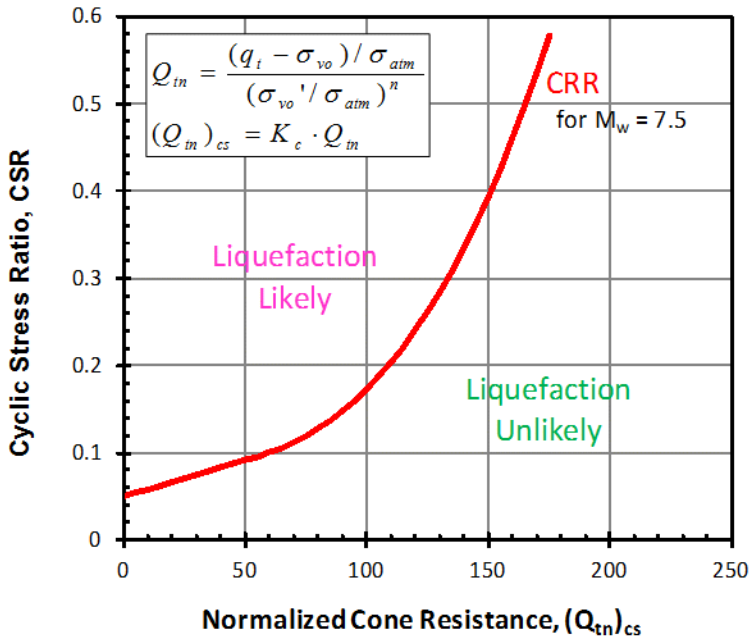

Figure 2-27 Cyclic resistance ratio (CRR) for evaluating soil liquefaction potential from CPT.

Probability of Liquefaction: Applying statistical evaluations to the datasets, CRR curves of different probabilities of occurrence have been developed from mapping functions (Chen and Juang, 2000; Juang and Jiang, 2000; Juang et al., 2006). These have been approximately related to the calculated safety factor *FS* to estimate the liquefaction probability P_L. For instance, based on a database of 225 CPT-based cases of sites having undergone a seismic event, Juang and Jiang (2000) develop sets of CRR vs. Q_{tn} probability curves, as presented in Figure 2.28. The relation between FS and P_L using the CPT database from Robertson & Wride (1998) that is included within the NCEER approach can be expressed:

$$P_L = \frac{1}{1 + FS^{3.34}}$$

A similar set of liquefaction probability CRR curves using stress-normalized shear wave velocity is presented in Appendix B based on recent work by Kayen et al. (2012).

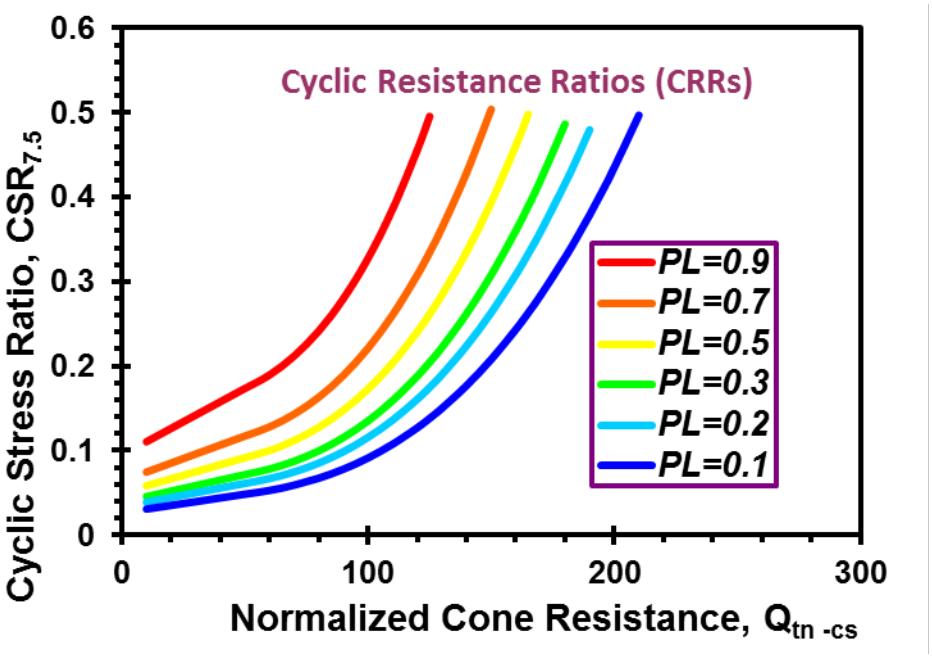

Figure 2-28 Family of CRR curves corresponding to different levels of probability of liquefaction (after Jiang and Juang, 2000).

Additional, considerations in liquefaction assessment can be given to the effects of sloping ground, very high overburden stresses, and limited sand layer thicknesses (Youd et al., 2001; Robertson, 2004; Robertson 2010). In addition, re-evaluation of compiled liquefaction case histories and re-examination of CPT data have been made independently by Idriss and Boulanger (2004) and Moss et al. (2006) with new formulations and algorithms for normalized CPT data and corrections for fines content. Appendix B presents the latest CRR trends for SPT and CPT developed by Boulanger & Idriss (2014). In general, the various methods tend to show similar results in the definition of the CRR curves, despite the differences in their stress-normalization schemes, as illustrated by Figure 2.29, particularly in the loose-firm sand regions where $Q_{tn} < 100$.

2.5.4.3.4 Advances in Testing

The amount of detail in subsurface exploration depends upon the type of test employed during field investigations and can be particularly important in paleoliquefaction studies since the depths and thicknesses of liquefied layers may be of limited extent. In the conventional rotary drilling and sampling operations, it is customary to conduct the SPT on 1.5-m depth intervals within the boreholes (Figure 2.30). Similarly, the conventional crosshole test (CHT) for collection of shear wave velocity (V_s) data obtains measurements at 1.5-m intervals. A somewhat better resolution is made during seismic cone tests since a geophysical downhole test (DHT) is performed at 1-m intervals for V_s determinations. In the DMT, readings are obtained at 20-cm intervals. CPT is particularly useful in paleoliquefaction analysis since multiple readings are made at 2-cm to 5-cm intervals, thus providing fine detailing of the soil profile. In addition, CPT results can be used to evaluate the magnitude of ground deformations (Appendix C).

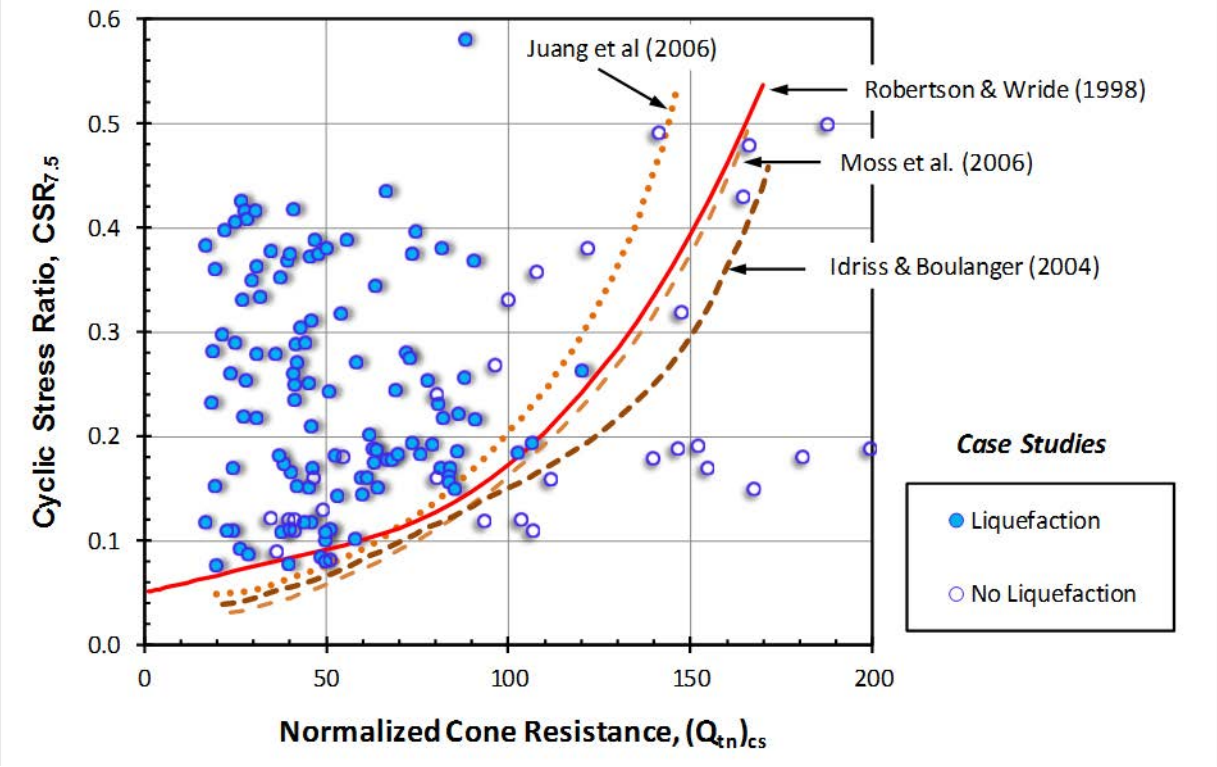

Figure 2-29 Comparison of the various CRR curves from different reviews of the available databases on seismic sites (Robertson, 2009). Note: Q_{tn} value is specific to its methodology.

A new type of downhole testing known as frequent-interval shear wave velocities (V_s) may help to reduce uncertainties related to measuring the properties of the sediment layers that liquefied during past earthquakes. The new technique employs either a seismic cone or a seismic dilatometer and allows detailed profiling of small-strain stiffness (Figure 2.30). Another technical advance includes the roto-autoseis, which is an electrically-driven surface source for shear wave generation that is high quality and repeatable, thus improving the resolution of V_s profiles and derived G_{max} profiles. Detailed profiles of two separate readings can be used independently to assess soil liquefaction potential at any given depth: (a) either q_{t1} and V_{s1} in the case of SCPT, or (b) K_D and V_{s1} in the seismic flat dilatometer test (SDMT). The results of a frequent-interval SCPTu from South Carolina is presented in Figure 2.31 showing very fine details in the shear wave velocity profile. The upper 15 m is within the vadose zone (i.e., above the groundwater table) and thus the higher expected values of V_s are in partially unsaturated soils. Based on the V_s profile, apparent cemented layers are evident at depths of 34 m and 44 m due to the calcareous constituency of the deeper Miocene to Eocene (5.3-56 Ma; Walker et al., 2012) deposits.

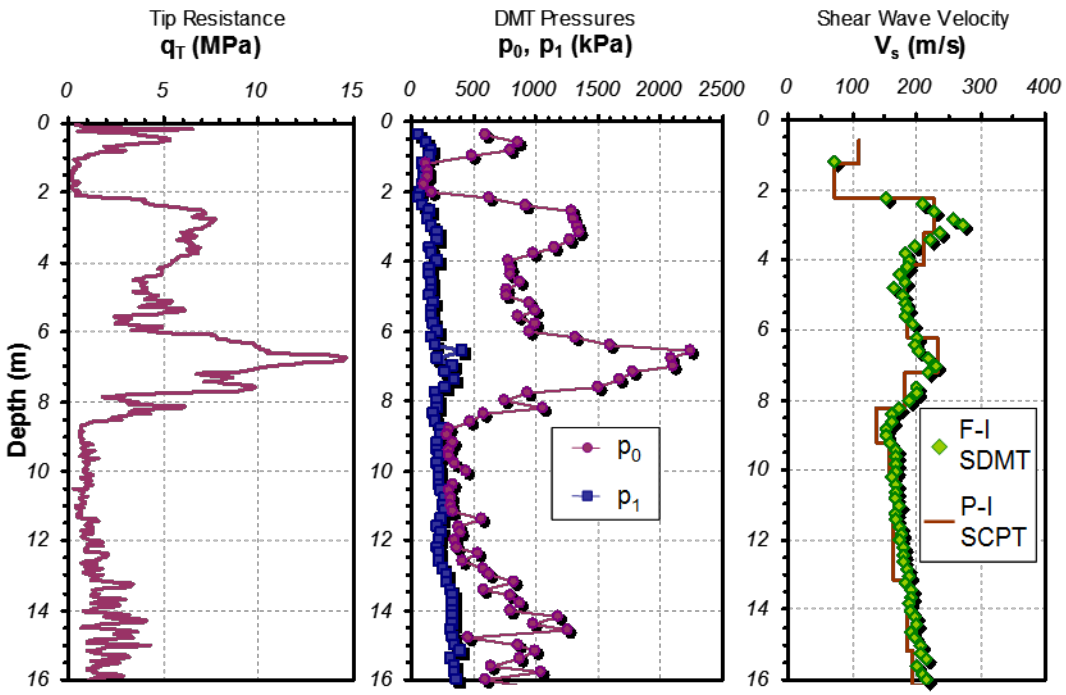

Figure 2-30 **Conventional SCPT cone tip resistance and neighboring seismic flat dilatometer test (SDMT) with frequent-interval V_s every 20 cm provides a detailed profile useful in paleoliquefaction (from McGillivray and Mayne, 2008). The normal SCPT increment for Vs readings is 1 m, CHT interval is 1.5 m (or 5 ft), and SASW interval 5 or 10 m.**

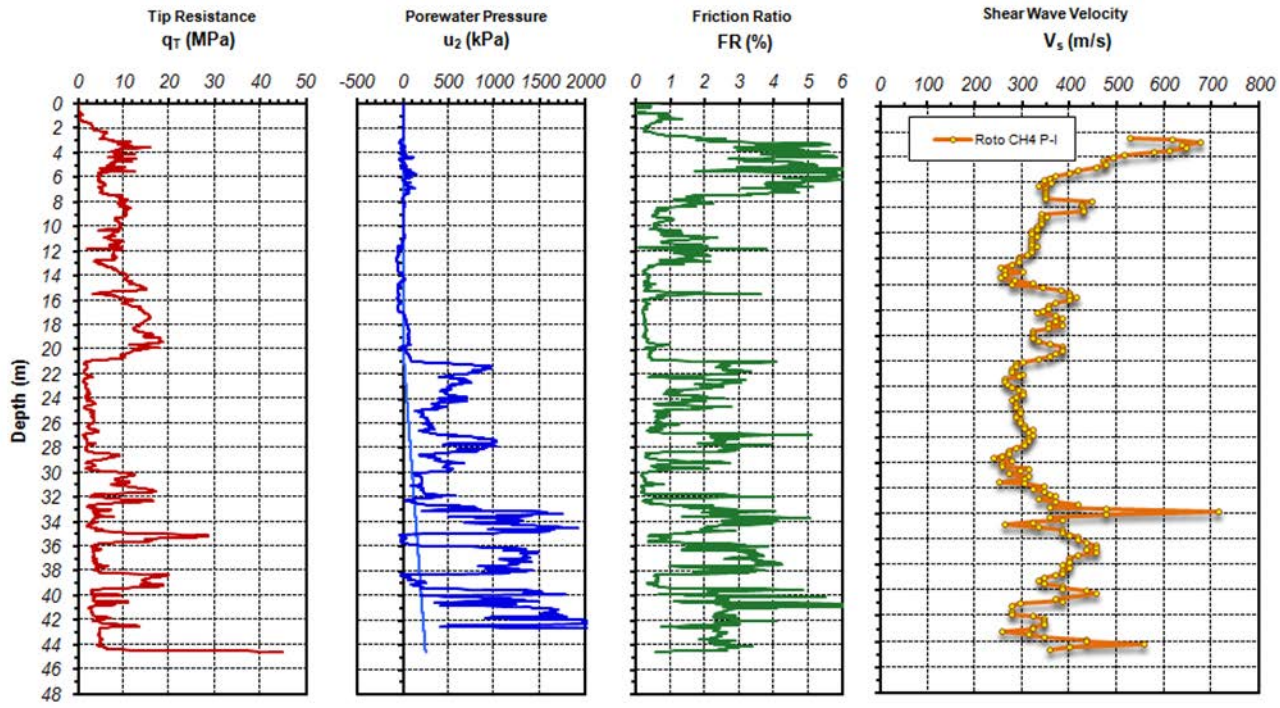

Figure 2-31 Representative frequent-interval SCPTu measurements near Aiken, South Carolina.

2.5.4.3.5 Liquefaction Potential Index

The liquefaction potential index (LPI) was originally proposed to assess the severity of liquefaction at a specific site, where severity is related to the degree of surface ground deformation. If LPI proves to be an effective tool for forward prediction of liquefaction, it also may be useful for inferring seismic parameters of past earthquakes from measurements at paleoliquefaction sites. LPI has been used to infer peak ground accelerations at a site shaken by the 2003 San Simeon, California, earthquake (Holzer et al., 2005). The inferred ground motions compared favorably to seismically based estimates. In addition, LPI has been used to infer possible seismic sources in southeastern Arkansas, although questions remain about the interpretation of paleoliquefaction features in that area (Cox et al., 2007; NUREG-2115).

LPI combines (for an individual boring or sounding) depth, cumulative thickness, and factors of safety of liquefiable intervals into a single parameter. It evaluates the factor of safety and thickness of potentially liquefiable layers to a depth of 20 m based on the proximity of layers to the ground surface. Iwasaki et al. (1978) define LPI as follows:

$$LPI = \int_0^{20m} F\mathcal{W}(Z)dZ,$$

where F = a function of the factor of safety against liquefaction (FS) defined as $F = 1 - FS$ for $FS \leq 1$ and $F = 0$ for FS > 1; z = depth in meters; and $w(z) = 10 - 0.5z$ is a linear depth-weighting factor. LPI values theoretically can range from 0 to 100. LPI evaluates the factor of safety and thickness of potentially liquefiable layers according to the proximity of layers to the ground surface.

Toprak and Holzer (2003) calibrated LPI by correlating computed values from CPT soundings at soil sites in California that had been strongly shaken during modern earthquakes, with locally observed surface manifestations of liquefaction. Their correlations indicate that the severity of liquefaction increases with increasing LPI. They observe that in general, sand boils or blows appear at $LPI = 5$ and lateral spreads occur at $\mathrm{LPI}=12$. Furthermore, they proposed that LPI could be used in probabilistic liquefaction hazard mapping by characterizing the statistical variability of liquefaction potential of surficial geologic units. Holzer et al. (2006a) attempted such an application of LPI for mapping the variability of liquefaction potential of geologic units in the Greater Oakland area, California. Their approach relied on field-based complementary cumulative frequency distributions of LPI for mappable surficial geologic deposits. Holzer et al. (2006b) used these distributions to develop liquefaction probability curves for a surficial geologic unit, where the probability of liquefaction is estimated from the ratio of peak ground acceleration $(\mathrm{a_{max}})$ to the liquefaction magnitude scaling factor (MSF), $\mathrm{a_{max}}/\mathrm{MSF}$. More recently, liquefaction probability curves have been proposed for a wide range of geologic units (Holzer et al., 2011).

Liquefaction hazard maps for future earthquakes using LPI, based on seismic cone penetration tests and measurements of pore water pressure (SCPTu), have been published for the Bay Area, California; Charleston, South Carolina; Evansville, Indiana; Memphis, Tennessee; and St. Louis, Missouri. For example, Heidari et al. (2011) characterize the liquefaction potential of the sandy portion of the 100,000-year-old Wando Formation (Qws) near Charleston, South Carolina, in terms of the LPI and corrected for the influence of diagenetic processes. They found that values of LPI are independent of the fault distance and suggest a uniform liquefaction susceptibility for Qws. In addition, liquefaction scenarios for historic earthquakes using LPI have compared favorably to liquefaction observations for these earthquakes.

2.5.5 Recurrence of Paleoearthquakes

A primary contribution of paleoliquefaction studies is a longer view of the seismic behavior of a fault zone or earthquake source area than afforded by the historical period. However, this view is limited by the completeness of the earthquake record. The paleoearthquake record may be incomplete in a particular region for a variety of reasons, including spatial variability in sedimentological and hydrological conditions, changes in liquefaction susceptibility over time, and availability of exposures and adequate sampling (NUREG-2115), and thus must be evaluated cautiously. The degree of completeness in space and time contributes to uncertainty in the locations, magnitudes, and recurrence times of paleoearthquakes. For regions where the paleoearthquake record is thought to be incomplete, paleoliquefaction features still can be used to determine the minimum number of earthquakes of a particular magnitude range for a given period. In this way, a minimum recurrence rate can be estimated. For regions in which the paleoearthquake record is reasonably complete for a certain time period (e.g., the Holocene), recurrence times for liquefaction-inducing earthquakes can be estimated.

The precision with which recurrence times can be calculated will depend on the precision of the estimated timing of the paleoearthquakes. Well-constrained age estimates of liquefaction features and paleoearthquakes contribute to well-constrained estimates of recurrence times (Table 2.3), providing that multiple earthquake cycles are recognized. The space-time diagram, in which the ages of liquefaction features are plotted against the locations of the features, is a graphical tool commonly used in paleoseismology (McCalpin, 1996 and 2009). In paleoliquefaction studies, the graphical representation of paleoliquefaction data aids in the correlation of similar-age features across a region, reducing the uncertainty associated with the timing of a paleoearthquake, the identification of paleoearthquake source areas, and the calculation of recurrence times for each source (Figures 2.16 and 2.32; Tuttle et al., 2002b). For regions with long and complete

paleoearthquake records, space-time diagrams of paleoliquefaction data may help in recognizing clustered versus non-clustered behavior and periodicity of seismicity. As more paleoliquefaction data become available over broad regions, the ability to evaluate the spatial and temporal distribution of paleoearthquakes produced by a single source or by multiple sources and to address questions related to long-term behavior and interaction of fault systems is improved.

McCalpin (1996) suggests using statistical tests (Z statistic) to determine whether clustered paleoearthquakes in a study zone are related (e.g., whether they occur on multiple segments of the same fault). This test examines the extent to which the probability distributions associated with the numerical ages for the paleoearthquakes overlap. As the timing of individual events becomes better constrained, the standard deviation of the age estimate is reduced and the probability that the earthquakes are related increases. Knowing whether individual earthquakes are contemporaneous contributes to understanding the potential for faults or fault segments to interact during an earthquake rupture. This has significant implications for seismic hazard in estimating the maximum probable earthquake for a regional assessment.

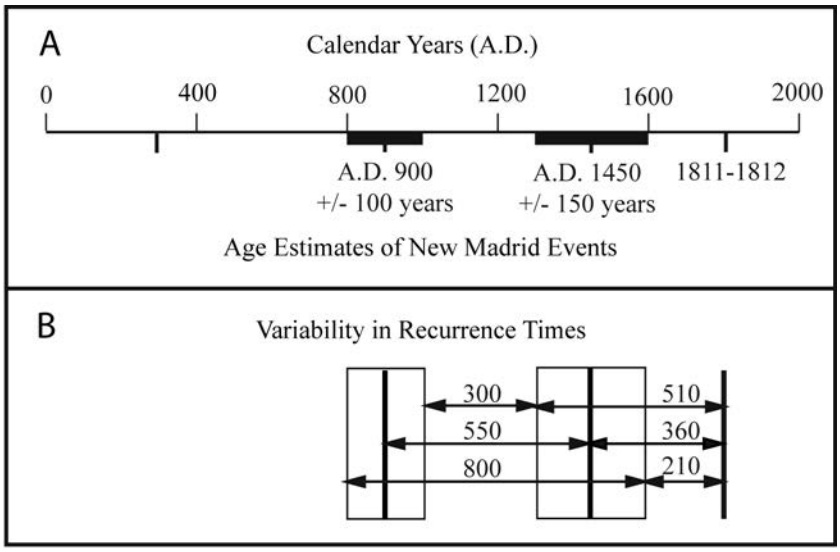

Figure 2-32 Example of graphical representation of age estimates and recurrences times of paleoearthquakes in the New Madrid seismic zone (from Tuttle et al., 2002b). (A) Age estimates and related uncertainties of New Madrid events during past 2,000 years. (B) Variability in recurrence times related to ranges of event ages. Average recurrence time for past two earthquake cycles is 500 years.

Regional space-time-histories can also be used to reveal information about the periodic behavior of fault systems. For example, as knowledge about the timing and source areas of large paleoearthquakes in the greater New Madrid region has accumulated, inferences have been drawn regarding migration of the locus of activity over time (Tuttle et al., 2006; Al-Shukri et al., 2009; NUREG-2115).

Although paleoliquefaction studies, when used in these ways, extend the earthquake record for seismic hazard estimation, it should be noted that it does so only for earthquakes larger than ~ M 6, which is generally accepted as the minimum magnitude required to produce liquefaction features over a large area. That is, the long-term behavior of low to moderate seismicity may notbe revealed by these studies, so a complete understanding of fault system dynamics cannot be achieved.

3 USE OF PALEOLIQUEFACTION DATA IN EARTHQUAKE SOURCE CHARACTERIZATION

Paleoliquefaction studies provide information about large earthquakes during the past 50,000 years, and possibly earlier, including their source areas, magnitudes, and recurrence times. In regions with fairly long and complete paleoearthquake records, paleoliquefaction data may also provide insights regarding clustered versus non-clustered behavior of earthquake sources and migration of seismicity within and/or between fault systems. This information is useful in the development of seismic source models, seismic hazard maps, and in site-specific seismic hazard assessments (e.g., Petersen et al., 2008 and 2014; Tuttle and Atkinson, 2010; NUREG-2115).

3.1 Development of Seismic Source Models

Over the past 10 years, paleoliquefaction data have increasingly shaped the seismic source model used in the National Probabilistic Seismic Hazard Maps developed and periodically updated by the U.S. Geological Survey. These maps display the ground-motion hazard component of the seismic provisions of national building codes and are used as input to design maps. The national seismic hazard maps also are used by the insurance industry to establish earthquake insurance rate and by government agencies concerned with national infrastructure. Given that they represent the best available data for estimating the sizes and frequencies of large Central and Eastern United States (CEUS) earthquakes, paleoseismic data were used to develop the fault model component of the seismic hazard model (Petersen et al., 2008). However, at the time, only the New Madrid seismic zone (NMSZ), the Charleston seismic zone, and the Meers and Cheraw faults were judged to have sufficient paleoseismic data to constrain recurrence times for large earthquakes.

As part of the more recent CEUS SSC project, a regional seismic source model was developed for use in probabilistic hazard analyses for nuclear facilities (NUREG-2115). The source model defines the frequency, spatial distribution, and rupture characteristics of potential earthquakes in the future (NUREG-2115). A master logic tree is used to establish the framework for the regional seismic source model. The framework includes a hierarchical approach to the identification and characterization of seismic sources. Sources of repeated large-magnitude earthquakes (i.e., RLMEs with magnitudes greater than 6.5, in this case) are included as a branch of the master logic tree. In the master logic tree, RLME sources help to define the Mmax zones for assessing the spatial and temporal characteristics of future earthquake sources. The project made unprecedented use of paleoliquefaction data, collected over the previous twenty to thirty years, to define the RLME sources. More specifically, paleoliquefaction data, where available, are used to evaluate whether a RLME source is in or out of an earthquake cluster and to define the range and weights of magnitudes and recurrence rates for RLMEs (Figure 3.1).

Relying heavily on the CEUS SSC project, the 2014 National Probabilistic Seismic Hazard Maps updated the information on the New Madrid, Charleston, Meers, and Cheraw sources and added six more fault-based sources of RLMEs, including the Wabash Valley (IL-IN), Commerce Geophysical Lineament (AR-IN), the Eastern Rift Margin (western TN) Marianna (east-central AR), and Charlevoix (southeastern Canada) areal source zones and the New Madrid (AR-KY) fault source (Petersen et al., 2014). Paleoliquefaction data figured largely in the Wabash Valley, Charlevoix, and New Madrid sources.

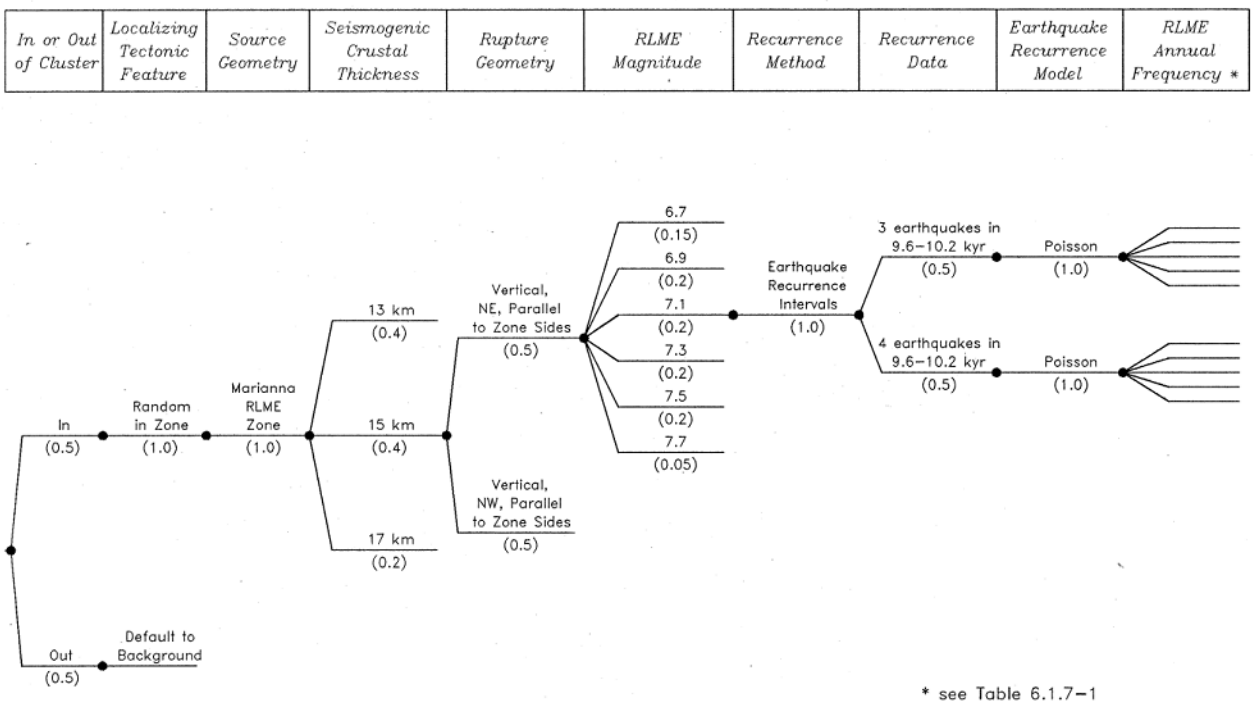

Figure 3-1 Example of logic tree for the Reelfoot rift-Marianna RLME source (from NUREG-2115). Paleoliquefaction data figure into evaluations of clustered behavior and magnitude and recurrence of RLMEs. The branch representing "out of cluster" behavior is not shown.

As part of the CEUS SSC project, a paleoliquefaction database including all major datasets was developed for use in the regional seismic source model. In addition, a technical report was written, summarizing the current state of knowledge for each region and reviewing uncertainties related to the identification and interpretation of earthquake-induced liquefaction features (Appendix E in NUREG-2115). Guidance for the use of paleoliquefaction data in seismic source characterization also was developed and is provided below:

- Ensure liquefaction features have an earthquake origin and are not the result of other non-seismic processes. Diagnostic criteria and characteristics of liquefaction features are described in Section 1.4.3.

- Use liquefaction features with well-constrained calibrated (2-sigma) ages to determine timing of paleoearthquakes (see Sections 2.4 and 2.5.2; Figure 2.11). Space-time diagrams illustrating age constraints and estimated ages of features can help to estimate timing of paleoearthquakes (e.g., Figure 2.16).

- Correlate features that are similar in age and/or occur in similar stratigraphic context within the same exposure or where strata are laterally continuous (Section 2.5.1 and Table 2.1).

- Compare size and distribution of paleoliquefaction features with those that formed during modern or historical earthquakes in the same or similar geologic and tectonic settings to help interpret the source areas and magnitudes of causative earthquakes (Sections 2.5.3 and 2.5.4.1).

- Use information on surficial geology, geologic and groundwater history, and geotechnical data and analysis, to help interpret the source areas and magnitudes of paleoearthquakes. Time-slice maps and animations may help to interpret earthquake source areas, and ground motion simulations may help to interpret earthquake magnitudes.

- Use empirical relations developed from case studies of modern earthquakes in similar geologic and tectonic settings to estimate magnitudes of paleoearthquakes on the basis of maximum distance of sand blows from the inferred epicenters (Section 2.5.4.2).

- If sufficient data are available, analyze the effect of ground motion parameters (e.g., attenuation and site response) on the size and distribution of liquefaction features and apply the geotechnical approach to help interpret source areas and magnitudes of paleoearthquakes (Section 2.5.4.3).

- Consider the completeness of the paleoearthquake record in both space and time when estimating source areas, magnitudes, and recurrence times of paleoearthquakes.

- If sufficient data are available, estimate recurrence times of paleoearthquakes that exhibit well-defined timing, source areas, and magnitudes of paleoearthquakes (Section 2.5.5).

3.2 Example - New Madrid Seismic Zone in Central United States

In 1811-1812, a major earthquake sequence including three mainshocks with moment magnitudes, **M** 7 to 8, and several large aftershocks, struck the central United States (Figure 2.16; e.g., Johnston, 1996; Hough et al., 2000; Bakun and Hooper, 2004). These earthquakes are inferred to have been centered in the NMSZ and to include some of the largest known intraplate earthquakes in the world (Johnston and Kanter, 1990). The 1811-1812 earthquakes destroyed several settlements along the Mississippi River and induced severe liquefaction and ground failure throughout the New Madrid region. A large liquefaction field (~10,000 km^2) has been attributed to the 1811-1812 earthquakes (Fuller, 1912; Saucier, 1977; Obermeier, 1989). In addition, the 1811-1812 earthquakes caused minor structural damage as far away as Cincinnati, Ohio, and St. Louis, Missouri, and induced liquefaction more than 240 km from their inferred epicenters (Street and Nuttli, 1984; Johnston and Schweig, 1996). The large liquefaction field and the great distance of liquefaction support the interpretation that the 1811-1812 mainshocks were very large-magnitude earthquakes (Fuller, 1912; Ambraseys, 1988; Johnston and Schweig, 1996; Tuttle et al., 2002b; Castilla and Audemard, 2007). There is considerable concern about possible impacts of a repeat of a New Madrid event to urban centers such as Memphis, TN, Little Rock, AR, and St. Louis, MO, and to engineered structures across the central United States.

Paleoliquefaction studies have made great strides in deciphering the prehistorical earthquake record of the NMSZ and improving understanding of the hazard it poses. By finding and dating hundreds of earthquake-induced liquefaction features across the region, earthquake sequences, similar to the 1811-1812 sequence, are thought to have occurred in A.D. 900 $\pm$ 100 yr, A.D. 1450 $\pm$ 150 yr, and 2350 $\pm$ 200 yr B.C. (Figure 2.16 and 2.17; e.g., Tuttle et al., 2002b and 2005b). From these paleoliquefaction data, a mean recurrence time of 500 years has been estimated for New Madrid events. Results of the paleoliquefaction studies, including insights on temporal clustering of earthquakes, timing, source area, and approximate magnitude of paleoearthquakes, as well as recurrence times of large-magnitude earthquakes, have been incorporated into seismic source models developed for seismic hazard assessments (NUREG-2115; Petersen et al., 2014).

3.2.1 Paleoliquefaction Studies in the New Madrid Region

During the past 30 to 40 years, various investigators have searched for and studied earthquake-induced liquefaction features in the NMSZ and surrounding region. In some of the studies, liquefaction features were assumed to have formed in 1811-1812. In other studies, pre-1811 sand blows and related sand dikes were recognized by their soil characteristics and stratigraphic and structural relationships (e.g., Russ, 1982; Saucier, 1991; Tuttle and Schweig, 1995; Tuttle et al., 1996). Since then, paleoliquefaction studies have focused on finding and dating paleoliquefaction features, constraining their ages, comparing their internal stratigraphy, sizes, and spatial distribution to features that formed during the 1811-1812 earthquakes, and estimating the locations, magnitudes, and recurrence times of their causative paleoearthquakes (e.g., Tuttle, 1999; Tuttle et al., 2002b and 2005b). In addition, magnitude-distance relations have been considered and liquefaction potential analyses have been performed to help constrain locations and magnitudes of paleoearthquakes.

Paleoliquefaction studies have been conducted in Holocene and Pleistocene fluvial deposits of the Mississippi River and its major tributaries. Some paleoliquefaction studies involved investigating sand blows at archeological sites (e.g., Saucier, 1991; Craven, 1995; Tuttle et al., 1996, 1999, and 2005b; Wolf et al., 2006), whereas others involved searching for liquefaction features along river cutbanks and drainage ditches (Figure 3.2; e.g., Vaughn, 1994; Tuttle, 1999 and 2010; Broughton et al., 2001). To date, more than 650 km of rivers and ditches have been searched and over 800 liquefaction features have been studied at about 210 sites (NUREG-2115; and NRC-HQ-11-C-04-0041). At the sites, liquefaction features were documented, described, and measured, and samples, where available, were collected for dating the liquefaction features. At more than 50 sites, half of which were also archeological sites, age estimates of sand blows and related sand dikes are well constrained (Figures 2.16 and 2.17; e.g., Tuttle et al., 1999, 2002b, 2005b).

The age estimates of liquefaction features across the region cluster around A.D. 1810 $\pm$ 130 years, A.D. 1450 $\pm$ 150 years, and A.D. 900 $\pm$ 100 years (Figure 2.16; Tuttle et al., 2002b). These dates are interpreted as the timing of paleoearthquakes. Age estimates of liquefaction features at several sites in northeastern Arkansas and southeastern Missouri cluster around 2350 B.C. $\pm$ 200 yr, suggesting an earlier event (Tuttle et al, 2005b). The sizes and spatial distributions of sand blows that formed during the paleoearthquakes are strikingly similar to those that formed during the 1811-1812 New Madrid sequence (Figure 2.17). In addition, there is a close spatial correlation of both historic and prehistoric sand blows with the NMSZ, which was almost certainly the source of earthquakes responsible for most, if not all, of the liquefaction features. The paleoliquefaction findings indicate that the NMSZ generated sequences including earthquakes similar to the 1811-1812 mainshocks (**M** 7 to 8) every 500 years on average during the past 1,200 years. The uncertainties in the timing of each New Madrid event allow for recurrence time to be as short as 160 years and as long as 1200 years (Figure 2.32; Cramer, 2001).

Many historic sand blows in the New Madrid region were found to be compound structures attributable to the three to four largest earthquakes in the 1811-1812 sequence (Saucier, 1989; Tuttle, 1999; Tuttle et al., 2002b). The compound sand blows range from 0.2 to 2 m total thickness and are composed of 1 to 4, generally fining-upward sedimentary units that are 20 to 60 cm thick, tens of meters wide, and hundreds of meters long (Figure 3.3). Often the depositional units are capped by silt or clay resulting from quiet water deposition following the cessation of ground shaking. During the 2010-2011 Canterbury sequence in New Zealand, recurrent liquefaction occurred during as many as ten earthquakes (Quigley et al., 2012), leading to the formation of compound sand blows composed of multiple depositional units capped by silt drapes

(Tuttle et al., 2012; Villamor et al., 2014). The compound sand blows in the Canterbury region range up to about 40 cm thick, 5 m wide, and 10 m long and are much smaller than those in the NMSZ (Tuttle et al., 2012). Sand blows in the New Madrid region are large, diameter ≈ 30 m ± 10 m, compared to sand blows worldwide (e.g. California sand boils have diameter ≈ 2 ± 1 m) (Castilla and Audemard, 2007).

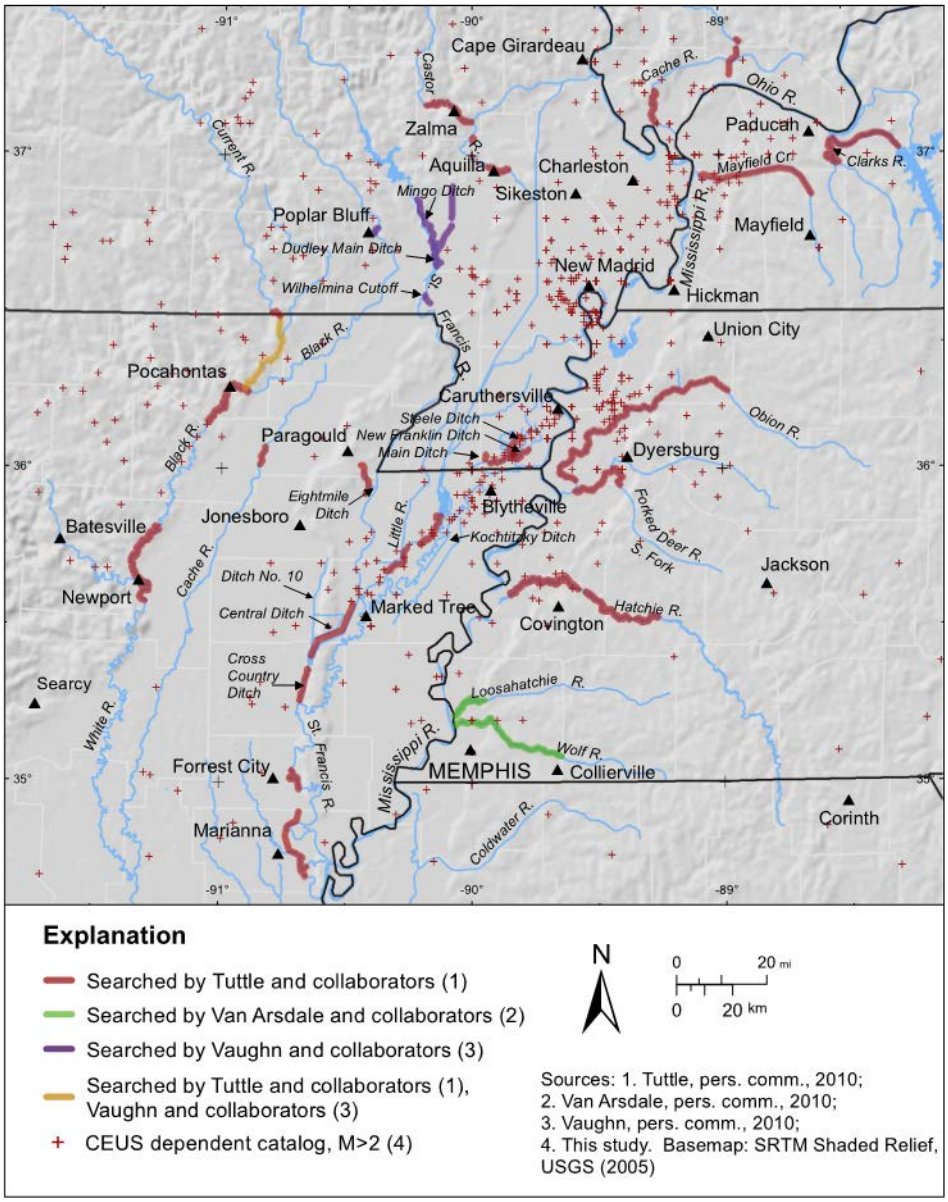

Figure 3-2 Map of NMSZ and surrounding region showing portions of rivers searched for earthquake-induced liquefaction features by various investigators (from NUREG-2115).

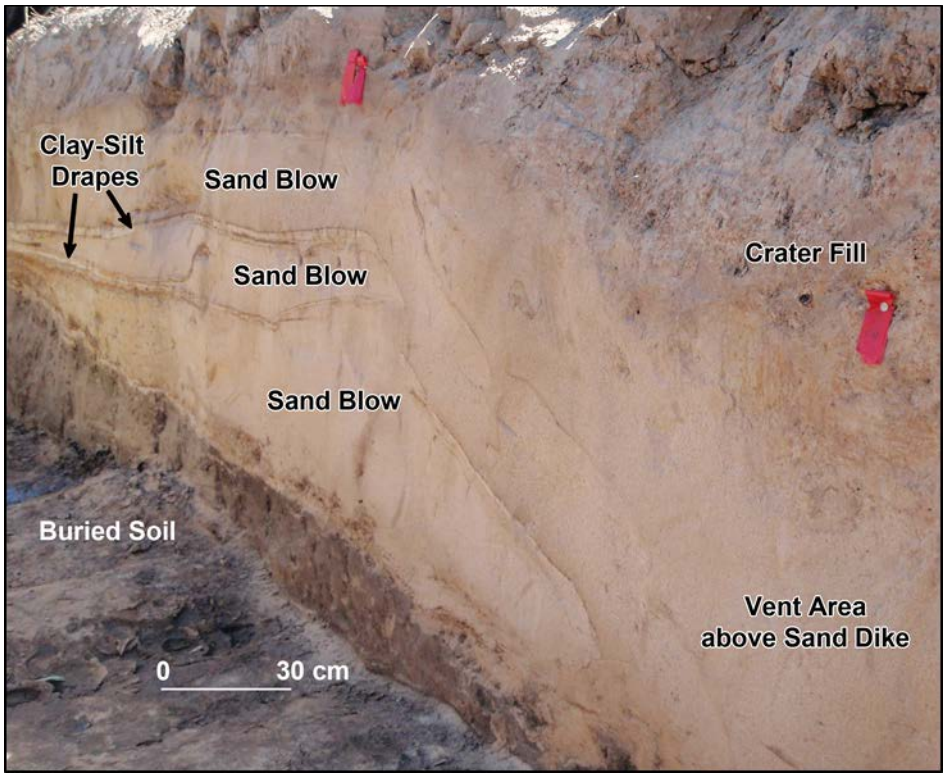

Figure 3-3 Compound sand blow composed of multiple depositional units capped by clay-silt drapes formed during 1811-1812 New Madrid earthquake sequence. See Figure 1.16 for view of vent area and related sand dikes below. Photograph by M. Tuttle

Like those that formed in 1811-1812, many of the pre-1811 sand blows are compound structures composed of multiple, fining upward units, indicating that they too formed as the result of several large earthquakes clustered in time (Tuttle, 1999; Tuttle et al., 2002b). The lack of inter-event soil development of depositional units argues for closely timed earthquakes over a period of only months. The total thickness of the pre-1811 compound sand blows, as well as the thickness of the depositional units (sand blows representing individual earthquakes) are similar in thickness and lateral extent to depositional units that formed in 1811-1812, suggesting that the A.D. 1450 and A.D. 900 events caused similar levels of ground shaking, and therefore were similar in magnitude, to the 1811-1812 earthquakes.

The spatial distribution of sand blows that formed in 1811-1812 are explained with three liquefaction fields, taking into account the internal stratigraphy or number and thickness of the major depositional units constituting sand blows across the region (Figures 2.17 and 3.4). The sand blows that formed in 1811-1812 usually have a maximum of three major sedimentary units. However, several sand blows located between Caruthersville and Marked Tree have a fourth unit that may have formed as a result of a large aftershock, on December 16th. In a review of intensity data, the December 16th aftershock has been attributed to the southeastern segment of the Reelfoot fault (Hough and Martin, 2002). It will be interesting to see if a fourth liquefaction field (dashed in Figure 3.4) becomes better defined near the southeastern segment of the Reelfoot fault as newly acquired data is incorporated into the liquefaction maps.

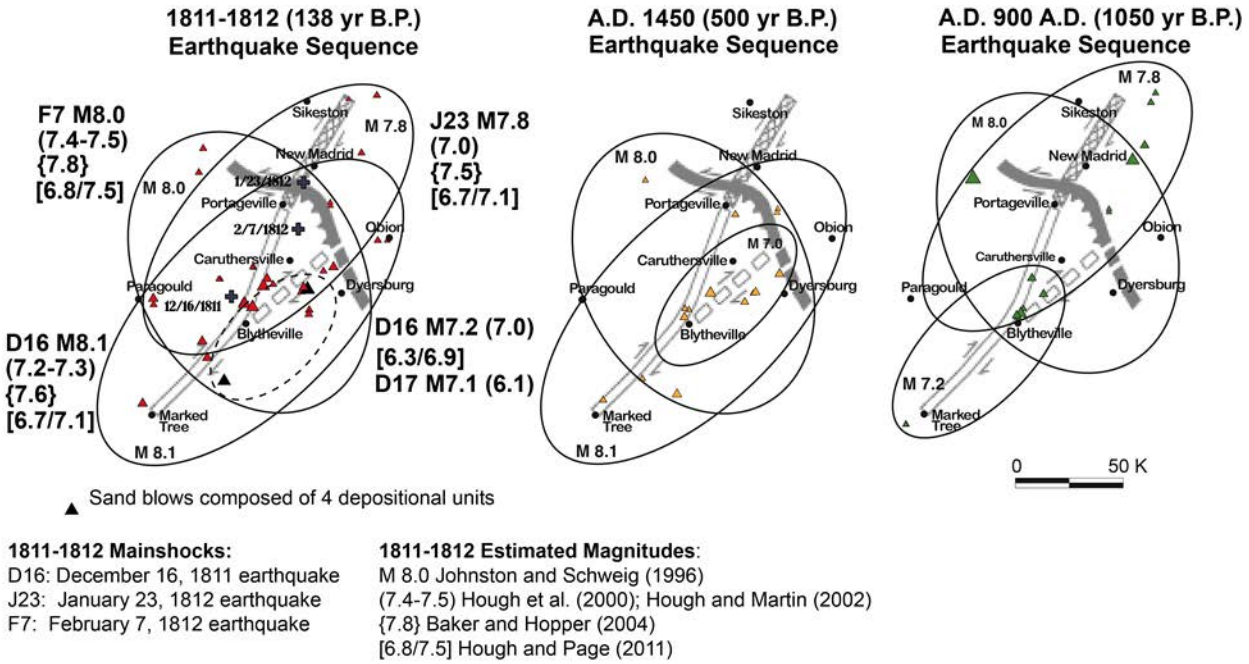

Figure 3-4 Liquefaction fields for the past three New Madrid events as interpreted from spatial distribution and stratigraphy of sand blows (from NUREG-2115). Ellipses define areas where similar-age sand blows have been mapped. Overlapping ellipses indicate areas where sand blows are composed of multiple units that formed during a sequence of earthquakes. Dashed ellipse outlines area where historical sand blows are composed of four depositional units. Magnitudes of earthquakes in A.D. 1450 and A.D. 900 are inferred from comparison with the 1811-1812 liquefaction fields. Magnitude estimates of December (D), January (J), and February (F) mainshocks and large aftershocks taken from several sources; rupture scenario from Johnston and Schweig (1996).

The liquefaction fields of the 1811-1812 earthquakes are constrained by sand blow data and encompass the preferred fault-rupture scenario for the 1811-1812 event of Johnston and Schweig (1996) (Figure 3.4). The liquefaction fields of the A.D. 1450 and A.D. 900 events can be modeled in a similar manner as the 1811-1812 earthquake sequence. The current interpretation of the sand blow data is that at least two earthquakes occurred during the A.D. 1450 and A.D. 900 events that were similar in locations and magnitudes to the 1811-1812 mainshocks. In addition, (1) faults associated with the northwest-oriented, central branch of the NMSZ, such as the Reelfoot fault, were the source of similar-size earthquakes during all three sequences, (2) faults associated with the southern branch of the seismic zone may have ruptured during each sequence, but produced a smaller magnitude earthquake in A.D. 900, and (3) faults associated with the northern branch of the NMSZ may have ruptured in A.D. 900 and 1812, but not in A.D. 1450 (Tuttle, 1999; Tuttle and Hartleb, 2012). Other interpretations of sand blow distribution and stratigraphy are possible, and the liquefaction fields will likely change as additional data are added to the maps. Using sand blow distribution and stratigraphy to map the liquefaction fields of multiple large events in an earthquake sequence is a powerful tool for identifying earthquake sources and studying the behavior of the complex fault system in the New Madrid region.

Overall, the similarity between the historical and prehistoric liquefaction fields suggest that the paleoearthquakes were generated by sources in the same area and had similar magnitudes to the mainshocks of the 1811-1812 sequence. Using the magnitude-distance relations developed from case studies of liquefaction around the world (e.g., Ambraseys, 1988; Castilla and Audemard, 2007), lower bound moment magnitude of 6.7 and 6.9 were estimated for the A.D. 1450 and A.D. 900 events, respectively, from the distance of observed sand blows. However, these are minimum magnitude values since the limits of liquefaction have not yet been defined for the paleoearthquakes, even though more than 650 km of river and ditch cutbanks have been searched. For the 1811-1812 event, the magnitude-distance relations suggest a lower bound **M** of 7.6 given a maximum distance of 240 km for surface manifestation of liquefaction. Since the paleoliquefaction features are similar to the 1811-1812 features in the meizoseismal area, it seems likely that they may extend to a similar maximum distance as the historical features. However, this is yet to be confirmed by additional reconnaissance in distant locations.

Several studies have used the geotechnical approach to estimate the magnitude of New Madrid events. Overall, the results are consistent with interpretations of the locations and magnitudes of historic and prehistoric earthquakes. Using electronic cone penetration soundings collected at six liquefaction sites in northeastern Arkansas and southeastern Missouri and within the NMSZ, it was concluded that the December 1811 New Madrid earthquake was likely in the **M** 7.6-8.0 range (Schneider and Mayne, 2000; Liao et al., 2002). Similarly, analysis of geotechnical data collected at a liquefaction site east of Memphis, TN, along the Wolf River, suggested that the December 1811 earthquake was larger than **M** 7.5 (Schneider et al., 2001). Another study using the same data from the NMSZ and the Wolf River found that magnitudes in the **M** 7.4 -8.4 range were necessary to cause liquefaction at the sites disregarding soil aging effects (Stark, 2002). Liquefaction analysis using geotechnical data from a bridge crossing close to liquefaction sites along the Hatchie River near Covington, TN suggested that the December 16, 1811 and February 7, 1812 mainshocks were ~**M** 7.6 and 7.8, respectively, and that the January 23, 2012 mainshock was located too far away to induce liquefaction in this area, even if it were of **M** 7.8 (Tuttle, 2004). Interestingly, these finding are supported by observations of compound sand blows along the Hatchie River, suggesting two episodes of liquefaction during the 1811-1812 event. The magnitude estimates, ~**M** 7.6 and 7.8, are similar to those derived from intensity data for the 1811-1812 mainshocks (Bakun and Hopper, 2004).

Taken together, the results of the various paleoliquefaction studies in the New Madrid region strongly suggest that the NMSZ generated earthquake sequences including very large, **M** 7 to 8, mainshocks in A.D. 1450 $\pm$ 150 years, A.D. 900 $\pm$ 100 years, and probably in 2350 B.C. $\pm$ 200. Therefore, the NMSZ can be characterized by an average recurrence time of 500 years, at least during the past 1,200 years, for 1811-1812 New Madrid-type events (Tuttle, 1999; Tuttle et al., 2002b and 2005b).

3.2.2 Seismic Hazard Models for the New Madrid Seismic Zone

As mentioned above in Section 3.1, paleoliquefaction data were used in the development of seismic source models for the 2012 CEUS SSC project's probabilistic hazard analyses and the 2014 National Probabilistic Seismic Hazard Maps. More specifically, the data were used to identify sources of RLMEs, to evaluate whether RLME sources are in or out of an earthquake cluster, and to define the range and weights of magnitudes and recurrence times for the RLMEs.

From paleoliquefaction data, it is clear that the NMSZ is a source of RLMEs. Also, the paleoliquefaction data indicate that the NMSZ produced three of the four events during the past 1200 years, suggesting that it is likely to be within a cluster or active period with New Madrid

events occurring on average every 500 years. There is significant uncertainty in magnitude estimates of the paleoearthquakes and the 1811-1812 mainshocks; however, most magnitude estimates fall within the 6.9-7.9 range. Furthermore, liquefaction data indicate that the NMSZ produced sequences including very large earthquake about A.D. 1450 and A.D. 900, as well as in 1811-1812, suggesting an average recurrence time of 500 years. These earthquake parameters are reflected in the NMSZ logic trees of the seismic source models in the CEUS SSC project and the National Probabilistic Seismic Hazard Maps. In the logic tree of the CEUS SSC project, a heavier weight (0.9) is placed on clustered earthquakes than on non-clustered earthquakes (0.1) and the dates of the last three New Madrid events (1811-1812, A.D. 1450 and A.D. 900) are included in the recurrence data (Figures 3.5; NUREG-2115). In the logic tree of the National Probabilistic Seismic Hazard Maps, weighting on earthquake sequence and on a recurrence time of 500 years is increased over the values used in the 2008 maps (Figure 3.6; Petersen et al., 2014). In addition, the 2014 logic tree includes the CEUS SSC project fault model as an alternative branch.

The NMSZ is recognized as having the highest hazard in the CEUS, but large uncertainties in the hazard models have spurred considerable debate and controversy. Sensitivity analysis of sources associated with the NMSZ suggests that earthquake rate has the greatest effect on hazard estimates, with uncertainties being greatest for the central New Madrid fault zone (McGuire, pers. comm., 2012). Mean recurrence interval estimates for this region are much more dependent on paleoseismology than anywhere else in the CEUS. To remedy this problem, the NRC is supporting a multi-year research project to recover additional paleoliquefaction information to reduce the uncertainties associated with earthquake rates before the near-surface record of past earthquakes is lost to land leveling and other agricultural practices.

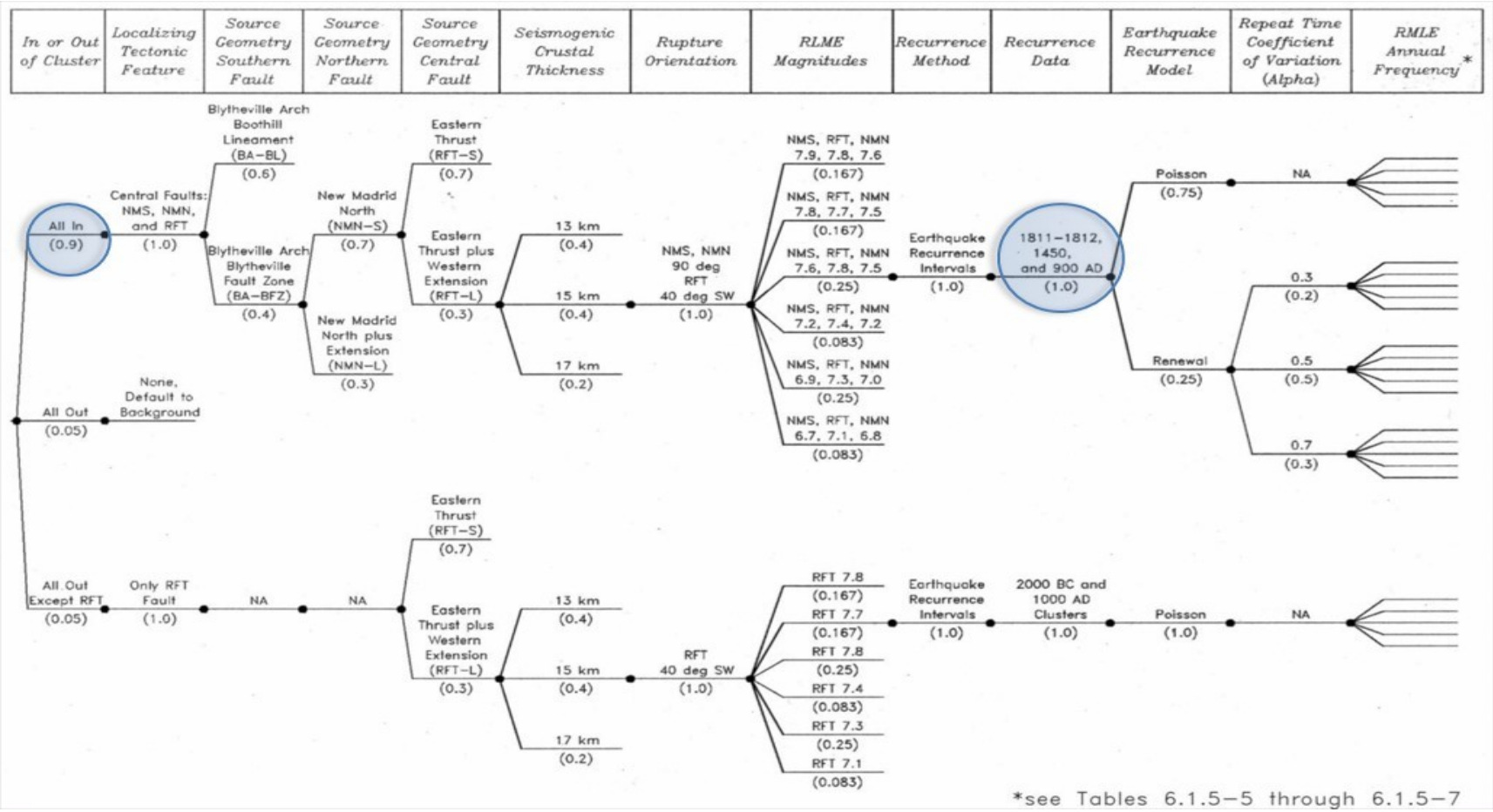

Figure 3-5 **NMSZ logic tree of the seismic source model in the CEUS SSC project (modified from NUREG-2115). Paleoliquefaction data are reflected in clustered behavior and in the recurrence data used in the seismic source model.**

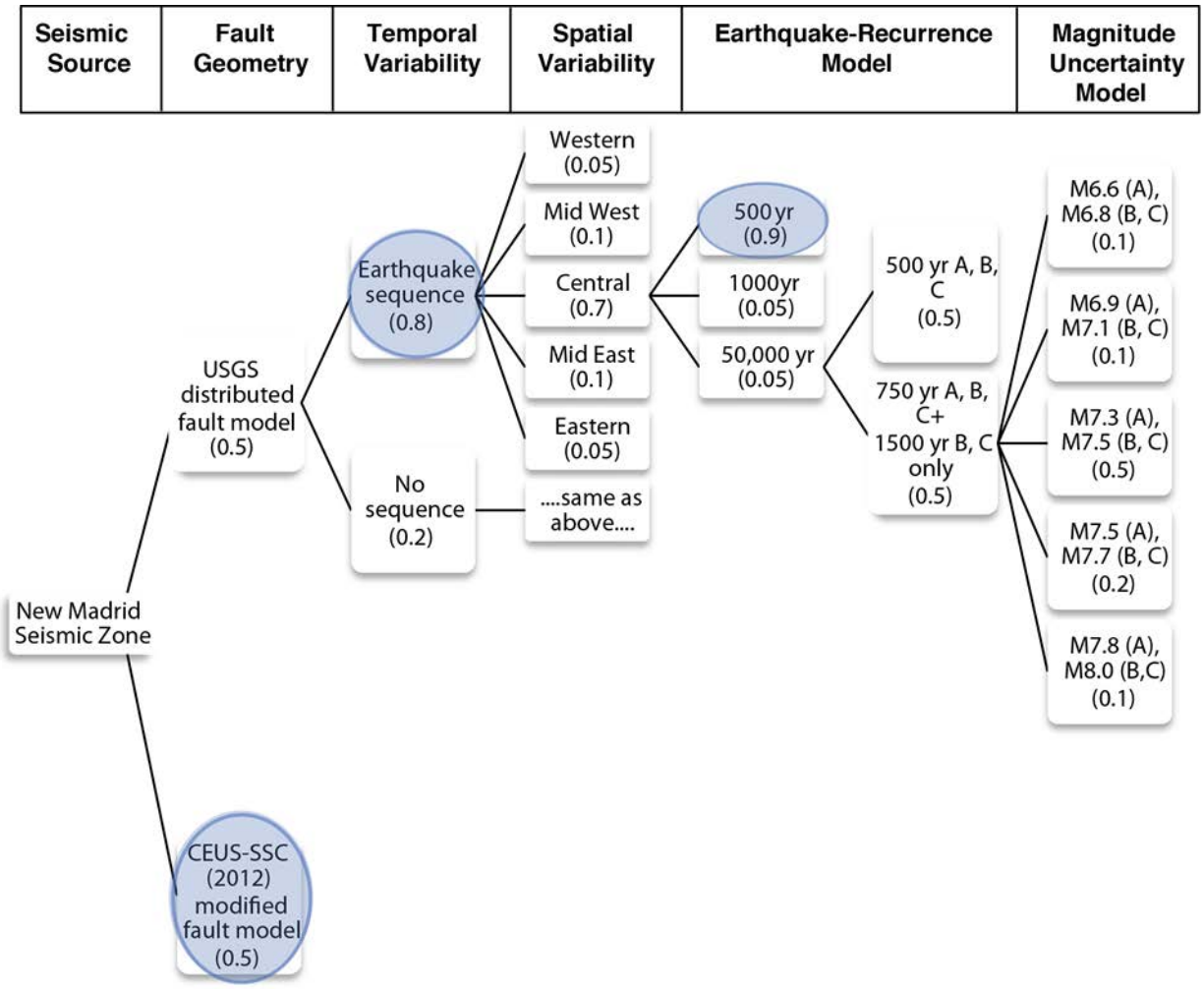

Figure 3-6 **NMSZ logic tree of the seismic source model in the National Probabilistic Seismic Hazard Maps (modified from Petersen et al., 2014). The ground motion model is not included in this figure. Paleoliquefaction data are reflected in increased weighting of earthquake sequence and 500 year recurrence time.**

4 RECOMMENDATIONS FOR FUTURE RESEARCH

Liquefaction studies contribute to understanding of seismic hazard by providing information about the timing, locations, magnitudes, and recurrence rates of paleoearthquakes. However, there are often large uncertainties associated with the derived earthquake parameters and there are many regions where paleoliquefaction studies have not yet been conducted. With additional research on various aspects of paleoliquefaction, it may be possible to reduce uncertainties associated with earthquake parameters and to advance the usefulness and application of this field of study.

Case Studies: Documentation of liquefaction induced by modern earthquakes, with well-constrained locations, magnitudes, and other earthquake parameters, is encouraged and would help to further characterize the size and spatial distributions of liquefaction features. The case studies should be regional in scope and include detailed descriptions of liquefaction features such as size and sedimentary characteristics of sand blows, dikes, sills and the soft-sediment deformation structures that formed within the liquefied layer. These case studies would provide calibration events for direct comparison as well as information that could be used to further improve empirical relations of earthquake and liquefaction parameters. Stratabound deformation structures, including convolute bedding and laminations, load casts, and pseudonodules, may be very useful in paleoliquefaction studies. However, additional research is needed to explore the full range of expression of these features as well as the ground motions and site conditions under which they form.

To gain a better understanding of both the processes of liquefaction and the effects on the source layers that liquefied, instrumentation of liquefaction-prone sites is encouraged, as is pre- and post-event measurement of geotechnical properties. This information may help to reduce uncertainties related to back-calculating magnitudes using post-event measurements. Field experiments of earthquake-induced liquefaction are more likely to be conducted in interplate settings where large earthquakes occur more frequently. It would be beneficial to better understand differences between characteristics, such as frequency content and attenuation of ground motion, of both intraplate and interplate earthquakes as they relate to liquefaction, so that results of field experiments could be applied to intraplate settings.

Mapping Using Remotely-Sensed Data: Modern technology provides new tools and techniques that make it possible to identify and map geologic and geomorphic features over large areas. It behooves us to develop methodologies that utilize these tools and techniques for mapping earthquake-induce liquefaction features and related ground failures, especially given the increasing human disturbance of the landscape and its impact of the geologic record of past earthquakes. Satellite imagery, image processing software, and geographical information systems provide the opportunity to combine data sets within a geographical framework and classify and map sand blows over large areas based on their spectral characteristics. For example, LANDSAT-7 Enhanced Thematic Mapper Plus (ETM+) imagery provides information on reflected or emitted radiation from the Earth's surface and holds promise for mapping sand blows of different ages based on soil characteristics. Light Detection and Ranging (LiDAR) high-resolution elevation data may be useful in mapping medium to large (greater than 2 m in diameter and 0.2 m in height) sand blows, if combined with other remotely-sensed data that reflect sediment and soil types. It should be recognized that liquefaction maps based on remotely-sensed data may be limited by feature size and depth of ground disturbance and will still require field validation.

Dating Techniques: Dating paleoliquefaction features is perhaps the most important aspect of any paleoliquefaction study. If the age estimates of paleoliquefaction features are not well

constrained, it is difficult to correlate similar age-features across a region and to interpret the locations and magnitudes of paleoearthquakes with confidence. Therefore, research to improve dating of paleoliquefaction features is a high priority.

Radiocarbon and optically-stimulated luminescence (OSL) are the two most commonly used dating techniques in paleoliquefaction studies. Because they are often collected stratigraphically above and below sand blows, samples for radiocarbon and OSL dating provide minimum and maximum constraining dates for liquefaction features, and thus the earthquakes that caused them. Although the individual dates may have precisions of ± 20–80 years, the age estimates of liquefaction features based on the combination of the minimum and maximum constraining dates will have uncertainties of about 100 years in the best of circumstances. Dating techniques and sampling strategies that provide more precise and accurate results would help to improve the utility of liquefaction features for identifying paleoearthquakes and characterizing regional seismicity.

OSL dating provides an opportunity to date soil and sediment buried by sand blows. Therefore, it is particularly useful at sites where organic samples necessary for radiocarbon dating cannot be found. However, uncertainties associated with OSL dating can be quite large, limiting its usefulness in paleoliquefaction studies, especially in regions where the repeat times of large earthquakes are on the order of hundreds of years. It is recommended that efforts be made to evaluate and improve both sampling and laboratory analysis used in OSL dating of sand blows, so that tighter age estimates can be derived from this technique.

Dendrochronology is one technique that could improve accuracy (annual, possibly seasonal) of age estimates of liquefaction features. Therefore, it is recommended that case studies be conducted of impacts of earthquakes on trees, including burial by sand blows, damage related to ground failures, and direct damage to the living tissue. Using lessons learned from these studies, efforts could be made to use dendrochronology to date paleoliquefaction features in regions where chronologies of long-lived tree species are already developed and where fossil wood is preserved by paleoliquefaction. If those efforts are successful, it may be worthwhile to extend those chronologies back in time to constrain the ages of older liquefaction features. In addition, chronologies could be developed for new regions where they could help to date paleoliquefaction features.

Geophysical Techniques: Geophysical surveys have proven a useful tool for locating sand dikes, mapping sand blows, and selecting locations for paleoseismic trenches. However, distinguishing between earthquake-induced liquefaction features and non-seismic sedimentary features and deposits in remotely sensed data can be difficult, particularly where sand blows are buried and have no surface expression. A better understanding of the morphological and spatial characteristic differences between features and sedimentary deposits could increase the usefulness of geophysical methods as a reconnaissance tool and as a means for tracing features beyond trench excavations.

Although geophysical methods yield results sensitive to the physical properties of rocks and sediment, better knowledge of empirical relations between these properties and the geophysical observations would increase confidence in data interpretations. This information could be used to better understand the soil and sediment characteristics that contributed to the occurrence of liquefaction in a particular environment. Specifically, the influence of stratigraphic and sedimentological properties in the development of pore water pressures at liquefaction sites could lead to a better understanding of the process of liquefaction and the conditions that contribute to a site's susceptibility. Further work on calibrating geophysical surveys with sedimentological and

geotechnical analyses is needed to extend the utility of site-specific geotechnical measurements and improve the ability to relate laboratory studies of liquefaction to actual field studies.

Geotechnical Approach: There are many uncertainties associated with the geotechnical approach for estimating the magnitudes of paleoearthquakes. Additional research is needed to further evaluate and reduce the sources of these uncertainties. The development and application of new techniques, devices, and procedures for *in situ* testing of soil properties in paleoliquefaction studies could help to reduce some of the uncertainties as follows:

1. Improved resolution

The traditional sampling interval of soil borings may be too gross to accurately reflect the properties of the deposit or layer that liquefied. The sampling interval for standard penetration test (SPT) N-values and crosshole/downhole shear wave velocities is 1.5-m. The conventional seismic cone test (SCPT) and seismic dilatometer test (SDMT) improve slightly on this as shear wave data are collected at 1-m intervals. However, the newest techniques such as frequent-interval shear wave velocities (V_s) using either a seismic piezocone or seismic dilatometer allows more detailed profiling of V_s and small-strain stiffness (G_{max}) at 0.2-m intervals that may help to reduce uncertainties. Also, the continuous-interval seismic piezocone test (CiSCPTu) is now available and permits profiling at 0.1-m intervals, although the data are noisier and less robust.

It may be possible to use of a mini-cone to construct stratigraphic profiles of compound sand blows as well as of buried sand blows. This could facilitate and compliment trench investigations and permit rapid characterization of sand blows at many sites across a region. Development of this technique, which will require field testing, has the potential to deliver a more accurate and detailed characterization of sand blows that have limited layer thickness, or that are composed of multiple depositional units related to recurrent liquefaction during an earthquake sequence. In addition, the technique may make it possible to identify ancient sand blows buried beneath the reach of trenches.

2. New testing devices and procedures

Several new devices are being developed that may help identify and evaluate the susceptibility and potential of soils to liquefy (Mayne, 2012), including the vibrocone penetrometer (Schneider et al., 1999; McGillivray et al., 2000; Bonita et al., 2004), large shaker tests (Rathje et al., 2005), the vision cone penetrometer (Saftner et al., 2011), and the piezovane (Charlie et al., 1995). These new devices may help to advance understanding and subsurface mapping via *in situ* testing at paleoliquefaction studies. Also, a newly developed procedure, the Rapid Soil Characterization System (RAPSOCHS) discussed by Kianirad et al., (2011) employs a manual-dynamic multi-channel penetrometer and may be useful testing at remote and difficult to access sites. Moreover, given the shallow occurrence and limited dimensions of paleoliquefaction features, mini-CPTs (Cha and Santamarina, 2013; Monfared, 2014) and micro-CPTs (Kim et al., 2010; Mayne, 2012) may help to better define layers, lenses, and liquefied zones and even to identify dikes and sills by the measured resistances (q_t, f_s, and u_2) with these reduced-scale penetrometers.

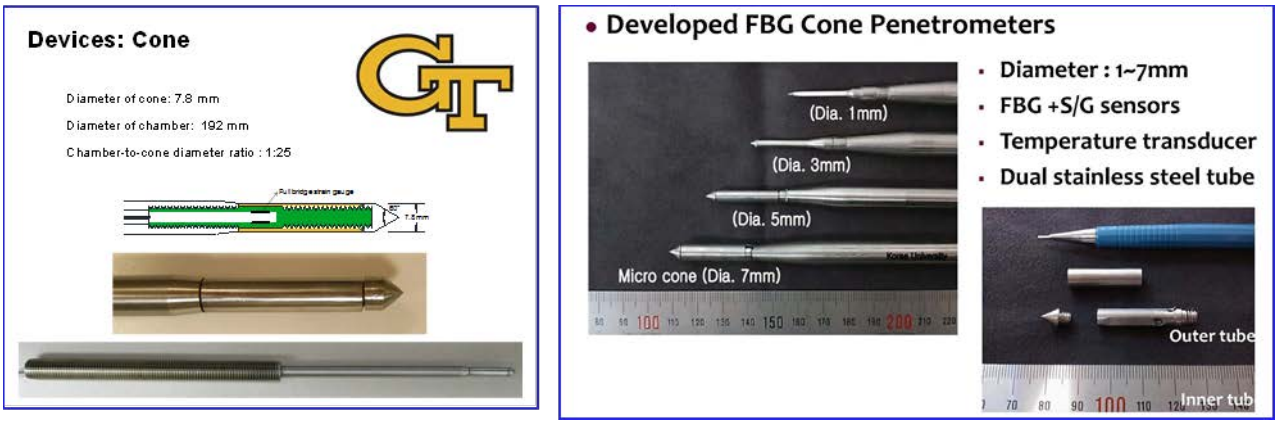

Figure 4-1 Scaled-down versions of the cone penetrometer including: (a) mini-CPT (Cha and Santamarina, 2013) and (b) micro-CPT (Kim et al., 2010).

Paleoearthquake Chronologies: In regions where paleoearthquake records exist but have not been fully developed, paleoseismic studies could be designed that would improve the completeness and extend the length of the paleoearthquake chronologies in order to improve recurrence estimates of large earthquakes and understanding of earthquake sources. It is also recommended that paleoliquefaction studies be conducted in regions of low seismicity that share geologic and tectonic characteristics with known seismogenic zones to better understand the earthquake potential of those regions and to test the hypothesis that inherited geologic structures, particularly faults that were active during the Mesozoic, controls seismicity.

5 REFERENCES

Adams, J., “Deformed Lake Sediments Record Prehistoric Earthquakes during the Deglaciation of the Canadian Shield,” *EOS,* 63(18):436, 1982.

Aiken, M.J., *Science-Based Dating in Archaeology*, Longman Group, London and New York, 1990.

Allen, J.R.L., *Sedimentary Structures: Their Character and Physical Basis*, Elsevier, Amsterdam, 1982.

Ambraseys, N.N., “Engineering Seismology: Earthquake Engineering and Structural Dynamics,” *Journal of the International Association of Earthquake Engineering*, 17:1-105, 1988.

ASTM International, “Standard Test Method for Standard Penetration Test (SPT) and Split-Barrel Sampling of Soils,” ASTM D1586-11, Soils and Rocks, American Society for Testing and Materials, West Conshohocken, PA, 04.08, 2015.

ASTM International, “Standard Test Method for Thin-Walled Tube Sampling of Soils for Geotechnical Purposes,” ASTM D1587-11, Soils and Rocks, American Society for Testing and Materials, West Conshohocken, PA, 04.08, 2015.

ASTM International, “Standard Test Method for Electronic Friction Cone and Piezocone Penetration Testing of Soils,” ASTM D5778-12, Soils and Rocks, American Society for Testing and Materials, West Conshohocken, PA, 04.08, 2015.

ASTM International, “Standard Test Methods for Maximum Index Density and Unit Weight of Soils Using a Vibratory Table," ASTM D4253-14, Soils and Rocks, American Society for Testing and Materials, West Conshohocken, PA, 04.08, 2015.

ASTM International, "Standard Test Methods for Minimum Index Density and Unit Weight of Soils and Calculation of Relative Density," ASTM D4254-14, Soils and Rocks, American Society for Testing and Materials, West Conshohocken, PA, 04.08, 2015.

ASTM International, “Standard Practice for Determining the Normalized Penetration Resistance of Sands for Evaluation of Liquefaction Potential,” ASTM D6066-11, Soils and Rocks, American Society for Testing and Materials, West Conshohocken, PA, 04.08, 2015.

Amick, D., G. Maurath, and R. Gelinas, “Characteristics of Seismically Induced Liquefaction Sites and Features Located in the Vicinity of the 1886 Charleston, South Carolina Earthquake,” *Seismological Research Letters,* 61(2):117-130, 1990.

Amick, D. and R. Gelinas, “The Search for Evidence of Large Prehistoric Earthquakes along the Atlantic Seaboard,” *Science*, 251:655-658, 1991.

Amoroso, S., C. Rodrigues, A. Viana da Fonseca and N. Cruz, "Liquefaction Evaluation of Aveiro Sands from SCPTu and SDMT," *Proceedings of the 3rd International Conference on Flat Dilatometer Tests, 14-16 June 2015*, Rome, Italy, 2015.

Andrus, R.D., and K.H. Stokoe, "Liquefaction Resistance of Soils from Shear Wave Velocity," *Journal of Geotechnical and Geoenvironmental Engineering,* 126(11):1015-1025, 2000.

Andrus, R.D., et al., “Predicting Shear-Wave Velocity from Cone Penetration Resistance, *in* K.D. Pitilakes, ed.,” *Proceedings of the 4th International Conference on Earthquake Geotechnical Engineering, 25-28 June 2007*, Springer, The Netherlands, 2007.

Annan, A.P., “The Principals of Ground Penetrating Radar, *in* D.K. Butler, ed.,” *Near-Surface Geophysics,* SEG– Investigations in Geophysics, 13:357-438, 2005.

Arlsoy, M.Ö., et al., “Images of Buried Graves in Bayat, Afyon (Turkey) from High-Resolution Magnetic Data and their Comparison with Preliminary Excavations,” *Journal of Archaeological Science*, 34(9):1473-1484, 2007.

Atkinson, G.M., and D.M. Boore, “Recent Trends in Ground Motion and Spectral Response Relations for North America,” *Earthquake Spectra*, 6, 1990.

Atwater, B.F., et al., "Earthquake Recurrence Inferred from Paleoseismology," *in* A.R. Gillespie, S.C. Porter, and B.F. Atwater, eds., *The Quaternary Period in the United States, Developments in Quaternary Science 1*, Elsevier, Amsterdam and New York, 331-350, 2004.

Audemard, F. and F. de Santis, “Survey of Liquefaction Structures Induced by Recent Moderate Earthquakes,” *Bulletin of the International Association of Engineering Geology*, 44:5-16, 1991.

Aylesworth, J.M. and D.E. Lawrence, “Earthquake-Induced Landsliding East of Ottawa; A Contribution to the Ottawa Valley Landslide Project,” *Proceedings, 3rd Canadian Conference on Geotechnique and Natural Hazards, (Geohazards 2003) 9-10 June 2003*, Edmonton, Alberta, 2003.

Bakun, W.H., and M.G. Hooper, “Magnitudes and Locations of the 1811-1812 New Madrid, Missouri, and Charleston, South Carolina, Earthquakes,” *Bulletin of the Seismological Society of America,* 94(1):64-75, 2004.

Bauer, L.M., *Studies of Historic and Prehistoric Earthquake-Induced Liquefaction Features in the Meizoseismal Area of the 1811-1812 New Madrid Earthquakes, Central United States,* M.S. Thesis, University of Memphis, Memphis, TN, 2006.

Birkeland, P.W., *Soils and Geomorphology, 3rd Edition,* Oxford University Press, New York and Oxford, 1999.

Bishop, A.W., “The Stability of Tips and Spoil Heaps,” *Quarterly Journal of Engineering Geology*, 6:335-376, 1973.

Bonita, J., J.K. Mitchell, and T.L. Brandon, *The Effects of Vibration on the Penetration Resistance and Porewater Pressure in Sands. Geotechnical and Geophysical Site Characterization, v. 1 (ISC-2, Porto),* Millpress, Rotterdam, 2004.

Boore, D.M., “Stochastic Simulation of High-Frequency Ground Motions Based on Seismological Models of the Radiated Spectra,” *Bulletin of the Seismological Society of America,* 73:1865–1894, 1983.

Boore, D.M., and G.M. Atkinson, Source Spectra for the 1988 Saguenay, Quebec, Earthquakes, *Bulletin of the Seismological Society of America,* 82(2):683-719, 1992.

Boore, D.M., "SMSIM — Fortran Programs for Simulating Ground Motions from Earthquakes: Version 2.3 — A Revision of OFR 96–80–A," U.S. Geological Survey, Menlo Park, CA, 2005. <http://www.daveboore.com/software_online.html>. Accessed July 12, 2015.

Boulanger, R.W. and I.M. Idriss, “Probabilistic Standard Penetration Test-Based Liquefaction: Triggering Procedure,” *Journal of Geotechnical and Geoenvironmental Engineering,* 138(10):1185-1195, 2012.

Boulanger, R.W. and I.M. Idriss, “CPT and SPT Based Liquefaction Triggering Procedures,” Report No. UCD/CGM-14/01, Center for Geotechnical Modeling, University of California, Davis, CA, 2014.

Bray, J.D. and R.B. Sancio, “Assessment of Liquefaction Susceptibility of Fine-Grained Soils,” *Journal of Geotechnical and Geoenvironmental Engineering,* 132(9):1165-1177, 2006.

Bray, J. and J.D. Frost, eds, “Geo-Engineering Reconnaissance of the February 27, 2010 Maule, Chile Earthquake,” GEER Report-022, May 25, 2010. <http://www.geerassociation.org/GEER_Post%20EQ%20Reports/Maule_Chile_2010/Ver2_Maule_Chile_2010_index.html>. Accessed May 6, 2015.

Bronk Ramsey, C., “Radiocarbon Calibration and Analysis of Stratigraphy: The OxCal Program,” *Radiocarbon,* 37(2):425-430, 1995.

Bronk Ramsey, C., “Development of the Radiocarbon Calibration Program OxCal,” *Radiocarbon,* 43(2A):355-363, 2001.

Brooks, G.R., “A Massive Sensitive Clay Landslide, Quyon Valley, Southwestern Quebec, Canada, and Evidence for a Paleoearthquake Triggering Mechanism,” *Quaternary Research,* 80(3):425-434, 2013.

Broughton, A., R. Van Arsdale, and J. Broughton, “Liquefaction Susceptibility Mapping in the City of Memphis and Shelby County, Tennessee,” *Engineering Geology,* 62:207-222, 2001.

Burger, H.R., A.F. Sheehan, and C.H. Jones, *Introduction to Applied Geophysics: Exploring the Shallow Subsurface,* W. W. Norton & Co., New York, 2006.

Carmichael, D.L., R.H. Lafferty III, and B.L. Molyneaux, *Excavation, the Archaeologist’s Toolkit, v. 3,* Altamira Press, Walnut Creek, CA, 2003.

Casagrande, A., “The Role of the "Calculated Risk" in Earthwork and Foundation Engineering. The Terzaghi Lecture,” *Journal of Soil Mechanics and Foundation Division,* American Society of Civil Engineers*,* 91(4):1-40, 1965.

Castilla, R.A. and F.A. Audemard, “Sand Blows as a Potential Tool for Magnitude Estimation of Pre-Instrumental Earthquakes,” *Journal of Seismology*, 11:473-487, 2007.

Castro, G., “On the Behavior of Soils During Earthquakes-Liquefaction, Soil Dynamics and Liquefaction, A.S. Cakmak, ed.,” *Elsevier,* 1987.

Castro, G., *Empirical Methods in Liquefaction Evaluation, Primer Ciclo de Conferencias Internationales Leonardo Zeevaert*, Mexico City, Mexico, 1995.

Cetin, K.O., et al., “Standard Penetration Test-Based Probabilistic and Deterministic Assessment of Seismic Soil Liquefaction Potential,” *Journal of Geotechnical and Geoenvironmental Engineering,* American Society of Civil Engineers*,* 1314-1340, 2004.

Cetin, K.O., et al., “Geotechnical Reconnaissance of the 2011 van Tabanli Earthquake in Eastern Turkey,” GEER Report-028, November 11, 2011. <http://www.geerassociation.org/GEER_Post%20EQ%20Reports/Turkey_Van_2011/Cover_Van-Tabanli_2011.html>. Accessed May 7, 2015.

Cha, M. and J.C. Santamarina, "Predissolution and Postdissolution Penetration Resistance", *Journal of Geotechnical and Geoenvironmental Engineering, American Society of Civil Engineers,* 139(12):2193-2200, 2013.

Charlie, W.A., et al., "Estimating Liquefaction Potential of Sand using the Piezovane," *Geotechnique,* 45(1):55-67, 1995.

Chen, C.J. and C.H. Juang, "Calibration of SPT- and CPT- Based Liquefaction Evaluation Methods. Innovations and Applications in Geotechnical Site Characterization" *(Proceedings GeoDenver), GSP 97,* American Society of Civil Engineers, Reston, VA, 2000.

Cox, R.T. and D. Larsen, "Investigation of Seismically-Induced Liquefaction in the Southern Mississippi Embayment," National Earthquake Hazards Reduction Program, Final Technical Report to U.S. Geological Survey, Award No. 1434-03HQGR0011, 2004.

Cox, R.T., et al., "Seismotectonic Implications of Sand Blows in the Southern Mississippi Embayment," *Engineering Geology,* 89(3-4):278-299, 2007.

Cramer, C.H., "A Seismic Hazard Uncertainty Analysis for the New Madrid Seismic Zone," *Engineering Geology,* 62:251-266, 2001.

Craven, J.A., *Paleoseismological Study in the New Madrid Seismic Zone Using Geological and Archeological Features to Constrain Ages of Liquefaction Deposits*, M.S. thesis, University of Memphis, Memphis, TN, 1995.

Cubrinovski, M., R.A. Green, and L. Wotherspoon, eds., "Geotechnical Reconnaissance of the 2011 Christchurch, New Zealand Earthquake," GEER Report-027, November 8, 2011. <http://www.geerassociation.org/GEER_Post%20EQ%20Reports/Christchurch_2011/Cover_Christchurch_2011.html>. Accessed May 7, 2015.

Dobry, R., "Some Basic Aspects of Soil Liquefaction during Earthquakes," *in* K.H. Jacob and C.J. Turkstra, eds., *Earthquake Hazards and the Design of Constructed Facilities in the Eastern United States,* Annals of the New York Academy of Sciences, New York, NY, 558:172-182, 1989.

Dougan, M., *An Arkansas Odyssey,* Rose Publishing, Little Rock, AR, 1995.

Douglass, A.E., *Climatic Cycles and Tree-Growth,* v. III. Carnegie Institution of Washington, Washington, D.C., 1936.

Douglass, A.E., "Crossdating in Dendrochronology," *Journal of Forestry*, 39(10):825-831, 1941.

Duller, G.A.T., *Luminescence Dating: Guidelines on Using Luminescence Dating in Archaeology*, English Heritage, Swindon, 2008.

Dutton, C.E., "The Charleston Earthquake of August 31, 1886," U.S. Geological Survey 9th Annual Report 1887–1888, 1889.

Electric Power Research Institute, "Seismic Evaluation Guidance Screening, Prioritization and Implementation Details (SPID) for the Resolution of Fukushima Near-Term Task Force Recommendation 2.1: Seismic," Technical Report 1025287, 2013.

Friedman, G.M. and J.E. Sanders, *Principles of Sedimentology*, John Wiley & Sons, New York, 1978.

Fuller, M.L., “The New Madrid Earthquake,” U.S. Geological Survey Bulletin 494, 1912.

Gassman, S., P. Talwani, and M. Hasek, 2009, *Maximum Magnitudes of Charleston, South Carolina Earthquakes from In-Situ Geotechnical Data, Abstracts Volume from Meeting of Central and Eastern U.S. Earthquake Hazards Program,* University of Memphis, Memphis, TN, October 28-29, 2009.

Gibbard, P. L., M.J. Head, M.J.C. Walker, and the Subcommission on Quaternary Stratigraphy, “Formal Ratification of the Quaternary System/Period and the Pleistocene Series/Epoch with a Base at 2.58 Ma.” *Journal of Quaternary Science*, 25:96-102, 2010.

Goldfinger, C., “Submarine Paleoseismology Based on Turbidite Records,” *Annual Review of Marine Sciences,* 3:35-66, 2011.

Grecheck, Eugene S., Dominion Nuclear North Anna, LLC, letter to U.S. Nuclear Regulatory Commission, "North Anna Early Site Permit Application, Response to Request for Additional Information No. 3,” October 2004, ADAMS Accession No. ML042800292.

Green, R.A., *Energy-Based Evaluation and Remediation of Liquefiable Soils,* Ph.D. Dissertation, Virginia Polytechnic Institute and State University, Blacksburg, VA, 2001.

Green, R.A., S.F. Obermeier, and S.M. Olson, “Engineering Geologic and Geotechnical Analysis of Paleoseismic Shaking Using Liquefaction Effects: Field Examples,” *Engineering Geology,* 76:263-293, 2005.

Green, R., et al., “Geotechnical Aspects in the Epicentral Region of the 2011 Mw 5.8 Mineral, Virginia, Earthquake, *in* J. W. Horton, Jr., M. C. Chapman, and R. A. Green, eds.,” The 2011 Mineral, Virginia, Earthquake, and Its Significance for Seismic Hazards in Eastern North America: Geological Society of America Special Paper 509, 2015.

Hajic, E.R., M.D. Wiant, and J.J. Oliver, “Distribution and Dating of Prehistoric Earthquake Liquefaction in Southeastern Illinois, Central U.S.,” National Earthquake Hazards Reduction Program, Final Technical Report to U.S. Geological Survey, Award No. 1434-93G2359, 1995.

Harden, J.W., “A Quantitative Index of Soil Development from Field Descriptions: Examples from a Chronosequence in Central California,” *Geoderma*, 28:1-28, 1982.

Harden, J.W. and E.M. Taylor, “A Quantitative Comparison of Soil Development in Four Climatic Regions,” *Quaternary Research,* 20:342-359, 1983.

Hashash, Y.M.A. and D. Park, "Non-Linear One-Dimensional Wave Propagation in the Mississippi Embayment," *Engineering Geology*, 62(1-3):185-206, 2001.

Hashash, Y.M.A., C. Phillips, and D. Groholski, "Recent Advances in Non-Linear Site Response Analysis", *Proceedings of the 5th International Conference: Recent Advances in Geotechnical Engineering and Soil Dynamics, 24-29 May 2010*, San Diego, CA, 2010.

Hatcher, R.D., Jr., J.D. Vaughn, and S.F. Obermeier, “Large Earthquake Paleoseismology in the Eastern Tennessee Seismic Zone – Results of an 18-Month Pilot Study,” *in* R.T. Cox, M.P. Tuttle, O.S. Boyd, and J. Locat, eds., *Recent Advances in North American Paleoseismology and Neotectonics East of the Rockies*, Geological Society of America, Special Paper 493:111-142, 2012.

Heidari, T., R.D. Andrus, and S. Moysey, “Characterizing the Liquefaction Potential of the Pleistocene-Age Wando Formation in the Charleston Area, South Carolina,” *GeoRisk 2011: Risk Assessment and Management,* American Society of Civil Engineers, 510-517, 2011.

Heaton, T.H. and S.H. Hartzell, “Earthquake Ground Motions,” *Annual Review of Earth and Planetary Sciences,* 16:121-145, 1988.

Holzer, T.L., et al., “Liquefaction at Oceano, California, during the 2003 San Simeon Earthquake,” *Seismological Society of America Bulletin*, 95(6):2396-2411, 2005.

Holzer, T.L., et al., “Liquefaction Hazard Mapping with LPI in the Greater Oakland, California, Area,” *Earthquake Spectra*, 22(3):693-708, 2006a.

Holzer, T.L., et al., “Predicted Liquefaction of East Bay Fills during a Repeat of the 1906 San Francisco Earthquake,” *Earthquake Spectra*, 22(S2):S261-S278, 2006b.

Holzer, T.L., T.E. Noce, and M.J. Bennett, “Liquefaction Probability Curves for Surficial Geologic Units,” *Environmental and Engineering Geoscience*, 17(1):1-21, 2011.

Hough, S.E., et al., “On the Modified Mercalli Intensities and Magnitudes of the 1811-1812 New Madrid Earthquakes,” *Journal of Geophysical Research,* 105(B10):23,839-23,864, 2000.

Hough, S.E., and S. Martin, “Magnitude Estimates of Two Large Aftershocks of the 16 December 1811 New Madrid Earthquake,” *Bulletin of the Seismological Society of America,* 92(8):3259-3268, 2002.

Hough, S.E., and M. Page, “Toward a Consistent Model for Strain Accrual and Release for the New Madrid Seismic Zone, Central U.S,” *Journal of Geophysical Research*, 116, 2011.

Housner, G.W. et al., “Liquefaction of Soils during Earthquakes,” Committee on Earthquake Engineering, Commission on Engineering and Technical Systems, National Research Council, National Academy Press, Washington, DC, 1985.

Hu, K., S.L. Gassman, and P. Talwani, “In-Situ Properties of Soils at Paleoliquefaction Sites in the South Carolina Coastal Plain,” *Seismological Research Letters,* 73(6):964-978, 2002a.

Hu, K., S.L. Gassman, and P. Talwani, “Magnitudes of Prehistoric Earthquakes in the South Carolina Coastal Plain from Geotechnical Data,” *Seismological Research Letters,* 73(6):979-991, 2002b.

Idriss, I.M. and R.W. Boulanger, “Semi-Empirical Procedures for Evaluating Liquefaction Potential during Earthquakes,” *Proceedings 11th International Conference Soil Dynamics and Earthquake Engineering, v. 1*: 32-46, Elsevier, Berkeley, CA, 2004.

Idriss, I.M. and R.W. Boulanger, “Soil Liquefaction during Earthquakes,” Earthquake Engineering Research Institute, Monograph 12, EERI MNO-12, 2008.

Idriss, I.M. and R.W. Boulanger, “SPT-Based Liquefaction Triggering Procedures, Report No. UCD/CGM – 10/02,” Department of Civil and Environmental Engineering, University of California at Davis, 2010. <http://faculty.engineering.ucdavis.edu/boulanger/wp-content/uploads/sites/71/2014/09/Idriss_Boulanger_SPT_Liquefaction_CGM-10-02.pdf>. Accessed May 8, 2015.

Imai, T and K. Tonouchi, "Correlation of N Value with S-Wave Velocity and Shear Modulus," *Proceedings of the 2nd European Symposium on Penetration Testing,* Amsterdam, The Netherlands, 1982.

Ishihara, K., "Stability of Natural Soils during Earthquakes," *Proceedings of the Eleventh International Conference on Soil Mechanics and Foundation Engineering, San Francisco, v. 1,* A.A. Balkema, Rotterdam, 1985.

Ishihara, K., R. Verdugo, and A.A. Acacio, "Characterization of Cyclic Behavior of Sand and Post-Seismic Analyses," *Proceedings of the Ninth Asian Regional Conference on Soil Mechanics and Foundation Engineering, 9-13 December, 1991, Bangkok, Thailand, v. 2,* Southeast Asian Geotechnical Society, Bangkok, 1991.

Ishihara, K. and M. Yoshimine, "Evaluation of Settlements in Sand Deposits following Liquefaction during Earthquakes," *Soils and Foundations,* 32(1), Japanese Geotechnical Society, 1992.

Iwasaki, T., et al., "A Practical Method for Assessing Soil Liquefaction Potential Based on Case Studies at Various Sites in Japan," *Proceedings 2nd International Conference on Microzonation, San Francisco,* National Science Foundation, Washington, D.C., 1978.

Jefferies, M. and K. Been, *Soil Liquefaction: A Critical State Approach*, Taylor & Francis Group, Oxon UK, 2006.

Jenny, H., *Factors of Soil Formation*, McGraw-Hill, New York, 1941.

Jenny, H., "Derivation of State Factor Equations of Soils and Ecosystems," *Proceedings, v. 25,* Soil Science Society of America, Madison, WI, 1961.

Johansson, J., "Soil Liquefaction Web Site," Department of Civil Engineering, University of Washington, Seattle, WA, January 2000. <http://www.ce.washington.edu/~liquefaction/html/main.html>. Accessed May 8, 2015.

Johnston, A.C., and L.R. Kanter, "Earthquakes in Stable Continental Crust," *Scientific American,* 262:68-75, 1990.

Johnston, A.C., "Seismic Moment Assessment of Stable Continental Earthquakes, Part III: 1811-1812 New Madrid, 1886 Charleston and 1755 Lisbon," *Geophysical Journal International,* 126:314-344, 1996.

Johnston, A.C., and E.S. Schweig, "The Enigma of the New Madrid earthquakes of 1811-1812," *Annual Review of Earth and Planetary Sciences,* 24:339-384, 1996.

Juang, C.H. and T. Jiang, "Assessing Probablistic Methods for Liquefaction Potential Evaluation. Soil Dynamics and Liquefaction 2000," *(Proceedings GeoDenver), GSP 107,* American Society of Civil Engineers, Reston, VA, 2000.

Juang, C.H., T. Jiang, and R.D. Andrus, "Assessing Probability-Based Methods for Liquefaction Potential Evaluation," *Journal of Geotechnical and Geoenvironmental Engineering,* 128(7):580-589, 2002.

Juang, C.H., S.Y. Fang, and E.H. Khor, "First-Order Reliability Method for Probablistic Liquefaction Triggering Analysis using CPT," *Journal of Geotechnical and Geoenvironmental Engineering*, 132(3):337-350, 2006.

Juang, C.H., C-H. Chen, and P.W. Mayne, "CPTu-simplified Stress-based Model for Evaluating Soil Liquefaction Potential," *Soils and Foundations*, 46(6):755-770, 2008.

Kattenhorn, S., “Earthquakes and Seismic Hazards, Geology 344 Course Materials,” Univ. of Idaho, 2011; www.webpages.uidaho.edu.

Kayen, R. et al., "Shear Wave Velocity-Based Probabilistic and Deterministic Assessment of Seismic Soil Liquefaction Potential,” *Journal of Geotechnical and Geoenvironmental Engineering*, 139(3):407-419, 2013.

Kelson, K.I., et al., “Multiple Holocene Earthquakes along the Reelfoot Fault, Central New Madrid Seismic Zone,” *Journal of Geophysical Research*, 101:6151-6170, 1996.

Kianirad, E., et al., “Equivalent Quasi-Static Estimation of Dynamic Penetration Force for Near Surface Soil Characterization,” *GeoFrontiers 2011: Advances in Geotechnical Engineering, GSP 211, Dallas,* American Society of Civil Engineers, Reston, Virginia, 2011.

Kim, R. et al., “Evaluation of the Smear Zone Using Micro Penetrometer, *Proceedings, GeoFlorida 2010: Advances in Analysis, Modeling, and Design*, (GeoCongress, GSP 199, West Palm Beach, FL), American Society of Civil Engineers, Reston, VA: 998-1007, 2010.

Kuenen, P.H., “Experiments in Geology, T*ransactions of the Geological Society of Glasgow,* 23:1-28, 1958.

Kramer, S.L., et al., “Site Response Modeling in Liquefiable Soil Deposits: Effects of Surface Geology on Seismic Motion,” *4th IASPEI / IAEE International Symposium,* University of California Santa Barbara, CA, 2011.

Kramer, S.L. and C-H. Wang, "Empirical Model for Estimation of Residual Strength of Liquefied Soil," *Journal of Geotechnical and Geoenvironmental Engineering*, 2015.

Kulhawy, F.H. and P.W. Mayne, “Manual for Estimating Soil Properties for Foundation Design,” Report EL-6800, Electric Power Research Institute, Palo Alto, 1990. <http://www.epri.com/abstracts/Pages/ProductAbstract.aspx?ProductId=EL-6800>. Accessed May 10, 2015.

Lafferty, R.H., III, “Archeological Techniques of Dating Ancient Quakes,” *Geotimes,* 41(11):24-27, 1996.

LDRL (Luminescence Dating Research Laboratory), *Luminescence Tutorial—Optically Stimulated Luminescence (OSL)*, University of Illinois at Chicago, 2010; http:// www.uic.edu/labs/ldrl/osl.html, Accessed June 10, 2010.

Leon, E., “Effect of Aging of Sediments on Paleoliquefaction Evaluation in the South Carolina Coastal Plain,” unpublished Ph.D. dissertation, University of South Carolina, 2003.

Leon, E., S.L. Gassman, and P. Talwani, “Effect of Soil Aging on Assessing Magnitudes and Accelerations of Prehistoric Earthquakes,” *Earthquake Spectra*, 21(3):737-759, 2005.

Leon, E., S.L. Gassman, and P. Talwani, “Accounting for Soil Aging when Assessing Liquefaction Potential,” *Journal of Geotechnical and Geoenvironmental Engineering*, 132(3):363-377.

Li, Y., et al., “Evidence for Large Prehistoric Earthquakes in the Northern New Madrid Seismic Zone, Central United States,” *Seismological Research Letters,* 69(3):270-276, 1998.

Lian, O., “Luminescence Dating, in Encyclopedia of Quarterly Science, S. A. Elias ed.,” Elsevier, New York, 2007.

Lian, O.B. and R.G. Roberts, “Dating the Quaternary: Progress in Luminescence Dating of Sediments,” *Quaternary Science Reviews*, 25:2449-2468, 2006.

Liao, S.S.C., D. Veneziano, and R.V. Whitman, “Regression Models for Evaluating Liquefaction Probability,” *Journal of Geotechnical Engineering*, 114(4):389–411, 1988.

Liao, T., et al., “CPT Site Characterization for Seismic Hazards in the New Madrid Seismic Zone,” *Soil Dynamics and Earthquake Engineering,* 22:943-950, 2002.

Liao, T. and P.W. Mayne, “Estimating Seismic Parameters Associated with Previous Earthquakes by SCPTU Soundings in the New Madrid Seismic Zone,” *Proceedings of the 5th International Conference: Recent Advances in Geotechnical Engineering and Soil Dynamics, San Diego, CA, 24-29 May 2010*, Paper 411a, 2010.

Liu, L. and Y. Li, “Identification of Liquefaction and Deformation Features using Ground Penetrating Radar in the New Madrid Seismic Zone, USA,” *Journal of Applied Geophysics*, 47:199-215, 2001.

Lowe, D.R., “Water Escape Structures in Coarse-Grained Sediment,” *Sedimentology*, 22:157-204, 1975.

Lowe, D.R. and R.D. LoPiccolo, “The Characteristics and Origins of Dish and Pillar Structures,” *Journal of Sedimentary Petrology*, 44:484-501, 1974.

Lunne, T., P.K. Robertson and J.J.M. Powell, *Cone Penetration Testing in Geotechnical Practice*, EF Spon/Routedge/Blackie Academic, London, England, 1997.

MacMurdo, J., *Papers Relating to the Earthquake which occurred in India in l819*, Trans. Lit. Soc., Bombay, III, 1822.

Mahan, S.A. and A.J. Crone, “Luminescence Dating of Paleoliquefaction Features in the Wabash River Valley of Indiana, in R. A. Wide, ed., *Proceedings of the 4th New World Luminescence Dating and Dosimetry Workshop, Denver, Colorado,* U.S. Geological Survey Open-File Report, Reston, VA, 2006-1351.

Mahan, S., et al., “Can OSL Be Used to Date Paleoliquefaction Events? Abstracts Volume from Meeting of Central and Eastern U.S. Earthquake Hazards Program,” University of Memphis, Memphis, TN, October 28-29, 2009.

Martin, J.R., et al., “Geotechnical Quick Report on the Affected Region of the 23 August 2011 M5.8 Central Virginia Earthquake near Mineral, Virginia,” GEER Report-026, October 2011. <http://www.geerassociation.org/GEER_Post%20EQ%20Reports/Virginia_USA_2011/index.html>. Accessed May 8, 2015.

Mayne, P.W., “Geotechnical Site Characterization in the Year 2012 and Beyond, SOA on in-situ Testing,” *Proceedings GeoCongress 2012: State-of-the-Art and Practice in Geotechnical Engineering, GSP 226, Oakland CA,* American Society of Civil Engineers, Reston, VA, 2012.

Mayne, P.W., "Keynote: Interpretation of Geotechnical Parameters from Seismic Piezocone Tests," in P.K. Robertson and K.L. Cabal, eds., *Proceedings of the 3rd International Symposium on Cone Penetration Testing*, (CPT'14), Las Vegas, NV, 2014.

Mayne, P.W., “NCHRP Synthesis 368 on Cone Penetration Test,” Transportation Research Board, National Cooperative Highway Research Program, National

Academies Press, Washington, DC, 2007. <http://onlinepubs.trb.org/onlinepubs/nchrp/nchrp_syn_368.pdf>. Accessed May 10, 2015.

Mayne, P.W., et al., "Subsurface Investigations -Geotechnical Site Characterization," Publication No. FHWA-NHI-01-031, National Highway Institute, Federal Highway Administration, Washington, D.C., 2002.

Mayne, P.W., et al., "State-of-the-Art Paper (SOA-1): GeoMaterial Behavior and Testing," *Proceedings 17th International Conference Soil Mechanics and Geotechnical Engineering, v. 4 (ICSMGE, Alexandria, Egypt),* Millpress/IOS Press, Rotterdam, 2009.

Mayne, P.W., J. Peuchen, and D. Bouwmeester, "Unit Weight Evaluation from CPT," *Proceedings, 2nd International Symposium on Cone Penetration Testing (CPT'10), v. 2,* Huntington Beach, CA, 2010a.

Mayne, P.W, J. Peuchen, and D. Bouwmeester, "Soil Unit Weight estimated from CPTu in Offshore Soils. Frontiers in Offshore Geotechnics II," *(Proceedings ISFOG 2010, Perth),* Taylor & Francis Group, London, 2010b.

McCalpin, J. P., ed., *Paleoseismology,* Academic Press, San Diego, CA, 1996.

McCalpin, J. P., ed., *Paleoseismology, 2nd edition,* Academic Press, Burlington, MA, 2009.

McCartan, L., E. M. Lemon, Jr., and R. E. Weems, "Geologic Map of the Area between Charleston and Orangeburg, South Carolina," U.S. Geological Survey, Miscellaneous Investigations Series Map I-1472, 1: 250,000-scale, 1984.

McGillivray, A., et al., *An Electro-Vibrocone for Site-Specific Evaluation of Soil Liquefaction Potential, Innovations and Applications in Geotechnical Site Characterization*, *GSP 97*, American Society of Civil Engineers, Reston, VA, 2000.

McGillivray, A.V. and P.W. Mayne, *An Automated Seismic Source for Continuous Shear Wave Profiling, Geotechnical and Geophysical Site Characterization*, Taylor & Francis, London, 2008.

McNulty, W.E. and S.F. Obermeier, "Liquefaction Evidence for at least two Strong Holocene Paleo-Earthquakes in Central and Southwestern Illinois, USA," *Environmental and Engineering Geoscience*, 5(2):133-146, 1999.

Monfared, S.D., "Miniature Cone Penetration Test on Loose Sand", Ph.D. dissertation, Paper 2533, University of Western Ontario, London, ON, 2014.

Morse, D.F. and P.A. Morse, *Archaeology of the Central Mississippi Valley*, Academic Press, Inc., New York, 1983.

Morse, D.F. and P.A. Morse, *Northeast Arkansas, in McNutt, C. H., ed., Prehistory of the Central Mississippi Valley,* University of Alabama Press, Tuscaloosa, AL,1996.

Moss, R.E.S., et al., "CPT-based Probablistic and Deterministic Assessment of in-situ Seismic Soil Liquefaction Potential," *Journal of Geotechnical and Geoenvironmental Engineering*, 132(8):1032-1051, 2006.

Munson, P.J. and C.A. Munson, "Paleoliquefaction Evidence for Recurrent Strong Earthquakes since 20,000 years BP in the Wabash Valley Area of Indiana," report submitted to the U.S. Geological Survey in fulfillment of National Earthquake Hazards Reduction Program Grant No. 14-08-0001-G2117, 1996.

Munson, P.J., et al., “Liquefaction Evidence for Holocene and Latest Pleistocene Seismicity in the Southern Halves of Indiana and Illinois: A Preliminary Overview,” *Seismological Research Letters,* 68:521-536, 1997.

National Research Council, *Liquefaction of Soils during Earthquakes*, National Academy Press, Washington, D.C., 1985.

Obermeier, S. F., *Using Liquefaction-Induced Features for Paleoseismic Analysis, in J. P. McCalpin, ed., Paleoseismology,* Academic Press, San Diego, CA, 1996.

Obermeier, S.F., “Liquefaction Evidence for Strong Earthquakes of Holocene and Latest Pleistocene Ages in the States of Indiana and Illinois, USA,” *Engineering Geology*, 50:227-254, 1998.

Obermeier, S.F., et al., “Geologic Evidence for Recurrent Moderate to Large Earthquakes near Charleston, South Carolina,” *Science*, 227:408-411, 1985.

Obermeier, S.F., et al., “Liquefaction Evidence for Repeated Holocene Earthquakes in the Coastal Region of South Carolina,” *Annals of the New York Academy of Sciences*, 558:183-195, 1989.

Obermeier, S.F., et al., “Earthquake-Induced Liquefaction Features in the Coastal Setting of South Carolina and in the Fluvial Setting of the New Madrid Seismic Zone,” U.S. Geological Survey Professional Paper 1504, 1990.

Obermeier, S.F., et al., “Liquefaction Evidence for one or more Strong Holocene earthquakes in the Wabash Valley of Southern Indiana and Illinois, with a Preliminary Estimate of Magnitude,” U.S. Geological Survey Professional Paper 1536, 1993.

Obermeier, S.F. and W.E. McNulty, “Paleoliquefaction Evidence for Seismic Quiescence in Central Virginia during Late and Middle Holocene Time, Eos,” Transactions of the American Geophysical Union, 79(17), Spring Meeting Supplement, Abstract T41A-9, 1998.

Obermeier, S.F., et al., “Paleoseismic Studies in Continental Settings-Geologic and Geotechnical Factors in Interpretations and Back-Analysis,” U.S. Geological Survey Open-File Report 01-29, 2001.

O’Brien, M.J. and R.L. Lyman, *Seriation, Stratigraphy, and Index Fossils: The Backbone of Archaeological Dating,* Plenum Press, New York, 1999.

Oldham, R.D., “The Cutch (Kachchh) Earthquake of the 16th June, 1819 with a Revision of the Great Earthquake of the 12th June, 1897,” India Geological Survey Memoir, No. 46., 1926.

Olson, S.M., S.F. Obermeier, and T.D. Stark, “Interpretation of Penetration Resistance for Back-Analysis at Sites of Previous Liquefaction,” *Seismological Research Letters,*72(1):46-59, 2001.

Olson, S.M., R.A. Green, and S.F. Obermeier, “Revised Magnitude Bound Relation for the Wabash Valley Seismic Zone of the Central United States,” *Seismological Research Letters,* 76(6):756-771, 2005a.

Olson, S.M., R.A. Green, and S.F. Obermeier, “Geotechnical Analysis of Paleoseismic Shaking using Liquefaction Features: A Major Updating,” *Engineering Geology,* 76:235–261, 2005b.

Olson, S.M. and C.I. Johnson, "Analyzing Liquefaction-Induced Lateral Spreads Using Strength Ratios," *Journal of Geotechnical and Geoenvironmental Engineering*, 134(8):1035–1049, 2008.

Oristaglio, M. and A. Dorozynski, *A Sixth Sense*, Gerald Duckworth & Co Ltd., London, 2009.

Owen, H.G., "Deformation Processes in Unconsolidated Sands," *Geological Society of London Special Publications,* 29:11-24, 1987.

Papadopoulos, G.A. and G. Lefkopoulos, "Magnitude-Distance Relations for Liquefaction in Soil from Earthquakes," *Bulletin of the Seismological Society of America,* 83(3):925-938, 1993.

Parasnis, D.S., *Principles of Applied Geophysics, 5th edition,* Chapman & Hall, New York, 1997.

Petersen, M.D., et al., "Documentation for the 2008 Update of the United States National Seismic Hazard Maps," U.S. Geological Survey Open-File Report 2008–1128, 2008.

Petersen, M.D., et al., "Documentation for the 2014 Update of the United States National Seismic Hazard Maps," U.S. Geological Survey Open-File Report 2014–1091, 2014.

Pierce, K., "Dating Methods, *in* Geophysics Study Committee, Geophysics Research Forum, National Research Council, Active Tectonics: Impact on Society," The National Academies Press, Washington, D.C., 1986.

Pond, E. C., "Seismic Parameters for the Central United States based on Paleoliquefaction Evidence in the Wabash Valley," Ph.D. Thesis, Virginia Polytechnic Institute, Blacksburg, Virginia, 1996.

Pond, E.C. and Martin, J.R., "Estimated Magnitudes and Accelerations Associated with Prehistoric Earthquakes in the Wabash Valley Region of the Central United States, *in* D. R. Kolata and T. G. Hildenbrand, eds., Investigations of the Illinois Basin Earthquake Region," *Seismological Research Letters,* 68:611-623, 1997.

Quigley, M.C., S. Bastin, and B.A. Bradley, "Recurrent Liquefaction in Christchurch, New Zealand, during the Canterbury Earthquake Sequence," *Geology* 41(4): 419-422, 2013.

Rathje, E.M., W-J. Chang, and K.H. Stokoe, "Development of an in Situ Dynamic Liquefaction Test," *ASTM Geotechnical Testing Journal,* 28(1):50-60, 2005.

Rattan, L., ed., *Encyclopedia of Soil Science*, Taylor & Francis Group, New York, 2006.

Reid, C.M., et al., "Sand Volcanoes in the Avon-Heathcote Estuary Produced by the 2010-2011 Christchurch Earthquakes: Implications for Geological Preservation and Expression," *New Zealand Journal of Geology and Geophysics,* 55(3):249-254, 2012.

Reimer, P.J., et al., "IntCal09 and Marine09 Radiocarbon Age Calibration Curves, 0–50,000 years cal BP," *Radiocarbon,* 51(4):1111–1150, 2009.

Rencz, A.N., ed., *Remote Sensing for the Earth Sciences, Manual of Remote Sensing, (3rd edition), 3*, John Wiley and Sons, New York, 1999.

Rhodes, E.J., "Optically Stimulated Luminescence dating of Sediments over the past 200,000 years," *Annual Review of Earth and Planetary Sciences,* 39:461-488, 2011.

Robertson, P.K., “Soil Classification using the CPT,” *Canadian Geotechnical Journal*, 27(1):151-158, 1990.

Robertson, P.K., “Evaluating Soil Liquefaction and Post-Earthquake Deformations using the CPT, Geotechnical and Geophysical Site Characterization, v.1,” *(Proceedings ISC-2, Porto),* Millpress, Rotterdam, 2004.

Robertson, P.K., “Performance-Based Earthquake Design Using the CPT. Performance-Based Design in Earthquake Geotechnical Engineering,” *(Proceeding International Symposium-Tokyo),* CRC Press- Taylor & Francis Group, London, 2009a.

Robertson, P.K., “Interpretation of Cone Penetration Tests: a Unified Approach,” *Canadian Geotechnical Journal*, 46(11):1335-1355, 2009b.

Robertson, P.K., “Evaluation of Flow Liquefaction and Liquefied Strength using the Cone Penetration Test,” *Journal of Geotechnical and Geoenvironmental Engineering*, 136(6):842-853, 2010.

Robertson, P.K., D.J. Woeller, and W.D. Finn, “Seismic Cone Penetration Test for Evaluating Liquefaction Potential,” *Canadian Geotechnical Journal*, 29(4):686-695, 1992.

Robertson, P.K. and C.E. Wride (Fear), “Evaluating Cyclic Liquefaction Potential using the Cone Penetration Test,” *Canadian Geotechnical Journal*, 35(3):442-459, 1998.

Russ, D.P., “Style and Significance of Surface Deformation in the Vicinity of New Madrid, Missouri *in* F.A. McKeown and L.C. Pakiser, eds., Investigations of the New Madrid, Missouri, earthquake region,” *U.S. Geological Survey Professional Paper 1236-H,* 94-114, 1982.

Saftner, D.A., et al., “Comparison of Predicted Cyclic Resistance Ratios from CPT, DMT, and Shear Wave Velocity Tests in Griffin, Indiana,” *Proceedings, GeoFrontiers 2011 (Dallas), GSP 211,* American Society of Civil Engineers, Reston, VA, 2011.

Salvi, S., et al., “Investigation of the Active Celano-L’Aquila Fault System, Abruzzi (central Apennines, Italy) with Combined Ground-penetrating Radar and Palaeoseismic trenching,” *Geophysical Journal International,*155:805–818, 2003.

Saucier, R.T., “Effects of the New Madrid Earthquake Series in the Mississippi Alluvial Valley,” *U.S. Army Corps of Engineers Waterways Experiment Station Miscellaneous Paper S-77-5,* 10, 1977.

Saucier, R.T., “Evidence for Episodic Sand-Blow Activity during the 1811-12 New Madrid (Missouri) Earthquake Series,” *Geology,* 17:103-106, 1989.

Saucier, R., “Geoarchaeological Evidence of Strong Prehistoric Earthquakes in the New Madrid (Missouri) Seismic Zone,” *Geology,* 19:296-298, 1991.

Saucier, R.T., “Geomorphology and Quaternary Geologic History of the Lower Mississippi,” *U.S. Army Corps of Engineers Waterways Experiment Station,* I and II, 1994.

Schnabel, P.B., J. Lysmer, and H.B. Seed, "SHAKE: A Computer Program for Earthquake Response Analysis of Horizontally Layered Sites", Report UCB/EERC-72/12, Earthquake Engineering Research Center, University of California, Berkeley, CA, 1972. <http://nisee.berkeley.edu/elibrary/getpkg?id=SHAKE91>. Accessed July 12, 2015.

Schneider, J.A., P.W. Mayne, and T.L. Hendren, “Initial Development of an Impulse Piezovibrocone for Liquefaction Evaluation, Physics and Mechanics of Soil Liquefaction,” *Proceedings of the International Workshop on the Physics and Mechanics of Soil Liquefaction, Johns Hopkins Univ.,* Rotterdam, 1999.

Schneider, J.A. and P.W. Mayne, “Liquefaction Response of Soils in Mid-America by SCPT,” *Innovations and Applications in Geotechnical Site Characterization (GSP 97),* American Society of Civil Engineers, Reston, VA, 2000.

Schneider, J.A., P.W. Mayne, and G.J. Rix, “Geotechnical Site Characterization in the Greater Memphis Area using CPT,” *Engineering Geology,* 62(1-3):169-184, 2001.

Seed, H.B., “State of the Art Paper: Evaluation of Soil Liquefaction effects on Level Ground during Earthquakes. Liquefaction Problems in Geotechnical Engineering,” *(Proceedings ASCE National Convention, Philadelphia),* Preprint 2752, American Society of Civil Engineers, Reston, VA, 1976.

Seed, H.B., “Soil Liquefaction and Cyclic Mobility Evaluation for Level Ground during Earthquakes,” *Journal of Geotechnical Engineering*, 105(GT2):201-256, 1979.

Seed, H.B. and I.M. Idriss, “Simplified Procedure for Evaluating Soil Liquefaction Potential,” *Journal of the Soil Mechanics and Foundations Division (American Society of Civil Engineers*), 97(SM9):1249-1273, 1971.

Seed, H.B. and I.M. Idriss, “Evaluation of Liquefaction Potential of Sand Deposits based on Observations of Performance in Previous Earthquakes, Pre-Print 81-544, Session on In-situ Testing to Evaluate Liquefaction Susceptibility,” ASCE National Convention, St. Louis, Missouri, October, 1981.

Seed, H.B. and I.M. Idriss, “Ground Motions and Soil Liquefaction during Earthquakes,” Earthquake Engineering Research Institute, Berkeley, CA, 1982.

Seed, H.B., I.M. Idriss, and I. Arango, “Evaluation of Liquefaction Potential using Field Performance Data,” *Journal of Geotechnical Engineering,* 109:458-482, 1983.

Seed, H.B., et al., “The Influence of SPT Procedures in Soil Liquefaction Resistance Evaluations,” *Journal of Geotechnical Engineering,* 111(12):1425–1445, 1985.

Sexton, J.L. and P.B. Jones, “Mini-Sosie High-Resolution Reflection Survey of the Cottonwood Grove Fault in Northwestern Tennessee,” *Bulletin of the Seismological Society of America,* 78(2):838-854, 1988.

Shedlock, K.M., “Seismic Hazard Map of North and Central America and the Caribbean,” *Annali di Geofisica,* 42(6):977-997, 1999.

Al-Shukri, H., H. Mahdi, and M. Tuttle, “Three-Dimensional Imaging of Earthquake-Induced Liquefaction Features with Ground Penetrating Radar near Marianna, Arkansas,” *Seismological Research Letters,* 77:505-513, 2006.

Al-Shukri, H., et al., “Spatial and Temporal Characteristics of Paleoseismic Features in the Southern Terminus of the New Madrid Seismic Zone in Eastern Arkansas,” National Earthquake Hazards Reduction Program, Final Technical Report to U.S. Geological Survey, Award No. 07HQGR0069, 2009.

Sims, J.D., “Earthquake-Induced Structures in Sediments of Van Norman Lake, San Fernando California,” *Science,* 182:161-163.

Sims, J.D., “Determining Earthquake Recurrence intervals from Deformational Structures in Young Lacustrine Sediments,” *Tectonophysics,* 29:141-153, 1975.

Sims, J.D., “Earthquake-induced Load Casts, Pseudonodules, Ball-and-pillow, and Convolute Lamination: Additional Deformation Structures for Paleoseismic Studies, *in* R.T. Cox, M.P. Tuttle, O.S. Boyd, and J. Locat, eds.,” Geological Society of America, Special Paper 493, 2012.

Sims, J.D. and C.D. Garvin, “Recurrent Liquefaction at Soda Lake, California, Induced by the 1989 Loma Prieta Earthquake, and 1990 and 1991 Aftershocks: Implications for Paleoseismicity Studies,” *Bulletin of the Seismological Society of America,* 85:51-65, 1995.

Skempton, A.W., “Standard Penetration Test Procedures and Effects in Sands of Overburden Pressure, Relative Density, Particle Size, Aging, and Overconsolidation,” *Geotechnique,* 36(3):425-447, 1986.

Sowers, G.F., *Introductory Soil Mechanics and Foundations: Geotechnical Engineering, 4th edition,* Macmillan Publishing Co., New York, 1979.

Stahle, D.W., E.R. Cook, and J.W.C. White, “Tree-Ring Dating of Baldcypress and the Potential for Millennia-Long Chronologies in the Southeast,” *American Antiquity,* 50:796-802, 1985.

Stahle, D.W., F.K. Fye, and M.D. Therrell, “Interannual to Decadal Climate and Streamflow Variability Estimates from Tree Rings, *in* A.R. Gillespie, S.C. Porter, and B.F. Atwater, eds., The Quaternary Period in the United States: Developments in Quaternary Science 1,” Elsevier, Amsterdam and New York, 2004.

Stark, T.D., “Interpretation of Ground Shaking from Paleoliquefaction Features,” National Earthquake Hazards Reduction Program, Annual Technical Report to U.S. Geological Survey, Award No. 01HQGR0030, 2002.

Stuiver, M., et al., “Calibration—1993,” *Radiocarbon,* 35(1):35-65, 1993.

Stuiver, M. and P.J. Reimer, “Extended ^{14}C Data Base and revised CALIB 3.0 ^{14}C age Calibration Program,” *Radiocarbon,* 35:215-230, 1993.

Stuiver, M., P.J. Reimer, and T.F. Braziunas, “High-Precision Radiocarbon Age Calibration for Terrestrial and Marine Samples,” *Radiocarbon,* 40(3):1127-1151, 1998.

Stuiver, M., P.J. Reimer, and R.W. Reimer, CALIB 6.0, 2005. <http://calib.qub.ca.uk/calib/>. Accessed May 8, 2015.

Talma, A.S. and J.C. Vogel, “A Simplified Approach to Calibrating C14 Dates,” *Radiocarbon,* 35:317-322, 1993.

Talwani, P. and J. Cox, “Paleoseismic Evidence for Recurrence of Earthquakes near Charleston, South Carolina,” *Science,* 228:379-381, 1985.

Talwani, P. and W.T. Schaeffer, “Recurrence Rates of Large Earthquakes in the South Carolina Coastal Plain based on Paleoliquefaction Data,” *Journal of Geophysical Research,* 106(B4):6621-6642, 2001.

Taylor, W.W., *A Study of Archeology,* Southern Illinois University Press, Carbondale, IL, 1967 (original 1948).

Telford, W.M., L.P. Geldart, and R.E. Sheriff, *Applied Geophysics, 2nd edition,* Cambridge University Press, Cambridge, U. K., 1990.

Terzaghi, K., *Theoretical Soil Mechanics,* Chapman and Hall, Wiley and Sons, New York, 1943.

Toprak, S., et al., “CPT- and SPT-based Probabilistic Assessment of Liquefaction Potential,” *Proceedings of the 7th U.S.–Japan Workshop on Earthquake Resistant Design of Lifeline Facilities and Countermeasures Against Liquefaction, Seattle, WA, 19 November 1999*, MCEER, Buffalo, NY, Technical Report MCEER-99-0019, 1999.

Toprak, S.A. and T.L. Holzer, “Liquefaction Potential Index: Field Assessment,” *Journal of Geotechnical and Geoenvironmental Engineering,* 129(4):315-322, 2003.

Trumbore, S.E., “AMS ^{14}C Measurements of Fractionated Soil Organic Matter: An Approach to Deciphering the Soil Carbon Cycle,” *Radiocarbon,* 31(3):644-654, 1989.

Tsai, P-H., et al., "Simplified DMT-Based Methods for Evaluating Liquefaction Resistance of Soils", *Engineering Geology*, 103:13-22, 2009.

Tuttle, M.P., “Late Holocene Earthquakes and their Implications for Earthquake Potential of the New Madrid Seismic Zone, Central United States,” Ph.D. dissertation, University of Maryland, College Park, MD, 1999.

Tuttle, M.P., “The Use of Liquefaction Features in Paleoseismology: Lessons Learned in the New Madrid Seismic Zone, Central United States,” *Journal of Seismology,* 5:361-380, 2001.

Tuttle, M.P., “Search for and Study of Sand Blows at Distant Sites resulting from Prehistoric and Historic New Madrid Earthquakes: Collaborative Research, M. Tuttle & Associates and Central Region Hazards Team,” National Earthquake Hazards Reduction Program, Annual Technical Report to U.S. Geological Survey, Award No. 1434-02HQGR0097, 2004.

Tuttle, M.P., “Re-evaluation of Earthquake Potential and Source in the Vicinity of Newburyport, Massachusetts,” National Earthquake Hazards Reduction Program, Final Technical Report to U.S. Geological Survey, Award No. 1434-01HQGR0163, 2007.

Tuttle, M.P., “Re-evaluation of Earthquake Potential and Source in the Vicinity of Newburyport, Massachusetts,” National Earthquake Hazards Reduction Program, Final Technical Report to U.S. Geological Survey, Award No. 1434-03HQGR0031, 2009.

Tuttle, M.P., “Search for and Study of Sand Blows at Distant Sites resulting from Prehistoric and Historic New Madrid Earthquakes: Collaborative Research, M. Tuttle & Associates and Central Region Hazards Team,” National Earthquake Hazards Reduction Program, Final Technical Report to U.S. Geological Survey, Award No. 1434-02HQGR0097, 2010.

Tuttle, M.P., “Study of Source, Magnitude, and Recurrence Time of Large Earthquakes affecting Northern Puerto Rico: Collaborative Research, M. Tuttle & Associates and Central Region Hazards Team,” National Earthquake Hazards Reduction Program, Final Technical Report to U.S. Geological Survey, Award No., 1434-06HQGR0023, 2011.

Tuttle, M.P., R. Such, and L. Seeber, “Ground Failure associated with the November 25th, 1988 Saguenay Earthquake in Quebec Province, Canada, *in* K. Jacob, ed., The 1988 Saguenay Earthquake of November 25, 1988, Quebec, Canada, Strong Motion Data, Ground Failure Observations, and Preliminary Interpretations,” National Center for Earthquake Engineering Research, Buffalo, New York, 1989.

Tuttle, M., et al., “Liquefaction and Ground Failure in Ferland, Quebec, triggered by the 1988 Saguenay Earthquake,” *Canadian Geotechnical Journal,* 27:580-589, 1990.

Tuttle, M. and L. Seeber, “Historic and Prehistoric Earthquake-induced Liquefaction in Newbury, Massachusetts,” *Geology,* 19:594-597, 1991.

Tuttle, M.P. and E.S. Schweig, “Archeological and Pedological Evidence for Large Earthquakes in the New Madrid Seismic Zone, Central United States,” *Geology,* 23:253-256, 1995.

Tuttle, M. and N. Barstow, “Liquefaction-related Ground Failure: A Case Study in the New Madrid Seismic Zone, Central United States,” *Bulletin of the Seismological Society of America,* 86(3):636-645, 1996.

Tuttle, M.P., et al., “Use of Archaeology to Date Liquefaction Features and Seismic Events in the New Madrid Seismic Zone, Central United States,” *Geoarchaeology: An International Journal,* 11(6):451-480, 1996.

Tuttle, M.P., et al., “New Evidence for a Large Earthquake in the New Madrid Seismic Zone between A.D. 1400 and 1670,” *Geology,* 27(9):771-774, 1999.

Tuttle, M.P., et al., “Observations and Comparisons of Liquefaction Features and Related effects induced by the Bhuj Earthquake,” *Earthquake Spectra,* 18(Supplement A):79-100, 2002a.

Tuttle, M.P., et al., “The Earthquake Potential of the New Madrid Seismic Zone,” *Bulletin of the Seismological Society of America,* 92(6):2080-2089, 2002b.

Tuttle, M.P., K. Dyer-Williams, and N.L. Barstow, “Paleoliquefaction Study of the Clarendon-Linden Fault System, Western New York State,” *Tectonophysics,* 353:263-286, 2002c.

Tuttle, M.P., et al., “Late Holocene Liquefaction Features in the Dominican Republic: A Powerful Tool for Earthquake Hazard Assessment in the Northeastern Caribbean,” *Bulletin of the Seismological Society of America,* 93(1):27-46, 2003.

Tuttle, M.P., et al., “Liquefaction induced by Historic and Prehistoric Earthquakes in Western Puerto Rico, *in* P. Mann, ed., Active Tectonics and Seismic Hazards of Puerto Rico, the Virgin Islands, and Offshore Areas,” Geological Society of America Special Paper 385, 2005a.

Tuttle, M.P., et al., “Evidence for New Madrid Earthquakes in AD 300 and 2350 B.C.,” *Seismological Research Letters,* 76(4):489-501, 2005b.

Tuttle, M.P., H. Al-Shukri, and H. Mahdi, “Very Large Earthquakes Centered Southwest of the New Madrid Seismic Zone 5,000-7,000 years ago,” *Seismological Research Letters,* 77(6):664-678, 2006.

Tuttle, M.P. and G.M. Atkinson, “Localization of Large Earthquakes in the Charlevoix Zone, Quebec, Canada, during the past 10,000 years,” *Seismological Research Letters,* 81(1):140-147, 2010.

Tuttle, M. and K. Dyer-Williams, “Paleoseismological Investigation in the Site Region of OPG’s New Nuclear — Darlington Project: New Nuclear - Darlington Environmental Assessment,” Prepared for Ontario Power Generation, Inc., 2010.

Tuttle, M.P., et al., “Repeated Large Earthquakes 4,800 to 38,000 years ago towards the Southwestern end of the Reelfoot Rift Fault System,” *Geological Society of America, Abstracts with Programs,* 42(5):218, 2010a.

Tuttle, M.P., et al., “Late Quaternary Earthquake-induced Liquefaction in Greater Toronto,” Seismological Society of America, Eastern Section Meeting, Program and Abstracts, 2010b.

Tuttle, M.P., et al., “Impact of Earthquake-induced Liquefaction and Related Ground Failure on a Mississippian Archeological Site in the New Madrid Seismic Zone, Central USA,” *Quaternary International,* 242:126-137, 2011.

Tuttle, M.P., P. Villamor, and P. Almond, “Paleoliquefaction Lessons Learned from the 2010-2011 Canterbury, New Zealand, earthquakes,” *in Proceedings of the Geological Society of America Annual Meeting, 4-7 November 2012,* Charlotte, NC, 2012.

U.S. Nuclear Regulatory Commission, Tuttle, M.P., P. Cowie, and L. Wolf, “Liquefaction Induced by Modern Earthquakes as a Key to Paleoseismicity: A Case Study of the 1988 Saguenay Earthquake,” in A. Weiss, ed., *Proceedings of the Nineteenth International Water Reactor Safety Information Meeting*, NUREG/CP-0119, 3:437-462, April 1992.

U.S. Nuclear Regulatory Commission, “Case Study of Liquefaction Induced by the 1944 Massena, New York-Cornwall, Ontario Earthquakes,” NUREG/CR-6495, September 1996.

U.S. Nuclear Regulatory Commission, “Dating of Liquefaction Features in the New Madrid Seismic Zone and Implications for Earthquake Hazard,” NUREG/GR-0017, September 1998.

U.S. Nuclear Regulatory Commission, “Paleoseismology Study Northwest of the New Madrid Seismic Zone,” NUREG/CR-5730, May 1999.

U.S. Nuclear Regulatory Commission, “Dating of Liquefaction Features in the New Madrid Seismic Zone, NUREG/GR-0018,” August 2000, ADAMS Accession No. ML003752771.

U.S. Nuclear Regulatory Commission, “Central and Eastern United States Seismic Source Characterization for Nuclear Facilities,” NUREG-2115, Vols. 1-6, February 2012, ADAMS Accession No. ML12048A776.

Van Arsdale, R.B., et al., “Earthquake Signals in Tree-Ring Data from the New Madrid Seismic Zone and Implications for Paleoseismicity,” *Geology,* 26(6):515-518, 1998.

Vaughn, J.D., “Paleoseismological Studies in the Western Lowlands of Southeastern Missouri,” National Earthquake Hazards Reduction Program, Final Technical Report to U.S. Geological Survey, 1994.

Villamor, P., et al., “Exploring methods to assess paleoliquefaction in the Canterbury area,” GNS Science Consultancy Report 2014/183, 2014.

Vogel, J.C., et al., “Pretoria Calibration Curve for Short Lived Samples,” *Radiocarbon,* 33:73-86, 1993.

Wair, B.R., J.D. DeJong, and T. Shantz, “Guidelines for Estimation of Shear Wave Velocity Profiles,” Pacific Earthquake Engineering Research Center, University of California, PEER Report 2012/08, 2012.

Walker, M., *Quaternary Dating Methods,* John Wiley and Sons, Ltd, West Sussex, England, 2005.

Walker, J. D. et al., compilers, *Geologic Time Scale v. 4.0*, Geological Society of America, 2012.

Wheeler, R.L., “Distinguishing Seismic from Nonseismic Soft-Sediment Features: Criteria from Seismic Hazard Analysis, *in* Ettensohn, F.R., N. Rast, and C.E. Brett, eds., Ancient Seismites,” Geological Society of America, Special Paper 359, 2002.

Wolf, L.W., “Geophysical Investigations of Earthquake-induced Liquefaction Features in the New Madrid Seismic Zone,” National Earthquake Hazards Reduction Program, Final Technical Report to U.S. Geological Survey, Award No. 01HQGR0003, 2004.

Wolf, L.W., et al., “Geophysical Reconnaissance of Earthquake-induced Liquefaction Features in the New Madrid Seismic Zone,” *Journal of Applied Geophysics,* 39:121-129, 1998.

Wolf, L.W., et al., “Geophysical Surveys of Earthquake-induced Liquefaction Deposits in the New Madrid Seismic Zone,” *Geophysics,* 71(6):B223-230, 2006.

Youd, T.L., “Liquefaction, Flow and associated Ground Failure,” U.S. Geological Survey, Circular 688, 1973.

Youd, T.L., “Geologic effects—Liquefaction and associated Ground Failure,” U.S. Geological Survey Open-File Report 84-760, 1984.

Youd, T.L., “A Look Inside the Debate over EERI Monograph MNO 12,” unpublished presentation, 2011.

Youd, T.L. and S.N. Hoose, “Liquefaction Susceptibility and Geologic Setting,” *Proceedings of th, 6th World Conference on Earthquake Engineering, v. 3,* United States Government Printing Office, Washington, D.C., 1977.

Youd, T.L. and D.M. Perkins, “Mapping of Liquefaction induced Ground Failure Potential,” *Journal of the Geotechnical Engineering Division,* American Society of Civil Engineers*,* 104(4):433-446, 1978.

Youd, T.L. and D.M. Perkins, “Mapping of Liquefaction Severity Index,” *Journal of Geotechnical Engineering,* 113(11):1374-1392, 1987.

Youd, T.L., D.M. Perkins, and W.G. Turner, “Liquefaction Severity Index Attenuation for the Eastern United States, Proceedings from the Second U.S.-Japan Workshop on Liquefaction, Large Ground Deformation and their Effects on Lifelines,” Technical Report NCEER-89-0032, 1989.

Youd, T.L. and I.M. Idriss, eds., *Proceedings of the NCEER Workshop on Evaluation of Liquefaction Resistance of Soils, Salt Lake City, Utah, Technical Report NCEER-97-0022, National Center for Earthquake Engineering Research,* Buffalo, NY, 1997.

Youd, T.L. and S.K. Noble, “Liquefaction Criteria based on Statistical and Probabilistic Analyses,” *Proceedings, NCEER Workshop on Evaluation of Liquefaction Resistance of Soils,* NCEER Technical Report No. 97-0022, Salt Lake City, 1997.

Youd, T.L., et al., “Liquefaction Resistance of Soils: Summary Report from the 1996 NCEER and 1998 NCEER/NSF Workshops on Evaluation of Liquefaction Resistance of Soils,” *Journal of Geotechnical and Geoenvironmental Engineering,* 127(10):817-833, 2001.

Youd, T.L., et al., “Closure to Liquefaction Resistance of Soils," *Journal of Geotechnical and Geoenvironmental Engineering,* 129(3):283-284, 2003.

Zhang, G., P.K. Robertson, and R.W.I. Brachman, “Estimating Liquefaction-Induced Ground Settlements from CPT for Level Ground,” *Canadian Geotechnical Journal,* 39(5):1168-1180, 2002.

Zhang, G., P.K. Robertson, and R.W.I. Brachman, “Estimating Liquefaction-Induced Lateral Displacements Using the Standard Penetration Test of Cone Penetration Test,” *Journal of Geotechnical and Geoenvironmental Engineering,* 130(8):861-871, 2004.

APPENDIX A

EVALUATION OF OVERBURDEN STRESS AND PORE WATER PRESSURE

The evaluation of the effective vertical (overburden) stress is one of the first and important steps in any situation involving geotechnics. The total vertical overburden stress (σ_{vo}) is calculated from the accumulation of total soil unit weight (γ_t) with depth:

$$\sigma_{vo} = \int_0^z \gamma_t \cdot dz$$

The above can be approximated on a spreadsheet using summation of unit weight times layer thickness with depth according to:

$$\sigma_{vo} \quad \sum_{i=1}^{z} (\gamma_{ti} \cdot \Delta z_i)$$

where the subscript *i* refers to each successive layer.

Measured Soil Unit Weight: Soil unit weight can be measured from undisturbed thin-walled tube samples (ASTM D1587) as total weight (W) divided by total volume (V), such that: $\gamma_t = W/V$. In this case, the soil mass density is obtained from: $\rho_t = \gamma_t/g$, where g = 9.8 m/s^2 = gravitational constant. Tube samples are readily obtained in fine-grained soils, however, granular soils especially clean sands are often difficult or very expensive to procure by this technique.

If the soil is dry, γ_t equals the dry unit weight (γ_{dry}) and if the soil is saturated, then $\gamma_t = \gamma_{sat}$. It is also possible to have soil unit weights between these two extreme values, yet it will be dependent on the existing degree of saturation (S). A primary soil identity relation can be used to assign unit weights based on index parameters:

$$G_s \cdot w_n = S \cdot e_0$$

where G_s = specific gravity of solids, w_n = natural in-place water content, and e_0 = void ratio. For most natural soils, a value $G_s = 2.70 \pm 0.10$. For saturated soils: S = 1 (or 100%), and for dry soils: $w_n = 0$. The general case for unit weight is given by the second soil identity:

$$\gamma_t = \frac{1 + w_n}{1 + e_0} \cdot G_s \cdot \gamma_w$$

where γ_w = unit weight of water (γ_w = 9.81 kN/m^3 for freshwater and = 10.0 kN/m^3 for salt water). For the two usual cases:

$$\gamma_{dry} = \frac{G_s \cdot \gamma_w}{1 + e_0}$$

$$\gamma_{dry} = \frac{G_s + e_0}{1 + e_0} \cdot \gamma_w$$

Estimated Unit Weight: In many cases, neither measured unit weight nor water content has been obtained for a soil layer. In these cases, values for various soils are often assumed or taken from published textbooks. A more rational approach for deriving values of soil unit weight can be made via direct statistical relations derived from large databases. In this appendix, methods for estimating soil unit weight are given for shear wave velocity, SPT, CPT, and DMT.

Figure A1 shows a clear link between the total unit weight and field shear wave velocity for a variety of soils, including clays, silts, sands, gravels, and mixed soils. For these sites, approximately 90% were submerged and thus represent the saturated unit weight. The shear wave velocity data were obtained primarily from downhole tests (85%), crosshole tests (10%), suspension logging (2%), and surface wave type methods (3%). A secondary effect with depth (z) is also shown. The general expression (units dependent) is given by:

$$\gamma_t = 8.63 \log (V_s) - 1.18 \log (z) - 0.53$$

where γ_t = unit weight (kN/m^3), V_s = shear wave velocity (m/s), and z = depth (meters). An alternate expression given in terms of effective overburden stress (σ_{vo}') rather than depth is also available (Mayne et al., 2009), which is more fundamental since groundwater table conditions are considered. However, the parameters σ_{vo}' or z are only secondary level effects to the regression.

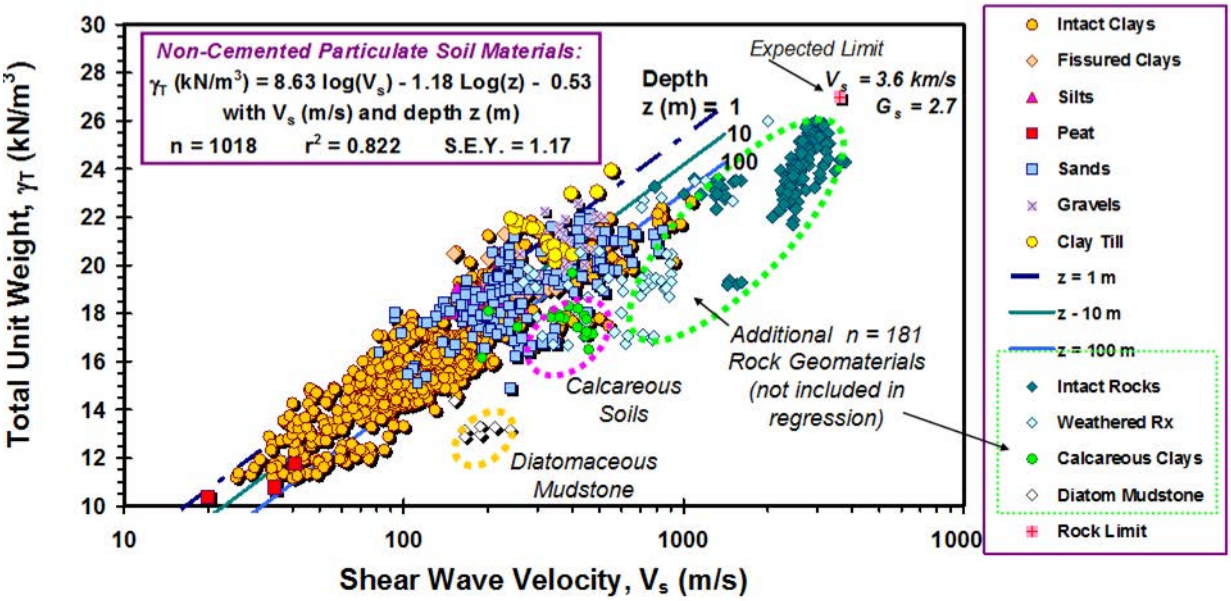

Figure A-1 Unit weight relation between shear wave velocity and depth (Mayne et al., 2009).

For the SPT, no direct means to estimate unit weight has been developed. However, many methods have empirically related shear wave velocity to SPT-N value (Wair et al., 2012). A rather quick and simple estimate is afforded from the large empirical dataset (n = 1654) reported by Imai and Tonouchi (1982) for all soil types:

$$V_s \text{ (m/s)} = 93 \, (N_{60})^{0.314}$$

whereby the estimated V_s and corresponding depth z can be entered into Figure A.1. to obtain an estimated soil unit weight. A more recent and rational approach has been developed that incorporates the corrected SPT resistance, influence of effective overburden stress (in KPa), and age (Wair et al., 2012):

$$V_s = 30 \cdot ASF \cdot (N_{60})^{0.215} \cdot (\sigma_{vo}')^{0.275}$$

where the age scaling factor (ASF) is taken as 0.87 for Holocene soils and 1.13 for Pleistocene soils. Slightly different values are used for fine-grained and coarse-grained soils. The above relation requires iteration with depth since σ_{vo}' depends on the unit weight. A means of estimating unit weight from the CPT sleeve friction also has been developed (Mayne et al., 2010a, 2010b). The results have been developed on the basis of 58 sites where statistical regression analyses were conducted on paired sets of laboratory-determined unit weights and CPT readings, as summarized in Figure A2. The summary expression is given by:

$$\gamma_t = 1.95 \cdot \gamma_w \cdot \left(\frac{\sigma_{vo}'}{\sigma_{atm}} \right)^{0.06} \cdot \left(\frac{f_{st}}{\sigma_{atm}} \right)^{0.06}$$

where γ_t = soil total unit weight, γ_w = unit weight of water, f_{st} = measured total sleeve friction from the CPT, and σ_{atm} = atmospheric pressure (= 1 atm ≈ 1 bar = 100 kPa). The relation appears valid for estimates in uncemented geomaterials including a variety of clays, silts, sands, tills, and mixed soil types, however, is apparently not valid for diatomaceous clays and perhaps of limited applicability in highly calcareous soils.

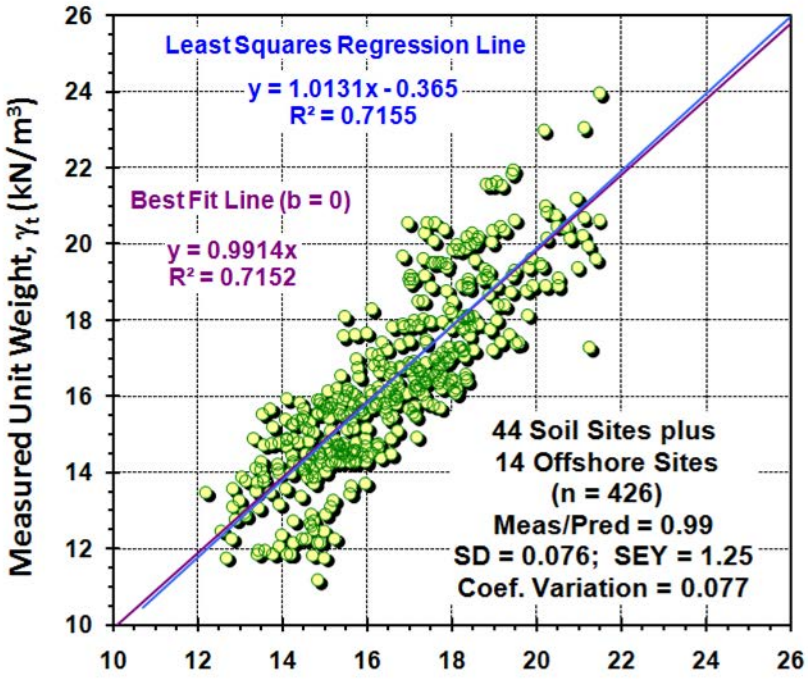

Figure A-2 Relation for soil unit weight from CPT sleeve friction resistance.

The above relation was expanded to over 80 sites and then simplified for direct use (Mayne, 2014) such that no iteration was necessary:

$$\gamma_t = \gamma_w \cdot [1.22 + 0.15 \cdot \ln(100 \cdot f_s / \sigma_{atm} + 0.01)]$$

The direct trend between soil unit weight and sleeve friction is presented in Figure A.3 along with corresponding statistical measures from regression analyses.

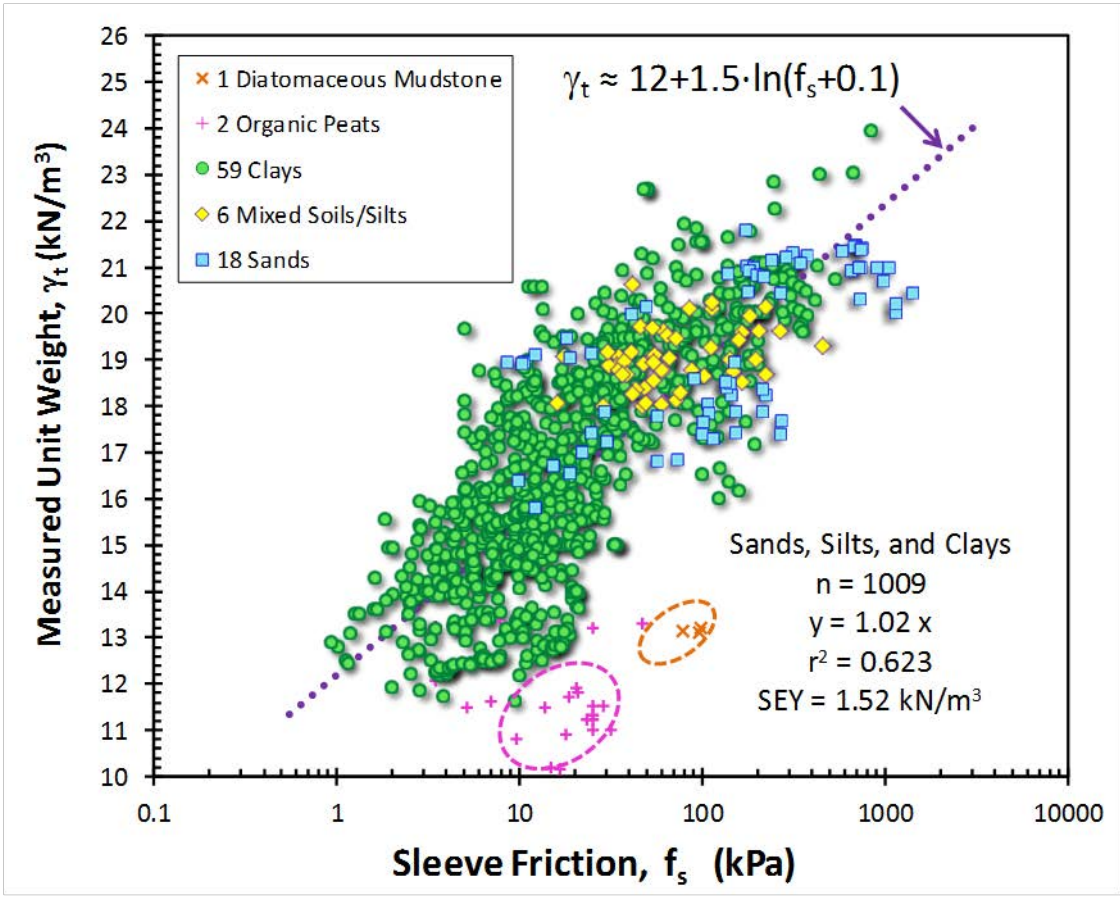

Figure A-3 Direct relation between soil unit weight and CPT sleeve friction for a variety of geomaterials (after Mayne, 2014).

For the flat plate dilatometer test (DMT), the soil unit weight can be estimated from the material index: $I_D = (p_1 - p_0)/(p_0 - u_0)$ and dilatometer modulus: $E_D = 34.7(p_1 - p_0)$ from (Mayne et al., 2009)

$$\gamma_t = 1.12\, \gamma_w \cdot (E_D/\sigma_{atm})^{0.1} \cdot (I_D)^{-0.05}$$

Hydrostatic Pore Water Pressure: The hydrostatic pore water pressure (u0) is obtained from the water table information (Mayne et al. 2002). For the case of unconfined aquifers, the depth to the groundwater (z_w) can be measured in open boreholes, observation wells, and by installation of piezometers. With CPTu, the depth of the water table can either be measured by allowing a full dissipation of the measured pore water pressures to hydrostatic ($u_2 \rightarrow u_0$) at selected test depth,

otherwise inferred from data in clean sand layers because the measured pressures are close to hydrostatic ($u_2 \approx u_0$) and therefore the height of the water is $h_w = u_2/g_w$. At that elevation, the depth of the groundwater table is then obtained as $z_w = z - h_w$.

Once z_w is known, then the profile of u_0 below this depth ($z > z_w$) can be calculated from:

Below groundwater table: $u_0 = (z - z_w) \cdot \gamma_w$

Above the water table ($z < z_w$), there are at least three possible cases (Mayne et al. 2002). The two simplest scenarios include completely dry soil and completely saturated soil due to capillary rise, where the u_0 conditions for these cases are:

Above water table (dry soil): $u_0 = 0$

Above water table (saturated soil): $u_0 = (z - z_w) \cdot \gamma_w$

The normal assumption is that clean sands are dry above the water table, while clays can be saturated (or dry) above the water table because of full capillarity. In the third possible case involving partially-saturated soils, the conditions could vary anywhere in-between, depending on many factors, including: the degree of saturation, recent rainfall or infiltration or irrigation, drought activity, humidity, temperature, and other environmental variables. In the case of special groundwater circumstances including artesian pressures and/or drawdown, it may be necessary to install permanent piezometers and monitoring wells to document the actual water table and its variations on a daily or weekly or seasonal basis.

APPENDIX B

UPDATED CRR CURVES FROM IN-SITU TESTS

Since the NCEER consensus reports were developed about two decades ago (Youd and Idriss, 1997), a number of new case studies from large seismic events worldwide have provided additional data to allow updating of the various cyclic resistance ratios (CRRs), as well as the cyclic stress ratios (CSR), for each of the *in-situ* test methods. Herein, a brief description will be provided for selected deterministic SPT, CPT, DMT, and V_s methods for soil liquefaction evaluation. Full details on the updated SPT and CPT methods are given by Idriss and Boulanger (2004, 2008, 2010) and Boulanger and Idriss (2012, 2014).

SPT: An updated SPT procedure for evaluating soil liquefaction triggering is presented by Idriss and Boulanger (2010) and Boulanger and Idriss (2014). Figure B.1 shows the new CRR for this method which depends upon specific procedures for the evaluation of the cyclic stress ratio for a magnitude **M** 7.5 and effective overburden stress of 1 atm, designated: $CSR_{7.5}$, σ_v'= 1 atm, and for obtaining the stress-normalized and energy-correction SPT resistance for an equivalent clean sand, designated: $(N_1)_{60\text{-}cs}$.

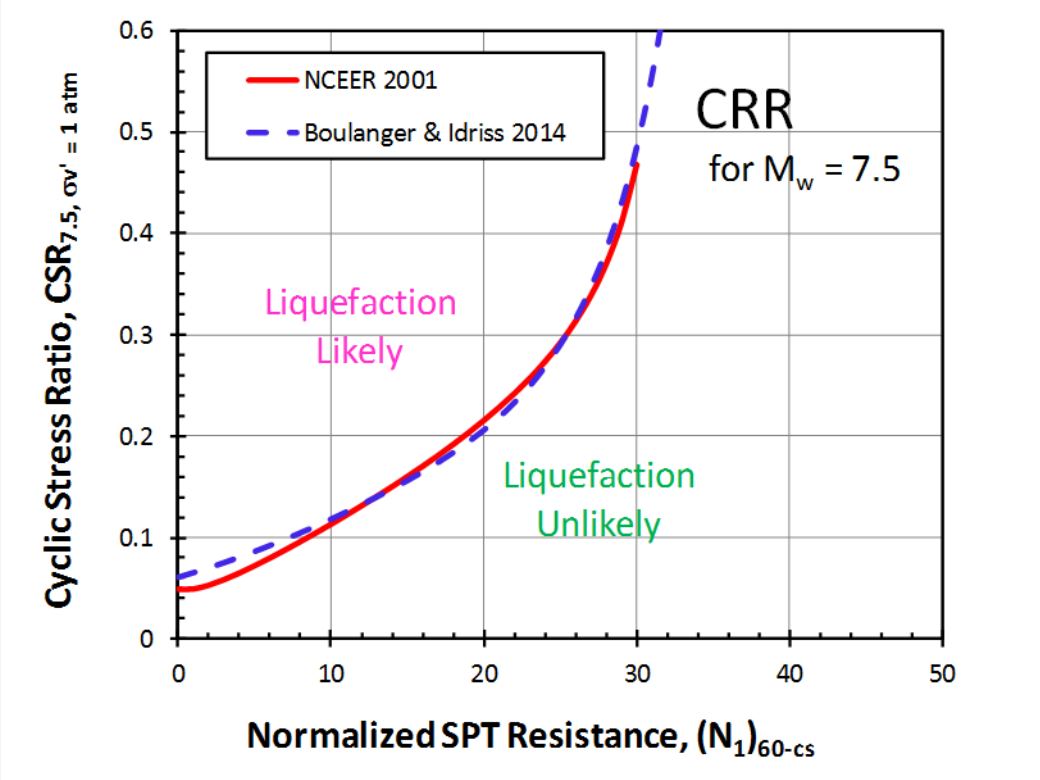

Figure B-1 Updated cyclic resistance ratio for SPT in clean sands (after Boulanger and Idriss 2014).

The normalized soil resistance for the updated method is given by:

$$(N_1)_{60} = C_{Ne} \cdot N_{60}$$

where the stress normalization factor is estimated by:

$$C_{Ne} = (\sigma_{atm}/\sigma_{vo}')^m \leq 1.7$$

The exponent *m* varies with relative density (D_R) of the sand, such that:

$$m = 0.785 - 0.521 \cdot D_R$$

For clean sands, the relative density can be estimated from the normalized penetration resistance (e.g., Skempton, 1986; Kulhawy and Mayne, 1990). For the updated approach, the relative density of clean sands is given by:

$$D_R \ (\%) = [\ (N_1)_{60}/46\ ]^{0.5}$$

For sands with fines, there is a correction for the fines content (FC in %) that provides a means to obtain a normalized penetration resistance that is equivalent to that for clean sands:

$$(N_1)_{60\text{-}cs} = (N_1)_{60} + \Delta(N_1)_{60}$$

where the fines correction is obtained from:

$$\Delta(N_1)_{60} = \exp\left(1.63 + \frac{9.7}{FC + 0.01} - \left[\frac{15.7}{FC + 0.01}\right]^2\right)$$

The combined effects of relative density and fines content can be expressed to give the exponent m in terms of the normalized and corrected SPT resistance:

$$m = 0.784 - 0.0768 \cdot [\ (N_1)_{60\text{-}cs}\ ]^{0.5}$$

where $0.264 \leq m$. This procedure of course requires iteration to resolve the final value for $(N_1)_{60\text{-}cs}$.

Once determined, the cyclic resistance ratio for **M** 7.5 and effective overburden stress at 1 atm (as shown in Figure B.1) is evaluated from:

$$CRR_{7.5,\,\sigma v'=1\,atm} = \exp\left[\frac{(N_1)_{60-cs}}{14.1} + \left(\frac{(N_1)_{60-cs}}{126}\right)^2 - \left(\frac{(N_1)_{60-cs}}{23.6}\right)^3 + \left(\frac{(N_1)_{60-cs}}{25.4}\right)^4 - 2.80\right]$$

The level of ground shaking by the earthquake is represented by the cyclic stress ratio (CSR) and is given by the following expression for flat horizontal ground:

$$CSR_{7.5,\,\sigma v'=1\,atm} = 0.65 \cdot \left(\frac{a_{max}}{g}\right)\left(\frac{\sigma_{vo}}{\sigma_{vo}'}\right) \cdot r_d \cdot \frac{1}{MSF} \cdot \frac{1}{K_\sigma}$$

where the first three terms have been detailed previously. For the Boulanger and Idriss (2014) approach, the stress reduction factor (r_d) is expressed as a function of depth (z) and magnitude (**M**), as presented in Figure B.2.

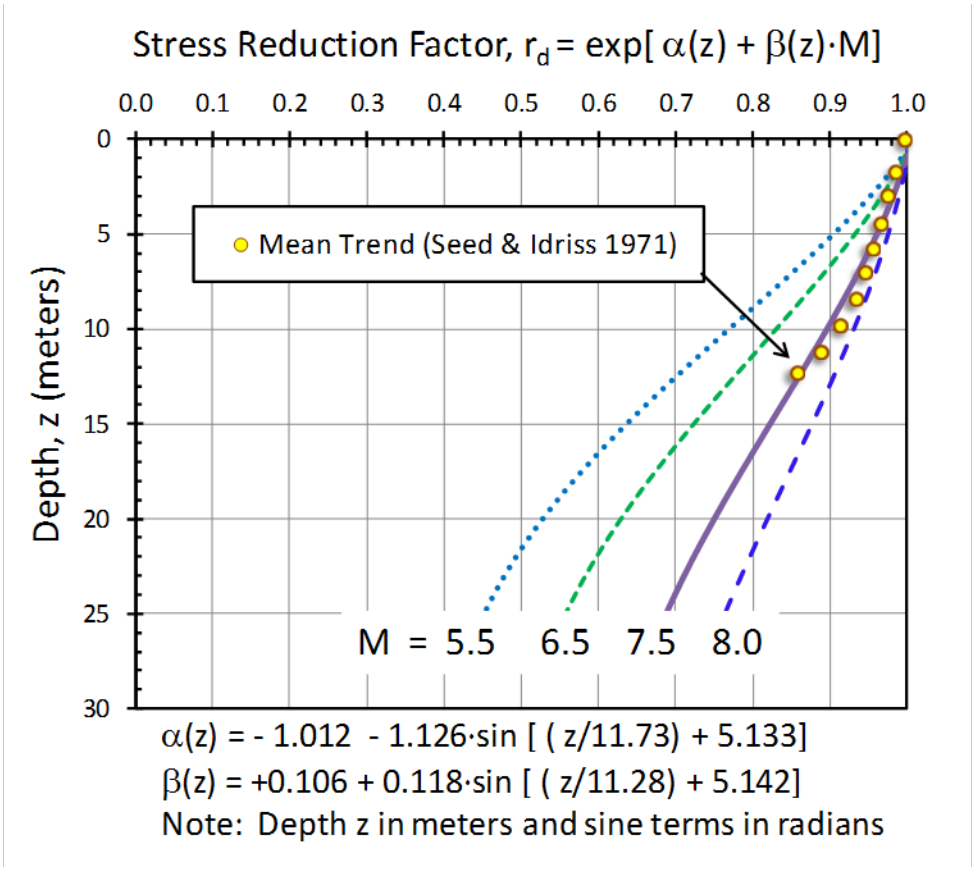

Figure B-2 Evaluation of the stress reduction factor (r_d) for the updated SPT-CPT approach (after Boulanger and Idriss 2014).

The MSF is evaluated from the magnitude earthquake and normalized-corrected penetration resistance:

$$MSF = 1 + (MSF_{max} - 1) \cdot [\, 8.64 \cdot \exp(-M/4) - 1.325 \,]$$

where $MSF_{max} = 1.09 + [\, (N_1)_{60\text{-}cs}/31.5 \,]^2 \leq 2.2$

The overburden stress factor is expressed as a function of normalized and corrected penetration resistance and effective stress:

$$K_\sigma = 1 - C_\sigma \cdot \ln(\sigma_{vo}'/\sigma_{atm}) \leq 1.1$$

where $C_\sigma = 1/[\, 18.9 - 2.55 \cdot \{(N_1)_{60\text{-}cs}\}^{0.5} \,] \leq 0.3$

The factor of safety for triggering liquefaction is finally calculated as the ratio of the resistance to the demand:

$$FS_{liq} = \frac{CRR_{7.5,\sigma v'=1\,atm}}{CSR_{7.5,\sigma v'=1\,atm}}$$

CPT: A number of updates to the cone penetration testing (CPT) methodologies for soil liquefaction assessment have occurred since the NCEER approach. Analogous to the aforementioned updated method for SPT, a parallel and consistent approach for CPT has also been developed (Boulanger and Idriss, 2014) where many additional case history records from the recent 2010 Canterbury **M** 7.1 and 2011 **M** 6.3 Christchurch earthquakes in New Zealand and 2011 **M** 9.0 Tōhoku earthquake in Japan have provided new data. The updated approach for calculating CRR and CSR from CPT data is discussed subsequently.

Also, clarification of the definitional types of soil liquefaction and ground failure conditions have been made using soil behavioral type (SBT) charts (Robertson, 2010). As detailed earlier in Figure 2.26 and Table 2.5, the normalized CPT parameters delineate nine different soil types within a plot of Q_{tn} versus F, as presented in Figure B.3. After screening out Zones 1, 8, and 9, the CPT material index (I_c) is used to delineate Zones 2, 3, 4, 5, 6 and 7.

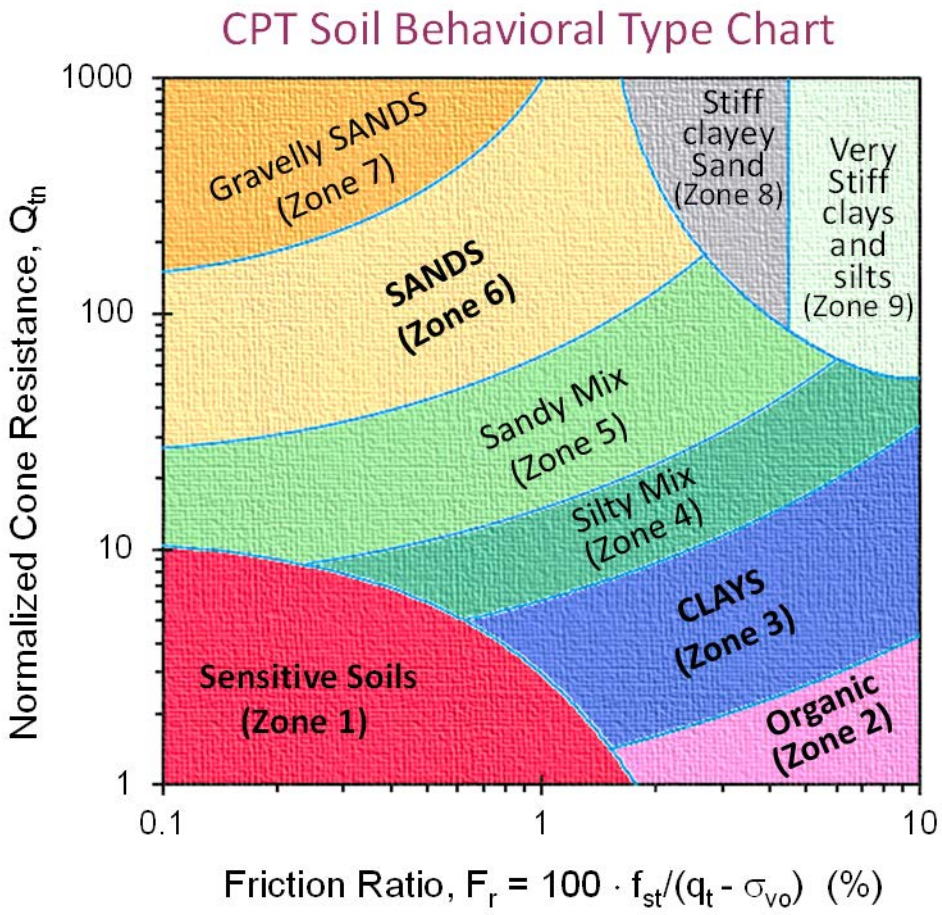

Figure B-3 Nine-zone chart of soil behavioral type for cone penetration tests (after Robertson, 2010).

Sandy soils may be susceptible to either flow or cyclic liquefaction and identified by a CPT material index $I_c \leq 2.60$. The identification of soils that are *contractive* versus *dilative* are demarcated by a normalized cone resistance for equivalent clean sand $(Q_{tn})_{cs} = 70$ (Robertson, 2010). Consequently, four regions are shown in Figure B.4 that categorize the expected types of soil behavior associated in seismic ground hazards.

- Region A_1 (cohesionless soils): Cyclic liquefaction possible
- Region A_2 (cohesionless soils): Cyclic and flow liquefaction possible
- Region B (cohesive soils): Cyclic softening possible
- Region C (cohesive soils): Cyclic softening and flow liquefaction possible.

Regions A1 and A2 include sands, sandy mixes, to gravelly sands and can be noted when:

$$Q_{tn} \geq 10^{[3.47-\sqrt{6.76-(1.22+\log F_r)^2}]}$$

Flow liquefaction may occur in Regions A2 and C, which can be approximately represented by:

$$Q_{tn-cs} \leq 10^{[0.6+1.25/[1+(F_r/2.2)^{1.8}]]}$$

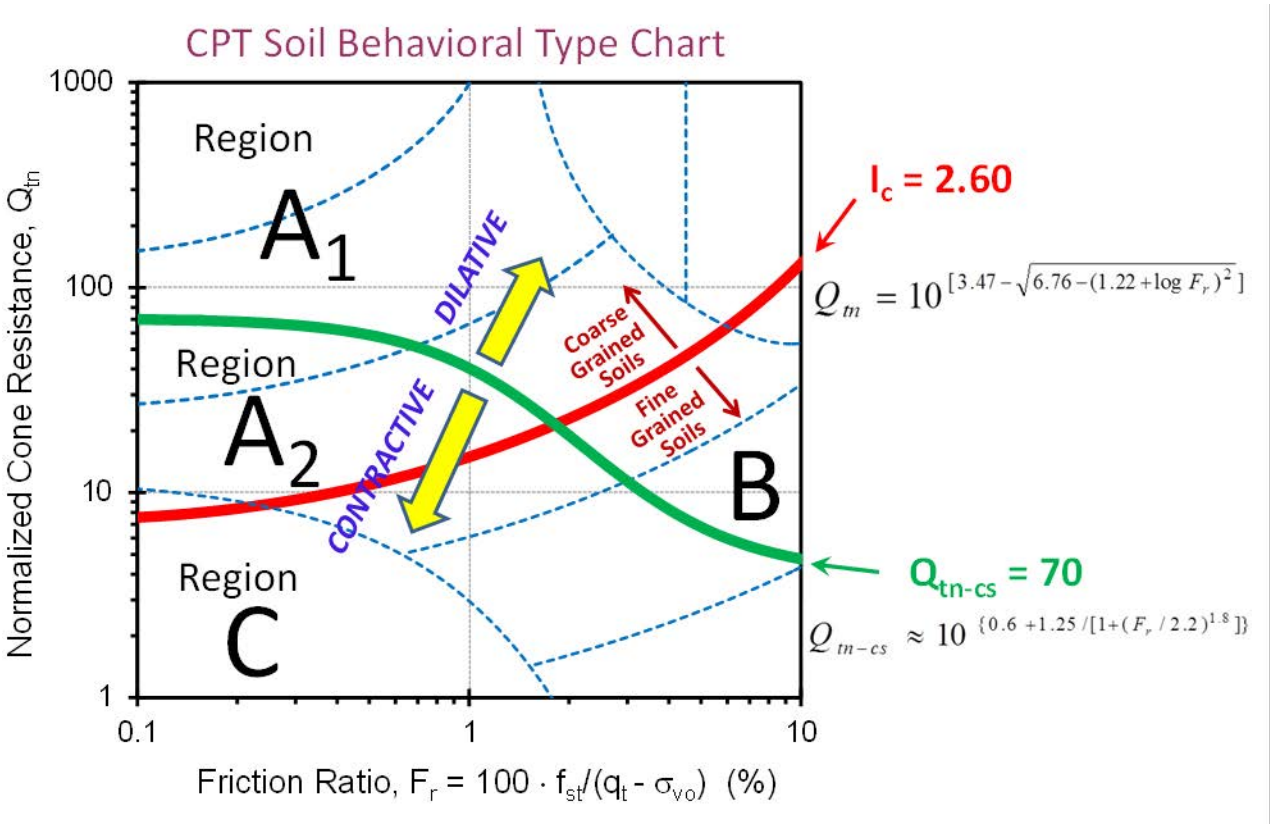

Figure B-4 Regions A_1, A_2, B, and C defining flow liquefaction, cyclic liquefaction, and/or cyclic softening (after Robertson, 2010).

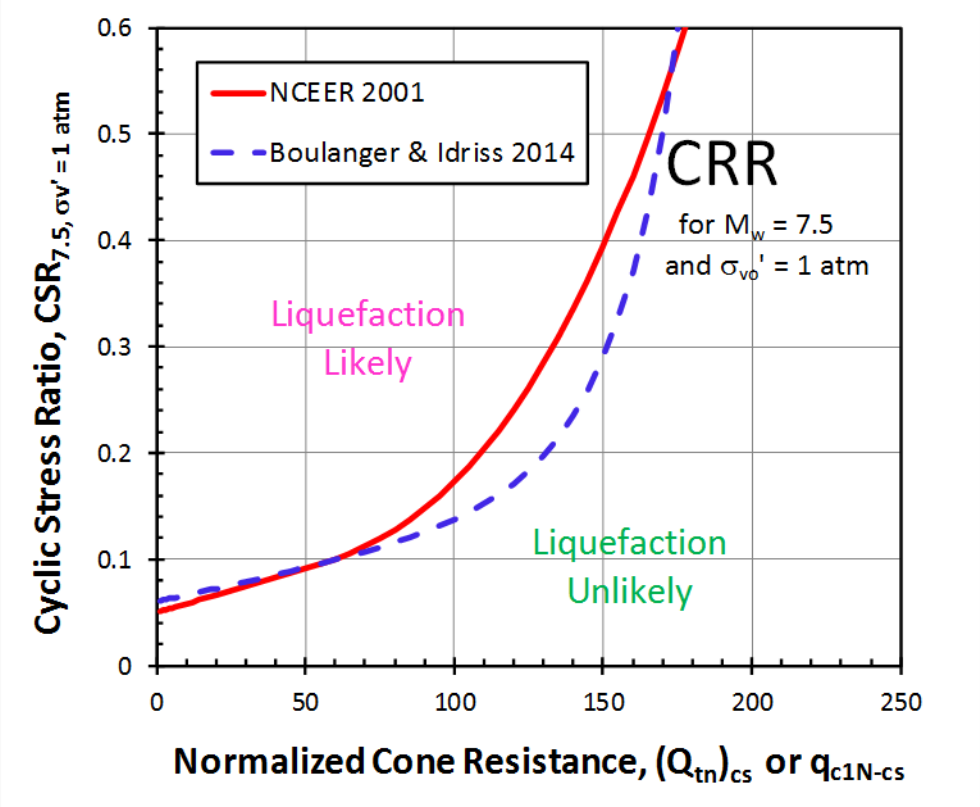

Figure B-5 Updated cyclic resistance ratio for CPTs in clean sands (after Boulanger and Idriss 2014).

The updated $CRR_{7.5}$ curve for CPT results is shown in Figure B.5 and seen to be a more conservative relationship for liquefaction triggering, in comparison with the NCEER (2001) curve.

Initially, the CPT material index (I_c) as defined by Robertson (2009a, 2009b, 2010) can be used to evaluate soil type and an estimate of the fines content of the sand, as discussed by Boulanger and Idriss (2014):

$$FC\ (\%) = 80\ (I_c + C_{FC}) = 137 \quad \text{where } 0\% \le FC \le 100\%$$

and the term C_{FC} is a site-specific calibration factor where the CPT readings can be calibrated with soil samples from adjacent side-by-side borings: $-0.29 \le C_{FC} \le +0.29$. In the event no samples are available, an initial estimate of $C_{FC} \approx 0$ may be used for preliminary efforts.

The stress-normalized cone resistance for clean sands is evaluated as a function of effective overburden stress and relative density:

$$q_{c1N} = C_{Ne} \cdot q_c/\sigma_{atm}$$

where the stress normalization factor is given by:

$$C_{Ne} = (\sigma_{atm}/\sigma_{vo}')^m \le 1.7$$

For general CPT interpretation in soils, the use of $q_{net} = q_t - \sigma_{vo}$ is essentially mandatory, where q_t = total cone tip resistance (Robertson, 1990; Lunne et al., 1997; Mayne, 2007). However, in clean sands, $q_t \approx q_c$ because induced penetration pore water pressures are low ($u_2 \approx u_0$). Also, since total overburden stress is small relative to cone tip resistance ($q_t >> \sigma_{vo}$) in clean sands at depths z < 30 m, essentially: $q_{net} \approx q_t \approx q_c$. Since liquefaction applies primarily to sands, the updated approach by Boulanger and Idriss (2014) has thus retained q_c in its formulations.

The exponent *m* varies with relative density (D_R) of the sand, such that:

$$m = 0.785 - 0.521 \cdot D_R$$

For this approach, the relative density of clean sands is given by:

$$D_R\ (\%) = 0.478\ (q_{c1N})^{0.264} - 1.063$$

For clean to silty sands, the measured (or estimated) fines content is used to adjust the normalized cone resistance to that for an equivalent clean sand:

$$q_{c1N\text{-}cs} = q_{c1N} + Dq_{c1N}$$

where the fines content correction term is expressed:

$$\Delta q_{c1N} = \left(\frac{q_{c1N}}{14.6} + 11.9\right) \cdot \left[1.63 - \left(\frac{9.7}{FC+2}\right) + \left(\frac{15.7}{FC+2}\right)^2\right]$$

Then this corrected and normalized CPT resistance is used to obtain the exponent *m*:

$$m = 1.338 - 0.249\ (q_{c1N\text{-}cs})^{0.264}$$

where it is restricted to the range: $0.264 \leq m \leq 0.782$.

The available strength of the ground to resist an earthquake is represented by the cyclic resistance ratio for a **M** 7.5 and effective overburden stress at σ_v' = 1 atm (as shown in Figure B.5), which is evaluated from:

$$CRR_{7.5,\sigma v'=1\,atm} = \exp\left[\frac{q_{c1N-cs}}{113} + \left(\frac{q_{c1N-cs}}{1000}\right)^2 - \left(\frac{q_{c1N-cs}}{140}\right)^3 + \left(\frac{q_{c1N-cs}}{137}\right)^4 - 2.80\right]$$

The level of ground shaking by the earthquake is represented by the cyclic stress ratio (CSR) and is given by the following expression for flat horizontal ground:

$$CSR_{7.5,\,\sigma v'=1\,atm} = 0.65 \cdot \left(\frac{a_{\max}}{g}\right)\left(\frac{\sigma_{vo}}{\sigma_{vo}'}\right) \cdot r_d \cdot \frac{1}{MSF} \cdot \frac{1}{K_\sigma}$$

where the first three terms have been detailed previously. For this updated approach, the stress reduction factor (r_d) is expressed as a function of depth (z) and magnitude (M), as presented in Figure B.2.

The MSF is derived from the earthquake magnitude and normalized-corrected penetration resistance:

$$MSF = 1 + (MSF_{max} - 1) \cdot [\, 8.64 \cdot \exp(-M/4) - 1.325 \,]$$

where $MSF_{max} = 1.09 + [\, (q_{c1N\text{-}cs})/180 \,]^2 \leq 2.2$

The overburden stress factor is expressed as a function of normalized and corrected penetration resistance and effective stress (Boulanger and Idriss 2014):

$$K_\sigma = 1 - C_\sigma \cdot \ln(\sigma_{vo}'/\sigma_{atm}) \leq 1.1$$

where $C_\sigma = 1/[\, 37.3 - 9.27 \cdot (q_{c1N\text{-}cs})^{0.264} \,] \leq 0.3$

The calculated factor of safety for triggering liquefaction is finally determined as the ratio of the resistance to the demand:

$$FS_{liq} = \frac{CRR_{7.5,\sigma v'=1\ atm}}{CSR_{7.5,\sigma v'=1\ atm}}$$

DMT: For the flat plate dilatometer test (DMT), an updated method has been developed by Tsai et al. (2009) that uses the NCEER evaluation of CSR (Youd et al., 2001) and the CRR shown in Figure B.6. The CRR for a magnitude **M** 7.5 event can be expressed in terms of the DMT horizontal stress index, $K_D = (p_0\text{-}u_0)/\sigma_{vo}'$:

$$CRR_{7.5} = \exp\left[\left(\frac{K_D}{8.8}\right)^3 - \left(\frac{K_D}{6.5}\right)^2 + \left(\frac{K_D}{2.5}\right) - 3.1\right]$$

Liquefaction studies reported by Amoroso et al. (2015) have shown this approach to give reasonable results when checked against sites in the L'Aquila earthquake.

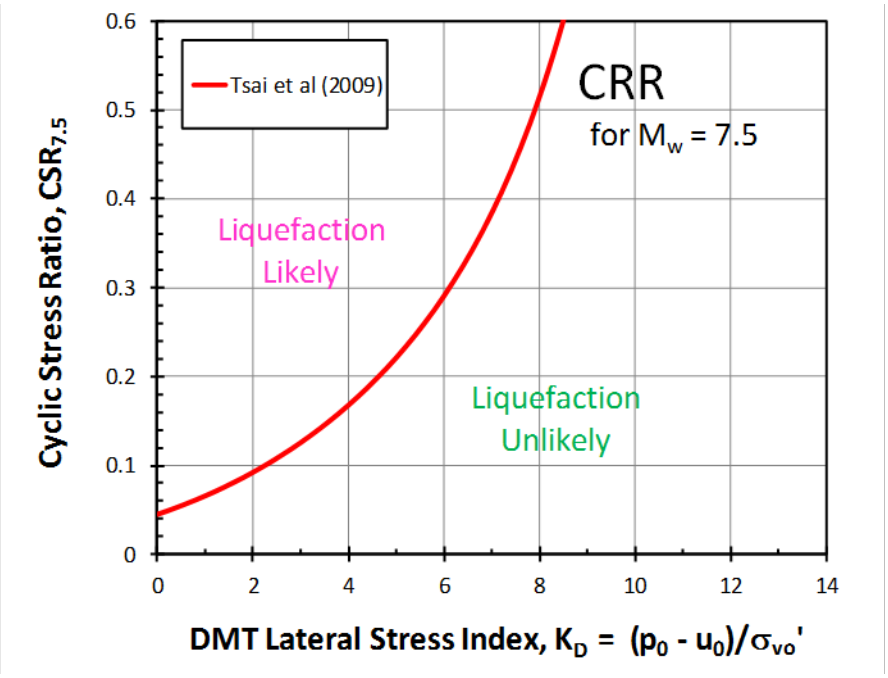

Figure B-6 Recommended $CRR_{7.5}$ for liquefaction evaluation using DMT in clean sands (after Tsai et al., 2009)

Shear Wave Velocity: The NCEER approach (Youd and Idriss, 1997) also includes a method for evaluating soil resistance using shear wave velocity (V_s), specifically the stress-normalized value:

$$V_{s1} = C_{Vs} \cdot V_s = \frac{V_s}{(\sigma_{vo}'/\sigma_{atm})^{0.25}}$$

where the term $C_{Vs} \leq 1.4$. The corresponding CRR is given by (Andrus and Stokoe, 2000):

$$CRR_{7.5} = 0.022 \cdot (V_{s1}/100)^2 + 2.8 \cdot \left[\frac{1}{*V_{s1c} - V_s} - \frac{1}{V_{s1c}} \right]$$

which has a hyperbolic form and the limiting asymptotes ($*V_{s1c}$ = 220, 210, and 200 m/s) are given in terms of fines contents: (a) FC < 5%; (b) FC = 20%, and (c) FC > 35%, respectively. Figure B.7 presents the CRR for V_{s1}. The $CSR_{7.5}$ is determined per the NCEER guidelines, as detailed earlier in this report.

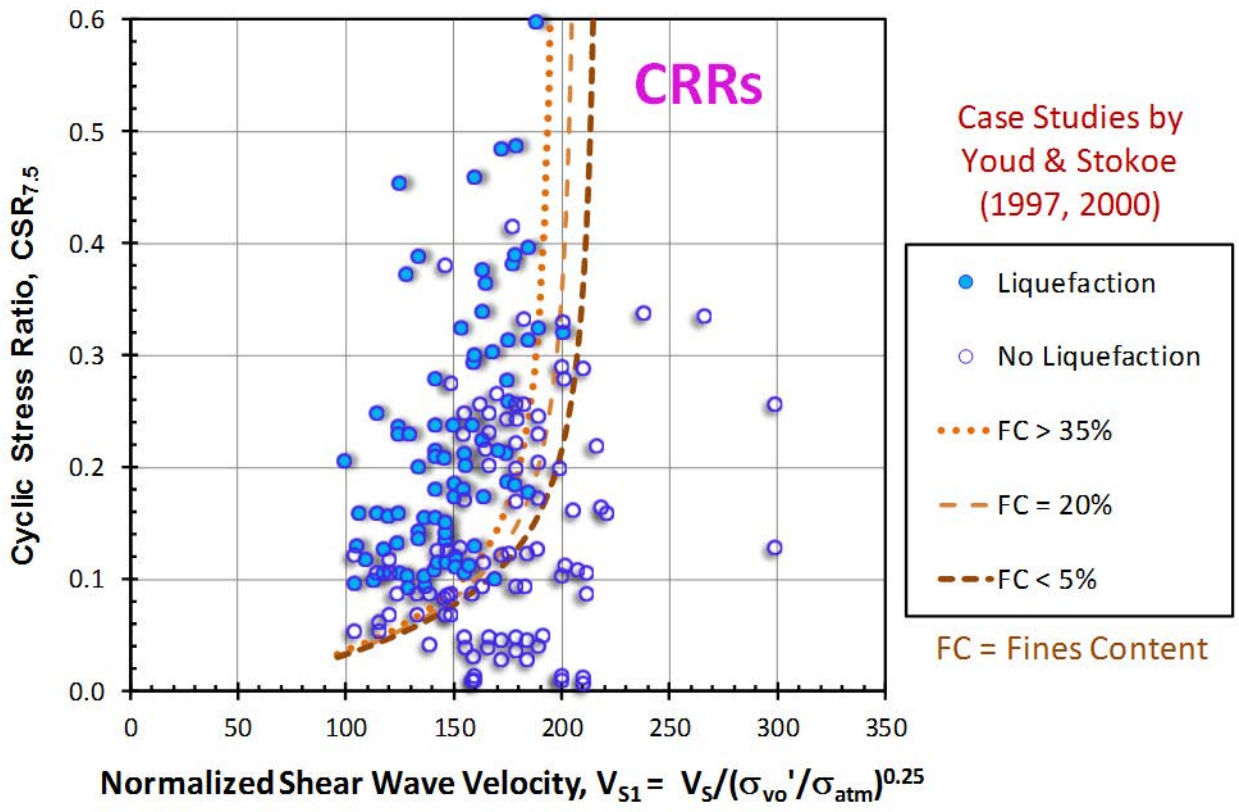

Figure B-7 NCEER recommended CRR for liquefaction evaluation using V_{s1} in sands

More recently, an updated approach using a larger database and recent case studies has been developed with both deterministic and probabilistic curves (Kayen et al., 2013), as presented in Figure B.8. In addition to adopting an exponential format (rather than the aforementioned hyperbolic algorithm), the method has a modified term for MSF and a rather more involved method for stress reduction factor, r_d.

The deterministic curve is associated with a probability of exceedance of 15% (PL = 0.15) and can be expressed simply as:

$$CRR_{7.5,\ sv'=1atm} = \exp[\ (V_{s1}/173.7)^{2.80} - 2.96\ ]$$

where the stress-normalized shear wave velocity has a cap of the term $C_{Vs} \leq 1.5$. The level of ground shaking represented by the cyclic stress ratio (CSR) is given by:

$$CSR_{7.5} = \frac{\tau_{ave}}{\sigma_{vo}^{'}} = 0.65 \cdot \left(\frac{a_{\max}}{g}\right) \cdot \left(\frac{\sigma_{vo}}{\sigma_{vo}^{'}}\right) \cdot r_d \cdot \frac{1}{DWF}$$

where DWF = duration weighting factor (essentially identical to the MSF = magnitude scaling factor), given here as:

$$DWF = 15\ M^{-1342}$$

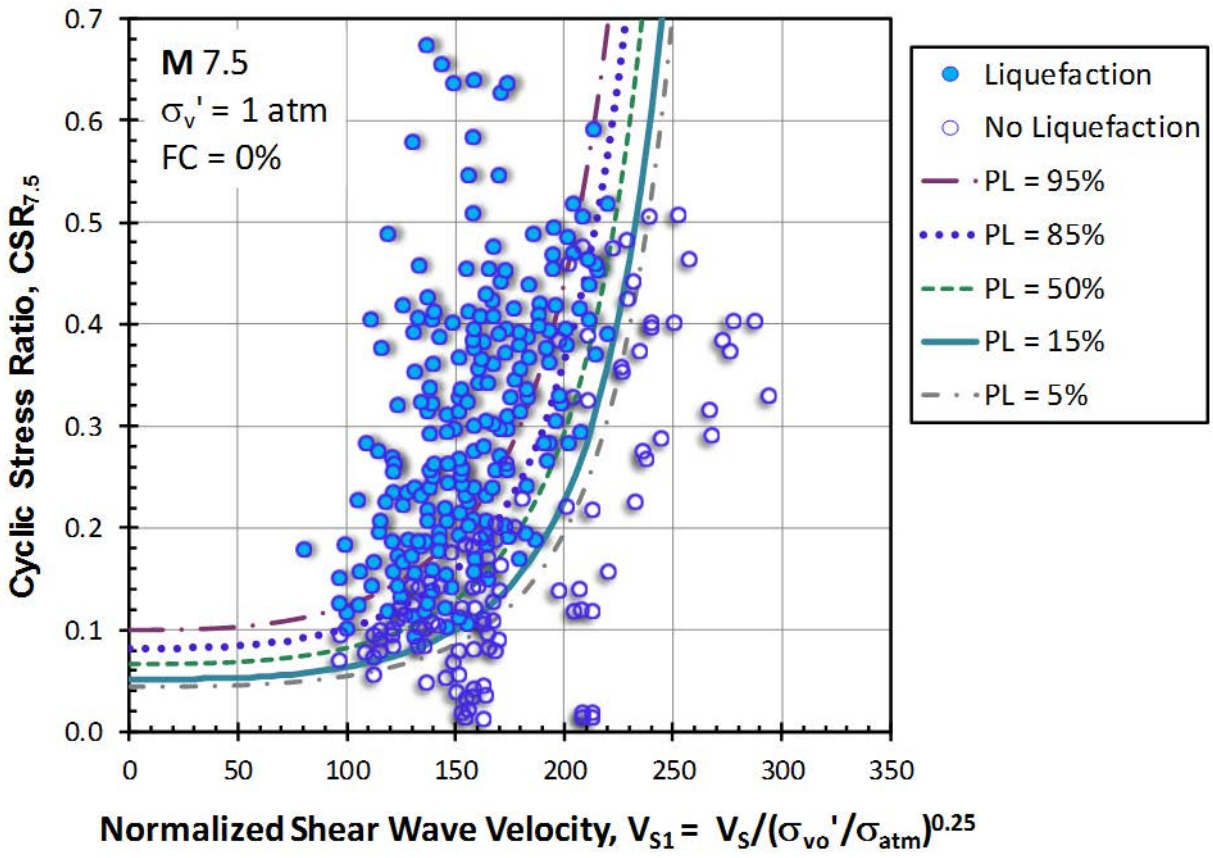

Figure B-8 Updated CRRs for normalized shear wave velocity using database methodology of Kayen et al., (2013).

More specifically, the generalized CRR for a range of probabilities is given by:

$$CRR=\exp\{[0.514\cdot[(0.0073\cdot V_{s1})^{2.80} -2.617\cdot\ln(\mathbf{M})-0.0099\cdot\ln(\sigma_{vo}'/\sigma_{atm}) +0.0028\cdot FC+0.481\cdot\varphi^{-1}(P_L)]\}$$

A detailed analysis on the stress reduction factor (r_d) has been conducted by Cetin et al. (2004). This permitted a statistical relation developed on the basis of depth (d) in meters, moment magnitude of the earthquake (**M**), level of ground shaking (a_{max}/g), and averaged shear wave velocity (V_s) in m/s over a particular depth range ($0 < d < 12$m), designated as $V_{s,12m}$. The mean value of r_d may be calculated as follows:

For depths d < 20 m:

$$r_d = \frac{1 + \dfrac{0.0525\cdot V_{s,12m} + M - 2.949\cdot(a_{\max}/g) - 23.013}{16.258 + 0.201\cdot\exp[0.341\cdot(7.586 - d + 0.0785\cdot V_{s,12m})]}}{1 + \dfrac{0.0525\cdot V_{s,12m} + M - 2.949\cdot(a_{\max}/g) - 23.013}{16.258 + 0.201\cdot\exp[0.341\cdot(7.586 + 0.0785 V_{s,12m})]}} \pm \sigma_{\varepsilon,r_d}$$

For depths d ≥ 20 m:

$$r_d = \frac{1 + \dfrac{0.0525 \cdot V_{s,12m} + M - 2.949 \cdot (a_{\max}/g) - 23.013}{16.258 + 0.201 \cdot \exp[0.341 \cdot (-12.414 + 0.0785 \cdot V_{s,12m})]}}{1 + \dfrac{0.0525 \cdot V_{s,12m} + M - 2.949 \cdot (a_{\max}/g) - 23.013}{16.258 + 0.201 \cdot \exp[0.341 \cdot (7.586 + 0.0785 \cdot V_{s,12m})]}} - 0.0046 \cdot (d - 20) \pm \sigma_{\varepsilon,r_d}$$

The standard deviations about the mean profile of r_d are given by:

For depths d < 12 m: $\sigma_{\varepsilon,rd} = 0.0198 \cdot d^{0.85}$

For depths d ≥ 12 m: $\sigma_{\varepsilon,rd} = 0.0198 \cdot 12^{0.85} = 0.164$

Residual Undrained Strength: After flow or cyclic liquefaction occurs, the shear strength of the liquefied sand is reduced to a smaller yet finite value, termed the *residual undrained strength*, s_r. Several new methods for evaluating the magnitude of s_r in sands from SPT resistance have been developed (Olson and Johnson, 2008; Boulanger and Idriss, 2014; Kramer and Wang, 2015). Using the latter method, which is shown in Figure B.9, the derived expression is:

$$S_r\ (atm) = \exp[0.109 \cdot (N_1)_{60} + 5.379 \cdot (\sigma_{vo}'/\sigma_{atm})^{0.1} - 8.444]$$

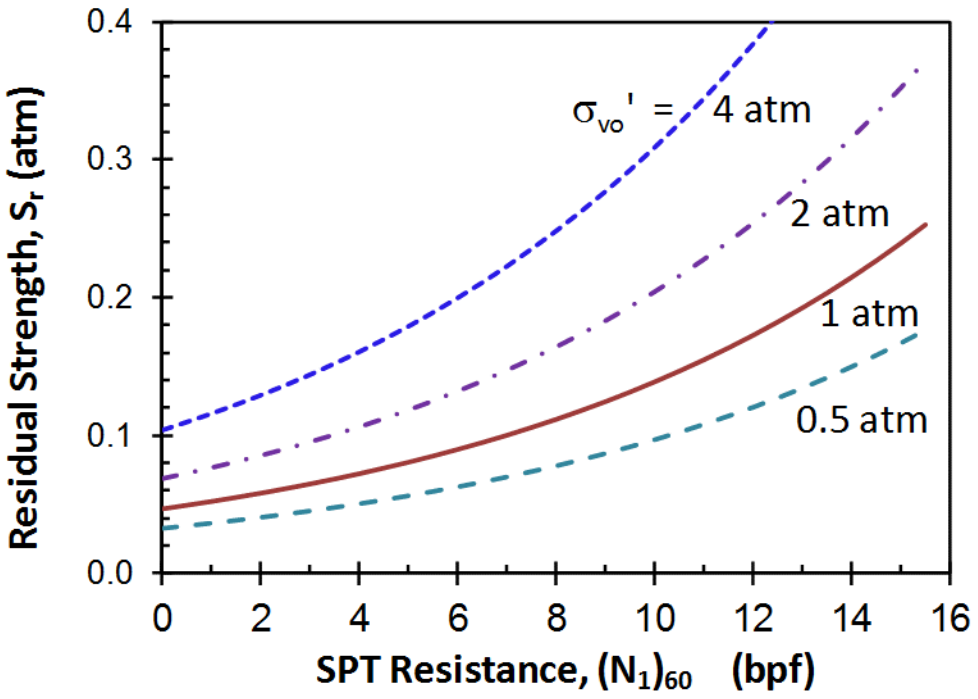

Figure B-9 Relation for residual undrained strength of sand, normalized SPT resistance, and effective overburden stress (Kramer and Wang, 2015).

Similiarly, new derivations for assessing the post-cyclic liquefied strength of sands from CPT results have been developed (Olson and Johnson, 2008; Robertson, 2010; Boulanger and Idriss, 2014). Using the approach reported by Robertson (2010), Figure B.10 shows the normalized

residual undrained strength to effective overburden ratio (s_r/σ_{vo}') with normalized CPT cone tip resistance for an equivalent clean sand that can be expressed:

$$\frac{S_r}{\sigma_{vo}'} = \frac{\frac{1}{45.5} - \frac{Q_{tn-cs}}{3201}}{1 - \frac{Q_{tn-cs}}{37.4} + \frac{(Q_{tn-cs})^2}{5608}}$$

where the ratio lies within the range: $0.03 \leq (s_r/\sigma_{vo}') \leq \tan\phi'$ and applies when $(Q_{tn})_{cs} < 70$.

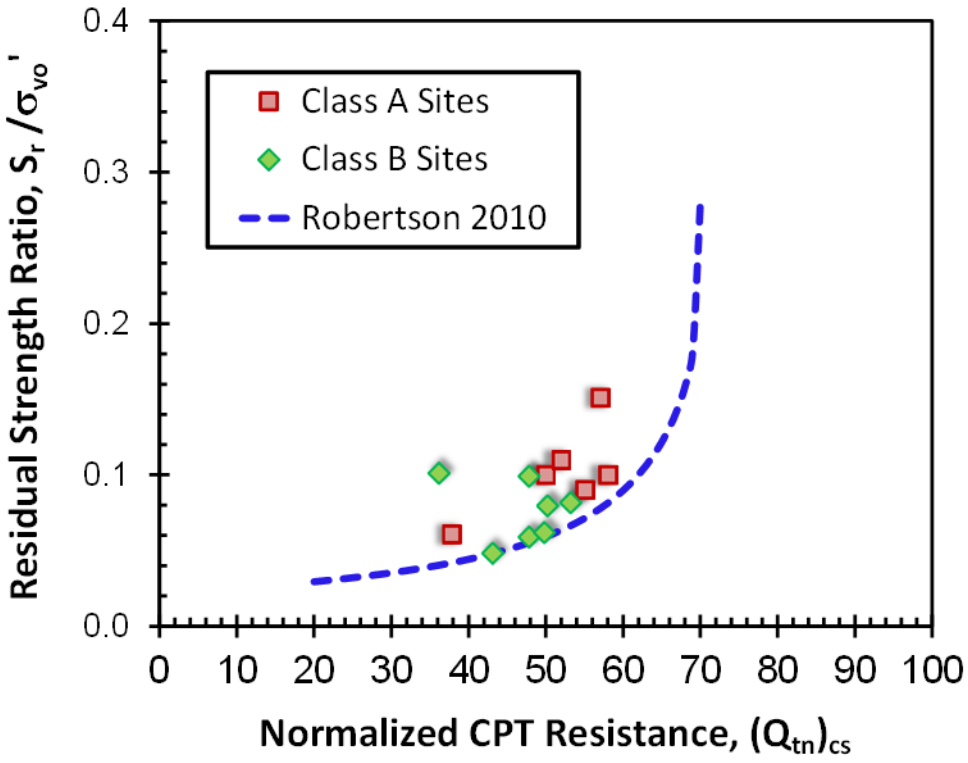

Figure B-10 Recommended strength of liquefied sands from CPT resistance (after Robertson, 2010).

APPENDIX C

SEISMIC GROUND DEFORMATIONS

Earthquake ground motions can result in collapse of the sand matrix structure resulting in ground deformations, including settlement and subsidence in level ground terrain. In sloped ground, there may be additional losses due to lateral spread. The use of the CPT results can be implemented in a systematic procedure to evaluate the magnitudes of seismic ground deformations in accord with the methodology described by Zhang et al. (2002, 2004).

Volumetric Strains: The magnitude of volumetric strains (ε_{vol}) are determined on the basis of the calculated factor of safety (FS) and the relative density (D_R) of the sands, as illustrated by Figure C.1. The seismic-induced permanent settlements (s_z) are calculated from:

$$s_z = \int_0^z \varepsilon_{vol}\, dz$$

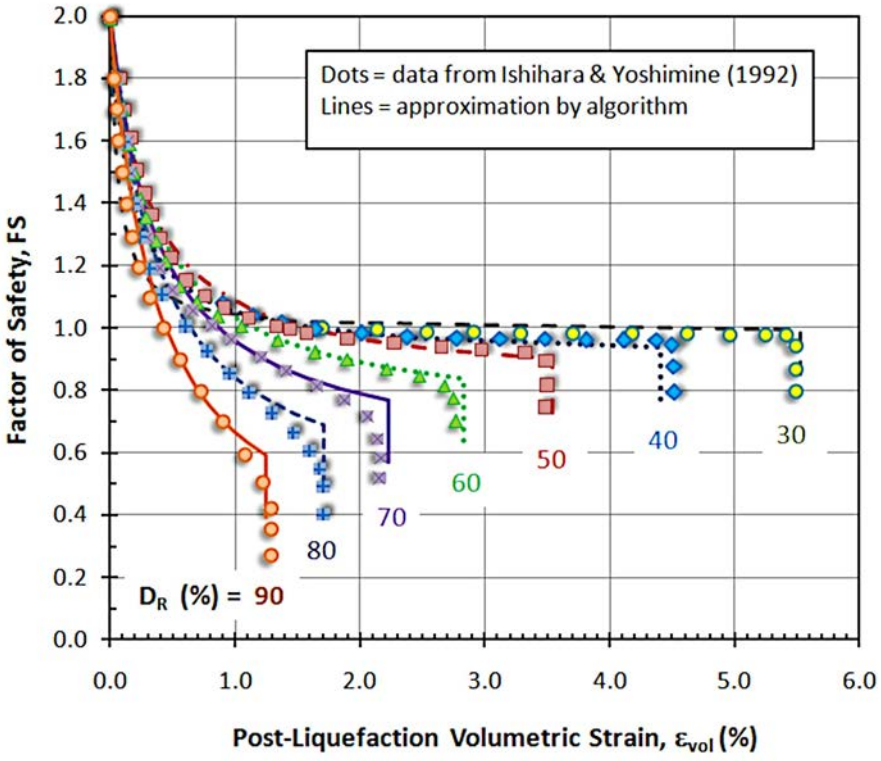

Figure C-1 Interrelationship of volumetric strain, safety factor, and sand relative density for evaluating seismically-induced settlements (after Ishihara and Yoshimine 1992).

Relative Density of Sand Layers: The relative density of sands (D_R) is a measure of the compactness of the state of packing of sand particles that range from its loosest (e_{max}) to its densest state (e_{min}), where e = void ratio and the limiting states are given by ASTM D4253 and

D4254. From a practical matter involving sands at a range of depths below the ground surface, the evaluation of D_R is empirically determined from the cone tip resistance:

$$D_R\ (\%) \quad = \quad 76 \cdot \log\ (Q_{tn\text{-}cs}) \ - \ 85 \qquad \leq \quad 100\%$$

where normalized cone tip resistance: $Q_{tn\text{-}cs} \leq 200$. Note for values of $Q_{tn\text{-}cs}$ above 200, set D_R = 100%.

Lateral Displacements: In sloping terrain and/or ground with a free-face condition, the occurrence of liquefaction can result in lateral spreading and horizontal movements downhill. The ground conditions include: (1) level ground, (2) gently sloping terrain, (3) level ground with free face, and (4) gentle slope with free face, as depicted in Figure C.2. The percent slope (S) and free face geometry (H = height and L = distance) are also defined here.

Figure C-2 Schematic drawings of ground surface conditions for lateral spread deformations.

The magnitudes of induced lateral displacements (LD) are estimated from the maximum cyclic shear strains (γ_{MAX}) which are integrated with depth to obtain the lateral displacement index (LDI):

$$LDI \quad = \quad \int_0^z \gamma_{MAX}\ dz$$

The level of cyclic shear strains was studied under laboratory controlled conditions on prepared sand specimens by Ishihara and Yoshimine (1992). They related magnitude of γ_{MAX} to the factor of safety (FS) and sand relative density (D_R). In addition, a limiting value of cyclic shear strain was established from the work of Seed (1976, 1979) and Housner et al. (1985). The resulting methodology is presented graphically in Figure C.3 (Zhang et al., 2004; Robertson 2004).

Depending upon the slope angle (0.2% < S < 3.5%), the calculated lateral displacements (LD) are obtained from:

$$LD/LDI \quad = \quad S \ + 0.2 \ (\%)$$

For free-face conditions (see Figure C.2), the geometry of distance from the CPT sounding location to the face location (L) and the height of the free face (H) are used to obtain the amount of lateral displacements (4 < L/H < 40):

$$LD/LDI \quad = \quad 6\ (H/L)^{0.8}$$

A number of case studies presented by Zhang et al. (2004) are used to develop these relations.

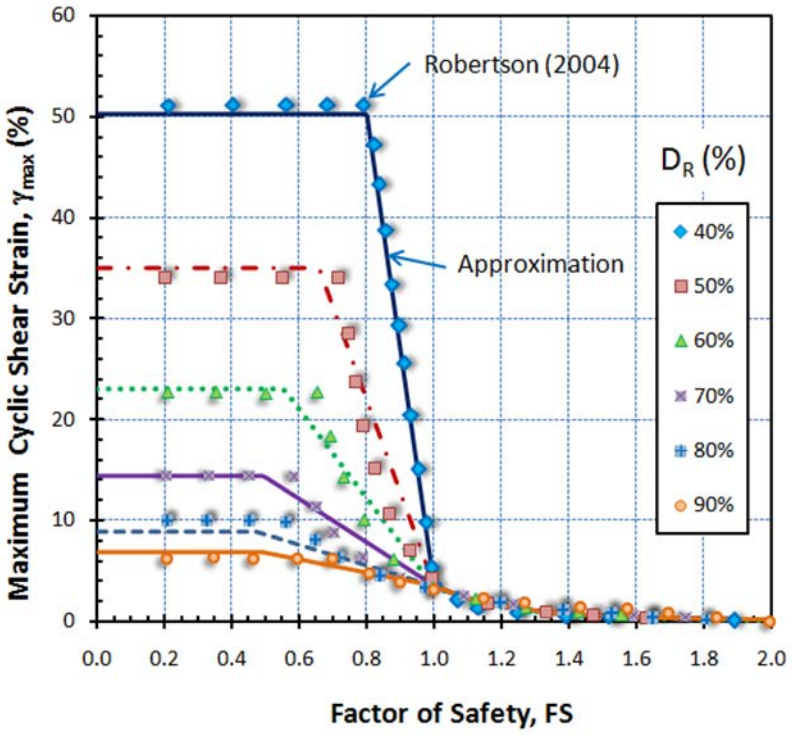

Figure C-3 **Relation of maximum cyclic shear strain (γ_{MAX}) with sand relative density (D_R) and calculated safety factor (FS) against liquefaction (after Zhang et al., 2004: Ishihara and Yoshimi, 1992).**

APPENDIX D

SITE DESCRIPTION FOR PALEOLIQUEFACTION STUDY

Site Name-Number: **1:24,000 Topo Map:**

GPS Waypoint: **Geographic Location:**

Latitude (degrees): **Longitude (degrees):**

Easting: **Northing:**

Access: **Permission:**

Logs: **Photographs:**

Exposure Length (m): **Exposure Height (m):** **Exposure Quality:** Ex Gd Fr Pr

Geological Setting:

Liquefaction Features:

Number of sand blows ( ) sand dikes ( ) sand sills ( ) SSD structures ( )

Other features ( ), briefly describe:

Diagram:

Samples Collected (see diagram):

Artifacts Charcoal OSL Soil Wood

Information Supplied By: **Name:**

Affiliation: Date: J F M A M J J A S O N D 2015

Liquefaction Feature Number: **Site Name-Number:**

Type of feature: blow dike sill diaper basal erosion load cast pseudonodule fold

Depth of termination or deformation below surface (or above water level) (m):

Thickness and length (cm):

Termination of dikes (blow, sill, pinch, truncation):

Widths of dikes (cm):

Strikes and dips of dikes (degrees):

Sediment type (grain-size, clasts):

Internal sedimentary structures (flow lamination, vertical/horizontal bedding):

Soil development or chemical weathering:

Distance between similar deformation features (m):

Cross-cutting relations:

Additional Notes (e.g., seismic vs non-seismic origin; relative age of features):

Information Supplied By: **Name:**

Affiliation: **Date:** J F M A M J J A S O N D 2015

APPENDIX E

ARCHEOLOGICAL EXCAVATION PROTOCOL DEVELOPED FOR PALEOSEISMIC INVESTIGATIONS AT ARCHEOLOGICAL SITES IN ARKANSAS

Documentation of archaeological features found during the excavation of a sand blow should begin with mapping and photographing the features as they appear on the surface of the sand blow once the plow zone has been removed. Archeological features are numbered sequentially for identification purposes and recorded on a feature log (Figure E.1). Features, such as post molds and pits, are usually cut in half and excavated with a 4½ inch masonry point trowel and other small hand tools. One half of the feature is excavated so that its cross section can be drawn and photographed. The features are documented on feature forms that standardize the observations made and samples collected.

Figure D-1 Archeologist, Robert Lafferty, documenting artifacts recovered from features intruding top of sand dike at archeological site 3MS557 in northeastern Arkansas. Photograph by M. Tuttle.

Observations include: feature dimensions (width, length, and depth), Munsell colors and textures of each stratum, and temporally diagnostic artifacts observed /collected in excavations. Documentation includes scaled, plan view and cross-sectional drawings on the grid paper (usually on the back of the form). The plan view drawing shows the north direction, feature limits and textures/color, as well as profile locations (Figure E.2). The cross sections show the position of the level line, feature limits, and soil descriptions of the feature fill and host. Other data shown on forms include: state site number, field serial number (FSN), excavator, date excavated, volume

excavated in liters. The excavated matrix is retained in large polyethylene bags and taken to the laboratory for flotation recovery of artifacts and charred botanical material. All of the exposed features intruding into the sand blow should be either excavated, if that part of the sand blow is to be excavated, or left in place and protected.

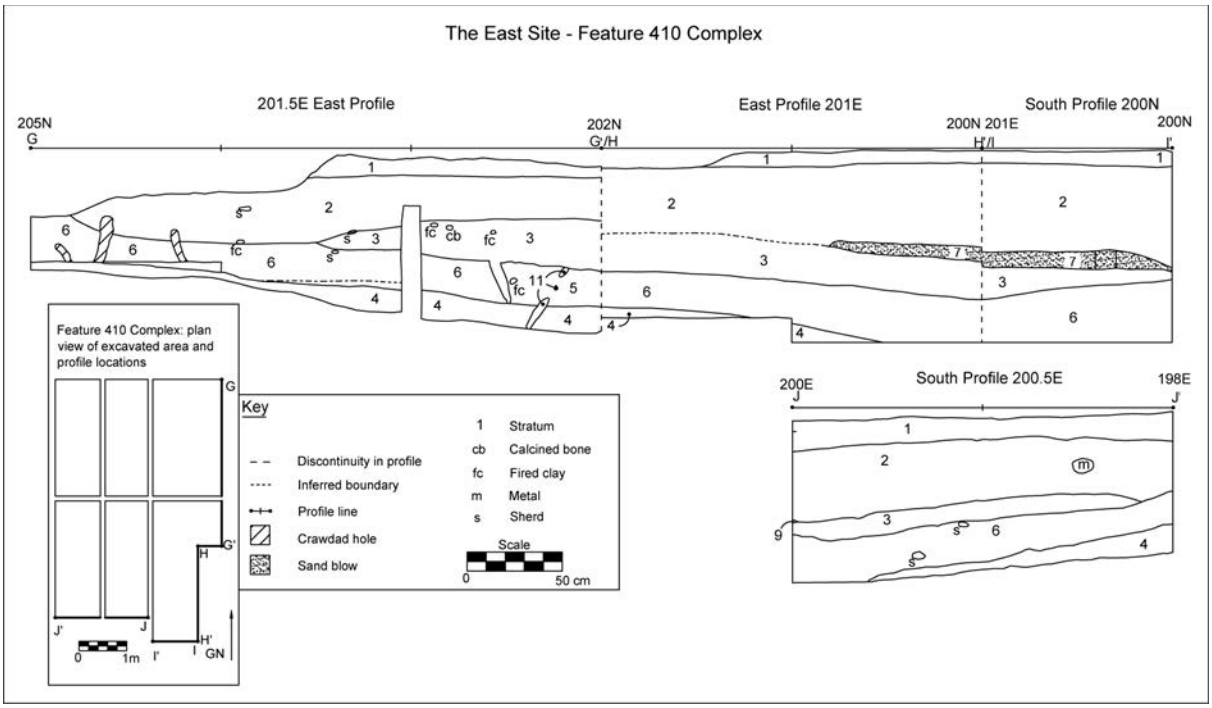

Figure D-2 Cross-sectional drawing G-G' to J-J' of archeological excavation at the East site (3PO610) in northeastern Arkansas (from Tuttle et al., 2011). Location of G-G' to J-J' profile indicated on plan view shown in lower left. Stratum 7 is sand blow indicated with stipple pattern.

The sand blow is excavated until the buried soil or sediment layer is encountered. The buried surface is examined by the archaeologist using a trowel, shovel, and/or a short-handled hoe. If there are intact archaeological deposits, one or more square meter test units (TU) are excavated through the deposit. Test units are excavated in 10-cm, or thinner, levels. Excavations are carried out with razor sharp shovels and trowels. A level is taken down in thin horizontal cuts of ½- to 1-cm thick shovel cuts. The matrix is put through 6.25 mm (¼ inch) screens and all recovered artifacts are placed in cloth bags that are labeled with site number, date, collector, depths, unit number, and field serial number. The excavation level is stopped at a depth of 10 cm and the whole unit floor is cleaned with a trowel. Stains or large artifacts are mapped at a scale of 1:10 or 1:20. Often, a flotation column (that is typically 25 x 25 x 10 cm; a volume of 6.26 liters for each 10-cm level) is taken from a corner of the unit. During excavation, artifacts and large samples of carbon may be point plotted and collected, and assigned an unique FSN. A level form is filled out for each excavation level. The soil matrix description, FSN's from the level, artifacts observed/collected, name, date, and a drawing of the level showing point-plotted artifacts, soil staining, and features are systematically recorded on the form. When the base of the excavation unit is reached, typically one or two levels below artifact bearing levels, one or more profiles are cleaned, photographed, and drawn. The profile drawings show soil strata and or horizons with colors and textures, feature staining, point-plotted artifacts, and any liquefaction features (Figure E.2). See Carmichael et al. (2003) for a more detailed discussion of techniques.

The profile of the sand blow is logged by a paleoseismologist. These large scaled (1:10) drawings show the sand blow layers, flow structures, soil textures, and colors, cultural deposits, including point-plotted artifacts, and collected samples.

NRC FORM 335
(12-2010)
NRCMD 3.7

U.S. NUCLEAR REGULATORY COMMISSION

BIBLIOGRAPHIC DATA SHEET

(See instructions on the reverse)

1. REPORT NUMBER
(Assigned by NRC, Add Vol., Supp., Rev., and Addendum Numbers, if any.)

NUREG/CR-7238

2. TITLE AND SUBTITLE

Guidance Document: Conducting Paleoliquefaction Studies for Earthquake Source Characterization

3. DATE REPORT PUBLISHED

MONTH	YEAR
January	**2018**

4. FIN OR GRANT NUMBER

5. AUTHOR(S)

M. Tuttle, L. Wolf, P. Mayne, K. Dyer-Williams, R. Lafferty

6. TYPE OF REPORT

Technical

7. PERIOD COVERED (Inclusive Dates)

8. PERFORMING ORGANIZATION - NAME AND ADDRESS (If NRC, provide Division, Office or Region, U. S. Nuclear Regulatory Commission, and mailing address; if contractor, provide name and mailing address.)

M. Tuttle & Associates, P.O. Box 345, Georgetown, ME 04548

9. SPONSORING ORGANIZATION - NAME AND ADDRESS (If NRC, type "Same as above", if contractor, provide NRC Division, Office or Region, U. S. Nuclear Regulatory Commission, and mailing address.)

Division of Engineering
Office of Nuclear Regulatory Research
U.S. Nuclear Regulatory Commission
Washington, DC 20555

10. SUPPLEMENTARY NOTES

Sarah Tabatabai

11. ABSTRACT (200 words or less)

The primary goal of this document is to provide detailed guidance for conducting paleoliquefaction studies in order to generate high-quality data for use in seismic source characterization and seismic hazard assessment. This document presents background information on paleoseismology, earthquake-induced liquefaction and related ground failures, and soft-sediment deformation structures that form as a result of liquefaction. It also provides guidance on all aspects of paleoliquefaction studies, including selection of study areas and the various types of information that should be consulted, performance of site investigations and surveys of river cutbanks and other exposures, relative and absolute dating techniques used to constrain ages of liquefaction features and thus important for estimating the timing and recurrence of paleoearthquakes, and geological and geotechnical approaches to estimating source areas and magnitudes of paleoearthquakes. The report identifies factors that contribute to uncertainty in paleoliquefaction data and observations and analyses that can help to reduce those uncertainties. The report also includes a discussion of the use of paleoliquefaction data in seismic hazard assessment through the development of regional seismic source models and presents recent examples of the use of paleoliquefaction data in seismic source models of the New Madrid seismic zone in the central U.S.

12. KEY WORDS/DESCRIPTORS (List words or phrases that will assist researchers in locating the report.)

Paleoliquefaction, earthquake-induced liquefaction, soft-sediment deformation, paleoseismology, paleoearthquakes, seismic source characterization, seismic hazard assessment.

13. AVAILABILITY STATEMENT

unlimited

14. SECURITY CLASSIFICATION

(This Page)
unclassified

(This Report)
unclassified

15. NUMBER OF PAGES

16. PRICE

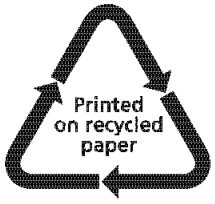

Federal Recycling Program

UNITED STATES
NUCLEAR REGULATORY COMMSSION
WASHINGTON, DC 20555-0001

OFFICIAL BUSINESS

UNITED STATES
NUCLEAR REGULATORY COMMISSION
WASHINGTON, DC 20555-0001

OFFICIAL BUSINESS

NUREG/CR-7238

Guidance Document: Conducting Paleoliquefaction Studies for Earthquake Source Characterization

January 2018